



# **River Training and Channel Protection**

## **Validation of a 3D numerical model**

**DJ Seed**

**Report SR 480  
March 1997**



Address and Registered Office: **HR Wallingford Ltd.** Howbery Park, Wallingford, Oxon OX10 8BA  
Tel: + 44 (0)1491 835381 Fax: + 44 (0)1491 832233

Registered in England No. 2562099. HR Wallingford is a wholly owned subsidiary of HR Wallingford Group Ltd.





---

## **Contract**

---

This report describes work funded by the Department of the Environment under research Contract PECD 7/6/110 for which the DoE nominated officer was P Woodhead and the HR nominated officer was WR White. The HR job number was RTS 50. It is published on behalf of the Department of the Environment, but any opinions expressed in this report are not necessarily those of the funding department. The work was carried out by David Seed and Manuela Escarameia and the project was managed by RWP May.

Prepared by David Seed Senior Scientist  
(name) (job title)

Approved by RWP. May Principal Engineer

Date 3 September 1997

© Crown Copyright 1997

Published by permission of the Controller of Her Majesty's Stationery Office





---

## ***Acknowledgements***

---

The author thanks the following for their contribution to this project. Richard Hibbert for the evaluation tests described in Section 5. Luca Barone for the tests in the rectangular channel. Esteban Azagra for tests in the trapezoidal channel. Norbert Jamot of the Ecole Centrale de Lyon for further tests in the rectangular and sinuous channel and for the computational tests.





---

## **Summary**

---

River Training and Channel Protection

Interim report, validation a of 3D numerical model

DJ Seed

Report SR 480

March 1997

Present methods of designing river training works rely mainly on empirical rules or require the use of expensive physical models. These models are themselves subject to uncertainties and errors due to scaling problems and are usually only justified for major schemes in localised areas. This report describes the initial phase of work to provide rational guidelines for the design of river training works. These guidelines will be based on the results of a numerical model which has been verified against physical experiments.

The initial phase of the work was the selection and validation of the numerical model. In the first year of work, a number of numerical models were tested and a package called SSIIM, developed by Dr N R B Olsen, was selected for its particular suitability to open channel flows. In the second phase of the work, SSIIM was tested against a number of physical models and was shown to give satisfactory results. During this work, sensitivity tests were conducted to establish the modelling parameters and discretisation which gave results that were sufficiently accurate while limiting the computer run times to acceptable levels. In the final phase, the SSIIM model is used to predict flows in fields of groynes. These simulations are used in the design guide for river groynes (SR 493). This work is partly funded by the Construction Sponsorship Directorate, of the Department of the Environment.





---

## **Notation**

---

$a$	:	groyne area
$A$	:	wetted area
$b$	:	unobstructed width of channel (B-L <sub>t</sub> )
$b^*$	:	width of recirculation zone
$B$	:	width of the channel
$C_{\mu}$	:	empirical constant of the k- $\epsilon$ model (0.09)
$C_{1\epsilon}$	:	empirical constant of the k- $\epsilon$ model (1.44)
$C_{2\epsilon}$	:	empirical constant of the k- $\epsilon$ model (1.92)
$F_r$	:	Froude number
$g$	:	acceleration due to gravity
$H$	:	depth of water at channel centreline
$h$	:	local depth of water
$h_g$	:	mean groyne height = $a/L_t$
$k$	:	turbulent kinetic energy
$k_s$	:	roughness
$L$	:	distance along the channel centreline (in sinuous channel)
$L_e$	:	embedded length of groyne
$L_m$	:	length of one meander (measured along the centreline of the channel)
$L_t$	:	exposed length of the groyne
$M$	:	Strickler coefficient (1/n)
$n$	:	Manning's roughness coefficient
$P$	:	pressure
$P$	:	wetted perimeter
$P_k$	:	term for the production of $k$
$Q$	:	discharge
$r_{\text{curv}}$	:	radius of curvature
$R_e$	:	Reynolds number
$R_h$	:	hydraulic radius
$s$	:	sinuosity of a channel
$S$	:	water surface slope
$S_L$	:	length of recirculation zone
$t$	:	time
$u$	:	velocity in x direction



---

## **Notation** *continued*

---

$u_*$	:	friction velocity
$U_i$	:	velocity (tensor notation)
$\overline{u_i u_j}$	:	Reynolds stress
$v$	:	velocity in y direction
$V_{\text{mean}}$	:	average velocity ( $Q/A$ )
$V_x$	:	velocity in x direction
$w$	:	velocity in z direction
$X$	:	length of experimental channel
$x_i$	:	direction x, y, z at $l = 1, 2, 3$
$x$	:	downstream direction (positive downstream)
$y$	:	lateral direction (positive away from groyne bank)
$z$	:	vertical direction (zero at bed)
$\beta_0$	:	empirical constant (3.0)
$\delta_{ij}$	:	Kronecker delta ( $\delta_{ii} = 1$ , $\delta_{ij} = 0$ for $i \neq j$ )
$\epsilon$	:	turbulent dissipation rate
$\theta$	:	angle between the centreline and the axis of the channel
$\theta_0$	:	maximum value of $\theta$
$\kappa$	:	von Karman constant for turbulent flow
$\nu$	:	viscosity
$\nu_t$	:	turbulent viscosity
$\rho$	:	density of water
$\sigma_\epsilon$	:	empirical constant of the k- $\epsilon$ model (1.0)
$\sigma_k$	:	empirical constant of the k- $\epsilon$ model (1.3)
$\tau_0$	:	shear stress of the wall
$\phi_e$	:	Arbitrary scalar variable at east face of cell
$\phi_E$	:	Arbitrary scalar variable at centre of east cell



---

# Contents

---

	<i>Page</i>
<i>Title page</i>	<i>i</i>
<i>Contract</i>	<i>iii</i>
<i>Acknowledgments</i>	<i>v</i>
<i>Summary</i>	<i>vii</i>
<i>Notation</i>	<i>ix</i>
<i>Contents</i>	<i>xi</i>
<b>1 Introduction</b> .....	<b>1</b>
1.1 Scope of work .....	1
1.2 Approach .....	1
<b>2 River training works</b> .....	<b>2</b>
2.1 Groynes .....	2
2.2 Impact of groynes .....	2
2.3 Overall design of groynes .....	3
2.4 Detailed Design of groynes .....	4
2.5 Previous Research into River Groynes .....	4
2.6 Characteristics in the region of a groyne .....	5
<b>3 Flow modelling software</b> .....	<b>5</b>
3.1 Turbulence modelling .....	5
3.2 Choice of numerical model .....	6
3.3 Phoenics .....	6
3.4 SSIIM .....	7
<b>4 Three dimensional flow modelling using SSIIM</b> .....	<b>7</b>
4.1 Introduction to SSIIM model .....	7
4.2 Creating the 3D Model Grid .....	8
4.3 Boundary conditions for the model .....	8
4.4 Water Surface .....	9
4.5 Numerical Schemes .....	9
4.6 Solution of the Pressure-Velocity Coupling using SIMPLE and SIMPLEC .....	10
4.7 Procedure for solving the flow equations .....	11
4.8 Block correction .....	12
4.9 Discussion .....	12
<b>5 Evaluation tests</b> .....	<b>13</b>
5.1 Introduction .....	13
5.2 Standard test cases .....	14
5.3 Simulation of impermeable groynes .....	14
5.4 Simulation of permeable groynes .....	14
<b>6 Comparative tests</b> .....	<b>15</b>
6.1 Test U0, U shaped flume .....	15
6.2 Test P0 - FCF flume (straight out of bank flow) .....	16
6.2.1 Comparison with Telemac .....	16
6.2.2 Comparison with experimental data .....	17
6.3 Test RAa - Hanover flume with a rectangular groyne .....	17
6.4 Summary .....	19



---

## Contents continued

---

<b>7</b>	<b>Physical model tests</b> .....	<b>19</b>
7.1	Experimental set-up .....	19
7.2	Velocity Measuring Equipment .....	19
7.3	Channel layout and model groynes .....	21
7.4	Preliminary tests .....	21
7.5	Tests in a rectangular channel .....	22
7.5.1	Single unsubmerged groyne (Test RAb) .....	22
7.5.2	Single submerged groyne (Test RB) .....	23
7.5.3	Two unsubmerged groynes, 1m apart (Test REa) .....	23
7.5.4	Two unsubmerged groynes, 2m apart (Test REb) .....	23
7.5.5	Permeable groynes .....	23
7.5.6	Tapered groyne (Test RM) .....	23
7.6	Tests in a trapezoidal channel .....	23
7.6.1	Single unsubmerged groyne (Test TA) .....	23
7.6.2	Single submerged groyne (Test TB) .....	24
7.6.3	Single unsubmerged groyne, 75° angle (Test TC) .....	24
7.6.4	Single unsubmerged groyne, 105° angle (Test TD) .....	24
7.6.5	Two unsubmerged groynes, 1m apart (Test TE) ..	24
7.7	Conclusions from the GP flume tests .....	24
7.8	Tests in a sinuous channel .....	24
<b>8</b>	<b>Validation tests for a rectangular channel</b> .....	<b>26</b>
8.1	Introduction .....	26
8.2	Test RAb - Rectangular groynes in a rectangular channel (GP Flume) .....	26
8.3	Test RB - submerged groyne .....	29
8.4	Tests RE - Two unsubmerged groynes .....	29
8.4.1	Test REa - Two groynes one metre apart .....	29
8.4.2	Test REb - Two groynes two metres apart .....	30
8.4.3	Summary .....	31
8.5	Tests RX and RY - Permeable groynes .....	31
8.6	Test RM - Tapered groyne .....	31
8.7	Summary of results from rectangular channel .....	32
<b>9</b>	<b>Validation tests for a trapezoidal channel</b> .....	<b>33</b>
9.1	Test TA - A single unsubmerged groyne in a trapezoidal channel .....	33
9.2	Test TB - A single submerged groyne in a trapezoidal channel .....	35
9.3	Test TC - An unsubmerged groyne angled upstream ..	36
9.4	Test TD - An unsubmerged groyne angled downstream ..	37
9.5	Test TE - Two unsubmerged groynes 1m apart .....	37
<b>10</b>	<b>Validation tests for a sinuous trapezoidal channel</b> .....	<b>39</b>
<b>11</b>	<b>Conclusions</b> .....	<b>40</b>
<b>12</b>	<b>References</b> .....	<b>42</b>



---

## Contents *continued*

---

### Tables

Table 1	Recommended groyne spacing for bank protection
Table 2	Orientation of groynes to upstream bank
Table 3	Test coding
Table 4	Description of Tests presented
Table 5	Physical parameters of tests
Table 6	Dimensionless parameters of tests
Table 7	Validation tests

### Figures

Figure 2.1	Typical impermeable groyne structures
Figure 2.2	Permeable timber pile groynes (after Chang)
Figure 2.3	Local vortex system around a groyne (after Copeland)
Figure 2.4	Stream flow around a single groyne (after Bognar and Hanko)
Figure 2.5	Typical layout of training work for channelisation (after Kinori and Mevotach)
Figure 2.6	Plan shapes of groynes
Figure 4.1	Notation for grid points and faces of control volumes
Figure 4.2	Flow chart for SSIIM numerical model
Figure 5.1	Test CA : 90° bend with obstruction - Bed layer
Figure 5.2	Test CA : 90° bend with obstruction - Mid layer
Figure 5.3	Test CA : 90° bend with obstruction - Surface layer
Figure 5.4	Test EO : straight channel - refined mesh - Bed layer
Figure 5.5	Test EO : straight channel - refined mesh - Mid layer
Figure 5.6	Test EO : straight channel - refined mesh - Surface layer
Figure 5.7	Test EE : Two groynes - Bed layer
Figure 5.8	Test EE : Two groynes - Mid layer
Figure 5.9	Test EE : Two groynes - Surface layer
Figure 5.10	Test EH : Two submerged groynes - Bed layer
Figure 5.11	Test EH : Two submerged groynes - Mid layer
Figure 5.12	Test EH : Two submerged groynes - Surface layer
Figure 5.13	Test EW-1 : Porous groyne (one vertical slot) - Bed layer
Figure 5.14	Test EW-1 : Porous groyne (one vertical slot) - Mid layer
Figure 5.15	Test EW-1 : Porous groyne (one vertical slot) - Surface layer
Figure 5.16	Test EW-2 : Porous groyne (3 vertical slots) - Bed layer
Figure 5.17	Test EW-2 : Porous groyne (3 vertical slots) - Mid layer
Figure 5.18	Test EW-2 : Porous groyne (3 vertical slots) - Surface layer
Figure 5.19	Test EW-3 : Porous groyne (submerged) - Bed layer
Figure 5.20	Test EW-3 : Porous groyne (submerged) - Mid layer
Figure 5.21	Test EW-3 : Porous groyne (submerged) - Surface layer
Figure 5.22	Test EW-4 : Porous groyne (horizontal slot) - Bed layer
Figure 5.23	Test EW-4 : Porous groyne (horizontal slot) - Mid layer
Figure 5.24	Test EW-4 : Porous groyne (horizontal slot) - Surface layer
Figure 5.25	Test EW-5 : Porous groyne (two horizontal slots) - Bed layer
Figure 5.26	Test EW-5 : Porous groyne (two horizontal slots) - Lower jet



---

**Contents**      *continued*

---

Figure 5.27	Test EW-5 : Porous groyne (two horizontal slots) - Mid layer
Figure 5.28	Test EW-5 Porous groyne (two horizontal slots) - Upper jet
Figure 5.29	Test EW-5: Porous groyne (two horizontal slots) - Surface layer
Figure 6.1	Test U0 : Velocity profiles in a U-shaped Channel (de Vriend)
Figure 6.2	Test U0 : Velocity profiles in a U-shaped Channel (SSIIM)
Figure 6.3	Test U0 : Velocity profiles in a U-shaped Channel (Phoenics)
Figure 6.4	Test P0 : Straight out-of-bank flow, layout of FCF flume
Figure 6.5	Test P0 : Straight out-of-bank flow, comparison of Telemac and SSIIM
Figure 6.6	Test P0 : Straight out-of-bank flow, comparison of SSIIM with experiment
Figure 6.7	Test RAa-1 : Hanover flume results from original grid
Figure 6.8	Test RAa-4 : Hanover flume results from non uniform grid
Figure 6.9	Test RAa : Hanover flume comparison of methods (longitudinal velocity)
Figure 6.10	Test RAa : Hanover flume comparison of methods (transverse velocity)
Figure 7.0	Layout of General Purpose flume (GP flume)
Figure 7.1	Minilab probe
Figure 7.2	Types of channel used for the laboratory in GP flume
Figure 7.3	Orientation of groynes in tests TC and TD
Figure 7.4	Dimensions of rectangular groynes in rectangular channel
Figure 7.5	Dimensions of permeable and tapered groynes in rectangular channel
Figure 7.6	Layout of Flood Channel Facility (FCF) - Series C
Figure 7.7	Dimensions of groynes in FCF
Figure 8.1	Experimental points and numerical grid for Test RAb
Figure 8.2	Test RAb - Unsubmerged groyne in a rectangular channel. Mid-depth velocities and cross-section profiles of X-velocity
Figure 8.3	Test RAb - Unsubmerged groyne in a rectangular channel. Plan velocity vectors near groyne and in the recirculation zone
Figure 8.4	Test RAb - Unsubmerged groyne in a rectangular channel. Plan velocity vectors (near-bed)
Figure 8.5	Test RAb - Comparison between SSIIM and experimental data. Vertical profiles of plan velocity and flow direction
Figure 8.6	Test RAb - Unsubmerged groyne in rectangular channel Long section view of velocity vectors (near groyne)
Figure 8.7	Recirculation lengths in rectangular channel
Figure 8.8	Experimental points and numerical grid for Test RB-1
Figure 8.9	Test RB - Submerged groyne in a rectangular channel Mid-depth velocities and cross-section profiles of X-velocity
Figure 8.10	Test RB - Submerged groyne in rectangular channel Plan velocity vectors above mid-depth
Figure 8.11	Test RB - Submerged groyne in rectangular channel Plan velocity vectors (near surface)



---

## **Contents**      *continued*

---

- Figure 8.12      Test RB - Submerged groyne in rectangular channel  
Plan velocity vectors (near-bed)
- Figure 8.13      Test RB - Submerged groyne in rectangular channel  
Long section - velocity vectors near groyne
- Figure 8.14      Experimental points and numerical grid for Test REa-1
- Figure 8.15      Test REa - Two groynes 1m apart in a rectangular channel.  
Mid-depth velocities and cross-section profiles of X-velocity
- Figure 8.16      Test REa - Two groynes 1m apart in a rectangular channel.  
Plan velocity vectors near groyne and in recirculation zone
- Figure 8.17      Test REa - Two groynes (1m apart) in a rectangular channel.  
Vertical profiles of plan velocity and flow direction
- Figure 8.18      Test REa - Two groynes (1m apart) in rectangular channel.  
Turbulent kinetic energy at three depths
- Figure 8.19      Experimental points and numerical grid for Test REb-1
- Figure 8.20      Test REb - Two groynes (2m apart) in a rectangular channel.  
Mid-depth velocities and cross-section profiles of X-velocity
- Figure 8.21      Test REb - Two groynes (2m apart) in a rectangular channel.  
Plan velocity near groyne and in recirculation zone
- Figure 8.22      Test REb - Test groynes (2m apart) in a rectangular  
channel. Vertical profiles of plan velocity and flow direction
- Figure 8.23      Test REb - Two groynes (2m apart) in rectangular channel.  
Turbulent kinetic energy at three depths
- Figure 8.24      Experimental points and numerical grid for Tests RX and RY
- Figure 8.25      Test RX - Permeable groyne with 25% obstruction  
Mid-depth velocities and cross-section profiles of X-velocity
- Figure 8.26      Test RY - Single groyne with 44% obstruction  
Mid-depth velocities and cross-section profiles of X-velocity
- Figure 8.27      Experimental points and numerical grid for Test RM-1
- Figure 8.28      Test RM - Tapered groyne in a rectangular channel  
Mid-depth velocities and cross-section profiles of X-  
velocity
- Figure 8.29      Test RM - Tapered groyne in a rectangular channel  
Plan velocity vectors near groyne and in recirculation zone
- Figure 8.30      Test RM - Tapered groyne in rectangular channel  
Vertical profiles of plan velocity and flow direction
- Figure 9.1      Experimental points and numerical grid for Test TA-9
- Figure 9.2      Test TA - Unsubmerged groyne in a trapezoidal channel  
Mid-depth velocity vectors and cross-section profiles of X-  
velocity
- Figure 9.3      Test TA - Unsubmerged groyne in a trapezoidal channel  
Plan velocity vectors near groyne and in the recirculation  
zone
- Figure 9.4      Test TA - Rectangular groyne in a trapezoidal channel  
Vertical profiles of plan velocity and flow direction
- Figure 9.5      Recirculation lengths in trapezoidal channel
- Figure 9.6      Test RAb-1 - Rectangular groyne in a rectangular channel.  
Plan velocities
- Figure 9.7      Test TA - Rectangular groyne in trapezoidal channel.  
Plan velocities
- Figure 9.8      Rectangular groyne in a rectangular channel  
Secondary flows upstream of the groyne



---

**Contents**      *continued*

---

Figure 9.9	Test TA - Rectangular groyne in a trapezoidal channel Secondary flows upstream of the groyne
Figure 9.10	Test TA - Rectangular groyne in trapezoidal channel Plan profiles of mid-depth velocity, $k$ and epsilon
Figure 9.11	Experimental points and numerical grid for Test TB-1
Figure 9.12	Test TB - Submerged in a trapezoidal channel Mid-depth velocities and cross-section profiles of X-velocity
Figure 9.13	Submerged in a trapezoidal channel. Plan velocity vectors near groyne and in the recirculation zone
Figure 9.14	Test TB - Submerged groyne in a trapezoidal channel Vertical profiles of plan velocity and flow direction
Figure 9.15	Long section of grid for submerged groyne
Figure 9.16	Test TB - Submerged groyne in a triangular channel Turbulent kinetic energy at three depths
Figure 9.17	Experimental points and numerical grid for Test TC-1
Figure 9.18	Test TC - A 75° angled unsubmerged groyne in a trapezoidal channel
Figure 9.19	Test TC - A 75° angled groyne in a trapezoidal channel Plan velocity vectors near groyne and in the recirculation zone
Figure 9.20	Test TC - Upstream angled groyne in trapezoidal channel Vertical profiles of plan velocity and flow direction
Figure 9.21	Experimental points and numerical grid for Test TD-1
Figure 9.22	Test TD - A 105° angled groyne in a trapezoidal channel Plan velocities
Figure 9.23	Test TD - A 105° angled groyne in a trapezoidal channel Plan velocity vectors near the groyne and in recirculation zone
Figure 9.24	Test TD - Downstream angled groyne in a trapezoidal channel. Vertical profiles of plan velocity and flow direction
Figure 9.25	Dependence of $k$ on groyne angle in a trapezoidal channel
Figure 9.26	Dependence of mid-depth velocity on groyne angle in a trapezoidal channel
Figure 9.27	Experimental points and numerical grid for Test TE-1
Figure 9.28	Test TE - Two unsubmerged groynes (1m apart) Plan velocities at mid-depth
Figure 9.29	Test TE - Two unsubmerged groynes (1m apart) Plan velocity vectors near the groyne and in recirculation zone
Figure 9.30	Test TE - Two groynes (1m apart) in a trapezoidal channel. Vertical profiles of plan velocity and flow direction
Figure 10.1	Test SPb-2 - FCF flume - numerical grid
Figure 10.2	Test SPO-1- Unobstructed sinuous channel Velocity contours at three depths
Figure 10.3	Test SPb-1 - Four groynes in a sinuous channel Velocities at three depths and depth averaged streamlines
Figure 10.4	Test SP - Four groynes in a sinuous channel Cross-section plan velocity profiles
Figure 10.5	Test SPb-1 - Four groynes in a sinuous channel Comparison of near-bed velocities



---

**Contents**      *continued*

---

Figure 10.6      Test SPb-1 - Four groynes in a sinuous channel  
Comparison of mid-depth velocities

**Plates**

Plate 1      Sontek Probe  
Plate 2      Test RAb - Unsubmerged groyne - Vortex shedding  
Plate 3      Test RAb - Unsubmerged groyne - Recirculation zone  
Plate 4      Test RB - Submerged groyne - Surface flow  
Plate 5      Test RB - Submerged groyne - Near-bed flow

**Appendices**

Appendix 1      Introduction to 3D Modelling Theory  
Appendix 2      Guidelines for running SSIIM  
Appendix 3      Numerical experiments to optimise the use of SSIIM





---

## 1 Introduction

---

### 1.1 Scope of work

Natural rivers commonly have a tendency to meander in an unstable manner so that the plan form of the river varies in time. This variation allows the river to modify the whole of the river valley in a time period that varies greatly throughout the world. Very rapid variations in plan form are most commonly associated with high flow velocities and non-cohesive bank materials. Such behaviour is unacceptable in many circumstances, particularly where man-made structures are located in close proximity to the river. In some cases, the problem may be avoided by preventing development near a mobile river. In other cases, such as bridges flood protection works, construction is necessarily located in close proximity to a river. Pressure for land use and established developments may also require development close to a mobile river. In such cases it is necessary to provide river training works which stabilise or modify the river plan form.

Bank protection works may be required to provide stability to river banks, which may be subject to erosion as a result of engineering works such as flood protection, dredging and reclamation. River training works are also installed to prevent siltation in the central region of the river to maintain sufficient depth for navigation.

Over a number of years, various designs of river bank protection have been employed but there has been little work done to systematically study the influence of these different designs. This report is part of a research project, funded by the Construction Sponsorship Directorate of the Department of the Environment and HR Wallingford, to compare the hydraulic effects of different river training works and to provide recommendations regarding the design and siting of such works.

### 1.2 Approach

It is recognised that physical modelling of the many different designs of river training works would be prohibitively expensive. Thus, it was decided to use a numerical model which had been validated against a number of physical model experiments conducted at HR and elsewhere. In the first phase of the study, a suitable numerical model was identified and tested. In the second phase, a number of physical model tests were conducted to validate the numerical model and to determine the best way of running the model, acceptable run times and accuracy.

In Section 2, the main types of river training work are described including current practice and design recommendations, in particular for groynes. In Section 3, turbulence modelling and turbulence models are considered. In Section 4, three-dimensional computational models are described, in particular SSIIM. In Section 5, the results of the evaluation tests are presented. This work confirmed SSIIM as a suitable model for the study. In Section 6, comparative tests are described. These tests compare the results of other numerical models with results from previous studies. In Section 7 the experimental work is described and in Sections 8, 9 and 10, validation tests are described for rectangular, trapezoidal and sinuous channels. These tests compare the results from the numerical model with those from physical model experiments. They are also used to determine the sensitivity of the computational model to various modelling parameters such as grid size, numerical scheme and relaxation factors. Section 11 concludes the



report, summarising the capabilities and limitations of the approach model. Tests using SSIIM to evaluate the performance of different arrangements of groynes are described in a separate HR report (SR 493 : Seed, 1997).

---

## **2 River training works**

---

### **2.1 Groynes**

River training works may consist of groynes, spur dykes, bank revetments or other measures. However for the purposes of this <sup>report</sup>, only groynes are considered. River groynes are structures designed to protect the river bank from erosion and encourage sediment deposition by locally reducing the velocity of the river. The groynes are fixed into the river bank and extend, across the direction of flow, towards the centre of the river. When designing a set of groynes for a reach of a river, consideration must be given to their length, spacing, orientation and crest elevation. River groynes may be classified as impermeable or permeable.

Impermeable groynes, also known as groins, spurs or spur dikes, completely prevent any flow passing through the structure and force the river away from the bank. By promoting siltation between groynes, impermeable groynes may be used to realign a main channel along the line traced by the tips of a group of groynes. They may also be used to deepen the main channel for navigation or to divert flow at a specific location, for example an intake. They are built from rock, concrete blocks, gabions or sheet piles. Various designs of impermeable groynes are shown in Figure 2.1.

Permeable groynes, also known as jetties or retards, allow some of the river flow to pass through the structure and so retard the flow locally around the groyne. Larger permeable groynes are constructed from timber or concrete piles or jacks. Some designs are shown in Figure 2.2. Smaller groynes may be made of wood or other natural materials.

Groyne design is influenced by the purpose of the groynes. Where erosion near the tip of the groyne is to be encouraged, impermeable groynes are appropriate but where such a response is undesirable, then permeable or tapered tipped groynes may be more appropriate. Different plan shapes of groynes may be used depending on local circumstances. These points are discussed further below.

### **2.2 Impact of groynes**

Groynes can be introduced into rivers for two main reasons: to increase sediment transport in the centre of the river channel, thus keeping the river clear for navigation and to reduce the sediment transport near the bank, thus preventing bank erosion and possibly encouraging accretion. In addition, groynes have also been used to create a riverine environment more suited to certain species of fish.

Installing river groynes along a reach of a river can have a strong local impact and the morphological effects of the groynes can be summarised as follows:

- \* local scour at the tip due to locally high velocities;



- \* local scour at the upstream and downstream faces due to intermittent weak vortices;
- \* low flow velocity zones behind, in front and between groynes;
- \* general scour due to channel contraction;
- \* diversion of the streamlines which may promote erosion of the bank opposite or adjacent to groynes.

The local effects of a groyne described by Copeland are shown in Figure 2.3. However, our tests did not confirm all these effects.

Figure 2.4 shows the flow lines of a river passing around a single impermeable groyne of length  $L_t$ . The length  $S_L$  downstream of the groyne can be considered as the length of protection afforded to the bank by the groyne. The area  $G_1$  downstream of the groyne is termed the recirculation zone and bank erosion may result due to the development of an eddy in this region. Unfortunately there is little information available on ways of predicting the strength of this eddy.

A variety of approaches have been employed to reduce the strength of the eddy and to improve the overall performance of the river training works. The following notes summarise the guidelines in common practice.

## 2.3 Overall design of groynes

Groynes should be used in groups or fields, and generally not in isolation. Measures should be taken to provide a transition to the groyne field, to steer the river flow away from the bank and limit potential erosion. Such measures include: aligning the upstream groyne to minimise the deflection of the flow; gradually increasing the length of the groynes at the upstream end of the groynes and combining the upstream groyne with a longitudinal dike. For bank protection works in the vicinity of a bend the first groyne should be placed at the start of any bend. A typical layout of training works for channelisation (after Kinori and Mevotach, 1984) is shown in Figure 2.5.

### Spacing of Groynes

The spacing of the river groynes along a reach of river depends upon the length of the groynes and the degree of protection required. A wide range of recommendations is made by different authors with the preferred spacing ranging from one to six times the exposed length of the groyne. Other sources recommend calculating groyne spacing based on the velocity head of the flow in the river. However, this method can lead to very wide groyne spacing in some cases. A number of recommendations are given in Table 1.

### Orientation of Groynes

After a thorough literature review and several experimental tests, Copeland (1983) concluded that placing groynes perpendicular to the river flow was perfectly acceptable. Other authors make specific recommendations regarding the orientation of groynes depending on the plan form of the river or local practice (see Table 2). Further recommendations on groyne orientation and spacing can be found in Przedwojski et al (1995).



## 2.4 Detailed Design of groynes

### Length of the Groynes

The alignment of the river channel is determined by the tips of the groynes in the groyne fields. The full length of a groyne is the exposed length of the groyne in the flow (the length  $L_1$  in Figure 2.4), plus a length  $L_e$  embedded into the bank. The embedded length is to allow for bank erosion at the junction of the bank and the groyne. Salikov (1987) recommended an exposed groyne length not exceeding 15-20% of the width of the river channel and Alvarez (1989) recommends an embedded length  $L_e$  of  $0.25L_1$ .

### Plan Shape of Groynes

There is a wide range of plan shapes for river groynes, for example straight, T-head, bayonet, hockey stick and L-shaped groynes. The preference for any particular shape depends upon local conditions and experience and there have been no systematic studies on this subject. Various plan shapes of groynes are shown in Figure 2.6.

### Crest Level and Crest Shape of Groynes

River groynes can be designed to have their crest levels above or below the water surface level. It is generally recommended that crests are above mean water level so that they do not become a hazard to the navigational or recreational use of the river. However, under flood conditions groynes may become submerged and this situation is considered later.

Alvarez recommends that groyne crests should slope downwards from the bank to the river bed. He recommends crest slopes between 0.1 and 0.25 and lists the following advantages of this design:

- \* practically no local scour at the groyne tip;
- \* less material to construct compared with a horizontal crest;
- \* quicker sand deposition between groynes.

### Permeability

As with sloping groynes, permeable groynes have the advantage of reducing scour at the tip of the groyne and reducing the strength of the recirculation, which may increase the rate of accretion downstream of the groyne. Permeable groynes are also attractive because they tend to produce smaller overall changes in flow pattern than impermeable groynes; this reduces the risk of serious erosion being triggered elsewhere. The major limitations on the use of permeable groynes in large rivers are the structural problems of their construction.

## 2.5 Previous Research into River Groynes

A theoretical study of an isolated groyne was made by Todten in 1975 as reported by Bognar and Hanko (1987). As shown in Figure 2.4, Todten found that the recirculation zone had a maximum width ( $b^*$ ), of  $1.67L_1$  and a maximum recirculation length ( $S_L$ ) of  $12.5 L_1$ .

Nwachukwu and Rajaratnam (1980) conducted a series of experiments on single perpendicular groynes. These experiments were carried out under normal flow conditions in a flume with a fixed rough bed. A yaw-probe was used to collect the data necessary to map the 3-D velocity and shear stress field around the



groyne. For a thin plate groyne, it was found that the recirculation zone had a width of  $2L_t$  and a length of  $12L_t$ ; however, this length reduced to  $5L_t$  when a thicker cylindrical groyne was used. The length of the disturbance to the flow upstream of the groyne was equal to about  $2L_t$ . From this work it was found that a depth averaged 2-D computational flow model could not represent this flow field correctly. This results from the fact that the plane of the outer boundary of the shear layer is tilted towards the recirculation zone near the bed.

## 2.6 Characteristics in the region of a groyne

The type of flow pattern that can be expected as a result of a groyne can be surmised from the pattern of flow at a bridge pier. The basic pattern of flow is that upstream of the obstruction a vortex with a horizontal axis is created. Towards the sides of the obstruction this vortex is drawn downstream. Behind the obstruction, an unstable wake is generated as vortices with a vertical axis are shed in the shear layer between the free flow and the region in the lee of the obstruction. The periodicity of a cylinder or other bluff body is associated with vortices breaking from either side with a frequency ( $f$ ) dependent on the width of a body ( $D$ ) such that  $f \approx 0.2U/D$ . However, for a groyne the representative width is less clear the frequency of vortex shedding is much less defined.

Overall, the pattern of flow behind a groyne is three dimensional and unsteady. Furthermore the turbulence generated by the vortices is likely to vary greatly throughout the flow (ie it is inhomogeneous) and the large scale turbulent velocities downstream of the obstruction are greater in plan than in the vertical ie (anisotropic).

A full numerical solution of such a flow field is not practical either from the point of view of the large computer storage requirements or the very long run times that would be necessary. Thus the simulation of the flow must be approximated to make both cost and run time acceptable. The first approximation which is considered acceptable is to model the flow as a steady state problem. The steady state approximation introduces some error in the velocities in the shear layer and will tend to under-estimate the maximum instantaneous velocities. However the errors are not likely to be large and are consistent with the fact that measurements in the field and in the laboratory are time averaged. The second approximation is in the turbulence modelling which is discussed below.

---

## 3 Flow modelling software

---

### 3.1 Turbulence modelling

Turbulence is a term used to describe the irregular, unsteady, three-dimensional flows which in general are too small to be studied in detail or to be simulated directly. Turbulent flows are said to be "modelled" by simulating a measure of the effects of the turbulence rather than the turbulent flows themselves. In a k-epsilon model, the turbulent flows are characterised by just two parameters at any one point:  $k$  - the turbulent kinetic energy and epsilon ( $\epsilon$ ) - the turbulent dissipation rate which is dependent on the turbulent strain rate. The consequence of this modelling is that the physical scale and direction of the turbulence are lost. The turbulent kinetic energy is modelled in much the same way as other scalar properties, such as temperature. Since the turbulence is considered to be the same in all directions, the model is said to be isotropic. This contrasts with the anisotropic turbulence described in the previous section.

that



Turbulent kinetic energy is not conserved. Physically, turbulence breaks down into smaller and smaller scales until the scale of the turbulence is at the molecular level at which point the energy is lost to heat. Numerically, the dissipation of turbulence is modelled through a negative source term (epsilon). The distribution of epsilon is modelled semi-empirically. Epsilon is determined by solving an advection-diffusion equation similar to that used for 'k'. However, in the case of epsilon, the terms in the equation are scaled by coefficients determined by experiment (Rodi, 1980). In theory, these coefficients could be adjusted depending on the particular circumstances, but in practice, the values used are usually those originally derived by Rodi. A brief mathematical description of k-epsilon models is given in Appendix 1, but for a fuller description the reader is referred to Rodi (1980), Patankar (1980) or Versteeg and Malalasekera (1995).

### 3.2 Choice of numerical model

Lavedrine (1996) reviewed a number of three-dimensional models applied to general river flows of straight and meandering rivers flowing in and out of bank. A number of different turbulence models were studied. It was confirmed that anisotropic turbulence models gave an improved prediction for the location of the maximum streamwise velocity but the effect on flows of engineering significance was small. That is to say, the near-bed velocities which give rise to erosion and the depth averaged velocities which are significant in navigation were adequately predicted using a k-epsilon model. The k - epsilon model has some limitations in how accurately the turbulence field is predicted near the free surface and it neglects the transient effects of the turbulence.

It is recognised from previous work (Rodi, 1984), that the size of the recirculation zone downstream of a rearward-facing step, is underpredicted when using an isotropic turbulence model (viz. the k-epsilon model). Similar behaviour can be expected for a groyne. Better predictions are given by anisotropic turbulence models such as the Reynolds stress models, but the run times and the risk of numerical instability are increased significantly. Thus, it was decided to use a k-epsilon model and to use physical model tests to characterise the size of the errors ~~that~~ which result from using such a model. In selecting a k-epsilon, 3D model for use in this study, the main consideration was that the model would be readily available to engineers when conducting their own studies. Two computational models were considered for use in this study: Phoenics and SSIIM.

### 3.3 Phoenics

PHOENICS has been widely used in many branches of engineering since its launch in 1981. Its application in hydraulics has included studies of river, coastal, estuarine, reservoir and lake flows. At HR it has been applied to sediment control at intakes, siltation under structures in estuaries and settling basin design.

PHOENICS (Parabolic, Hyperbolic Or Elliptic Numerical Integration Code Series) solves the Navier-Stokes equations on a grid of computational cells, which may have straight or curvilinear cell boundary lines. A solution is derived iteratively to a specified accuracy using the SIMPLEST algorithm for the pressure-velocity linkage. The approach is finite-volume, but with a choice of interpolation schemes. Pressures are solved over the whole domain, while other scalars and velocities are solved layer by layer.



PHOENICS can use a range of turbulence models but the k-epsilon energy dissipation model was used in this study due to its widespread acceptance and successful application for river flow simulations.

At the bed, the effect of the friction on turbulence and velocities is modelled using log-law wall functions.

In summary the model takes account of the following effects:

- (i) vertical accelerations, such as in the vicinity of a low level sluice;
- (ii) momentum effects in the flow, such as the secondary flow in a curved open channel which sweeps the near-bed flow towards the inside of the curvature;
- (iii) turbulence and its effect on friction within the flow;
- (iv) bed roughness, and the resulting bed shear stress;
- (v) convection and diffusion of sediment concentrations in the flow, together with the siltation and sediment entrainment at the bed. (This produces a prediction of the deposition rate at each point in plan) and
- (vi) free surface effects, such as local drawdown due to flow acceleration.

### 3.4 SSIIM

SSIIM (Sediment Simulation In Intakes with Multiblock Option) was developed by Nils Olsen at the Norwegian Institute of Technology, University of Trondheim. At present it can be used free of charge by any organisation provided that its origin is properly recognised. It uses a control volume method to solve the k-epsilon model. It has been used to model river flows with sediment transport, although this ~~latter~~ feature has not been tested at HR. It has many of the capabilities of Phoenix, but is less developed particularly in its input and output capabilities. The Phoenix model is widely used and this would have been acceptable. However, it was decided to use SSIIM since this runs on an IBM-compatible PC, and is available at no cost on the Internet, and is easier to apply because it was specifically developed for fluvial applications. SSIIM is described in greater detail in the next section.

---

## 4 *Three dimensional flow modelling using SSIIM*

---

Although this section describes the capabilities and limitations of SSIIM, many of the comments apply to any 3D, k-epsilon model. The numerical experiments which were conducted to investigate the capabilities and limitations of SSIIM are described in Appendix 3. Notes on the particular operational aspects of SSIIM are contained in Appendix 2.

### 4.1 Introduction to SSIIM model

SSIIM was designed to model 3D flow and sediment transport for free surface conditions. However in this study sediment transport was not considered. The program solves the Navier-Stokes equations with the k-epsilon model on a three dimensional structured grid, which is non-orthogonal in plan but regular in the



vertical direction. A control volume method is used with cell centred nodes. Two numerical schemes are available : the power-law scheme which is accurate where the flow is aligned with the grid and the second order upwind scheme which is less susceptible to false diffusion which may occur where the flow is at an angle to the grid.

The continuity constraint is imposed using the SIMPLE or SIMPLER method. These methods use pressure coupling to generate corrections to the (incomplete) solutions to the momentum equations. Rhie and Chow interpolation is used to smooth checkerboard oscillations. The overall matrix equations are solved using a line Gauss-Seidel method with an option for block correction, which is a method for accelerating convergence of the solution. By contrast, the term "Multiblock" used in the acronym SSIIM, refers to the ability to "cut and paste" blocks of cells from a rectangular grid to generate more complex shapes such as a cruciform. This capability was not used in the present study.

## 4.2 Creating the 3D Model Grid

To construct an SSIIM model, it is necessary to develop a grid on which all the model's calculations will be performed. The grid is defined by a number of intersecting lines. For each intersection in defined plan, a fixed number of points are defined in the vertical direction. The bed level is defined by the user and the free surface is initially determined from a backwater calculation. The location of intermediate points in the water column are determined as a proportion of the depth of water. These points define the corners of the control volume cells but variables are calculated at the nodes at the centre of each cell. Since there is a fixed number of points in the vertical direction, the depth must be finite at all locations. Thus when modelling a trapezoidal channel, a small vertical bank must be included in the numerical grid. In order to model a groyne in the grid, the corresponding cells are blocked out, i.e. made inactive. This is referred to in the SSIIM documentation as "outblocking".

It was found that about ten layers in the vertical were necessary to obtain a good representation of the vertical velocity profiles in the region of the groyne. A three layer model was adequate for determining the overall effects of the groyne as indicated by the recirculation length. A 2-D simulation gave only an approximate solution to the flow, with the recirculation length being under-estimated by 20%.

Resolution may need to be increased for one of two reasons. Firstly the grid must be fine enough to represent significant features of the flow. For example, it is necessary to represent the recirculation downstream of an obstruction in order that the resultant energy loss is modelled (even where the details of the recirculation are not of direct relevance). Secondly, the resolution must be sufficient to minimise false diffusion and similar errors related to grid size. Tests on grid resolution are discussed in Sections A3.5 and A3.6 of Appendix 3.

## 4.3 Boundary conditions for the model

The downstream boundary condition is a given water level. At the upstream boundary, the inflowing discharge is specified. By default, this discharge is distributed as a fully developed velocity profile but a velocity field may be specified.

At the walls, the boundary conditions may be specified as being either a friction law as applied at the bed or as a free slip boundary condition. At the bed, the log



law is used to describe the law of the wall which defines the friction in the boundary cells. The roughness term  $k_s$  may be specified in each cell or it can be determined globally from a specified Strickler roughness coefficient (M) using the formula  $k_s = (26 \cdot n)^6$ , where  $k_s$  is in metres,  $n$  is the Manning's coefficient and  $M = 1/n$ . Tabulated below are some commonly used roughness values.

S

Strickler (M)	Manning (n)	Roughness $k_s$ (m)
50	0.0200	0.0198
60	0.0167	0.0066
70	0.0143	0.0026
77	0.0130	0.0015
80	0.0125	0.0012
90	0.0111	0.0006
100	0.0100	0.0003

Tests on the effects of varying the roughness are discussed in Appendix 3 Section A3.9.

#### 4.4 Water Surface

In common with many models for open channel flow, the free surface is modelled as a 'rigid lid' and vertical accelerations cause variations in surface pressure. The initial position of the surface is determined by a backwater calculation. For a more accurate representation of the surface, it is possible to adjust the position of the surface such that the surface is located where the pressure is zero. The effect of this adjustment is to slightly modify the height of the water column and thus modify the strength of the velocities. For reasons of stability, this adjustment is not made every iteration but less frequently, typically every 20 iterations. The significance of this effect is dependent on the square of the Froude number, and in the majority of tests conducted, the Froude number was low and the effect of the water surface update was negligible. Furthermore, the inclusion of water surface update reduced the speed of convergence and thus was not included in the majority of tests. Tests on water surface update are discussed in Appendix 3 Section A3.7.

#### 4.5 Numerical Schemes

SSIIM stores the computed velocity components and various scalar variables at the nodes at the geometric centres of the control volumes; the value of a quantity  $\phi$  at a node is denoted as  $\phi_p$ . To calculate the advection of  $\phi$  into the control volume it is necessary to calculate effective values at the faces of the cells e.g. at the east face  $\phi_e$ . Different numerical schemes use different formulae in the calculation of  $\phi_e$ .

In the central differencing scheme  $\phi_e = (\phi_E + \phi_P)/2$  where  $\phi_E$  is the value at the next node on the eastern side of point P. In the upwind scheme  $\phi_e = \phi_E$  is the value at the eastern node for flow into the cell and  $\phi_e = \phi_P$  for flow out of the cell. These schemes are rarely used due to problems of accuracy and stability. In SSIIM, two schemes are available: POW and SOU.



In the power law (POW) scheme,  $\phi_e$  is determined using the upwind scheme, but the diffusive flux is reduced by a factor which is dependent on the Peclet number. The Peclet number ~~which~~ represents the relative significance of convection and diffusion. At high Peclet numbers, convection predominates and the diffusive flux is zero. This method is accurate and stable where the flow is aligned to the grid.

However, the POW scheme is highly susceptible to false diffusion. In essence, false diffusion is numerical diffusion ~~which~~ increases with the size of the grid and occurs where the flow is not aligned to the grid. The effects of false diffusion may be reduced by refining the mesh but the computational time and memory requirements may preclude this approach. Alternatively, false diffusion can be reduced by using a second order upwind scheme (SOU) in which  $\phi_e$  is determined from the linear extrapolation of the two cells upwind of the face (e). Thus for flow out of the cell  $\phi_e = \phi_P + \frac{1}{2} (\phi_P - \phi_W)$  and for flow into the cell  $\phi_e = \phi_E + \frac{1}{2} (\phi_E - \phi_{EE})$  where  $\phi_{EE}$  is the value of  $\phi$  two cells to the east of the current cell. However, the SOU scheme is less stable than the POW scheme and more computationally intensive for the same grid size. Thus, where the flow is aligned to the grid, the POW scheme is preferred.

Conversely, the use of the SOU scheme is indicated where the flow is not aligned to the grid. This will necessarily occur in a recirculation zone such as downstream of an impermeable groyne. However, as shown by Tamamidis and Assanis (1993), this scheme is subject to undershoots. Although negative velocities are meaningful and acceptable in the numerical scheme, negative values of  $k$  (kinetic energy) and epsilon (turbulent dissipation) are unrealistic and might be the cause of numerical instability. In SSIIM, different numerical schemes can be applied to different equations. Tests were conducted using SOU, POW and a mixed scheme where SOU was used for velocity but POW was used for  $k$  and epsilon. In some cases there was little difference between the schemes, but it was found that in most cases the mixed scheme performed best in terms of speed, reliability and accuracy. These tests are discussed further in Appendix 3, Section A3.1.

#### **4.6 Solution of the Pressure-Velocity Coupling using SIMPLE and SIMPLEC**

The SIMPLE (Semi-Implicit Method for Pressure Linked Equations) family of algorithms is based on using a relationship between velocity and pressure corrections. This relationship is derived from the momentum equation. In these methods, an assumed pressure field is used to determine a predicted velocity field. The above relationship, combined with the continuity equation is used to calculate corrections for the velocity and pressure fields. The system of equations is then solved iteratively. In SSIIM both the standard SIMPLE and the SIMPLEC (SIMPLE-Consistent) algorithms are available. SIMPLE is used by default, but problems in which convergence is limited by pressure-velocity coupling can converge more quickly using SIMPLEC. This method has been found to be successful by other researchers, but in our tests it was found that the convergence rates were mostly limited by other factors, particularly the convergence of  $k$  and epsilon. Thus for the majority of tests, the more robust scheme was used, namely SIMPLE.



## 4.7 Procedure for solving the flow equations

### Main iterative Procedure

The equations of flow, shown in Appendix 1, are a set of nonlinear, simultaneous differential equations. The numerical scheme reduces these differential equations to a set of simultaneous matrix equations. The matrix equations are solved by an iterative scheme ~~which~~ <sup>that</sup> starts from arbitrary initial conditions, except at the boundaries, and converges to a solution after performing a number of iterations. The main steps are described below:

- The  $u$ ,  $v$ ,  $w$  momentum equations are each solved in turn using current values for pressure, in order to update the velocity field.
- The “pressure correction” equation is then solved using the SIMPLE or SIMPLER equations to obtain the corrections to the pressure and velocity fields.
- The  $k$  and  $\epsilon$  equations are solved using the updated velocity field.
- The water surface is updated if required.
- The above steps are repeated until convergence is reached (i.e. when all the equations are solved to sufficient accuracy).

The overall scheme is shown in Figure 4.2.

### Matrix solution method

Within the above iterative procedure, SSIIM also uses iterative techniques to obtain an approximate solution to each of the matrix equations. In large systems, solving equations iteratively requires less effort than solving them directly. One technique used by SSIIM is the line-by-line solution technique, known as the Line-Gauss-Seidel (LGS) method. In LGS, the equations are solved simultaneously for each line of cells, where a line is a complete row or column of cells. During the solution of a line, the neighbouring lines are treated as correct and are kept constant. The solution of all lines in the  $x$ ,  $y$  and  $z$  directions is referred to as a ‘sweep’ of the solver. SSIIM provides the facility to specify the number of sweeps performed for each equation. The default number of sweeps is set at 5 for the pressure correction equation and 1 for the other equations. Tests on the number of sweeps indicated that the default system could not be adjusted (see Appendix 3, Section A3.3).

### Relaxation factors

Because of the non-linearity of the equations being solved, it is not generally possible to obtain a solution by fully substituting the “improved” values for each variable which have been generated by the approximate solution of the matrix equations. Convergence can be achieved by under-relaxation which reduces the difference between the old and new values of the variable from successive iterations. In essence, the new variable value at any node equals the old value at that node plus the computed change of the value multiplied by the relaxation factor. In SSIIM, the standard values used for the relaxation factors are 0.8 for the velocities, 0.2 for pressure and 0.5 for turbulence ( $k$  and  $\epsilon$ ). In some circumstances, it may be necessary to use reduced relaxation factors to achieve convergence. For example, when modelling a groyne with two vertical slots, the appropriate relaxation factors were found to be 0.2 for velocities, 0.03 for pressure, and 0.05 for turbulence.



### Residuals

The residuals of a numerical scheme are a measure of how close the model is to convergence. At any node, the residual is the difference between the old and new values. When using residuals to test for convergence an average residual is used and this is normalised with reference to a characteristic flux entering the domain. The convergence criterion for SSIIM is that all the normalised residuals are less than  $10^{-3}$ . After the first 10-20 iterations, the residuals should decrease steadily. A plot of the log of the residuals against the number of iterations should decrease approximately linearly to convergence is to be reached after an acceptable time. Other possibilities are: a) the model diverges b) the residuals fall and rise c) the residuals fall monotonically but one or more of the residuals falls very slowly. The reasons for non-convergence may be: a grid that is too coarse or uneven; a flow pattern that is unstable; or a numerical method (such as block correction) that should not be applied. A slower but more steady reduction in residuals may be achieved by reducing the relaxation coefficients. This should be done in decrements of 0.05 or 0.1 and applied to the equations ~~that~~ <sup>that</sup> which have non-convergent residuals, typically the k and ε equations. These matters are discussed further in Appendix 3, Section A3.4.

### **4.8 Block correction**

SSIIM provides an optional block-correction procedure for accelerating the convergence of the POW scheme. The block correction technique, as described by Patankar, speeds up convergence by applying a quasi-one-dimensional correction to the current solution field in order to satisfy global conservation. The global correction vanishes as the local convergence is achieved throughout the domain. The one-dimensional grid is made by summing the values in the other two directions. For example, all the values in each horizontal layer are summed to create a 1D vertical grid. Then an iteration is performed on the one dimensional grid and a correction applied to all points in each layer. This is repeated in all three directions.

Block correction usually gives greater stability and better convergence. It reduces long-wavelength errors in the direction where they are applied, but may introduce large short-wavelength errors. In particular, there may be some problems when the geometry has blocked out regions, which is typically the case when modelling groynes. Our initial tests showed that although block correction gave accelerated convergence during the early part of the solution (i.e. for the first few hundred iterations), after that block correction could lead to a slowly oscillating solution ~~which~~ <sup>that</sup> would not converge.

If the computational run is to be attended, ~~then~~ the best strategy may be to use block correction for a few hundred iterations, and then, if oscillations are noticed, to turn off the block correction. If the run is to be unattended, for example when the model is to be run overnight, then it is prudent to avoid block correction. This was the strategy adopted for most of the runs conducted.

### **4.9 Discussion**

~~that~~ <sup>that</sup> Three-dimensional computational models contain many non-physical parameters ~~which~~ may affect the accuracy, stability and speed of solution. For a complete knowledge of the behaviour of the model it would be necessary to test each parameter thoroughly and in every combination. Clearly this is impractical even for a single situation. The recommendations in the use of the numerical model described above were derived from experience, published works and private correspondence with the originator of the model, Dr Nils Olsen. The following



table summarises the influence of the various parameters available in 3D modelling.

Item	For accuracy	For stability	For Speed
Resolution	increase	sufficient to resolve shear layers.	decrease
Numerical Scheme	SOU (with recirculation)	POW	POW
Block Correction	No influence	avoid	use with caution
Relaxation factors	No influence	reduce	increase

---

## 5 Evaluation tests

---

### 5.1 Introduction

Tests conducted in this work have been coded to give an indication of the circumstances of the run. The initial letter indicates the shape of the channel and the phase of the work. For example, the letter C indicates flow in a curved channel. The second character indicates the general physical circumstances of the test. For example the letter A indicates a single rectangular impermeable groyne at right angles to the channel, and the digit 0 indicates an unobstructed channel. The third letter, if present, is in lower case and indicates variations in the physical circumstances. Digits after this indicate different computational modelling options. Thus, run code EW-2 indicates the second simulation of a 40% permeable groyne in the evaluation tests. Table 3 describes the coding scheme in detail and a full list of the run codes is given in Table 4. The physical circumstances of each test are given in Table 5. In all tests, results are presented as plan views of horizontal velocity vectors. Additional views are also provided in certain cases.

The evaluation tests were conducted as an initial investigation into the capabilities of SSIIM and k-epsilon models in general. All these tests were in a rectangular channel either straight or curved. These straight channel tests were coded E and the curved channel tests were coded C. The first two tests were derived from standard tests provided with the SSIIM software.

CA : 90 degree bend and blunt groyne

E0 : straight section

The remaining tests were used to investigate the capability of SSIIM to simulate slender groynes. The later tests (EW) investigated the capability of SSIIM to model porous groynes using groynes constructed with vertical or horizontal holes.

EE : 2 groynes

EH : 2 submerged groynes

EW-1 : groyne with one vertical slot

EW-2 : groyne with 3 vertical slots

EW-3 : submerged groyne

EW-4 : groyne with horizontal slot

EW-5 : groyne with two horizontal slots



## 5.2 Standard test cases

### Test CA - Rectangular channel with a 90° bend (blunt groyne)

This test is based on a standard test case supplied with the software. The SSIIM grid editor was used to insert an irregular obstruction on the inside of the channel. The velocity at the upstream end is 1.0 m/s. A vector plot of the near-bed velocities can be seen in Figure 5.1. The velocities at the mid and surface layers are shown in Figures 5.2 and 5.3. A recirculation zone is generated behind the obstruction. The recirculation is larger and the velocities higher at the surface than at the bed. The influence of the obstruction is still noticeable at the outlet. The velocities are lower on the inside of the bend downstream of the obstruction but at the outside of the bend, it can be seen that the flow is slightly directed towards the inner bank, indicating that the flow is "recovering" from the influence of the obstruction.

### Test E0 - Straight rectangular channel

This test shows the development of the lateral velocity profile along a channel 2m wide. It can be seen that the profile stabilises after about 20 metres i.e. 10 channel widths. Figures 5.4 to 5.6 show plan views of the velocity field at three levels in the flow. In SSIIM, the log law velocity distribution in the vertical is applied at the inlet boundary.

## 5.3 Simulation of impermeable groynes

In these tests, the impermeable groynes were constructed by blocking out a row of cells to about 35% of the channel width. In the first case (EE), the cells were blocked out to the full depth of flow. In the second case (EH) the cells were blocked out to approximately half the depth of flow. The length of the groyne was approximately 7m and the groynes were positioned at 25m and 45 m from the upstream end of the channel.

### Test EE - Straight rectangular channel with two groynes

Flow upstream of the groyne is diverted away from the groyne. In the bed layer, the lower streamwise momentum allow a greater change in the direction of the flow. Just past the tip of the groyne, velocities in all layers are similar and this gives rise to a recirculation zone which is similar at all levels. The length of the recirculation zone is constrained by the second groyne. The centre of rotation of the recirculating flow is downstream of the mid point between the two groynes. (See Figures 5.7 to 5.9)

### Test EH - Straight rectangular channel with two submerged groynes

In this case, the upper layers appear unaffected by the submerged groynes. The recirculation in the bed layer is similar to the case for the unsubmerged (full height) groynes but the centre of rotation is to the upstream of the mid point between the groynes. (See Figures 5.10 to 5.12)

The results from the model seem realistic. Comparison between Test EE and the later Test REa, shows that the coarse grid used in these tests has caused some details of the flow to be omitted.

## 5.4 Simulation of permeable groynes

These tests were conducted for a straight rectangular channel of width 8m, length 100m, discharge 20 cumecs, downstream level 2m and Manning's  $n = 0.02$ . The groyne was positioned at 25m from the upstream end of the channel. The groyne thickness was 100mm and the permeability was 40%, that is to say the total obstruction area was 60% of the total submerged area of the groyne.



Each of the following tests uses a different geometry or “schematisation” to simulate a permeable groyne.

Test EW-1 Permeable groyne simulated by a single vertical hole

The vertical hole was 2m wide and extended from bed to surface. A large recirculation zone can be seen downstream of the groyne near the left bank and a smaller recirculation zone can be seen downstream of the isolated section of groyne. The velocity profile continues to show signs of the groyne schematisation some 50m downstream of the groyne. Such a schematisation is unlikely to be satisfactory because of the influence of the schematisation on any further groynes which may need to be positioned downstream of the first. (See Figures 5.13 to 5.15)

Test EW-2 Permeable groyne simulated by three vertical holes

In this test, the effects of the schematisation are barely noticeable some 20m (ie more than groyne lengths) downstream of the groyne. It appears that such a simulation of a permeable groyne may prove acceptable provided that the groyne separation is less than 3 groyne lengths and if local effects do not need to be evaluated. (See Figures 5.16 to 5.18)

Test EW-3 Permeable groyne simulated by 60% submergence

A smooth velocity profile is to be found some 60m downstream of the groyne. However, the very strong recirculation zone in the bed layer immediately downstream of the groyne probably makes this simulation unacceptable regardless of the distance downstream. (See Figures 5.19 to 5.21)

Test EW-4 Permeable groyne simulated by one horizontal hole at mid-depth

In this simulation, an eddy with a horizontal axis forms behind the groyne. This will not adequately simulate a permeable groyne, since in a permeable groyne, bed velocities downstream of the groyne are streamwise and increase with porosity whereas in this simulation the bed velocities are upstream and are unlikely to be of the correct magnitude. (See Figures 5.22 to 5.23)

Test EW-5 Permeable groyne simulated by two horizontal holes

The flow pattern in this case suffers from similar limitations to those in the case of the single horizontal hole. (See Figures 5.25 to 5.29)

In conclusion, although the groynes with holes may give satisfactory simulation of the flows remote from the groyne, the poor simulation of the near field probably renders this approach unacceptable unless a method can be found to avoid the unrealistic jets and recirculation zones near the holes. The question of calibrating the simulated porosity remains to be resolved.

---

## **6 Comparative tests**

---

### **6.1 Test U0, U shaped flume**

This case is based on the work of de Vriend(1981). Measurements were taken in a U shaped flume at LFM (the Laboratory of Fluid Measurements at Delft University of Technology). A rectangular channel of width 1.7m is curved through 180° with a radius of 4.25m. The straight inflow and outflow sections are 6m long. The bed ~~is~~<sup>is</sup> made of concrete and the walls are plastered brick except for glass panels on the outside of the bend. The upstream depth of water is ~~in~~<sup>in</sup> the experimental model the discharge was 0.19m<sup>3</sup>/s, but in the numerical tests



the inlet velocity was set to 1m/s so that the graphs can be viewed as normalised velocities. The corresponding discharge for the numerical tests is 0.289m<sup>3</sup>/s. Figure 6.1 shows the depth-integrated velocities for the experimental measurements and values predicted by de Vriend's laminar model. The boundary layer of the model is thicker than that measured and the velocities at the outside of the bend show a significant peak in the numerical model which is absent from the measured results. This consistent with the lack of turbulent diffusion in de Vriend's numerical model.

Two numerical models were set up using the same schematisation as de Vriend. The velocity vectors for the bed and surface layers are shown for SSIIM in Figure 6.2 and in Figure 6.3 for Phoenix. It can be seen in each case that the velocities at the outer bank do not show the peaks modelled by de Vriend. Both SSIIM and Phoenix show signs of a secondary current with surface flows being directed towards the outer bank and a weaker counter flow towards the inside of the bend at the bed of the flume. The results are not strictly comparable since the models use different roughness conditions. Nonetheless, the results from both Phoenix and SSIIM are reasonably compatible with the measurements presented by de Vriend.

## 6.2 Test P0 - FCF flume (straight out of bank flow)

### 6.2.1 Comparison with Telemac

This test case is based on experimental data taken from the Flood Channel Facility at HR Wallingford (see Figure 6.4). In the series A tests, this out-of-bank model comprised a straight trapezoidal channel with flat floodplains. The whole model had a longitudinal slope of approximately 1 to 1000. The total width of the flume was 6.3 metres. In the centre of the flume a trapezoidal channel of depth 0.15m was moulded. The channel width was 1.5m at the base and 1.8m at bank top. The results from SSIIM were compared both with the experimental data and with data taken from the Telemac model. Telemac is a widely used 3D Finite Element model with k-ε turbulence developed by Electricite de France. In the SSIIM run, default values were used for all modelling parameters except that Second Order Upwinding (SOU) was used for the velocity equations.

The results of Telemac-3D are taken from the work of Lavedrine (1996). For this test, the upstream boundary condition was not consistent with the experimental conditions. Therefore, when comparing the results of the Telemac model with the SSIIM model, the velocities were normalised by dividing them by the mean upstream velocity. Also, since the friction was not calibrated to the model results, the water levels at the test section (x=36m) were also different from the experimental case. This difference was resolved by considering a modified unit discharge (q)

$$\text{where } q = \frac{Vh}{V_{\text{mean}}}$$

It can be seen in Figure 6.5, that the values of q from SSIIM and Telemac are well correlated, both in the main channel and on the floodplain. It should be noted that since SSIIM is a cell centred model, it cannot predict values at the boundary of the model.

The values of velocity (U<sub>x</sub> and U<sub>y</sub>) are not well correlated since the Telemac results predict slightly incorrect levels. The error causes a significant change in



the depth on the floodplain but not in the deeper main channel. Thus the floodplain velocities are higher in the Telemac results.

The reduced depths on the floodplain in the Telemac results cause a reduction in lateral velocities, but the overall shape of the two sets of results are similar. It can be seen that the lateral flow is anti-symmetric with flows towards the centre of the channel.

The uneven shape of the graph in the outer floodplain appears to be non-physical and may be related to the relatively coarse grid size in this region.

### **6.2.2 Comparison with experimental data**

A detailed survey of longitudinal velocity was carried out in the FCF so it is possible to compare both the depth averaged and surface velocities with the results from the numerical model (SSIIM).

The water levels in the flume were adjusted to obtain uniform flow conditions. The measured discharge, water depth and slope ( $1.027 \times 10^{-3}$ ) were used to determine an overall Manning's coefficient for the test. This value was then supplied to SSIIM to generate the water levels in the numerical model. The modelled water slope was 3% greater ( $1.055 \times 10^{-3}$ ), but this difference was considered to be acceptable.

The streamwise velocity distribution measured in the flume is compared with the numerical model in Figure 6.6. The predicted velocities are within 3% of the measured velocities and the overall shape of the velocity distribution is well predicted.

The mesh size of SSIIM is indicated by the spacing of the data points which are located at the centres of the computational cells. More reliable results from the numerical model might be obtained by a more refined mesh, particularly at the edges of the main channel and at the edge of the floodplain. However the accuracy obtained is still satisfactory and indicates that SSIIM is able to model this type of situation well.

### **6.3 Test RAa - Hanover flume with a rectangular groyne**

Comparisons were made between the SSIIM results and the results from a numerical model developed by Mayerle, Toro and Wang (1995) at the Center for Computational Hydroscience and Engineering in the University of Mississippi, Oxford, USA. The results were also compared with corresponding data from physical model tests carried out at the Frenzies Institute of Fluid Mechanics, University of Hanover, Germany.

The co-ordinate system used in this test was also adopted for all the tests with straight channels described later in this report. The origin is at the root of the groyne (or the upstream groyne if there is more than one); x is positive downstream; y is positive away from the near bank (ie the bank is protected by the groyne) and z is zero at the bed and positive upwards. All distances on the graphs are shown in metres. Where the z co-ordinate is indicated in percentage terms, it is normalised to the local depth.

The dimensions of the straight rectangular flume were length 32.4m; width 2.5m; and depth 0.23m. The plan dimensions of the unsubmerged groyne were length 0.25m and thickness 0.05m. The discharge was 0.2 cumecs. In making a



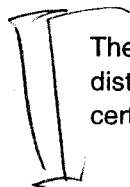
comparison with the results from the physical model tests and the numerical model from Mississippi University, consideration was given to the vertical velocity profiles of  $u$  and  $v$  at two points close to the groyne tip. The initial test (RAa-1) was modelled with a coarse grid as can be seen from Figure 6.7. The whole of the experimental channel was modelled in SSIIM. However the flow patterns downstream of the groyne change very little and thus a revised grid was used in test RAa-3. Here the modelled length of channel was reduced to 6 metres. This increased the resolution by a factor of about 6 in the  $x$  direction. However to further improve the resolution, in Test RAa-4 (Figure 6.8) the number of cells was increased and the cells were refined in the region of the groyne tip. Although this gave improved results, the grid was still not fine enough to resolve the details of the flow in the region of the groyne tip and thus the length of the recirculation zone was under-estimated. A comparison of longitudinal and lateral velocities is given in Figures 6.9 and 6.10. In Test RAa-6, the overall resolution was coarsened to improve run times, but the grid was refined in the region of the groyne tip. When this schematisation was used with the SOU scheme, the correlation between the experimental data and the numerical model was good.

Further tests were conducted with this schematisation to investigate the best choice of tuning parameters in SSIIM; these are presented in Appendix 3. The optimum parameterisation was found in Test RAa-12. Results from this test are discussed below.

The velocities at mid-depth are shown in Figure A-17. It can be seen that the correlation with experimental results is quite good. The width of the recirculation zone, is indicated by the velocities at sections D and E. It can be seen that the recirculation zone is about 0.5m wide and that velocities in this region are accurately predicted. This zone width is twice the length of the groyne which corresponds with the experiments of Nwachukeua and Rajaratnam which were discussed in Section 2.5.

The length of the recirculation zone is defined by the point on the bank at which the longitudinal velocity is zero. This can be seen in the plan view in Figure A-17 at the end of the reverse flow region (for a depth of 37.5% from the bed). A more accurate view of the reattachment length is shown in Figure A-19. The length of the recirculation zone at this depth is found to be 2.88m but at the surface the reattachment length is slightly less (2.72m). The reattachment length measured by Mayerle et al was 2.88m which corresponds closely to the values predicted by SSIIM.

The numerical model predicts a longer reattachment length near the bed; this is reflected in the change of flow direction near the bed point C3 in Figure A-18. However this behaviour is not seen in the experimental measurements at that point. Similarly the vertical velocity profile at point A3, shows a significant discrepancy. The experimental data shows a peak at about mid-depth but this is not seen in the numerical model.



These results indicate that the numerical model can predict the overall distribution of flow, but that the vertical velocity profile is not well predicted at certain locations.



## 6.4 Summary

In each of the tests conducted, the numerical model predicts velocity fields which are close to those measured in the laboratory. Although some details of the flow are not well represented, the overall accuracy is good.

Thus, the k-epsilon SSIIM model was considered suitable for numerical simulations of flow patterns around groynes. However, like all such models care is needed in the choice of grid and the use of alternative solution algorithms.

---

## 7 Physical model tests

---

### 7.1 Experimental set-up

A number of laboratory tests were carried out with two main objectives, to provide experimental data for validation of SSIIM and to allow direct visual observation of the three-dimensional flow around structures used in river training works. The majority of the tests were carried out in the General Purpose Flume (GP Flume) at HR. Tests conducted in a sinuous channel are described in Section 7.8. The GP Flume has a test section 15.24m long by 2.3m wide and 0.6m deep. The flume had wooden floor and walls, and the flow was smoothed at the upstream end by means of a screen baffle positioned across the whole width of the flume. A pump with a capacity of about 0.13m<sup>3</sup>/s supplied the water to the flume which was then discharged back into a sump, thus producing recirculating conditions.

A thin rectangular plate weir, located at the upstream end of the flume, was used to measure the flow rate; the water depth above the crest of the weir was measured by means of a tapping point connected to a stilling well fitted with a micrometer screw point gauge. The repeatable accuracy of the point gauge was estimated to be  $\pm 0.3$ mm. A tailgate at the downstream end of the GP Flume was used to control the water depth, ~~in the flume~~ which was varied from 0.18m to 0.20m.

A diagram of the GP flume is shown in Figure 7.0.

Water depths in the test flume were measured by a point gauge with vernier scale mounted on an instrument carriage. The velocity probes were also fixed onto this carriage which could move along a central section of the flume approximately 7.5m long. The section of flume covered by the carriage was sufficiently long to allow the collection of data in the whole of the flow field affected by the presence of the training structures, ~~but it~~ was occasionally necessary to take a few readings outside the carriage range. On these occasions the probe was held by hand.

### 7.2 Velocity Measuring Equipment

#### Sontek

The three-dimensional velocity field was monitored in most tests by a Sontek acoustic doppler velocimeter probe (since renamed Nortek). The acoustic sensor of the probe is formed by one transmit transducer and three receive transducers; these are oriented in such a way that the receive beams intercept the transmit beam in a sample volume 50mm below the sensor (see Plate 1). Velocity components in three directions are measured in this sample volume (approximately 3-9mm in height and 6mm in diameter) which is largely



undisturbed by the presence of the probe. A printed circuit board, installed in a personal computer (minimum 386/387), performs the digital signal processing and the data acquisition software, which is supplied with the instrument, gives real-time display in graphical and tabular form. The velocity data was recorded at 10Hz in binary form. The data was then converted into ASCII format for the analysis of results using a spreadsheet. From the data analysis it was possible to determine the mean and fluctuating velocity components in each of the 3 directions. The equipment is able to use the time of a reflected signal to accurately determine the height of the measuring volume above the bed.

#### Minilab

When the Sontek was not available, tests were performed with a Minilab SD-12. This probe (shown in Figure 7.1) is a three-component ultrasonic instrument. However, only two of the velocity components could be measured with confidence due to malfunction of one of the probe's channels. It was decided for these tests to monitor in the streamwise and transverse directions since the vertical component is less important in the definition of the flow field around training works. The Minilab instrument consists mainly of a probe which contains three pairs of transducers. The flow speed is determined from the transit time of an acoustic beam between each pair of transducers, from transmitter to receiver via the reflector. The beam path length for the x and y transducers is 5cm. The measured velocity is the average flow velocity along the beam path. The Minilab display unit allows the direct reading of the velocity components. The averaging time for the velocity measurements was usually selected to be 20 seconds. Previous experience of using this type of probe showed that it required regular monitoring of the signal offset at zero flow velocity. This is due to the sensitivity of the probe to temperature changes and impurities in the water.

#### Comparison

The use of the Minilab probe, when the more modern Sontek was not available, was essentially due to the decision to minimise delays in the test programme and to obtain as much experimental data as possible. In doing so, it was therefore necessary to check whether the results given by the probes were comparable.

The accuracy of the velocity readings obtained in the laboratory tests depends on the accuracy of the probes used and also on the precision of the manual positioning of the instruments at each measurement point. At the beginning of the test programme some tests were carried out to compare the readings given by the Minilab and the Sontek probes. It was found that the Minilab gave generally lower values; this was more apparent in the readings of the x-component of the velocity and particularly for positions close to the channel bed. The discrepancy at points near the bed can be possibly explained by inaccuracies in the positioning of the instrument, which would affect mainly the Minilab, since the Sontek instrumentation gives the experimenter the vertical coordinate of the point. Due to the steep velocity gradient usually present near the bed, small positioning errors can result in relatively big differences in the readings. This can account for the maximum differences of about 8% that were observed in the streamwise velocity components. In view of the closeness of the readings given by the two probes in the comparison tests, the results from both instruments were considered valid.

Position of the sample volume

In general, the Sontek is considered more accurate than the Minilab probe because the positioning is more accurate, the sampling volume is smaller and the obstruction effects are less. This last factor is particularly true in the



recirculation zone where reverse flows may cause the Minilab reflector support to interfere with the measured flow.

### 7.3 Channel layout and model groynes

Two types of channel cross-section were considered in the experimental programme: rectangular and trapezoidal (see Figure 7.2). In the rectangular layout (Tests RAb to RE), the channel modelled was 2.3m wide and the tests were carried out with one or two model groynes positioned at right angles in relation to the flow direction (see Figure 7.4). In later tests (RM, RX, RY), the channel was 2m wide (see Figure 7.5). The model groynes (which were 0.2m high and 0.025m thick) were made of wood and had vertical faces. Some of the model groynes used in the rectangular channel had a semi-cylindrical tip (see Figure 7.4). The groynes introduced an obstruction of  $0.072\text{m}^2$  which is 17% of the width of the flume.

In the trapezoidal layout, the side slopes of the channel were 1V:2.5H and were moulded in sand/cement mortar (Figure 7.2). In plan, a 2m long transition was included in the flume to allow a gradual change between the rectangular cross-section of the flume and the trapezoidal test section. In this case the model groynes were designed to cause an obstruction to the flow equal to that in the rectangular channel case (ie  $0.072\text{m}^2$ ). However, due to the smaller size of the trapezoidal channel this represents an obstruction of about 26%.

The length of the groynes measured from the toe of the embankment to the tip of the groyne was therefore chosen to be 0.18m, and the height and width remained at 0.2m and 0.025m, respectively. With this layout, tests were carried out with the model groynes at right angles to the flow and also at  $75^\circ$  and at  $105^\circ$  to the upstream bank (see Figure 7.3). Note that in the GP Flume the flow is from the right, but in all the results presented, flow is shown from the left according to the usual convention.

The plan of the sinuous channel is shown in Figure 7.6. The dimensions of the groynes used in the sinuous channel are shown in Figure 7.7. The dimensions of all tests are given in Table 5. Dimensionless parameters are given in Table 6. Experimentally determined recirculation lengths are given in Table 7 together with some data from the computational model.

### 7.4 Preliminary tests

Before the start of the test programme, preliminary tests were conducted to assess whether: 1) the boundary layer was fully developed at the start of the test section; 2) the flow conditions were smooth (i.e. absence of surface waves); and 3) the two probes (Minilab and Sontek) gave comparable measurements.

To assess the development of the boundary layer, velocity measurements were taken at a section sufficiently upstream of the groynes to represent undisturbed flow conditions and far enough from the flow entry point to be unaffected by entry disturbances. These measurements were taken with the two probes used in the tests (to allow a comparison between them) and also with a miniature propeller meter. The velocity profile was thus determined and showed a smooth, developed shape. Visual observation of the flow indicated that the screen baffle at the upstream end of the flume created smooth flow conditions. To compare the measurements given by the Minilab and Sontek probes, velocity profiles were determined at two points in the centre of the flume, one upstream of the test section and another at the downstream end. The profiles were found to be



similar in shape, and only minor differences were observed in the magnitude of the velocity values. These were mostly close to the bed, where positioning error may be significant as discussed in Section 7.2.

Consideration was also given before the start of the tests to the location of points where the measurements would be taken. In plan, it was decided that several points would be required to define the velocity field in the vicinity of the groynes and particularly at the groyne tip. All the tests also included a point far upstream of the groyne(s) and another one far downstream, both close to the centreline of the flume. These points would allow the assessment of the velocity conditions in the flow undisturbed by the groynes. Four measurement points through the depth of the flow were used to enable the definition of the vertical velocity profile. The location of the measurement points for each of the main tests are shown by the corresponding Figure in the following table.

Test	RAb	RB	REa	REb	RM	RX, Y	TA	TB	TC	TD	TEa
Figure	8.1	8.8	8.14	8.19	8.27	8.24	9.1	9.11	9.17	9.21	9.27

## 7.5 Tests in a rectangular channel

### 7.5.1 Single unsubmerged groyne (Test RAb)

This test was carried out with a flow rate of  $0.131\text{ m}^3/\text{s}$  and flow depth of  $0.18\text{ m}$ . Since the model groyne was  $0.2\text{ m}$  high, this meant that the top of the groyne was above the mean water level and the groyne was therefore unsubmerged.

It was found that the groyne diverted the flow from the channel wall quite markedly, producing a long re-circulation zone behind the groyne. Dye was introduced into the water to visualise the flow and photographs taken from above. Vortex shedding was visible just downstream of the groyne, as can be seen in Plates 2 and 3. Plate 3 illustrates the acceleration of the flow at the tip of the groyne and the lower velocities in the re-circulation zone.

The length of the re-circulation zone was assessed by using a fine thread fixed to the tip of a rod. This rod was held by hand at various distances from the groyne and the flow direction determined. At the end of the recirculation zone the predominant velocities were those caused by eddies generated in the shear layer between the recirculation zone and the main flow. Thus the flows were unsteady in this region and it was difficult to determine the extent of the recirculation zone exactly. In this test, the length of this zone was found to be between  $3\text{ m}$  and  $4\text{ m}$ .

The velocity field was measured with the Minilab probe (in the streamwise and transverse directions): four measurements were taken at each position in plan to define the vertical velocity profile. These points corresponded to positions  $0.04\text{ m}$ ,  $0.09\text{ m}$ ,  $0.12\text{ m}$  and  $0.15\text{ m}$  above the bed.

With a flow straightening baffle installed upstream of the test section, velocity measurements were also taken with a Sontek probe. These results are discussed in the next chapter together with the results from the numerical model.



### **7.5.2 Single submerged groyne (Test RB)**

The Sontek probe was used in this test which was carried out with a flow rate of  $0.135\text{m}^3/\text{s}$  and water depth of  $0.25\text{m}$ . The groyne tested ( $0.2\text{m}$  in height) was therefore submerged by approximately  $0.05\text{m}$  of water.

As in the previous test, dye was introduced in the flow to help visualise the direction of the flow at various levels above the bed. Examples of this procedure are shown in Plates 4 and 5. The re-circulation zone was found to be under  $6\text{m}$  in length. However, as in the unsubmerged groyne test, the limits were ill-defined, with signs that the flow occasionally reversed at approximately  $3\text{m}$  downstream of the groyne.

### **7.5.3 Two unsubmerged groynes, 1m apart (Test REa)**

In this test, two groynes were positioned in the flume separated by  $1\text{m}$ . The flow depth was  $0.18\text{m}$  and the flow rate was  $0.131\text{m}^3/\text{s}$ . The velocity readings were taken with the Minilab probe. It was found that the length of the re-circulation zone in this test was between  $2$  and  $4\text{m}$  (measured from the downstream groyne).

### **7.5.4 Two unsubmerged groynes, 2m apart (Test REb)**

This test was carried out with the same flow conditions of test REa and the Minilab probe was also used for the measurements of flow velocity. Using the rod-and-thread technique, it was found that at  $4.25\text{m}$  downstream of the second groyne the re-circulation zone had definitely ended. As in all the other tests, it was found that the direction of the flow started to oscillate far upstream of the reattachment point, in this test at about  $2\text{m}$  from the downstream groyne.

### **7.5.5 Permeable groynes**

This test was conducted in the GP flume into which a wooden insert had been constructed, reducing the channel width to  $2\text{m}$ . The water depth was  $0.18\text{m}$  and the discharge was  $0.114\text{m}^3/\text{s}$ . Velocities were measured using the Sontek probe. Two permeabilities were tested: Test RX with  $25\%$  obstruction and Test RY with  $44\%$  obstruction. The design of the model groynes are shown in Figure 7.5. Velocity measurements were taken at the points indicated in Figure 8.24.

### **7.5.6 Tapered groyne (Test RM)**

This test was conducted with similar conditions to those for the permeable groynes. The discharge was  $0.106\text{m}^3/\text{s}$ . The water depth at the groyne was  $0.18\text{m}$ . Velocity measurements were taken at positions indicated in Figure 8.27.

## **7.6 Tests in a trapezoidal channel**

### **7.6.1 Single unsubmerged groyne (Test TA)**

In this test, the flow rate was reduced to  $0.0922\text{m}^3/\text{s}$  and the water depth was  $0.18\text{m}$ . The velocity measurements were taken using the Sontek probe which was also used in all the other tests of the trapezoidal channel. Visual observation of the flow indicated that the length of the re-circulation zone was approximately  $6\text{m}$  and that shedding of vortices was quite noticeable at the tip of the groyne and over a distance of  $1\text{m}$  downstream of the groyne.



### **7.6.2 Single submerged groyne (Test TB)**

Test TB was carried out with  $0.0927\text{m}^3/\text{s}$  and  $0.25\text{m}$  water depth. Because the groyne was submerged, it was observed that there was streamwise flow along the inclined banks of the channel downstream of the groyne. The re-circulation zone was found to be a little over  $4\text{m}$  long and less well defined than in the unsubmerged groyne case. The vortex shedding observed was also much less pronounced than in the previous test.

Subsequent analysis of the velocity data from the Sontek probe showed that some points were unreliable (possibly due to reflections of the acoustic signal). Such points were discarded.

### **7.6.3 Single unsubmerged groyne, $75^\circ$ angle (Test TC)**

The orientation of a groyne relative to the bank is defined in this report as the angle between the groyne and the upstream bank. In this test, the model groyne was positioned in the flume at an angle of  $75^\circ$  to the upstream bank and was therefore facing upstream (see Figure 7.3).

The flow rate in the test was  $0.0940\text{m}^3/\text{s}$  and the water depth was  $0.18\text{m}$  so that the groyne was unsubmerged. It was found that the re-circulation zone created by the groyne was about  $5.8\text{m}$  long; vortex shedding was also observed downstream of the groyne, particularly within a distance of one metre from the groyne.

### **7.6.4 Single unsubmerged groyne, $105^\circ$ angle (Test TD)**

This test was carried out with the model groyne facing downstream, at an angle of  $105^\circ$  to the upstream bank. The flow conditions were similar to those of the previous test: flow rate of  $0.0902\text{m}^3/\text{s}$  and water depth of  $0.18\text{m}$ . Visual observation of the flow indicated that the re-circulation zone was approximately  $6.5\text{m}$  long and relatively well defined.

### **7.6.5 Two unsubmerged groynes, $1\text{m}$ apart (Test TE)**

In this test the groynes were positioned at right angles to the bank, one metre apart. The flow rate was  $0.0956\text{m}^3/\text{s}$  and the water depth was  $0.18\text{m}$ . This layout produced a re-circulation zone of about  $2.5\text{m}$  in length (measured from the downstream groyne).

## **7.7 Conclusions from the GP flume tests**

Data was collected to validate the numerical model for a number of conditions. The unsteady flow resulting from eddies hindered the estimation of the recirculation length. The recirculation lengths are given in Table 7 and in Figures 8.7 and 9.5. This unsteadiness also necessitated long averaging times at each measurement point. The results from the physical model are discussed further in Sections 8 and 9 where they are compared with results from the numerical model.

## **7.8 Tests in a sinuous channel**

The sinuous channel in the flood channel facility at HR was chosen for some of the tests because this provides circumstances similar to those in a natural river where groynes may be used to stabilise plan form.

The model consisted of a sinuous trapezoidal channel with a top width of  $1.6\text{m}$  and a side slope of  $45^\circ$  degrees. The meander width measured at the channel centreline was  $5.92\text{m}$  and the wavelength of the sine generated curve measured



along the channel centreline was 20.107m. The meander length measured along the floodplain was 14.96m giving a sinuosity of 1.344.

The curve defining the channel was given by:

$$\theta = \theta_0 \cos \left( 2\pi \frac{L}{L_m} \right) \quad \text{with } \theta_0 = 60^\circ \text{ and } L_m = 20.107\text{m}$$

$$r_{\text{curv}} = \frac{L_m}{\theta_0 \times 2\pi \times \sin \left( 2\pi \frac{L}{L_m} \right)}$$

where  $\theta$  is the angle between a cross-section and the axis of the channel  
 $L_m$  is the length of one meander measured along the centreline  
 $L$  is distance along the channel centreline  
 $r_{\text{curv}}$  is the local radius of curvature

The length of the channel was approximately 50m which provided two full meanders with lead-in and lead-out sections. The overall design of the facility is shown in Figure 7.6. The model contained a mobile bed of 0.8m sand. The channel bed was levelled to give a depth of 0.25m below bank level. The flow conditions were set so as to prevent sediment transport in the bulk of the channel. This meant that the flow was not "normal" and the flow depth increased along the length of the channel. The flow depth at the test section was 0.2m. In the test section, groynes were inserted into the sand. The dimensions are shown in Figure 7.7. In the vicinity of the groynes, where the flow was accelerated, the sand was stabilised using cement dust.

Velocities were measured using a miniature propeller current meter (MPCM). The flow direction was determined using wool and the MPCM was orientated in the predominant direction of flow. The flow was visualised using dye and polystyrene balls.

Velocity measurements in the unobstructed channel showed that the maximum velocity occurred at the inside of the bend. This is as expected for a channel of constant cross-section, as can be seen from the test in a curved channel of rectangular cross-section discussed in Chapter 6. However it is different from the flow in a natural river where secondary currents at the bend cause erosion at the outside of the bed and deposition on the inside. This results in greater depths and larger velocities at the outside of the bend.

In the first test, two groynes were placed near the inner bank followed by two groynes at the outer bank. This created highly erosive conditions. In the second test, the order of the groynes was reversed and this test (SPb) is used for comparison with the numerical model.

*Is there a standard reference for this observation regarding natural and domestic meandering channels*



## 8 Validation tests for a rectangular channel

### 8.1 Introduction

The object of these tests is to validate SSIIM in the modelling of river groynes by comparison with the experimental work in a rectangular flume described in Chapter 7. This work has three aims. First, to check that SSIIM is capable of performing such simulations with sufficient accuracy. Second, to confirm the most suitable choice of numerical parameters, including the grid resolution, for speed, accuracy and stability. Third, to lay the groundwork for the predictive study in which model simulations will be used to develop guidelines for river training works.

The following pages give a brief description of each of the tests. Plots are included to compare the results from the SSIIM simulations with results from the HR experiments. Velocity vectors are shown in the units measured (m/s). The flow angle is indicated as positive clockwise from the predominant flow direction ie towards the near bank at  $y = 0$  (see Figure 8.1). Contours and other comparisons are shown normalised the average upstream velocity ie  $V_{norm} = V/V_{mean}$ , where  $V_{mean} = Q/A$ . Brief conclusions have been drawn from the test results.

In Section 6.3, various simulations of the SSIIM model were compared with results for a single groyne obtained in an experimental flume at the University of Hanover (Mayerle et al). In Section 8.2 comparisons are made against similar experimental conditions studied at HR. In Section 8.3 conditions for two groynes are presented and in Section 8.4 submerged groynes are considered.

### 8.2 Test RAb - Rectangular groynes in a rectangular channel (GP Flume)

The physical conditions for these tests are described in Section 7.1. The channel is 2.3m wide and the water 0.18m deep. The full width of the groyne extends 0.4m into the flow. The groyne height is above the water surface, and thus the groyne is unsubmerged (see Figure 7.4). Although the experimental channel was 15m long, it was found that satisfactory upstream and downstream boundary conditions could be established with a numerical model of 8m in length.

To compare the results from the experimental model with those from the numerical model, graphs of velocity vectors are shown for both the models. Figure 8.1 shows the points where experimental velocity measurements were taken. Figure 8.1 also shows a plan view of the grid. The grid intersections indicate the centres of the cells where the numerical model calculates velocity and other data. Figure 8.2 shows an overall view of the velocity field and the lateral velocity profiles of streamwise velocity at sections upstream and downstream of the groyne. Figure 8.3 shows velocity vectors upstream of the groyne and in the recirculation zone. These figures show velocities in the upper layer of the flow (at 66% of the depth ie 12cm from the bed). Figure 8.4 shows the velocity vectors at 22% of the depth (ie 4cm from the bed). Figure 8.5 shows the vertical profiles of velocity and flow direction at selected points in the flow. Figure 8.6 shows long section views of longitudinal and vertical velocity at various distances from the near wall. The groyne is located at the near wall.

*Positive angles are towards the near bank as indicated in Figure 8.1*



The results from the test are considered in two parts, upstream of the groyne and elsewhere.

#### Upstream of the groyne

The flow upstream of the groyne can be seen in Section A of Figure 8.2 and the upper part of Figure 8.3. The vertical distribution of flow is shown at the tip of the groyne at point 6 in Figure 8.5 and at various points in the flow in Figure 8.6.

The experimental results are shown by the thicker vector lines. Upstream of the groyne, the flow is diverted away from the groyne but the diversion angle is not great. The flow near the surface (see Figure 8.3) is less than the velocities near the bed (see Figure 8.4). Increased velocities near the bed were not expected, since the normal behaviour of open channel flow is for the flows near the bed to be reduced due to the frictional effects of the bed.

At first it was thought that these results might be due to some failing in the flume or the measuring equipment. Measurements were taken 1.5m upstream of the groyne which was about 3m from the start of the flume. The velocity profile at those points showed the normal velocity profile with below average velocities at the lower layers, confirming the accuracy of the measurements.

Another possible cause of the velocity profile at the location might be an uneven horizontal velocity profile upstream of the groyne. This possibility was eliminated by the introduction of a baffle at the start of the flume. As a further precaution a different velocity probe was substituted. There is a difference between the results obtained using the Sontek probe without the baffle and those obtained using the Minilab probe after the baffle was installed. However, as can be seen in Figure 8.6 the general pattern of the flow upstream of the groyne in the two cases is the same:

- a general reduction of velocities,
- velocities higher near the bed than at the surface and
- no reverse flow.

It should be noted that vertical velocity components were not measured by the Minilab probe (see Section 7.2).

One possible explanation for the behaviour in the physical model is that a small roller vortex may be present at the upstream face of the groyne. Another possibility is the presence of lateral surface eddies on the upstream face of a groyne as indicated by Copeland and shown in Figure 2.3. The effect of either condition would be to divert flow to the lower layers.

If such a disturbance was smaller than 10cm in the x direction, it would not have been detected by the velocity measurements. Also, if the disturbance was unsteady, then its detection would have been difficult due to the long averaging times for the velocity measurements (some 50 seconds). This view is to some extent supported by the dye tests, in which it was seen that the flow near the surface dispersed the dye more quickly than near the bed.

It is not clear whether any vortex is present at the face of the groyne, and the magnitude and effect of surface eddies are also difficult to measure since the Sontek probe could not measure within 8cm of the water surface. Velocity



measurements close to the groyne are difficult because of the physical size of the velocity probes. Further investigations of this behaviour could not be carried out within the timescale allowed by the project.

Whatever the cause of the behaviour in the physical model, it is clear that the numerical model does not predict this effect. Instead a full depth roll vortex is seen at the upstream face of the groyne. Here and downstream of the groyne, bed velocities are on the whole lower than average.

Three possible explanations were considered for this discrepancy.

First, the numerical model assumes isotropic turbulence but, where surface eddies are present, it is clear that the turbulence in plan is greater than the vertical turbulence thus the turbulence is anisotropic. A second possible cause of the problem results from the rigid lid assumption used in the model (see Section 4.4). However comparative tests between RAa-11 and RAa-12 show that the effect of updating the water surface is very slight. This comparison is considered in Appendix 3.7.

Finally, the experimental method had a groyne with a semi-cylindrical tip. This shape more closely corresponds to the shape used in prototype groynes but, because of practical difficulties associated with the mesh, this was not simulated in the numerical model. The rounded tip of the experimental groyne will tend to streamline the flow and may thus reduce the angle of deflection.

The significance of these effects cannot be readily estimated without a comparison using other numerical models. In summary, the details of the flow upstream of the groyne are not well modelled by SSIIM.

Recirculation zone

The main features of the flow to be considered in validating the numerical model are: the length and width of the recirculation zone, and the distribution of flow downstream of the groyne.

The experimental and numerical recirculation lengths are shown in Figure 8.7. The length of the recirculation zone was measured experimentally at between 3 and 4m and the computation model indicates that the length is approximately 5m. This is an acceptable degree of correspondence when the uncertainty in the experimental measurements (see limits of position in Figure 8.7) is considered.

The width of the recirculation zone was not measured directly in the experimental model but the lateral velocity profiles downstream of the groyne (Sections B and C in Figure 8.2) shows a good correspondence.

The recirculation width was estimated from the maximum width of the plan velocity contour ( $V/V_{\text{mean}} = 0.5$ ) at mid-depth. Recirculation widths and lengths for each test are listed in Table 7.

Summary

The overall parameters of flow are reasonably well predicted. The length and width of the recirculation zone are close to measured values. Velocities upstream of the groyne and at the groyne tip are significantly overpredicted, which errs on the conservative side when considering the possible effects of scour in this region.

Roller vortex not well modelled full depth vortex seen

Handwritten mark resembling a large 'Y' or bracket.



The lateral velocity profiles downstream of the groyne indicate a good correspondence.

The vertical velocity distribution is not well predicted by the numerical model. This limitation is not very important when considering the overall effects of the groyne.

### 8.3 Test RB - submerged groyne

This test was run under similar conditions to Test RAb, except that the water level was increased to 0.25m so that the groyne was submerged. This test showed many of the features of the previous test. The positions of the measurement points are shown in Figure 8.8, plan velocity profiles are in Figure 8.9; velocity vectors in plan are shown in Figures 8.10, 8.11 and 8.12. Velocity vectors in long section are shown in Figure 8.13.

As in test RAb, a roll vortex upstream of the groyne was found in the numerical test but not in the experiments. The flow near the groyne tip is deflected by a greater angle in the numerical test. Upstream of the groyne ( points 1 and 2) and near the groyne tip (points 3, 4, 5, 6), the observed velocities near the surface are less than at the bed but this pattern is not predicted by the numerical tests. Despite these differences, the overall pattern of flow predicted is close to that observed. The recirculation length is predicted as <sup>between 3 and 3.5m</sup> while the observed value was between 3m and 6m. The flow patterns downstream of the groyne are well predicted.

The depth <sup>of</sup> submergence of the groyne was less than the minimum needed by the velocity probe so the flow over the groyne could not be measured. However, the effects of submergence can be seen by the reduced recirculation length and the greatly reduced recirculating velocities. Both measured and predicted velocities in the lee of the groyne show very low upstream velocities (~ 5mm/s). Overall the predictive ability of the numerical model is reasonable as the main features of the flow are predicted with acceptable accuracy.

### 8.4 Tests RE - Two unsubmerged groynes

In these tests, the Minilab probe was used for the experimental measurements. Two groynes were placed at 1m separation in Test REa and 2m separation in REb. In each case, comparisons are shown at cross-sections in the recirculation zones beyond the first and second groyne.

In addition to graphs of velocity, turbulent kinetic energy is shown to the influence of the wake of the first groyne on the second groyne.

#### 8.4.1 Test REa - Two groynes one metre apart

The experimental points are shown in Figure 8.14. Figure 8.15 shows a good correlation between numerical and experimental data for the flow between the two groynes. Between the groynes at Section A the flow is well predicted. However downstream of the groynes at Sections B and C, the correlation is not so good. At Section B, the strength and width of the recirculation zone is over-estimated. This can also be seen in velocity vectors in the recirculation zone (Figure 8.16). At Section C, 4m downstream of the second groyne, it can be seen that the length of the recirculation zone is over-estimated since at this section, the numerical model incorrectly predicts reverse flow. This fact is



confirmed by the length of the recirculation zone estimated by using a string on the water surface see Figure 8.7, graph REa. The numerical recirculation length, measured from the downstream groyne, is 4.5m and the experimental length is about 3.5m. Similarly the numerical recirculation width at 0.55m is about 20% greater than the experimental value of 0.45m. The widths are determined from the location of  $(V/V_{\text{mean}}) = 0.5$  in Section B at mid-depth. This can be seen in the lower centre graph in Figure 8.15. This difference is also evident in the discrepancy in flow direction seen at point 18 in Figure 8.17.

The numerical model shows reverse flow at the tip of the second groyne. This was not recorded in the experimental model since the flows were very unsteady due to the shear layer generated by the first groyne. However this phenomenon was demonstrated by the movement of polystyrene balls floating on the water surface. The unsteadiness of the shear layer cannot be modelled in SSIIM since it is a steady state model. However a high degree of turbulence near the water surface at the groyne tip ( $x = 1\text{m}$ ,  $y = 0.4\text{m}$ ,  $z/h = 0.95$ ) can be seen in Figure 8.18.

### Conclusion

Between the two groynes, SSIIM models the flow quite accurately although the recirculation zone is slightly over-estimated. However, the velocity downstream of the second groyne are not well predicted. The width of the recirculation zone at Section B is over-estimated by some 50%. The reattachment length is similarly over-estimated.

### **8.4.2 Test REb - Two groynes two metres apart**

The Minilab probe was used to measure the components of the plan velocity for this test. The experimental points and the numerical grid are shown in Figure 8.19. The graphs of the comparison between SSIIM results and laboratory experiments for this test can be seen in Figures 8.20 to 8.22. The experimental sections A and B were located between the groynes to check the accuracy of SSIIM in this area.

Most of the observations from the previous test apply also to this case. Between the two groynes, the width of the recirculation zone is over predicted by about 20%, as can be seen from the velocity profile in Section B. At Section C in Figure 8.20, it can be seen that the experimental velocities are close to zero, indicating the end of the recirculation zone at this point. Thus the recirculation length measured from the downstream groyne, is approximately 1.5m. This is less than the recirculation length measured using the rod and string method of between 2 and 4.25m. However, the velocity measurements should be considered more reliable since the velocities were averaged over a relatively long period (about 50 seconds). The computed recirculation length is 4.3m which is larger than the experimental value.

This significant error may result from the very high turbulence of the tip of the second groyne. Here the numerical model predicts significant reverse flows but these are not observed in the experimental tests. This discrepancy may result from a much higher level of turbulent dissipation in the shear layer than is predicted by the k- $\epsilon$  model. Turbulence levels in the numerical model are shown in Figure 8.23.

The vertical velocity profiles (Figure 8.22) corroborate the fact that SSIIM results are satisfactory in the first recirculation zone (at points 8 and 12) but poor in the



second one. Both the velocity magnitude and the flow direction are wrongly predicted at points 22 and 24.

### 8.4.3 Summary

Overall, the effect of flow separation at the groynes may be seen by comparing the results from the tests of rectangular groyne(s) in a rectangular channel. The predicted recirculation lengths were as follows: 5m for a single groyne (Test RAb); 4.6m for two groynes set 1m apart (REa); and 4.3m for two groynes set 2m apart (REb).

The effect of the upstream groyne is to cause the flow approaching the second groyne to be more aligned with the flow. When the groynes are separated by 1m, the flow is still diverging as can be seen by the vectors between the two groynes. When the groyne separation is increased to 2m, the flow approaching the second groyne is approximately parallel with the channel. Thus the length of the recirculation zone downstream is reduced.

## 8.5 Tests RX and RY - Permeable groynes

In these tests, the permeable groynes were modelled experimentally using square vertical bars shown in Figure 7.5. Velocity measurements immediately behind the groynes were taken just behind each bar and in each jet from between the bars. In the numerical model, the porous groyne was modelled by using 'porous' cells defined in SSIIM.

The experimental points for these tests are shown in Figure 8.24 and velocity profiles are shown for 25% obstruction (Test RX) in Figure 8.25 and for 44% (Test RY) in Figure 8.26. In each case, the jets measured in the physical experiments are not reproduced by the numerical model because the latter assumes the porosity to be uniformly distributed along the full length of a groyne. However, the mean experimental flow can be estimated, and it can be seen that at all locations the experimental velocities are greater than those predicted. In Test RX, the mean flow behind the groyne is under-estimated at Section A and this under-estimation continues downstream of the groyne at Sections B and C. The under-estimation of flow through the groyne is matched by over-estimated velocities in the main channel, away from the lee of the groyne.

Test RY shows very similar results, with the numerical model over-estimating the blockage effect of the porous groyne. This is probably ~~due to the fact that~~ <sup>because</sup> the porosity parameter in the numerical model is based on a random porous medium such as loosely packed stones. These would cause much greater headloss than the regular structure created by the vertical bars in the experimental tests.

Comparison of the experimental results of Test RY with the numerical test of RX shows a better correspondence than the individual tests. This indicates that permeable structures can be modelled, provided tests are conducted to determine their effective permeability. Experimental tests using a porous structure made with a fine or composite structure such as a perforated plate or several rows of piles may give results ~~which~~ <sup>that</sup> would help to clarify this point.

## 8.6 Test RM - Tapered groyne

The experimental measurements for these tests were carried out with the Sontek probe at the positions indicated in Figure 8.27. The grid used in this test was the same as that used in test RX and RY. The tapered groyne which was shaped as shown in Figure 7.5 was simulated numerically by raising the bed and



blocking out the bed layer. The graphs which compare the SSIIM results with the laboratory experiments can be seen in Figure 8.28 to 8.30.

The three test sections were chosen downstream of the groyne so that the accuracy of the numerical model in the recirculation zone could be checked. As can be seen in Figure 8.28, the numerical predictions are excellent in Sections A and B. The velocity increase due to the constriction is well predicted and the boundary between the main flow and the recirculation zone is correctly positioned. The Section C shows a slight difference, with the magnitude of the reverse flow being under-estimated. This corresponds to an under-estimate of the reattachment length. The accuracy of the velocity predictions in Figure 8.29 is generally very satisfactory. The direction and magnitude of the flow are accurately predicted, both close to the groyne and in the recirculation zone. Figure 8.30 shows the vertical velocity profile and the direction of the flow for the points 7, 24, 12 and 30. The results for points 7 and 12 (either side of the groyne) are very good. The velocity is over-estimated for the points 24 and 30 which are located at the boundary between the main channel and the low velocity area downstream of the groyne.

At point 24, one metre downstream of the groyne, the experimental data shows near-bed velocities that are 50% higher than those at mid-depth. This behaviour is not modelled by SSIIM. The explanation for this discrepancy follows the same lines as for Test RAb.

Considering the complexity of the flow, the results are good. The numerical model is able to calculate the flow around a 3-dimensional structure with acceptable accuracy.

### 8.7 Summary of results from rectangular channel

There are two main factors to consider in the performance of groynes.

The first is the width of the recirculation zone which controls the increased velocities in the main channel. In the majority of these tests, the width and the associated velocities ~~was~~<sup>were</sup> over-estimated by up to 20%. However, the accuracy of the prediction of main channel velocities is better than this value, since the main channel velocities are determined by the width of the unobstructed channel.

The second factor is the length of the recirculation zone, which indicates the amount of protection afforded by the groyne. Rodi indicates that the recirculation length is usually underpredicted in a channel in which the influence of the opposite wall is negligible. Here, by contrast, the numerical model tended to over-estimate the recirculation length. This was associated with an over-estimate of the reverse flows in the recirculation zone except in the case of the tapered groyne (RM) and the submerged groyne (RB) where results were generally better.

In all experimental tests, there were points in the flow where the maximum velocity was located below the water surface. This behaviour in general was not predicted by the numerical model.

Overall the results from the numerical model are acceptable for ~~the purpose of~~<sup>general</sup> modelling the ~~overall~~<sup>general</sup> behaviour of groynes in a rectangular channel. However, such a channel shape is not representative of many practical cases, and thus further tests were performed in a trapezoidal channel.



---

## 9 Validation tests for a trapezoidal channel

---

The trapezoidal channel and groyne is shown in Figure 7.2. The channel is approximately 2m wide with a flow depth of 0.18m for the majority of tests and *a depth* 0.25m for the submerged flow tests. For these tests, the Sontek probe was used to measure the velocity.

### 9.1 Test TA - A single unsubmerged groyne in a trapezoidal channel

The location of the experimental points and sections are shown in Figure 9.1. The comparison between SSIIM results and laboratory experiments are shown in Figures 9.2 to 9.4. Figure 9.2 shows the longitudinal velocity at three locations. At Section A, 0.15m upstream of the groyne, the velocities are accurately predicted. At Section B (0.15m downstream of the groyne) and at Section C ( $x = 2m$ ), the width of the recirculation zone is under predicted by about 10cm which is 15% of the groyne length. The length of the recirculation zone as indicated in Figure 9.5 is measured as 6m but predicted as 5m.

Figure 9.3 shows the velocity vectors at the groyne tip and in the recirculation zone. The velocities approaching the groyne tip are accurately predicted. However, as the flow passes the groyne, it starts to decelerate and here the predictions are less accurate. The observed flow direction is mostly downstream whereas the numerical results show a significant lateral component. This discrepancy has been discussed in previous tests and is thought to be mostly due to problems in modelling the flow upstream of the groyne. The main behaviour of the flow is predicted by the numerical model although the recirculation zone is slightly too short. The numerical model results are presented at mid-depth. Thus for flows over the sloping banks, the 50% level is closer to the water surface. The flows in this shallow water are driven by surface flows in deeper water. It can be seen that relatively high velocities are generated near the bank. The experimental probe in use did not permit measurements in water less than 6 to 8cm deep and thus this behaviour could not be confirmed.

Vertical velocity profiles are shown in Figure 9.4. Point 6 is located near the tip of the groyne. The near-bed velocity is over-estimated, thus providing a conservative estimate of the likelihood of scour around the groyne. Points 19, 22 and 25 are located at the toe of the bank at 0.3m, 1m and 2m downstream of the groyne respectively. Velocities are under-estimated at these points and the discrepancy is greater near the bed. However it can be seen from Figure 9.3 that the numerical model predicts larger velocities close to the bank. These results indicate that selection of particular points in the flow for predictive purposes may give unreliable results. Perhaps, a better strategy would be to consider the maximum of the velocities in the lee of the groyne. This gives a more acceptable correlation with both the experimental and numerical tests, indicating mid-depth velocities in the region of 0.1 m/s for this test.

#### Comparison with rectangular channel Test (RAb)

Comparison of Test TA-3 and Test RAb shows the effect of channel shape on the results. The groyne length in the rectangular channel test was 400mm long and in the trapezoidal case was 670mm long. This size was chosen so that the blockage area of the two groynes is the same  $\approx 0.72m^2$ . The groynes are shown in Figure 7.4. However, because of the sloping side of the trapezoidal channel, the mean width is reduced and this increased the blockage ratio from 0.174 to



0.274. The velocity profiles in Figure 9.6 for RAb can be compared directly with those in Figure 9.7 for Test TA. The main features of the flow are as follows:

- For Test RAb, a roller vortex is to be seen in the numerical simulation in the long section (Figure 8.6) and in the cross-sectional view (Figure 9.8). This behaviour is not seen in the experimental data. In the trapezoidal case, a roller vortex is not discernable in the numerical simulation, which corresponds also with the experimental observations (Figure 9.9).
- One metre downstream of the groyne ( $x = 1\text{m}$ ), the reverse currents near the bank appear stronger in the trapezoidal case but this is mostly due to the increasing influence of surface velocities on mid-depth flows.
- At  $x = 3\text{m}$ , the velocity profiles in the two cases are similar - the overall length of the recirculation zone is 5m in the rectangular channel and 4.9m in the trapezoidal case.
- The width of the recirculation zone in the rectangular case is predicted to be 0.62m (ie 0.22m beyond the groyne tip). In the trapezoidal case, the recirculation zone is predicted to be 0.75m from the bank (0.25m from the groyne tip).

Thus it can be seen that the recirculation zone width is dependent on the channel shape, but that the length of the recirculation zone is largely unaffected. Despite this difference, the behaviour of the flow near the groyne is broadly similar in the two cases. The general similarity of flow patterns is not repeated on the far side of the bank. This can be seen by comparing the shapes of the velocity contours of average flow in the range  $x = 0$  to  $x = 5\text{m}$ . The average flow contour is the line where the normalised horizontal velocity ( $V/V_{\text{mean}}$ ) is equal to one. In the rectangular case, the average flow contour is nearly parallel to the far bank. The range of movement of the contour downstream of the groyne is approximately 0.15m (which is 75% of the width of the channel). (See Figure 9.6.) In the trapezoidal case, the range is about 0.30m. Upstream of the groyne in a trapezoidal channel, the lateral slope and the reduced depth cause near bank velocities to be lower than in the rectangular channel.

In the region of the groyne, the constriction causes increased flows near the bank opposite the groyne. The high velocities and shallow depths in the trapezoidal channel cause high turbulence. In this test, the grid was not fine enough on the far bank to give an accurate prediction in this area, but the results do indicate a trend which deserves further investigation in the next phase of the work, because these conditions can be associated with bank erosion. Indeed, river bank failures have been associated with obstructions on the opposite bank.

Beyond the constriction caused by the groyne, flow velocities are reduced at the far bank. The computational model shows significant turbulent dissipation at the toe of the far bank for 4m downstream of the groyne. This is associated with a significant reduction in streamwise velocity. Near the downstream boundary of the numerical model reverse flows are predicted, but it is thought that this is related to the boundary condition applied in the model and is not a true effect.



Velocity measurements were not taken on the far bank in the experiments, and so this cannot be confirmed.

In order to investigate this discrepancy, predicted values of turbulence ( $k$  and  $\epsilon$ ) are plotted in Figure 9.10. This shows a very high level of turbulent kinetic energy ( $k$ ) along the shear layer between the main flow and the recirculation zone. High levels of  $k$  and  $\epsilon$  are also to be seen on the far bank. These values may be the cause of the reduced (and reserved) flows on the far bank. It can be seen that the maximum turbulent dissipation ( $\epsilon$ ) occurs at the groyne tip (here the shear is greatest since the width of the shear layer is limited by the presence of the groyne). In contrast, the value of  $k$  increases along the line of the shear layer, as turbulence is generated faster than it is dissipated. The different distributions of  $k$  and  $\epsilon$  are in contrast to the results from an eddy viscosity model which only uses a single parameter to model turbulence.

The results from this test indicate that the model can give acceptable results. The schematisation used was found to take an unacceptably long time. This may be related to the very thin cells adjacent to the near bank. Alternative gridding will be investigated in the next phase of the project.

## 9.2 Test TB - A single submerged groyne in a trapezoidal channel

The submerged groyne has the same dimensions as in the previous test but the water level was raised to 0.25m to submerge the groyne. This caused an increase in water surface width. In the numerical model, the submerged groyne was created by raising the bed and blocking off one cell above the raised bed as can be seen in Figure 9.15. This method enables the height of the groyne to be modelled accurately, but the grid is distorted and this increases the run times. However, the method is preferable to maintaining an orthogonal grid and blocking out the cells corresponding to the groyne. The chosen method has the advantage that the grid is refined where the flow accelerates over the groyne and so provides a more accurate and stable solution. The location of the experimental points is shown in Figure 9.11. The comparisons between SSIIM results and laboratory experiments are shown in Figures 9.12. to 9.14. Figure 9.12 shows that the longitudinal velocity is well predicted over the cross-section both upstream and downstream of the groyne. The separation between the main flow and the low velocity area is well predicted in Section B. The peak of velocity near the bank in Sections B and C is due to the shallower depths on the banks. <sup>This</sup> ~~which~~ brings the mid level closer to the faster moving surface water. The velocity vectors in Figure 9.13 serve to confirm the accuracy of the numerical model for this test. It should be noted that some unreliable experimental points were removed from the comparison (see Section 7.6.2). The flow direction and the velocity magnitude are well predicted in the whole channel, especially at the tip of the groyne and downstream of the groyne. The vertical velocity profiles in Figure 9.14 show that the flow is fully three dimensional. Thus, the recirculation zone has a height ~~which~~ <sup>that</sup> reduces downstream of the groyne.

Points 19, 22 and 25, correspond to positions at the toe of the bank 0.3m, 1m and 2m downstream of the groyne. The height of the recirculation zone can be seen from the change in flow at each point. At point 19 the flow is streamwise near the surface and reversed nearer the bed. The boundary between the two flows is at 0.16m ie just below the height of the groyne at 0.20m. At point 22, the mixing between upper and lower layers is shown. The flow in this region is complex and unsteady; it can be seen that the flow near the bed is towards the



bank (angle  $\approx 90^\circ$ ), but at the higher levels the flow is away from the bank (angle  $\approx -90^\circ$ ). At 2m downstream of the groyne (point 25), the recirculation zone has ended and all flow is in the streamwise direction (angle  $\approx 0^\circ$ ). These observations are confirmed by the numerical results and indicate the value of a 3D model in this case. The flow direction and magnitude is also well predicted near the tip of the groyne as can be seen for point 6. The experimental data shows a greater deflection of the flow at the groyne tip when compared with the unsubmerged case (Test TA, see Figure 9.4).

Examination of the longitudinal profile (Figure 9.15) shows that in the lower layers beyond the groyne, a recirculation zone is formed but at higher levels, the flow continues in a streamwise direction. Thus, immediately downstream of the groyne, the flow forms a roller <sup>in which</sup> ~~with~~ reverse flows near the bed <sup>rising</sup> ~~rising~~ into the stream which passes over the top of the groyne. This has the net effect of increasing near-bed velocities immediately downstream of the groyne which increases the likelihood of scour. The velocity field is accurately predicted in this case. The flow is more complicated than in the case of an unsubmerged groyne but the results are still very good. The accuracy at the tip of the groyne is better in this test than in the Test TA. This is probably due to the fact that the flow is accelerated less because the net obstruction is smaller. The turbulence shown in Figure 9.16 is generally lower than in the unsubmerged case. As a conclusion, SSIIM results are suitable for predicting the velocity and the flow direction for this test.

### 9.3 Test TC - An unsubmerged groyne angled upstream

In this test, a full depth groyne is angled upstream at  $15^\circ$  from normal ie at  $75^\circ$  from the upstream bank. The groyne length was extended so that the obstruction to the flow viewed in the x direction is the same as in the case where the groyne is at right angles to the bank (Test TA). In the numerical model, a non-orthogonal grid was required as can be seen in Figure 9.17. The grid irregularity tended to cause oscillations in the solution and to prevent these, the relaxation factors were set very low. This caused the number of iterations needed for convergence to increase to 4688; the run time increased from about 24 hours to 65 hours.

The comparison between SSIIM results and laboratory experiments are shown in Figures 9.18 to 9.20. Lateral profiles of longitudinal velocity are shown in Figure 9.18. In Section A, the low velocity zone in the upstream corner between the groyne and the bank is correctly predicted. The velocity profile in Section B corresponds to the experimental measurements even for the points which are close to the opposite bank. The velocity profile for Section C shows that the recirculation zone is accurately predicted but at the toe of the opposite bank, the difference is large. The experimental results in this region were highly variable in space and time. The flow near the bed at this location was recorded as 0.55m/s compared to 0.24m/s at the mid level where the velocities are plotted. The standard deviation of the recorded velocity was about 0.4m/s.

In Figure 9.19, the predicted values of flow direction and velocity magnitude are compared with the experimental measurements. The measured velocities are somewhat lower than the predicted values and are more varied in direction. Nonetheless, the strong deflection of the flow at the tip of the groyne is confirmed by the numerical model. Immediately downstream of the groyne, the recirculation zone is accurately predicted but further downstream the correspondence is less good. The vertical velocity profile (Figure 9.20) and the



flow direction for points 3 and 12 show reasonable agreement but the differences in velocity and in direction at point 21 are significant. This point is at the toe of the bank in the recirculation zone. In this area, the velocity gradients are very high and the flow is unsteady. If numerical results at point 21 were shifted 5cm towards the bank, the correspondence between the experimental and the numerical results would be significantly improved. This indicates that the numerical results predict a recirculation zone which is closer to the bank than found by experiment. The flow direction at point 24 indicates that the reattachment length is under-estimated. In Figure 9.5 it can be seen that the recirculation length was measured as 5.8m but is predicted at 3.5m. The measured length of 5.8m is uncertain because of the highly turbulent conditions in this test. The direction of flow measured at point 24 ( $x = 3\text{m}$ ), is largely towards the bank. This indicates a shorter recirculation length than 5.8m. Overall, the numerical model is able to simulate the attracting nature of an upstream facing groyne. That is, the groyne “attracts” flow towards the bank on which the groyne is located.

#### **9.4 Test TD - An unsubmerged groyne angled downstream**

The comparisons between SSIM results and laboratory experiments are shown in Figures 9.21 to 9.25. This test is identical to the previous test except that the groyne is placed at an angle  $15^\circ$  downstream (ie  $105^\circ$  to the upstream bank). The numerical grid is as shown in Figure 9.22. As in the previous test, the non-orthogonal grid caused a greatly increased run time. The transverse velocity profiles seen in Figure 9.22 show a good correspondence between numerical and experimental data. However there is insufficient experimental data near the bank in the recirculation zone to confirm the high near bank velocities which were predicted at Section C (2 metres downstream of the groyne). The high predicted velocities in the recirculation zone can also be seen in the lower part of Figure 9.23. Figure 9.23 also shows that the flow directions are well predicted beyond the groyne tip. This contrasts with the relatively poor predications of flow direction seen in Figure 9.19 for Test TC where the groyne is angled upstream. This difference may result from the greater turbulence and unsteadiness of the flow where the groyne is angled upstream (Test TC). The downstream facing groyne may be said to be more “streamlined”. Numerical plots of turbulent kinetic energy in the two cases (Figure 9.25) show that where the groyne is angled upstream, the turbulence at the groyne tip is greater but the turbulence is dissipated more quickly. This turbulent dissipation has the effect of reducing the length of the recirculation zone. Comparison of the velocity contours (Figure 9.26) for the two angled groynes show that the length of the recirculation zone is much longer where the groyne is angled downstream and this results in increased midstream velocities at a point 5m downstream of the groyne. However, closer to the groyne the difference is negligible.

Overall the numerical results are able to identify flow patterns which are confirmed by experiment.

#### **9.5 Test TE - Two unsubmerged groynes 1m apart**

In this test, two unsubmerged groynes were placed one metre apart at right angles to the flow. The locations of the experimental points are shown in Figure 9.27. This situation is closer to that used in practical situations where it is usual to place several groynes in a row. An orthogonal grid was used in the numerical model as can be seen in Figure 9.27. The grid is refined in the region of both groynes. The test results are shown in Figures 9.28 to 9.30. The behaviour of



the flow upstream of the first groyne is very similar to that of a single groyne (Test TA). The effect of the second groyne is to 'break up' the recirculation zone downstream of the first groyne.

Between the first and second groynes a smaller recirculation zone is created. The size of this zone is constrained by the length and separation of the groynes. The flow direction is correctly predicted but the strength of the flow is under predicted as can be seen from the upper half of Figure 9.29. This under prediction is confirmed by consideration of the velocity profile at Section B in Figure 9.28 and the vertical velocity profiles at the toe of the bank between the two groynes, points 8, 12 and 16 in Figure 9.30. Point 12 is midway between the two groynes and points 8 and 16 are close to the upstream and downstream groynes respectively. The flow velocity is significantly under predicted at the edge of the recirculation zone between the two groynes. This can be seen in the vertical velocity profile for point 13 in Figure 9.30 and in the plan view in Figure 9.29. The discrepancy here is largely due to the over-estimation of the width of the recirculation zone which has been discussed in earlier tests.

The strength of the recirculation zone between the groynes is much greater in the trapezoidal channel compared to a similar configuration in the rectangular channel (Test REa ); see Figures 8.16 and 9.29. The greater velocities in the present case are associated with the shape of the region between the two groynes. In each case, the cross-sectional area of the groynes is the same, but in the trapezoidal case the width at the surface is greater. This greater width allows stronger surface currents to be generated. The effect is enhanced by the fact that the blockage ratio in the trapezoidal case is greater. This effect is seen to varying extent in both the experimental data and the numerical predictions.

Downstream of the second groyne, the recirculation zone is shorter than in the case of a single groyne. The flow approaching the second groyne is mostly aligned downstream, and thus there is no tendency for the width of the recirculation zone to increase. The flow velocity past the tip of the second groyne is lower than at the first groyne, <sup>and</sup> ~~so~~ <sup>compared to</sup> the length of the recirculation zone in the experiments was reduced to 2.5m (from 6m for the equivalent case of the single groyne in Test TA). A much smaller reduction in recirculation length is found in the numerical results. The recirculation length is reduced from 5m for a single groyne to 4.1m for two groynes. The direction of flow measured at the toe of the groyne, two metres downstream of the first groyne ( $y = 0.45$ ,  $x = 2$ ) can be seen in Figure 9.28 (Section C). The measured velocity at this point indicates that the recirculation zone is shorter than that predicted. Experimental methods using a string floating on the water surface indicated a recirculation length of 3.5m, whereas the numerical prediction is 4.1m. <sup>See</sup>

Although the values of velocity are not very accurate, the correct trends that are obtained when considering the influences of groyne positioning and channel shape, indicate that the numerical model can be used in a predictive capacity.



---

## 10 *Validation tests for a sinuous trapezoidal channel*

---

The experimental work was conducted in the flood channel facility. The plan geometry of the sinuous channel is described in Section 7.8 and can be seen in Figure 7.6. The geometry of the channel cross-section and the groynes can be seen in Figure 7.7. The channel bed was formed in 0.8mm sand but the flow velocities were reduced to avoid bed movement. The velocity measurements were made with a miniature propeller meter.

A plan of computational grid is shown in Figure 10.1 which contains 2700 cells in plan. Because of the large extend of the grid, it was necessary to limit the vertical resolution to 3 cells. The groynes were simulated in the numerical model by using a raised bed and blocked-off top cells. The computational solution was achieved using very low relaxation factors. The flow in the first meander is not fully developed (Figure 10.2). Therefore, it was decided to set up the groyne field in the second meander of the channel. The results of the numerical model are shown in Figure 10.3.

Figure 10.4 shows the profiles of normalised plan velocity at sections between the groynes. The predictions of SSIIM roughly match the experimental measurements. The velocity increase in the main channel is well estimated. However, the velocities in the shelter of the groynes are over predicted. Figure 10.5 shows the near-bed velocities as measured and predicted in the region of the groynes. The mid-depth velocities are shown in Figure 10.6.

Upstream of the bend, the flow tends to the inside of the bend with significantly reduced velocities at the outside of the bend. Upstream of the first groyne a small horizontal circulation zone is predicted but there is little sign of this in the physical model. Experimental results show that the first groyne diverts flow away from the outside of the bend. This leads to a recirculation zone between the first two groynes. Five centimetres in front of the third groyne, the experimental measurements show strong lateral currents as the flow is diverted to the outside of the bend. A small recirculation zone is seen upstream of the fourth groyne at the mid-depth in both the experimental and the numerical results. Downstream of the fourth groyne, the diverted flow remains at the outer part of the bend, forming a long recirculation zone on the opposite side. Although few velocity measurements were taken in this region, observations from dye tests indicate that this recirculation zone continued almost to the next bend. The predicted velocities also show this effect.

Some of the details of the flow in the vicinity of the groynes are not well predicted. However, essential features are as follows.

- Upstream of the groynes velocities are greater near the inside of the bend.
- Downstream of each groyne, a recirculation zone is formed; the smallest is downstream of the second groyne; the largest is downstream of the fourth and final groyne.
- Downstream of the groynes, the velocities are greater near the outside of the bend.



- These results indicate the adequacy of the numerical model in predicting flows in this situation and show that the use of a 3 layer model was justified.

---

## **11 Conclusions**

---

A 3-D numerical flow model called SSIIM (with k- $\epsilon$  turbulence modelling) has been compared with data obtained from laboratory experiments on arrangements of groynes as used for river training purposes. Three-dimensional experimental and numerical data has been collected for over 20 test cases. It has been shown that the 3-D model performs better than an equivalent 2-D model.

The following general recommendations are made about how 3-D models should best be used to predict groynes in rivers.

1. The horizontal grid should be refined in regions of highly varying flow, particularly at the groyne tip. This improves the accuracy of the solution both locally and downstream of the groyne.
2. A minimum level of grid refinement is required on a sloping bank to ensure realistic flows even if the location is not of interest, but the overall level of refinement may need to be coarser than ideal to ensure acceptable run times.
3. A two-dimensional model may be used for determining the general flow pattern but does not give accurate results.
4. The number of layers required depends on the geometry of the groyne and other features which give rise to depth varying flow. Sensitivity tests for the number of layers should be performed for each situation. The influence of bed roughness and channel curvature deserve further investigation.
5. SSIIM has the choice of a second order upwinding scheme (SOU) or a first order power law scheme (POW) for solution of the governing hydrodynamic equations.
  - a) The SOU is recommended for the momentum equations since it improves accuracy for flow that is not aligned to the grid and may reduce run times.
  - b) The POW scheme is recommended for the turbulence equations because of its greater stability. The use of SOU can cause negative values of k and  $\epsilon$  which may cause the solution procedure to fail.
6. In addition, to the above parameters which may apply to any numerical scheme, SSIIM has the possibility of using block correction and altering the relaxation factors.
  - a) Block correction can significantly reduce run times, particularly where the domain is relatively long.
  - b) Relaxation factors are difficult to determine. If they are chosen too small, solution times are increased unnecessarily but if they are chosen too high the model may oscillate and fail to



converge. The need to adjust relaxation factors is a drawback of SSIM

7. The time for each iteration was approximately proportional to the number of cells. The number of iterations required for convergence depends on the complexity of the problems particularly where reduced relaxation factors are required.  
  
Factors which significantly increase the number of iterations required for convergence are:
  - a) Large variations in depth in a cell.
  - b) A non-orthogonal grid plan, as used for angled groynes.
  - c) Porosity cells as used for permeable groynes.
8. In the tests conducted, SSIM was found to be generally acceptable in predicting flows around river groynes.
9. The accuracy of simulations in a trapezoidal flows channel were generally more accurate than those in a rectangular channel.
10. For trapezoidal channels, the length of the recirculation zone downstream of a groyne is reduced by the presence of an upstream groyne. The upstream groyne has the effect of aligning the flow that impinges on the downstream groyne.
11. Modelling the detailed flows in a porous groyne is impractical due to the very fine grid that would be needed. We were not able to represent groynes accurately using porosity cells. However, suitably calibrated, porosity cells appear to be the most promising possibility for modelling permeable groynes.
12. Further work is required to investigate the error in the predicted flow upstream of a rectangular groyne.
13. With the above two exceptions, the numerical model correctly simulated the general behaviour of the flow in all the tests conducted.
14. Velocities at key points around groynes were mostly predicted with an accuracy of better than 20% which may be considered acceptable for design purposes provided a suitable safety margin is allowed. However, larger errors did occur and thus it is recommended that predictions are based on the maximum velocity in a given region of interest.



---

## 12 *References*

---

- Alvarez JAM, 1989, State-of-the-art Report: Mexico - Design of Groins and Spur Dikes, Proceedings of the 1989 National Conference on Hydraulic Engineering, ASCE, pp. 296-301.
- Bettess (1990) "Groynes and Training Works affecting River Planform - A literature review". HR Wallingford. Report SR 229.
- Bognar G and Hanko Z (Eds), 1987, Fluvial Hydraulics and River Training. Recent trends in research and development. Hungary's Contribution to the State-of-the-art. IAHR, Budapest, Hungary.
- Chang HH, 1988, Fluvial Processes in River Engineering, John Wiley & Sons, New York, USA.
- Copeland RR, 1983, Bank Protection Techniques Using Spur Dikes, US Army Engineer Water ways Experimental Station, Vicksburg, USA.
- de Vriend HJ, 1981, Steady Flow in Shallow Channel Bends. Part II: Figures and Appendices. Report No. 81-3. Department of Civil engineering, Delft University of Technology, pp 97, Figure 63.
- Garg SP, 1980, Training of Rivers, Proceedings of the International Workshop on Alluvial River Problems, Rookee, India, pp. 3(114).
- Jansen P, Van Bendegom L, Van den Berg J, De Vries M and Zanen A, 1979, Principles of River Engineering. The Non-Tidal Alluvial River, Pitman. London, England.
- Kinori BZ and Mevorach J, 1984, Manual of Surface Drainage Engineering. Volume II; Streamflow Engineering and Flood Protection, Elsevier, Amsterdam, The Netherlands.
- Lavedrine IA, 1996, Evaluation of 3D Models for river flood applications. HR Wallingford. Report TR 6.
- Mayerle R, Toro RM, Wang SSY, 1995, Verification of a three-dimensional numerical model simulation of flow in the vicinity of spurdikes. Journal of Hydraulic Research Vol. 33 No. 2, pp 243-256.
- Maccaferri, 1980, Gabions for Flexible River Groins. Technical Booklet No. 10, Maccaferri Organisation for River and Sea Gabions, London, England.
- Nwachukwu BJ and Rajaratnam N, 1980, Flow and Erosion Near Groynelike Structures, Department of Civil Engineering, University of Alberta, Canada.
- Neill CR (Ed), 1973, Guide to Bridge Hydraulics, University of Toronto Press, Canada.
- Olsen NRB and Melaaen MC, 1993. Three-dimensional numerical modelling of scour around cylinders. ASCE Journal of Hydraulic Engineering, Vol. 119, No. 9. Sept. pp 1048-1054.



Patankar SV, 1980, Numerical Heat transfer and fluid flow. Hemisphere Publishing Corporation, New York, USA.

Przedwojski B, Błażejowski R and Pilarczyk 1995 " River Training Techniques - Fundamentals, Design and Applications". AA Bakerna, Rotterdam, ISBN 90 5410 196 2.

Rodi W, 1980, Turbulence models and their application in hydraulics - A state-of-the-art review. IAHR Section on fundamentals on division II: experimental and mathematical fluid dynamics, Delft, The Netherlands.

Rodi (1984), Turbulence models and their application in hydraulics: A state of the art review. IAHR (2nd edition).

Salikov VG, 1987, Protection of Banks and Roadbeds from Erosion on River "Nips", Hydrotechnical Construction, 20 (10), pp. 575-580.

Seed DJ, 1997, Design Guide for river groynes. HR Wallingford, England. Report SR 493.

Tamamidis P and Assanis DN, 1993, "Evaluation of various high-order-accuracy schemes with and without flux-limiters". International Journal for Numerical Methods in Fluids, Vol. 16, pp. 931-948.

UNECAFE, 1953, River Training and Bank Protection. Flood Control Series No. 5, Bangkok, Thailand.

Versteeg HK and Malalasekera W, 1995, "An Introduction Computational Fluid Dynamics - The finite volume method" pub, Longman Scientific and Technical, England, 0-582-21884-5.





## Tables





**Table 1**      **Recommended groyne spacings for bank protection**

Reference	Bank	Spacing	Comment
Grant	Concave	$3L_t$	
UNECAFE	Concave	$1L_t$	General practice
UNECAFE	Convex	2 to $2.5L_t$	General practice
Richardson & Simons, 1973	Concave	4 to $6L_t$	Bank may need riprap
Neill, 1973	Either	2 to $4L_t$	
Los Angeles District, 1980	Straight	$2L_t$	Bank may need riprap
Los Angeles District, 1980	Concave	$1.5L_t$	Bank may need riprap
Los Angeles District, 1980	Convex	$2.5L_t$	Bank may need riprap
Garg et al, 1980	Either	3 to $4L_t$	Upstream orientation
Maccaferri, 1980	Concave	$4L_t$	Gabions
Maccaferri, 1980	Convex	$6L_t$	Gabions
Copeland, 1983	Concave	up to $3L_t$	Bank may need riprap
Bognar & Hanko, 1987	Either	$1.2L_t$	Maximum siltation
Alvarez, 1989	Concave	2.5 to $4L_t$	



**Table 2**      **Recommended orientation of groynes to upstream bank**

Reference	Angle	Comment
UNECAFE, 1953	60° to 80°	For bank protection
Jansen et al, 1979	90°	Shortest and therefore cheapest
Garg et al, 1980	75° to 80°	Indian practice
Copeland, 1983	90°	Most effective bank protection
Bognar & Hanko, 1987	115°	Hungarian practice



**Table 3**      **Test coding**

<p><u>First letter</u> : channel</p>	<p>T : trapezoidal channel - GP Flume  R : rectangular channel - GP Flume and Hanover flume  S : trapezoidal sinuous channel - SERC flume series C  P : straight channel with floodplain - SERC flume series A  E : rectangular channel - Evaluation tests  C : curved channel - 90° bend (rectangular)  U : U-bend channel (rectangular) - LFM flume</p>
<p><u>Second letter</u> : groyne</p> <p>Rectangular groynes</p> <p>Tapered groynes</p> <p>Porous groynes</p>	<p>0 : no groyne</p> <p>A : one rectangular unsubmerged groyne  B : one rectangular submerged groyne  C : one rectangular unsubmerged groyne angles 15° upstream  D : one rectangular unsubmerged groyne angles 15° downstream  E : two rectangular unsubmerged groynes  F : three rectangular unsubmerged groynes  G : four rectangular unsubmerged groynes  H : two rectangular submerged groyne</p> <p>M : one tapered unsubmerged groyne  N : two tapered unsubmerged groynes  P : four tapered unsubmerged groynes</p> <p>U : one porous unsubmerged groyne porosity = 0.5  V : one porous unsubmerged groyne porosity = 0.3  W : one porosity unsubmerged groyne porosity = 0.4  X : one porous unsubmerged groyne porosity = 0.25  Y : one porous unsubmerged groyne porosity = 0.44</p>
<p><u>Third letter</u>  <small>(small letter)</small> : physical values</p>	<p>Flow conditions or/and configuration of groynes</p>
<p><u>A number</u> : numerical values</p>	<p>Meshes and parameters in the numerical model</p>



**Table 4**      **Description of tests presented**

Test	Description	Comparison data
CA	Rectangular Channel, 90° bend with obstruction	-
EO	Straight rectangular channel	-
EE	Two groynes	-
EH	Two (50%) submerged groynes	-
EW-1	"Porous" groyne, 1 vertical hole	-
EW-2	"Porous" groyne, 3 vertical holes	-
EW-3	"Porous" groyne, 40% submerged	-
EW-4	"Porous" groyne, 1 horizontal hole	-
EW-5	"Porous" groyne, 2 horizontal holes	-
UO	Semi circular LFM flume	de Vriend (1981),
PO	Trapezoidal channel with flood plain (FCF-A)	MCPM, Telemac
RAa	Rectangular channel with groyne (Hanover flume)      (3)	Mayerle et al (1995)
RAb	Rectangular channel with groyne (G.P. flume)	Sontek, Minilab
RB	Rectangular channel with submerged groyne	Sontek, Minilab
REa	Rectangular channel with two groynes (1m apart)	Minilab
REb	Rectangular channel with two groynes (2m apart)	Minilab
RM	Rectangular channel with tapered groyne	Sontek
RX	Rectangular channel with permeable groyne (25%)	Sontek
RY	Rectangular channel with permeable groyne (44%)	Sontek
TA	Trapezoidal channel with groyne      (3)	Sontek
TB	Trapezoidal channel with submerged groyne	Sontek
TC	Trapezoidal channel with upstream groyne	Sontek
TD	Trapezoidal channel with downstream groyne	Sontek
TE	Trapezoidal channel with two groynes (1m apart)	Sontek
SO	Sinuuous channel in FCF- series C	-
SPb	Sinuuous channel in FCF- series C - 4 groynes	MCPM

Note :

- (1) Groynes are Rectangular, impermeable, full-depth, and perpendicular to the bank unless otherwise stated.
- (2) The flume is the (straight) GP flume unless stated.
- (3) Sensitivity tests were conducted for conditions RAa and TA

**Table 5 Physical dimensions of tests**

run code	Channel width B (m)	Channel depth H (m)	Channel flow area A (m <sup>2</sup> )	Channel length X (m)	Discharge Q (m <sup>3</sup> /s)	Mean velocity $V_{\text{mean}}$ (m/s)	Groyne length (2) $L_t$ (m)	Groyne height $h_g$ (m)	Groyne area a (m <sup>2</sup> )	conditions
CA	1.4	1.00	1.4	5.5	1.2	0.857	0.255	1.000	0.255	90° bend
E0	2.0	1.00	2	50	4	2.000	0.000	0.000	0.000	2 m channel
EE,EH	20.0	8.00	160	150	160	1.000	7.000	8.4	56.28	2 groynes
EW	8.0	2.00	16	100	20	1.250	6.000	2.000	12.000	"permeable"
U0	1.7	0.17	0.285	26	0.289	1.013	0.000	0.000	0.000	U bend flume
P0 main channel	1.8	0.19	0.315	50	0.254 (1)	0.806	0.000	0.000	0.000	over bank test
P0 flood plain	4.5	0.04	0.169	50	0.070 (1)	0.414	0.000	0.000	0.000	over bank test
RAa	2.5	0.23	0.575	32	0.200	0.348	0.250	0.230	0.058	Hanover
RAb,RH	2.3	0.18	0.414	12	0.131	0.316	0.400	0.180	0.072	rectangular
REa,REb	2.3	0.18	0.414	12	0.131	0.316	0.400	0.180	0.072	2 groynes
RB	2.3	0.25	0.575	12	0.135	0.235	0.400	0.200	0.080	submerged
RM	2.0	0.18	0.36	12	0.090	0.25	0.340	0.132 (2)	0.045	tapered
RX	2.0	0.18	0.36	12	0.114	0.316	0.320	0.045	0.0144	25% obstruction
RY	2.0	0.18	0.36	12	0.114	0.0316	0.320	0.079	0.0252	44% obstruction
TA	2.0	0.18	0.266	12	0.091	0.342	0.405	0.180	0.073	trapezoidal
TB	2.3	0.25	0.414	12	0.092	0.223	0.493	0.200	0.086	submerged
TC	2.0	0.18	0.266	12	0.096	0.359	0.405	0.180	0.073	upstream
TD	2.0	0.18	0.266	12	0.094	0.353	0.405	0.180	0.073	downstream
TE	2.0	0.18	0.266	12	0.090	0.339	0.405	0.180	0.073	2 groynes
SPb	1.5	0.2	0.26	~50	0.040	0.154	0.62	0.103 (3)	0.064	sinuous

Note:

- (1) Split of flow between main channel and flood plain estimated from experimental data
- (2) Measured plan from bank to tip
- (3) Average groyne height ( $a/L_t$ )





**Table 6** *Dimensionless parameters of tests*

run code	Channel aspect ratio B/H	Length ratio B/X	Froude number Fr	Manning's n	Relative groyne length $L_g/B$	Relative groyne height $h_g/H$	Blockage ratio a/A	Groyne shape
CA	1.400	0.255	0.274	0.020	0.182	1.000	0.182	round
E0	2.000	0.040	0.639	0.020	0.000	0.000	0.000	no groyne
EE,EH	2.500	0.133	0.113	0.020	0.350	1, 0.5	0.35, 0.175	rectangular
EW	4.000	0.080	0.282	0.020	0.750	1.000	0.750	permeable
U0	10.131	0.065	0.790	0.012	0.000	0.000	0.000	no groyne
P0 main channel	9.595	0.036	0.591	0.00835	0.000	0.000	0.000	no groyne
P0 flood plain	119.681	0.090	0.661	0.00835	0.000	0.000	0.000	no groyne
RAa	10.870	0.078	0.232	0.020	0.100	1.000	0.100	rectangular
RAb,RH	12.778	0.192	0.238	0.020	0.174	1.000	0.174	rectangular
RE	12.778	0.192	0.238	0.013	0.174	1.000	0.174	rectangular
RB	9.200	0.192	0.150	0.013	0.174	0.800	0.139	rectangular
RM	11.111	0.167	0.188	0.020	0.17	0.733	0.125	tapered
RX	11.111	0.167	0.238	0.020	0.16	1.000	0.04	25% obstruction
RY	11.111	0.167	0.238	0.020	0.16	1.000	0.07	44% obstruction
TA	11.111	0.167	0.257	0.020	0.203	1.000	0.274	rectangular
TB	9.200	0.192	0.142	0.020	0.214	0.800	0.208	rectangular
TC	11.111	0.167	0.270	0.020	0.203	1.000	0.274	rectangular
TD	11.111	0.167	0.266	0.020	0.203	1.000	0.274	rectangular
TE	11.111	0.167	0.255	0.020	0.203	1.000	0.274	rectangular
SPb	7.5	-0.03	0.110	-	0.413	0.515	0.246	sinuous

**Table 7 Validation tests**

run code	notes	block correction	Number of cells				comp. time (minutes)	number of iterations	seconds/iteration	Recirculation Length measured from d/s groyne		Separation width
			X	Y	Z	total				Experiment (1)	SSIIM (2)	
RAa-13	Hanover	k,ε	35	19	10	6650	-	349	3.1			
RAb-1	Rectangular	k,ε	45	31	13	13950	-	782	-	3 to 4	5 to 5.2	0.62
RB-1	Submerged	k,ε	45	39	13	13950	650	700	55.7	3 to 6	3 to 3.5	0.52
REa-1	1m apart	no	56	31	10	17360	-	-	-	2 to 4	4.6	0.62
REb-1	2m apart	no	59	31	10	18290	1017	860	70.9	4 to 4.3	4.3 to 4.5	0.62
RM-1	Tapered	no	45	31	10	13950	388	454	51	-	2.2 to 2.5	0.32
RX-1	25% obstruction	no	45	31	10	13950	1201	1389	51.9	-	-	-
RY-1	44% obstruction	no	45	31	10	13950	2298	2658	51.8	-	-	-
P0	No groyne	no	49	20	4	3920	-	-	-	-	-	-
TA-9	Rectangular	k,ε	54	29	12	18792	1200	1010	85.9	6	5	0.75
TB-1	Submerged	no	54	29	10	15660	786	864	54.58	4	3	0.85
TC-1	Upstream	no	57	29	10	16530	3925	4688	50.2	5.8	3.5	0.75
TD-1	Downstream	no	57	29	10	16530	3300	3932	49.7	6.5	5.4	0.75
TE-1	1m apart	no	63	29	12	21924	-	-	-	2.5	4.1	0.75

**Notes**

- (1) Recirculation length was determined experimentally using the rod and string method described in Section 7.
- (2) This was determined numerically from the location of  $V_x = 0$  close to the bank at various heights as shown in Figures 8.7 and 9.5.
- (3) Separation width is determined numerically from the maximum distance from the bank of the contour of  $V_x = 0.5V$  measured at mid-depth







## Figures



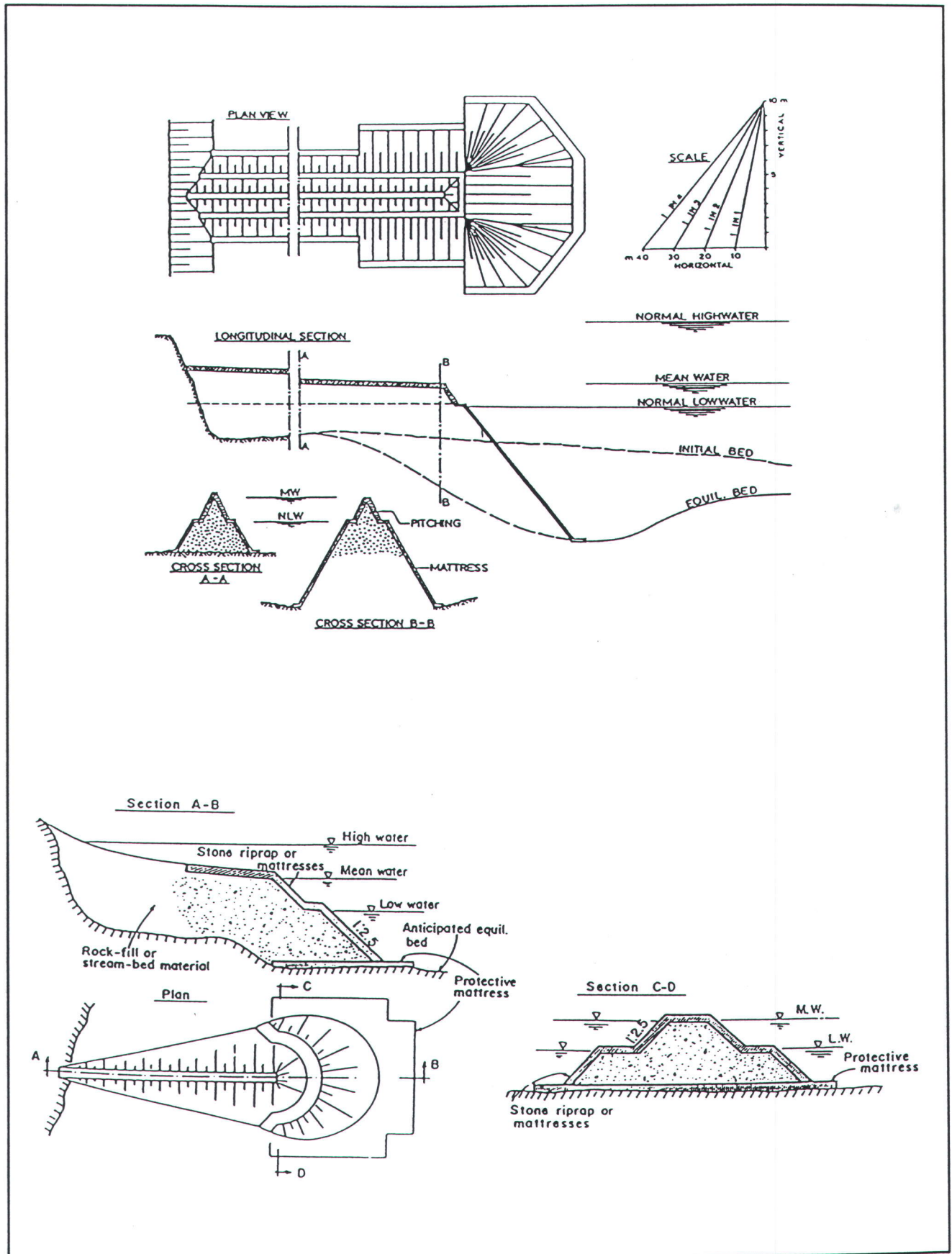
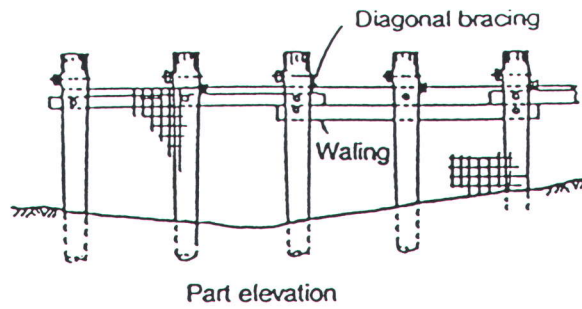
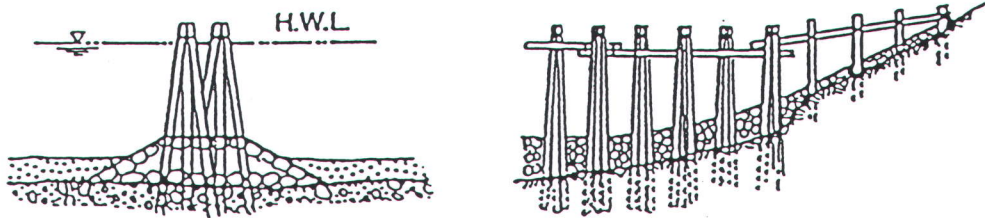


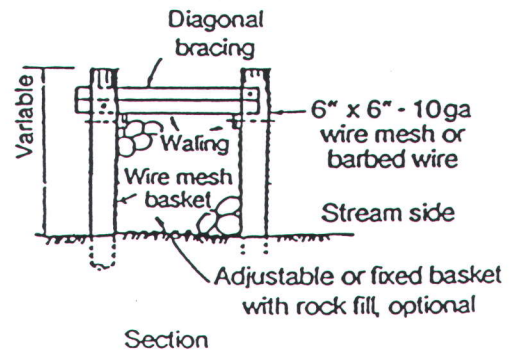
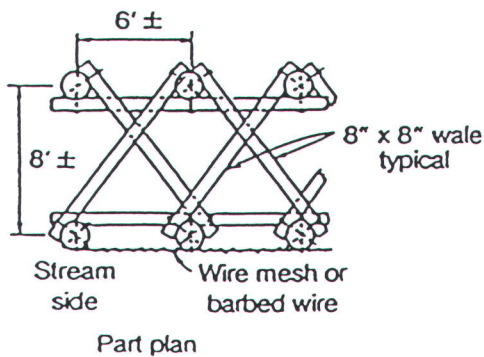
Figure 2.1 Typical impermeable groyne structures



(a) Single row timber pile with wire fence

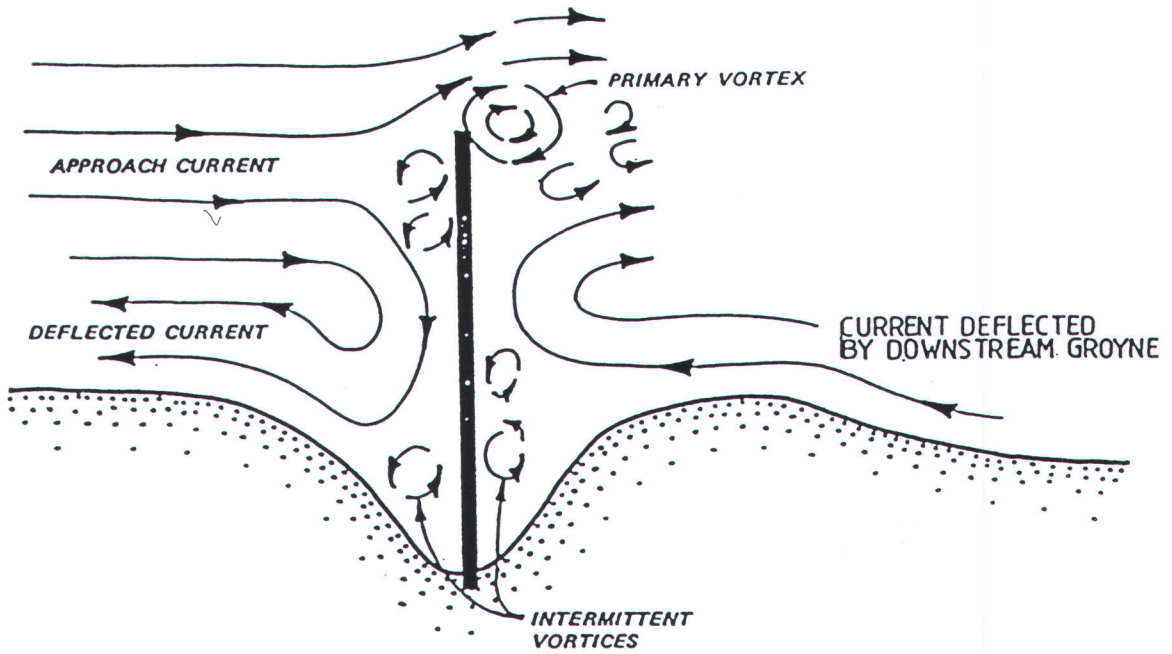


(c) Pile clusters

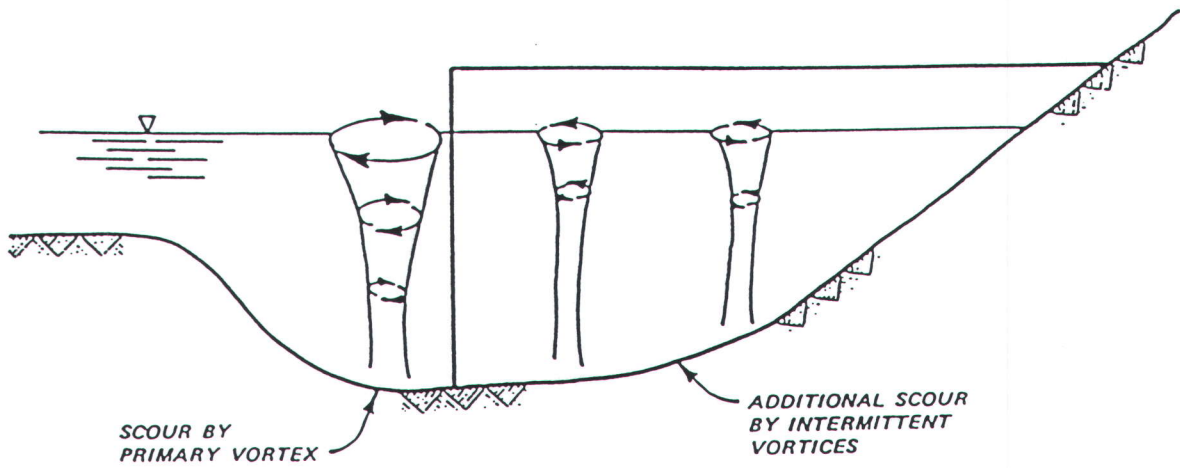


(b) Double row timber piles with rocks and wire fence

Figure 2.2 Permeable timber pile groynes (after Chang)



Planview: Flow patterns at groyne



Elevation : Scour hole profile along groyne

Figure 2.3 Local vortex system around a groyne (after Copeland)

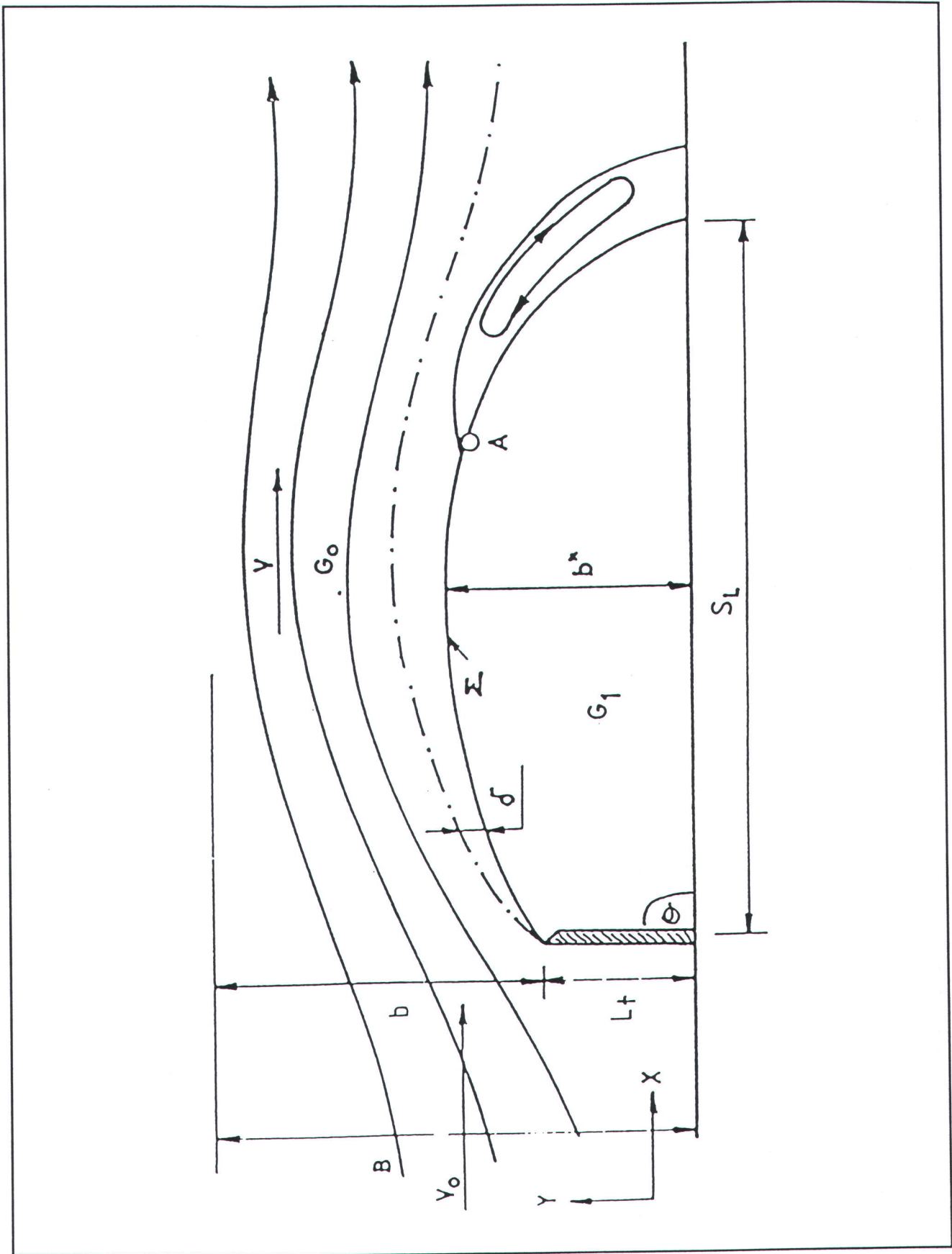
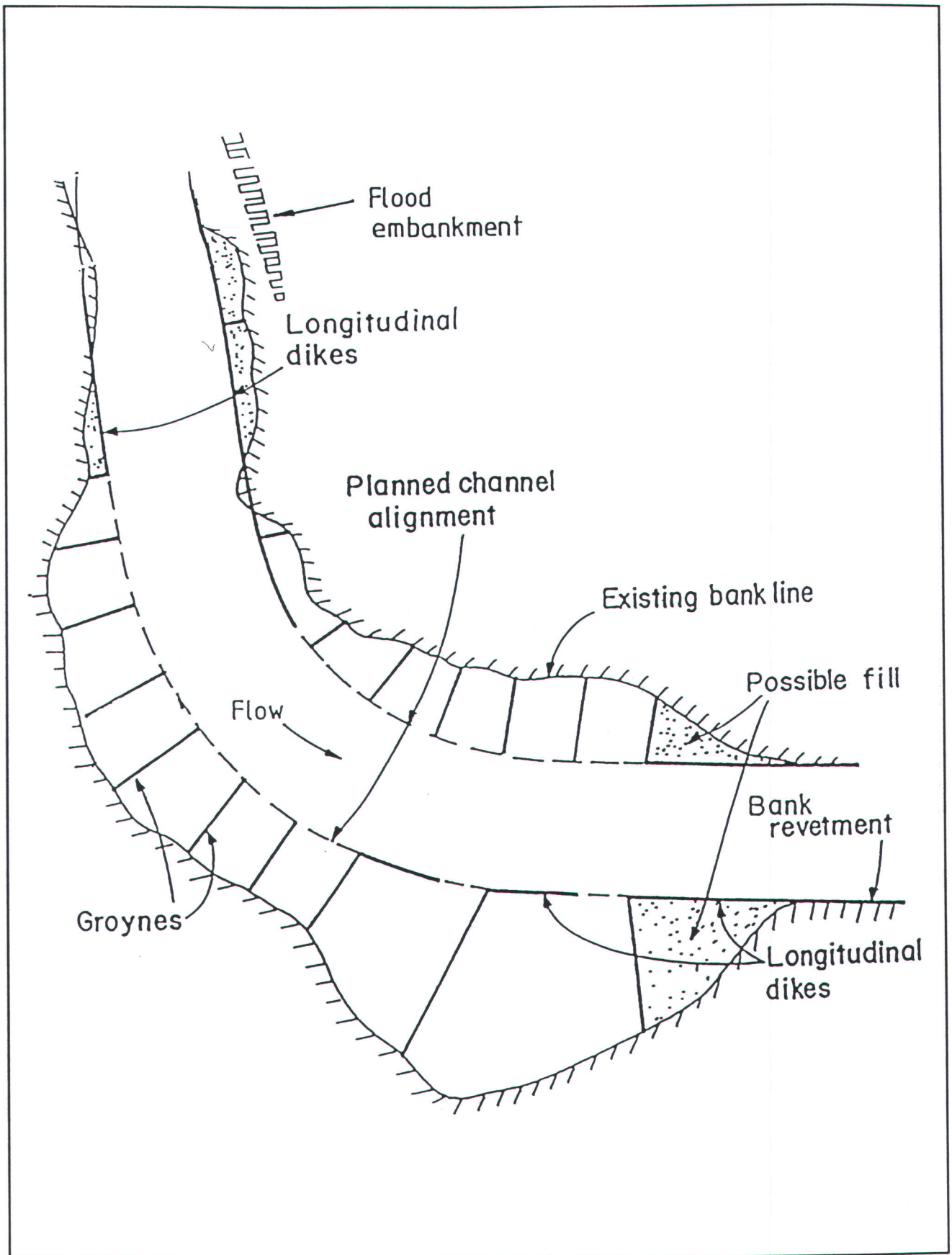


Figure 2.4 Plan view of flow around a groyne (after Bognar and Hanko)



**Figure 2.5** Typical layout of training work for channelisation (after Kinori and Mevotach)

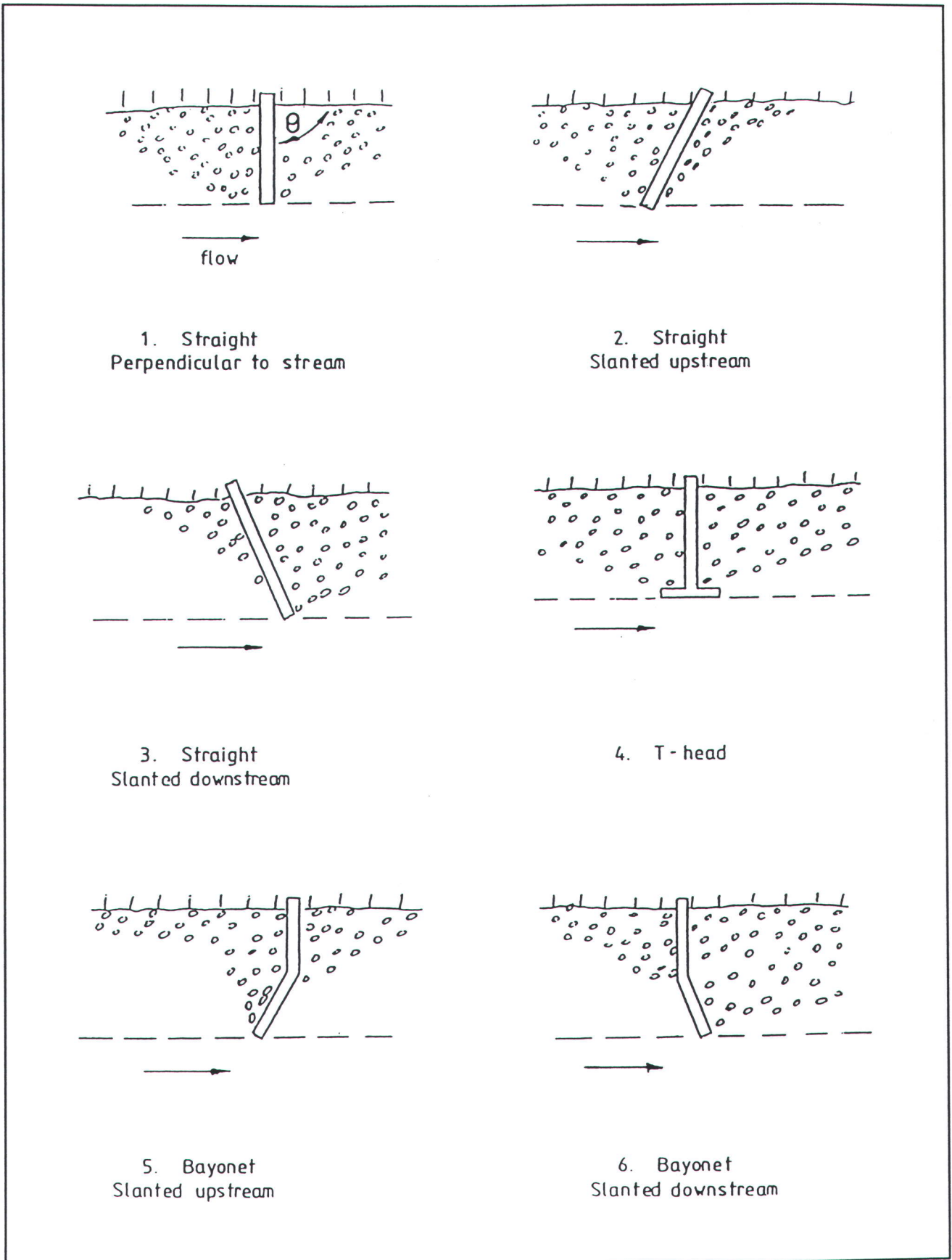
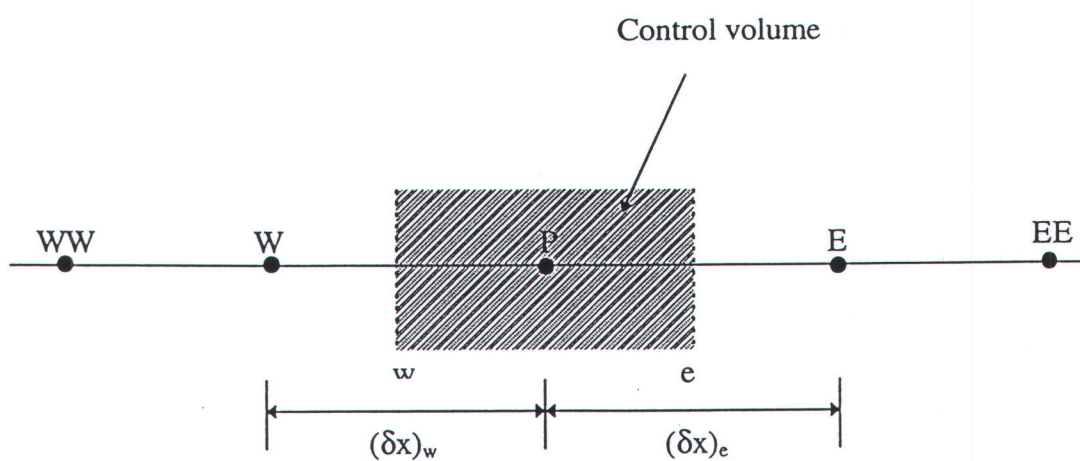


Figure 2.6 Plan shapes of groynes



Typical 1-D grid-points

Figure 4.1 Notation for grid points and faces for control volumes

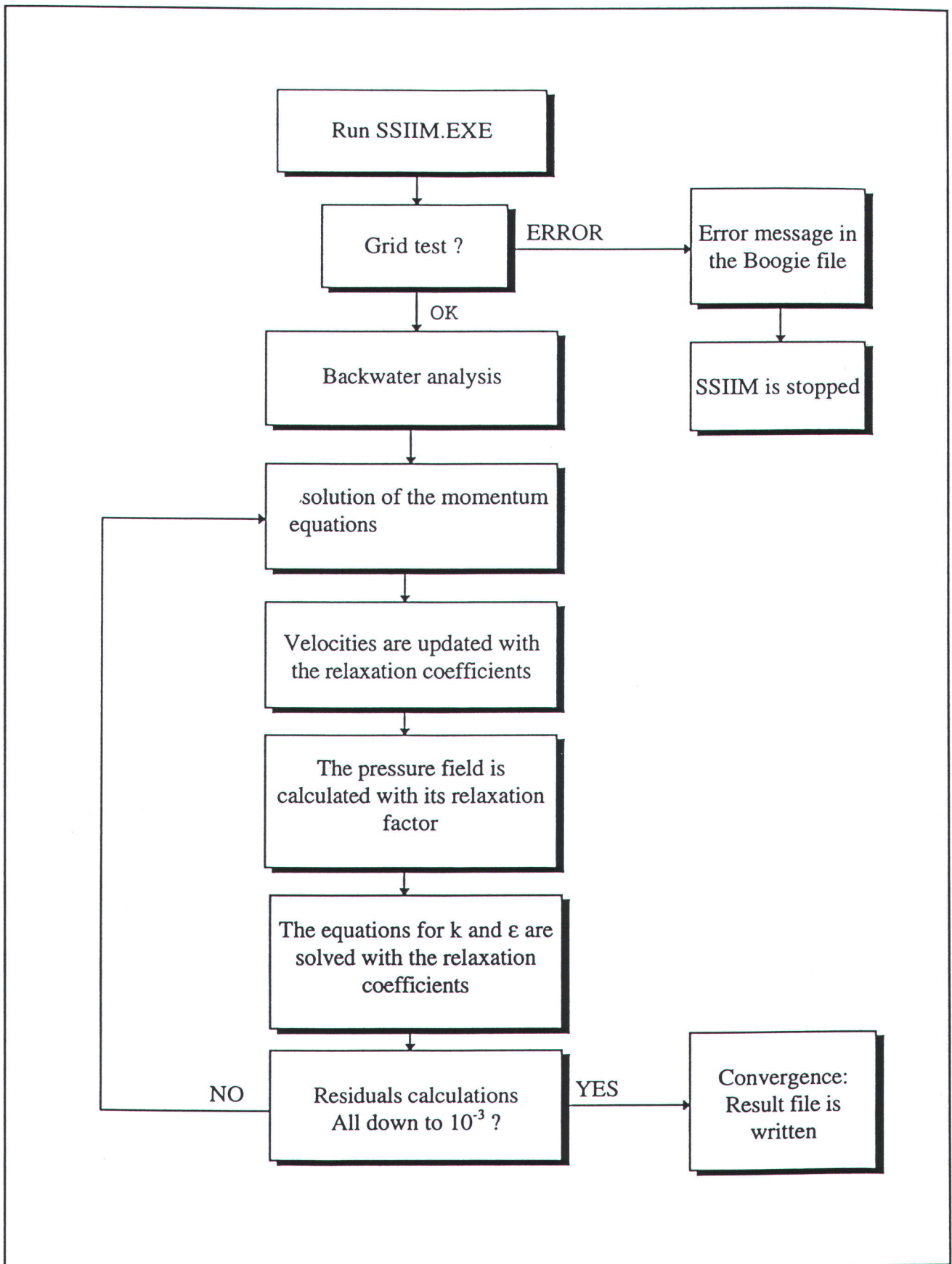


Figure 4.2 Flow chart for SSIIM numerical model

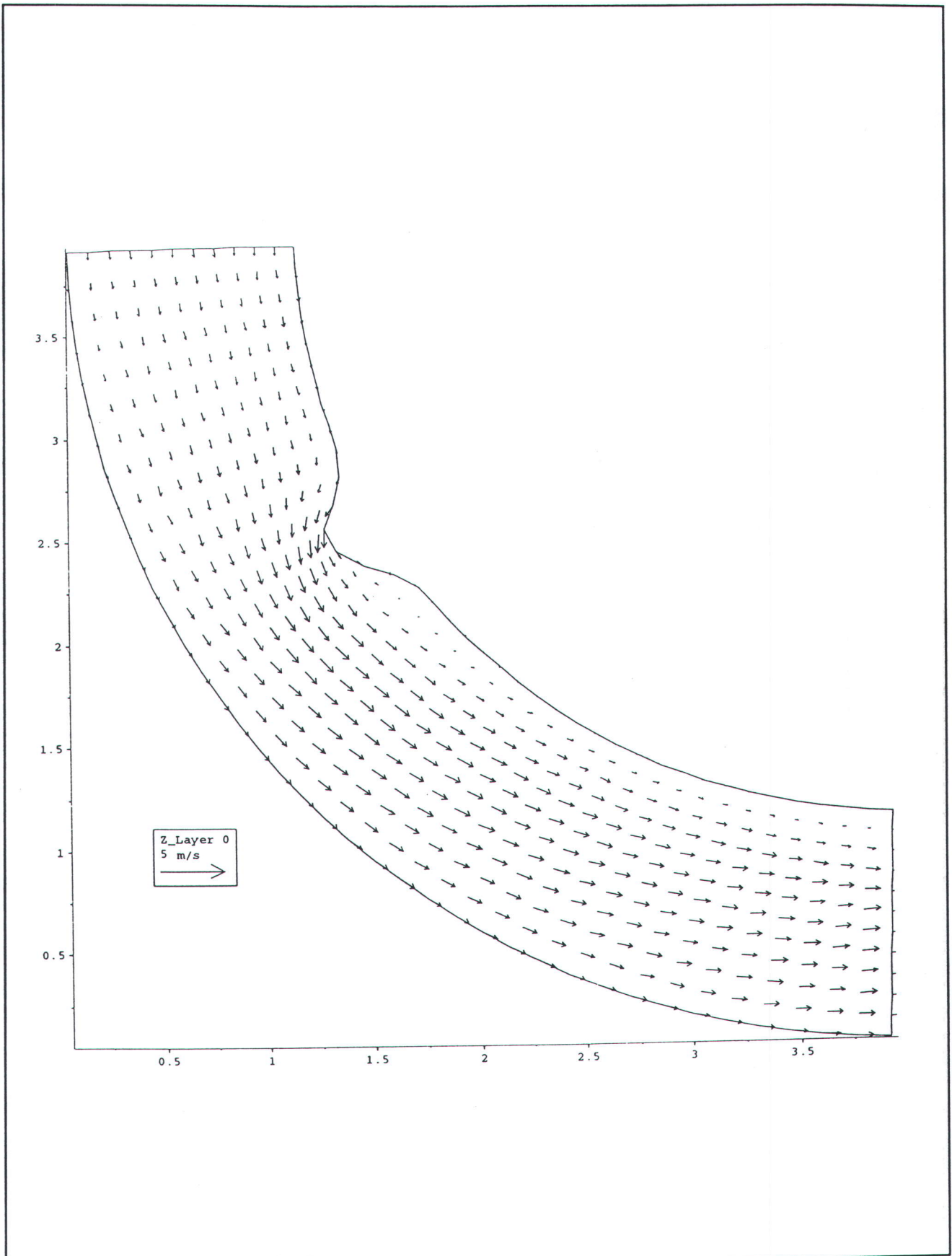


Figure 5.1 Test CA : 90° bend with obstruction - Bed layer



FIG 2 Mid Layer - Rectangular Channel with Half a U-Bend with Obstruction

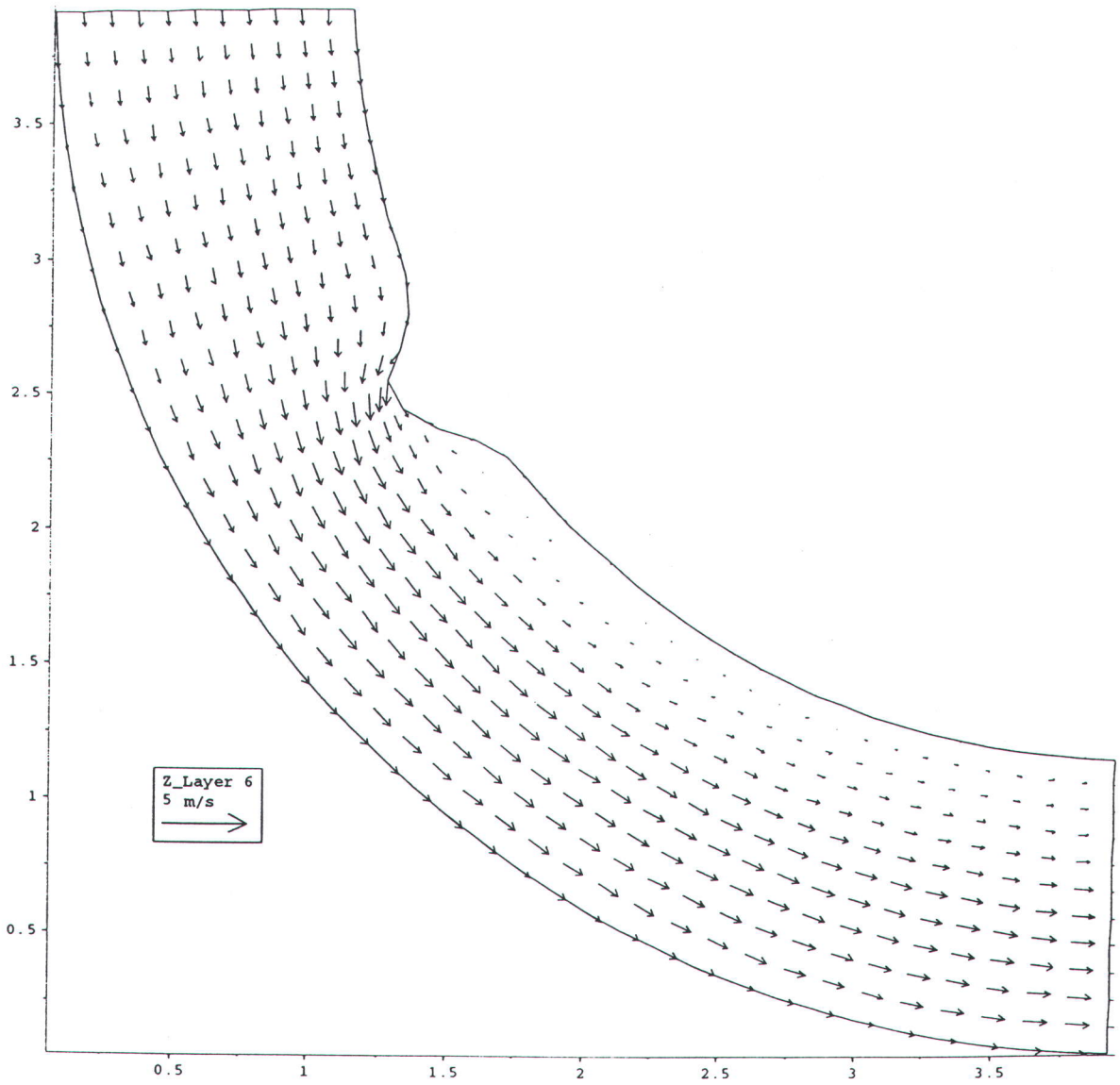


Figure 5.2 Test CA : 90° bend with obstruction - Mid layer



FIG 3 Surface Layer - Rectangular Channel with Half a U-Bend with Obstruction

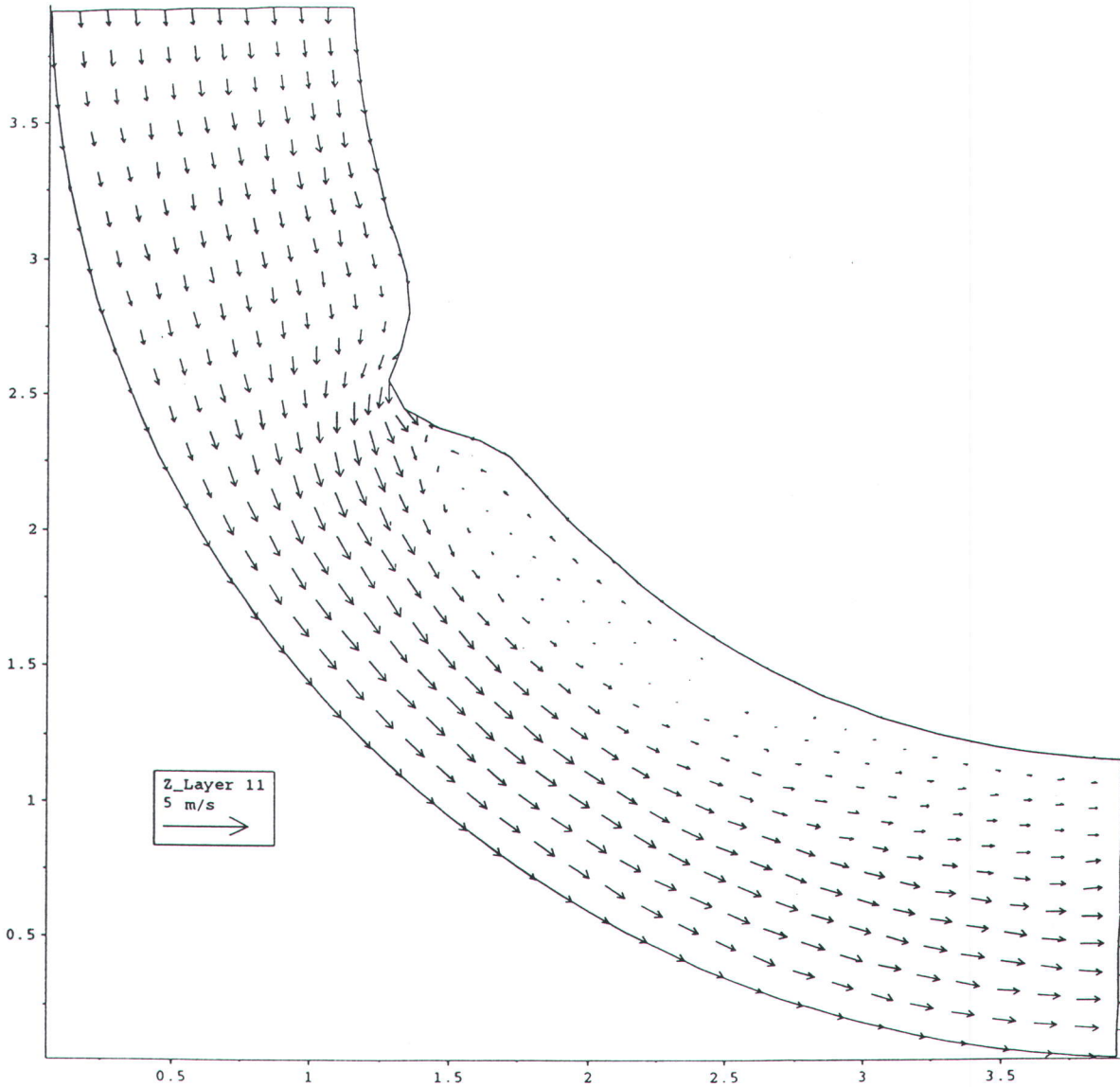


Figure 5.3 Test CA : 90° bend with obstruction - Surface layer

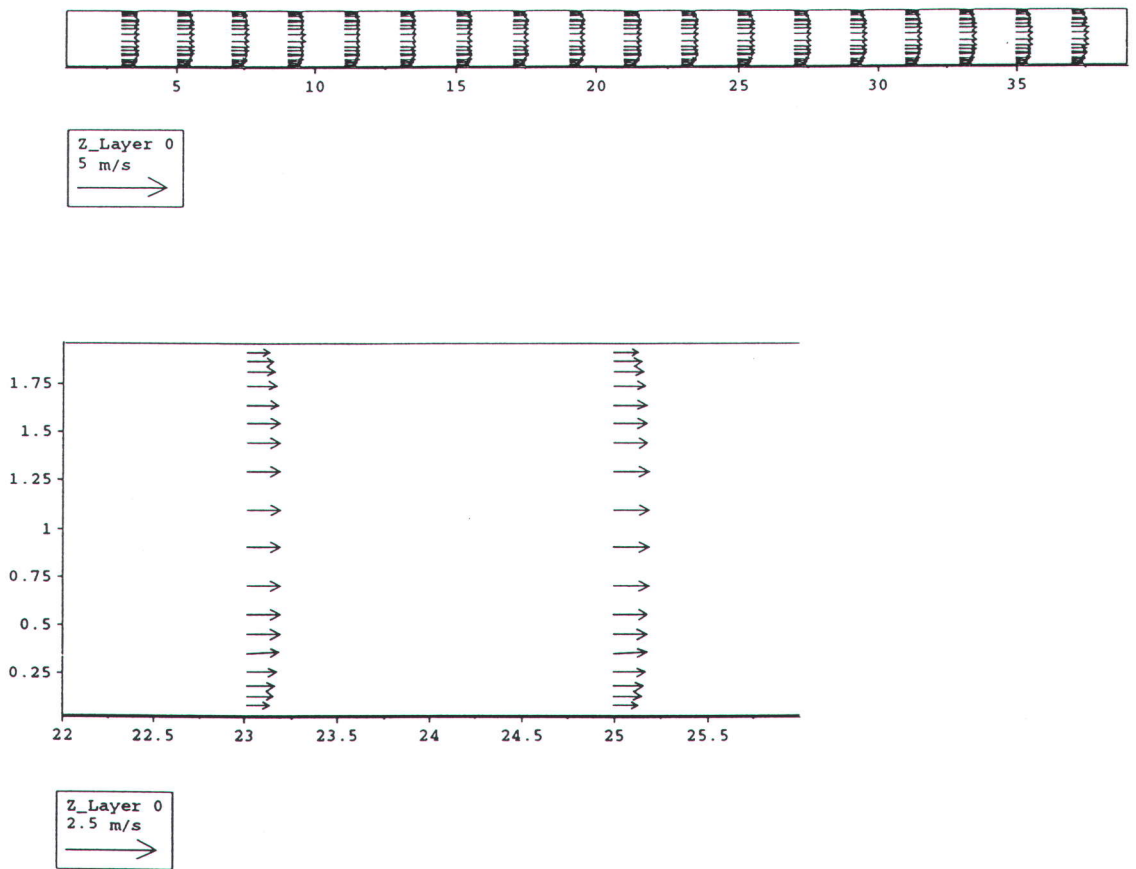
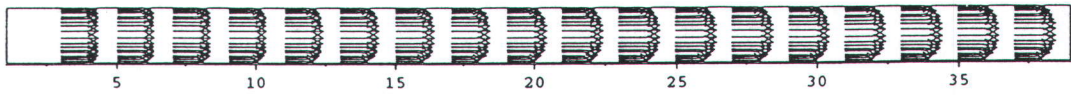
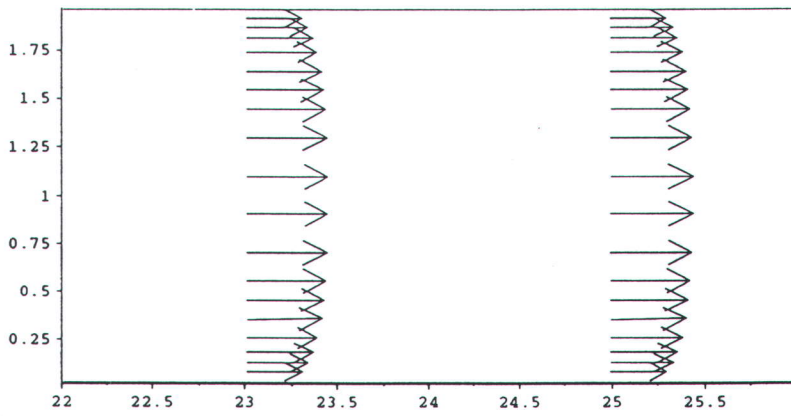


Figure 5.4 Test EO : straight channel - refined mesh - Bed layer

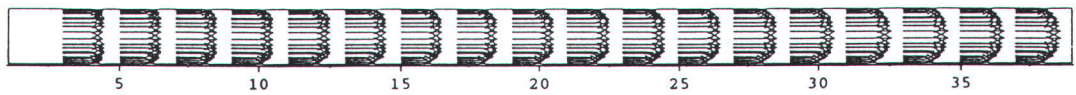


z\_Layer 7  
5 m/s  
→

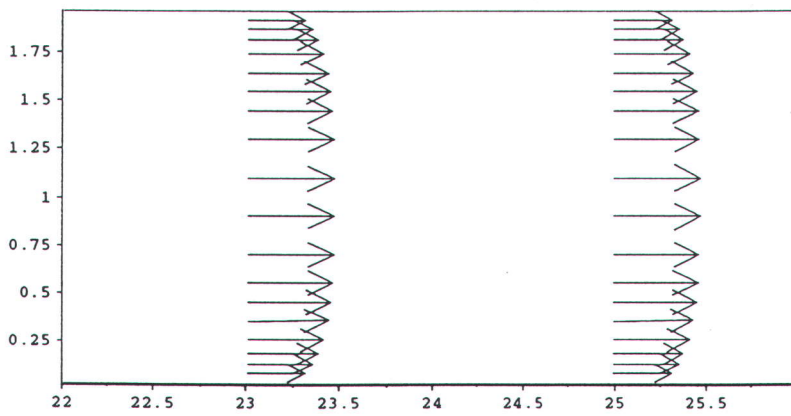


z\_Layer 7  
2.5 m/s  
→

Figure 5.5 Test EO : straight channel - refined mesh - Mid layer



Z\_Layer 13  
5 m/s  
→



Z\_Layer 13  
2.5 m/s  
→

Figure 5.6 Test EO : straight channel - refined mesh - Surface layer

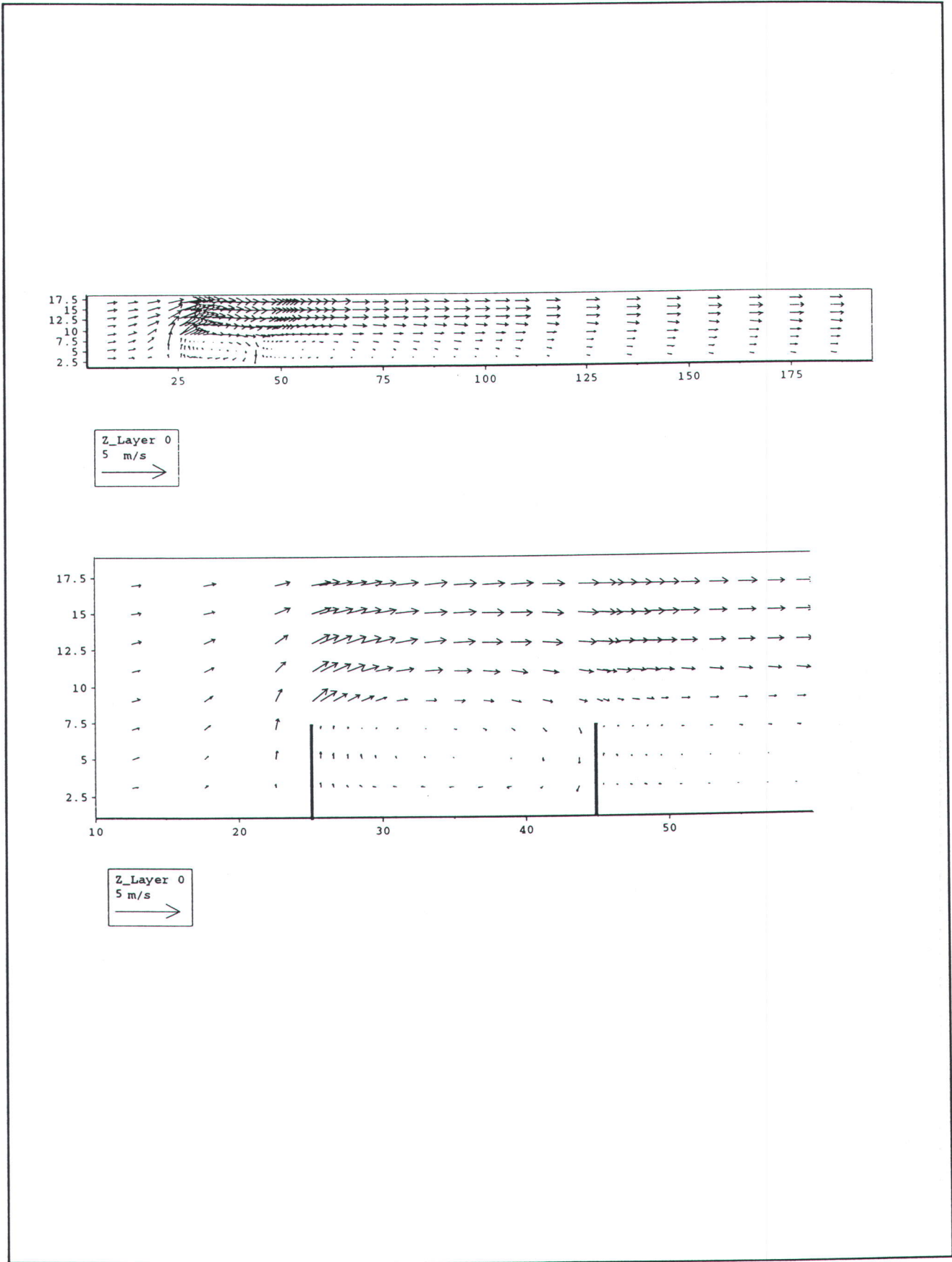


Figure 5.7 Test EE : Two groynes - Bed layer

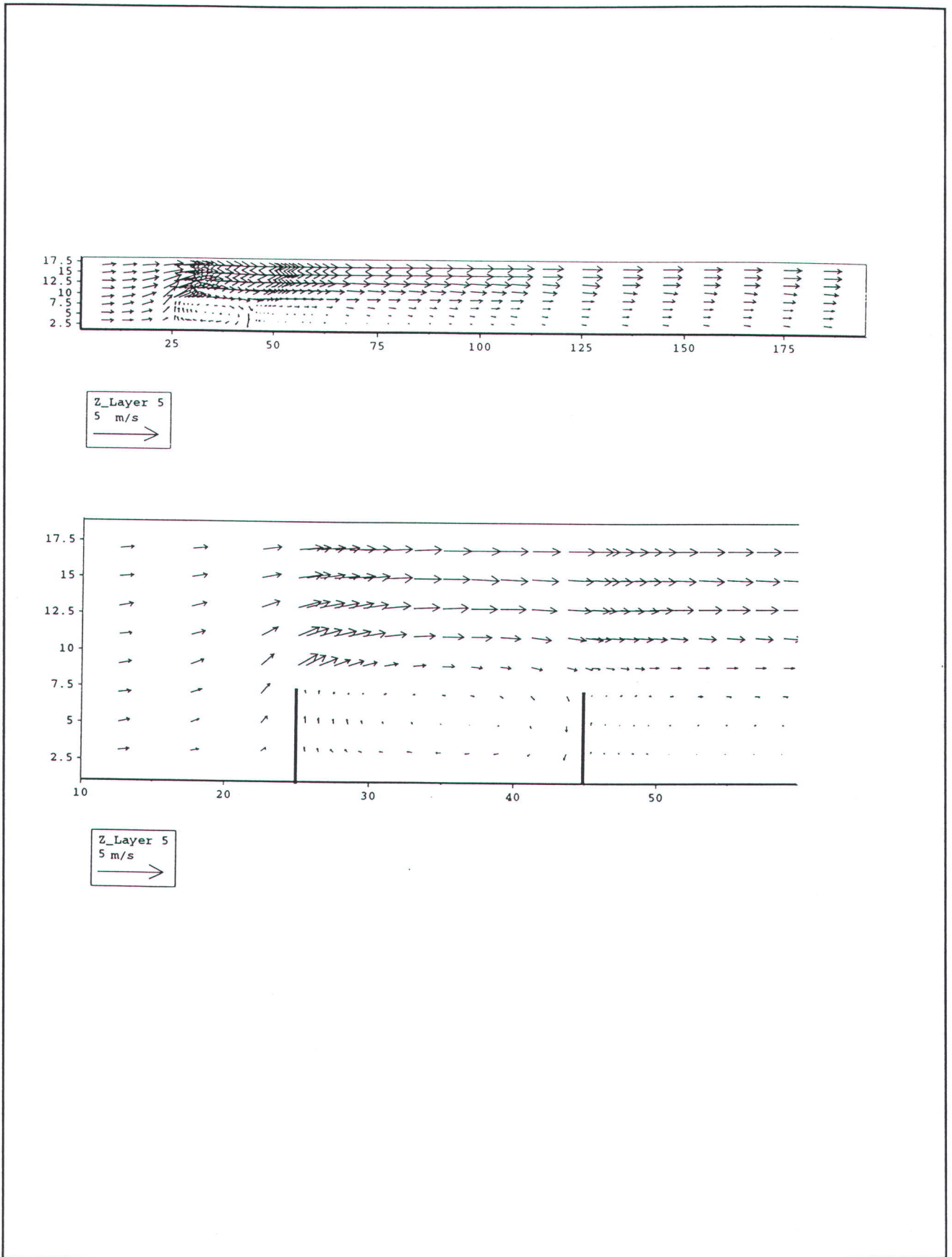
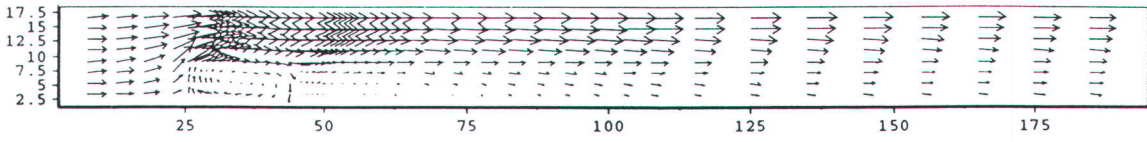
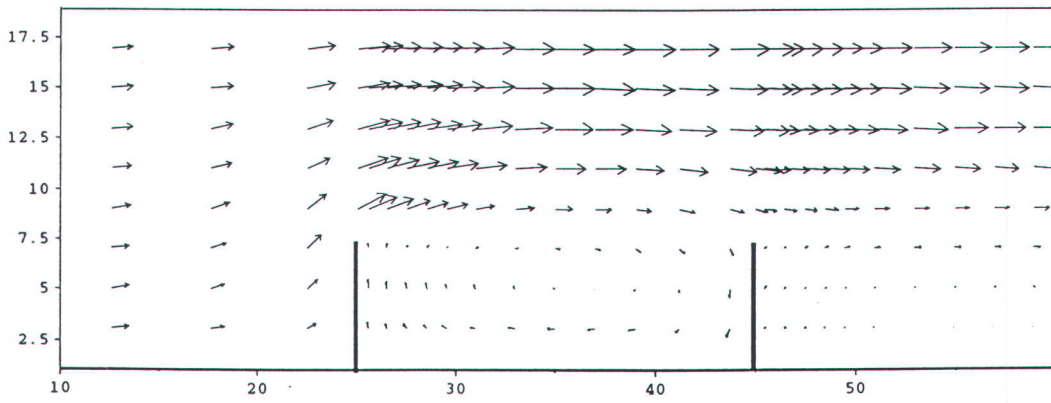


Figure 5.8 Test EE : Two groynes - Mid layer



Z\_Layer 9  
5 m/s  
→



Z\_Layer 9  
5 m/s  
→

Figure 5.9 Test EE : Two groynes - Surface layer

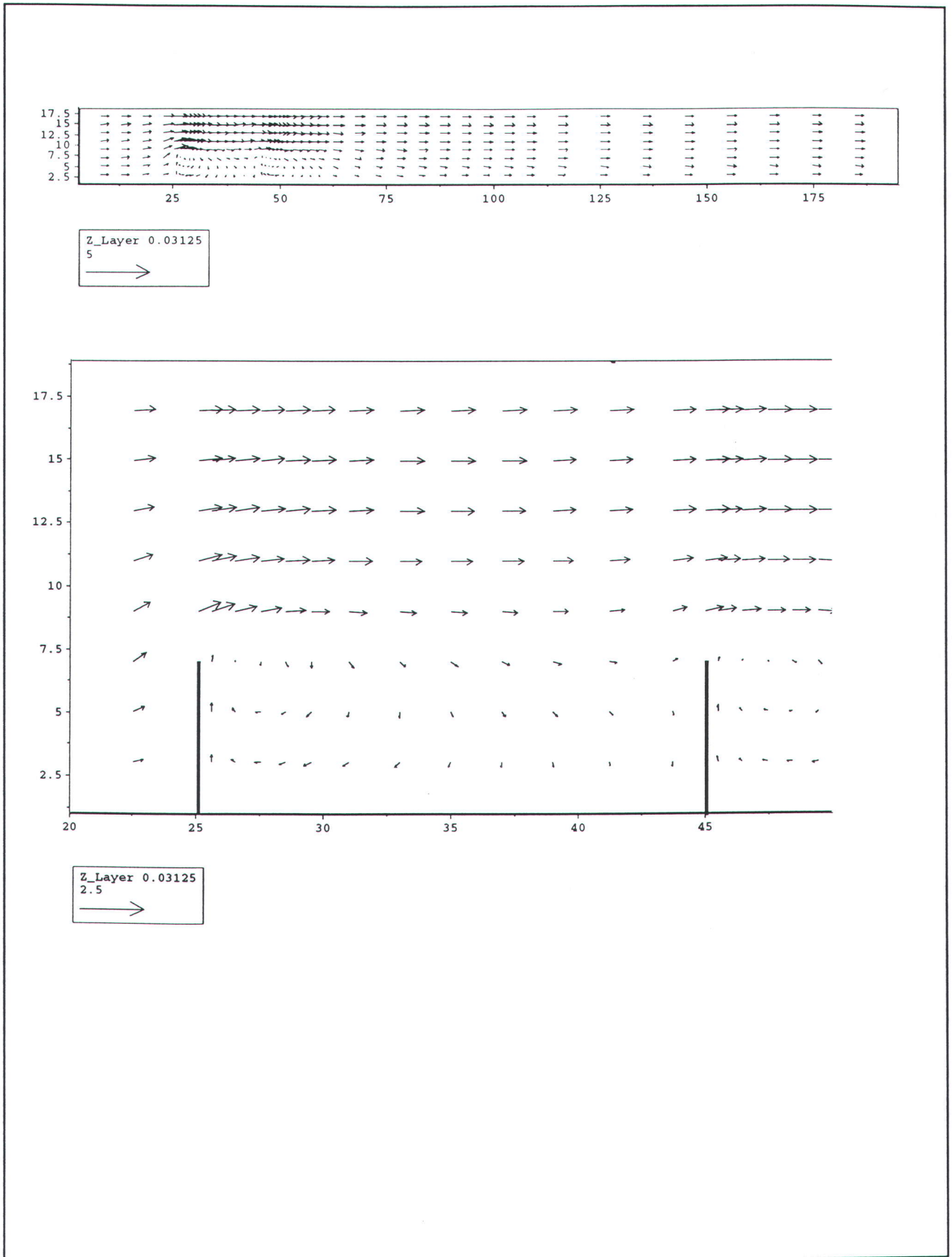
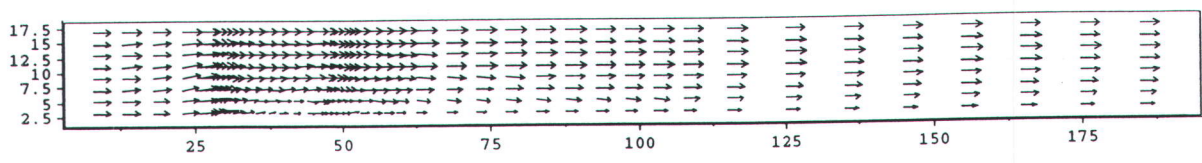


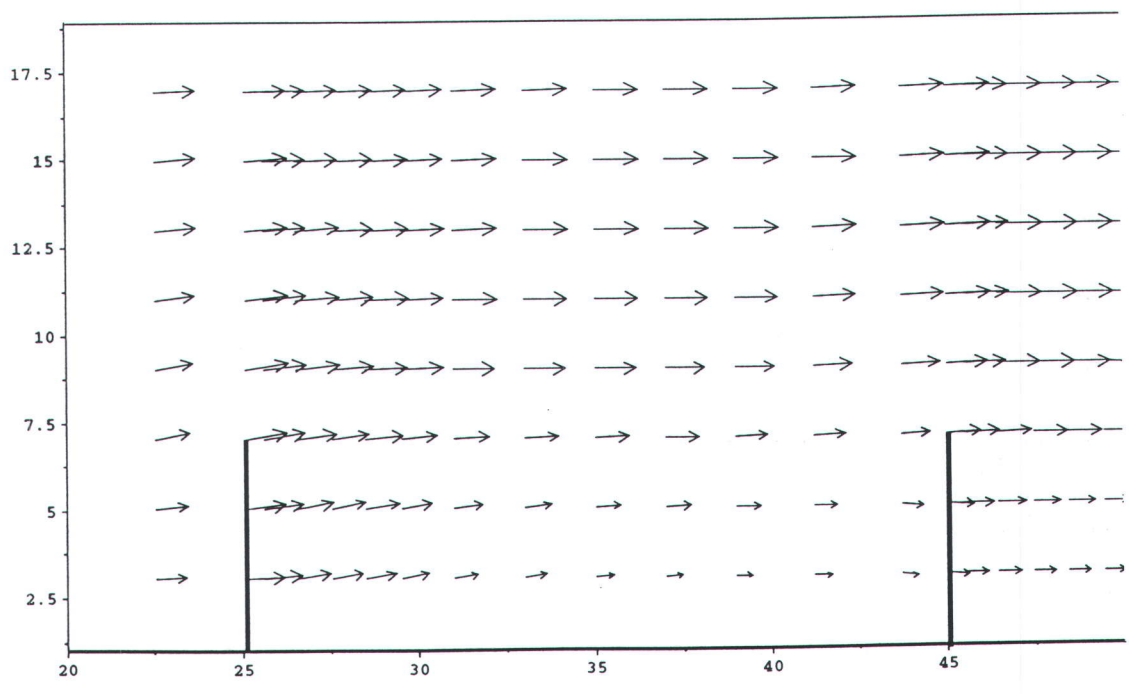
Figure 5.10 Test EH : Two submerges groynes - Bed layer



Velocity vectors at approx. half water depth cell level (m/s)



Z\_Layer 0.437501  
5  
→



Z\_Layer 0.437501  
2.5  
→

Figure 5.11 Test EH : Two submerged groynes - Mid layer

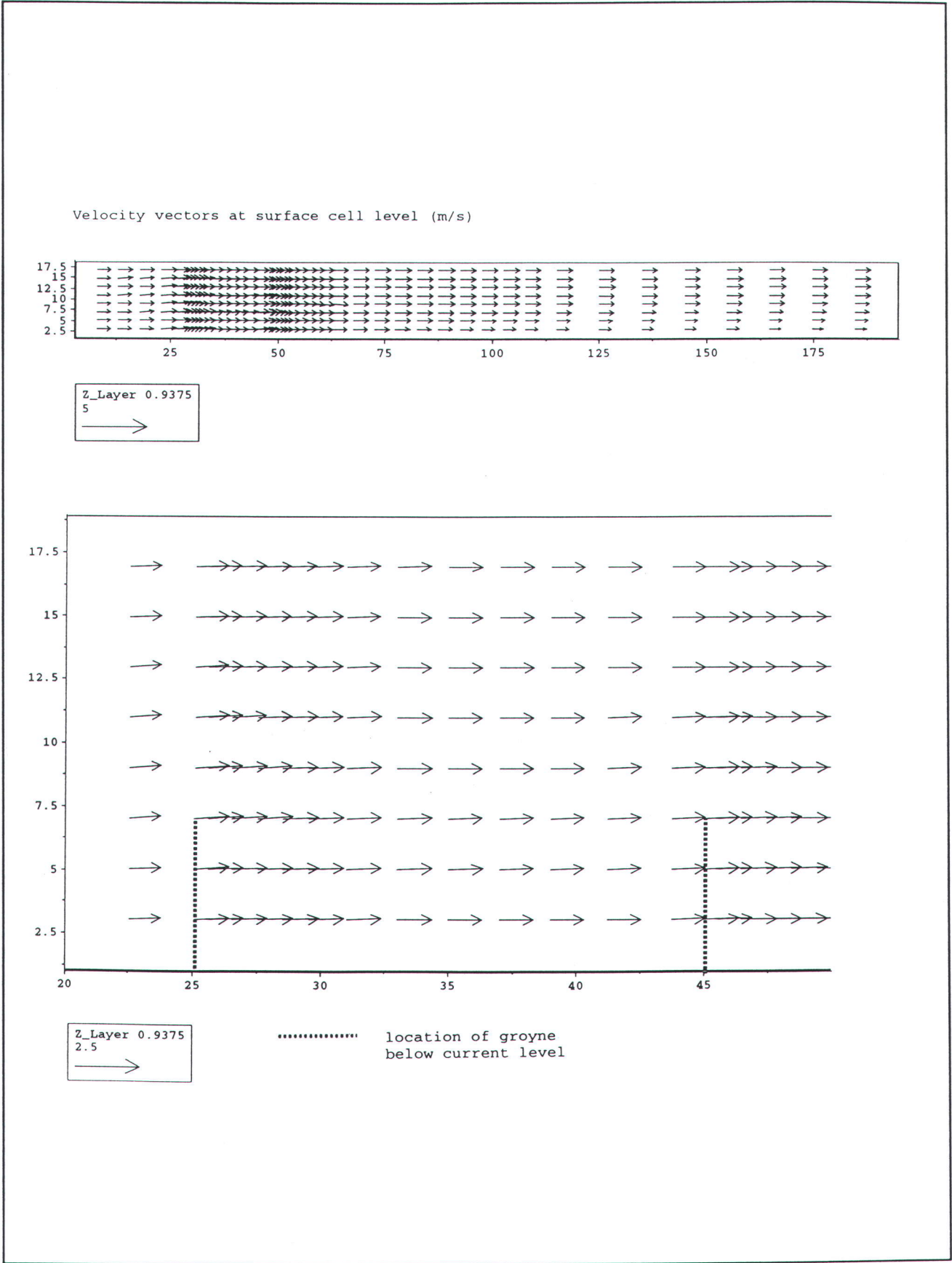
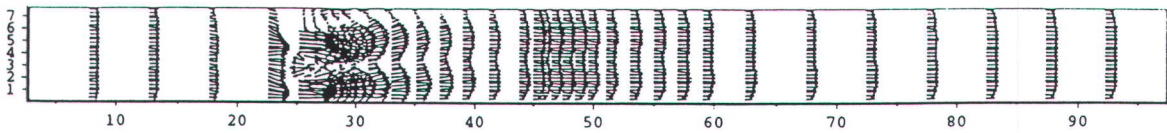


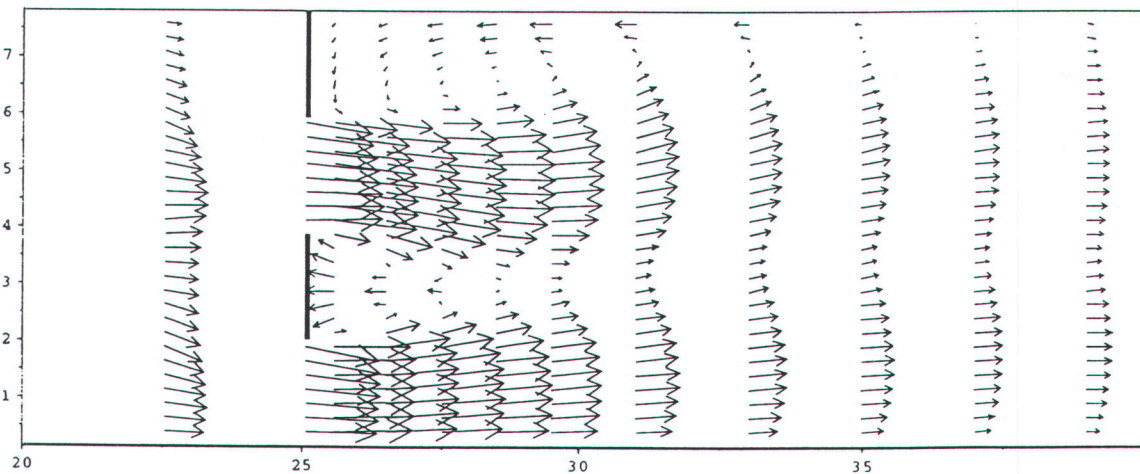
Figure 5.12 Test EH : Two submerged groynes - Surface layer



Velocity vectors at bed cell level (m/s)



Z\_Layer 0.0625  
5



Z\_Layer 0.0625  
2.5



Figure 5.13 Test EW-1 : Porous groyne (one vertical slot) - Bed layer

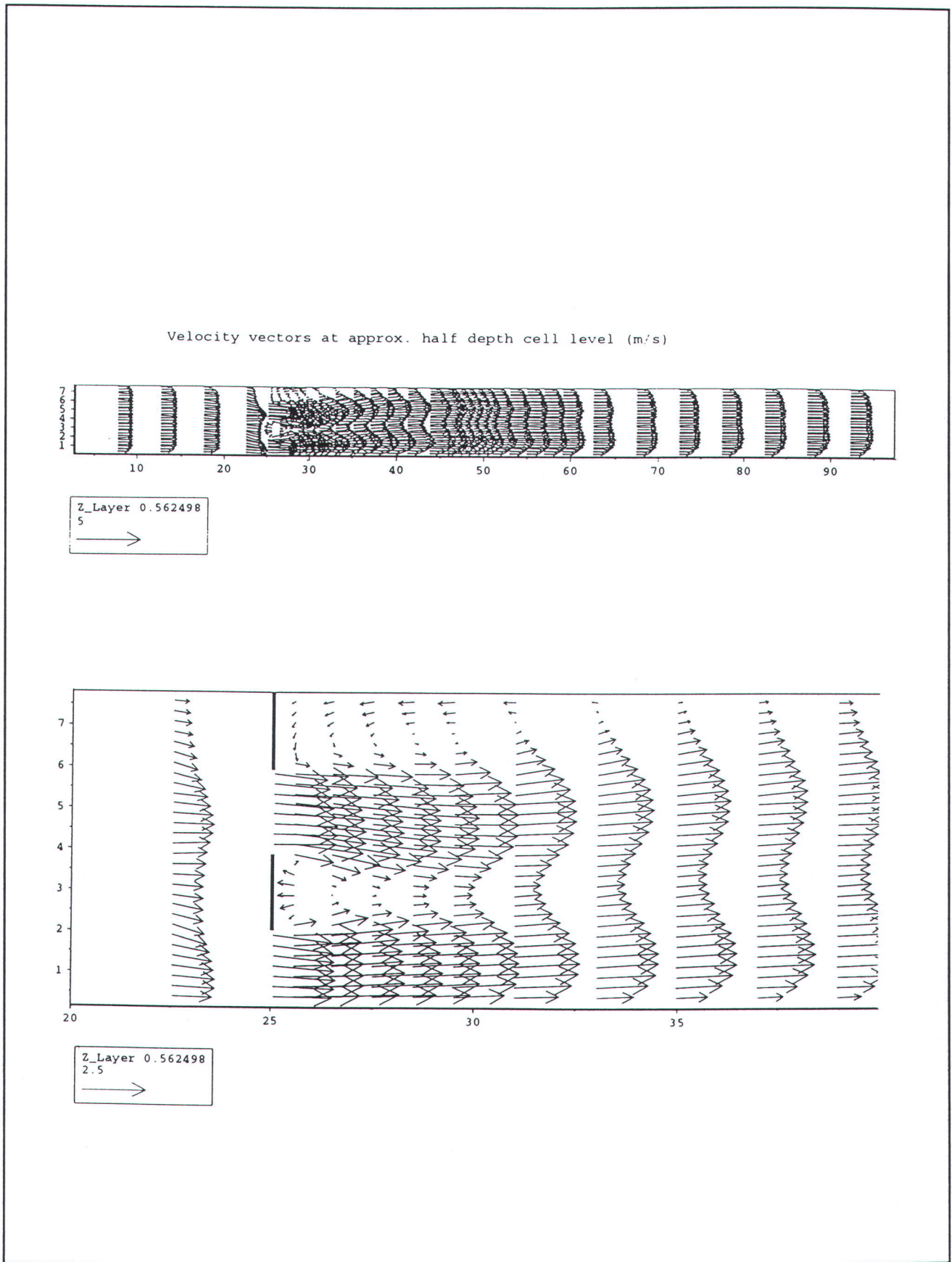
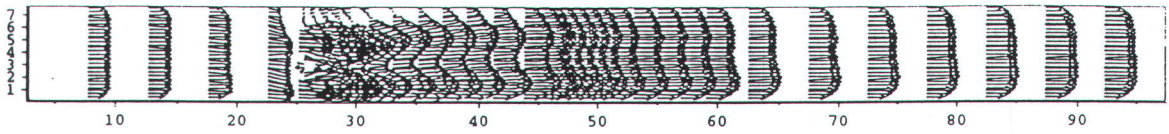


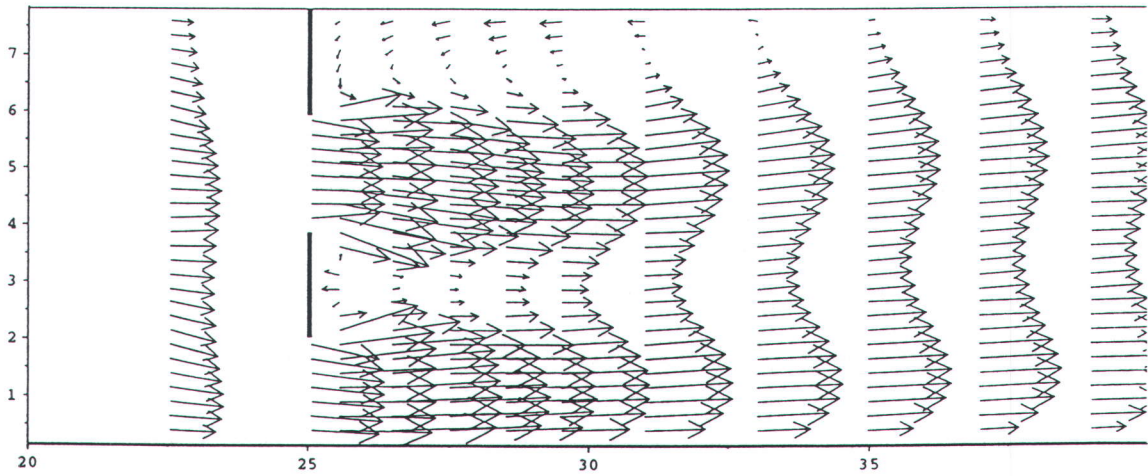
Figure 5.14 Test EW-1 : Porous groyne (one vertical slot) - Mid layer



Velocity vectors at surface cell level (m/s)



Z\_Layer 0.9375  
5  
→

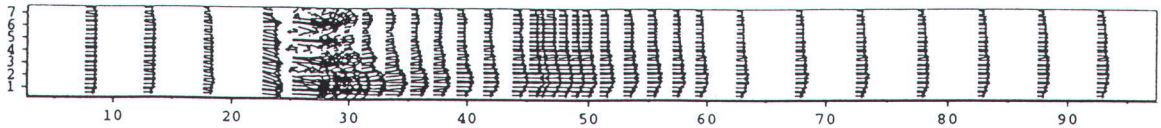


Z\_Layer 0.9375  
2.5  
→

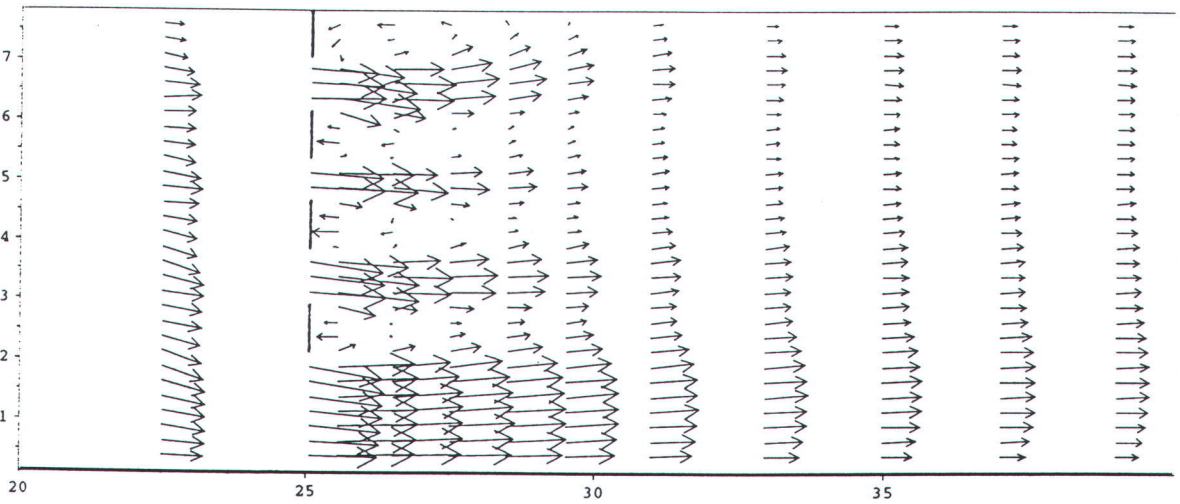
Figure 5.15 Test EW-1 : Porous groyne (one vertical slot) - Surface layer



Velocity vectors at bed cell level (m/s)



Z\_Layer 0.062499  
5  
→

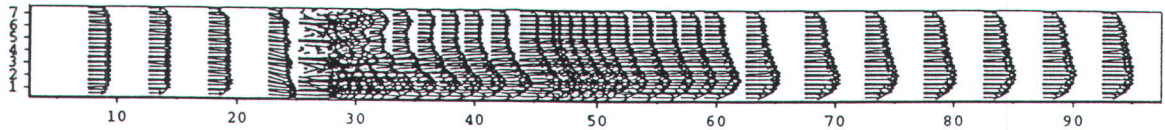


Z\_Layer 0.062499  
2.5  
→

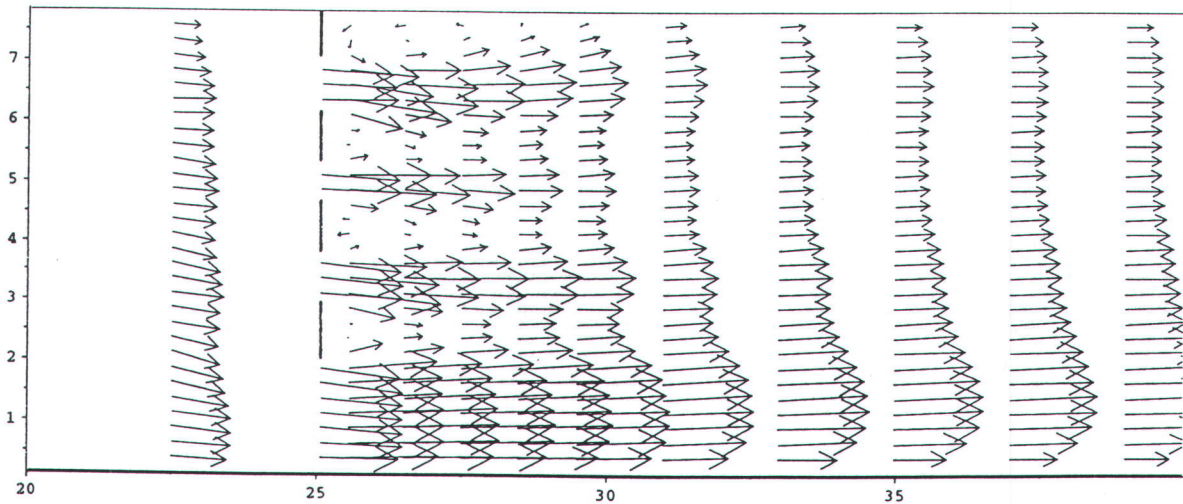
Figure 5.16 Test EW-2 : Porous groyne (3 vertical slots) - Bed layer



Velocity vectors at approx. half depth cell level (m/s)



Z\_Layer 0.562499  
5  
→



Z\_Layer 0.562499  
2.5  
→

Figure 5.17 Test EW-2 : Porous groyne (3 vertical slots) - Mid layer

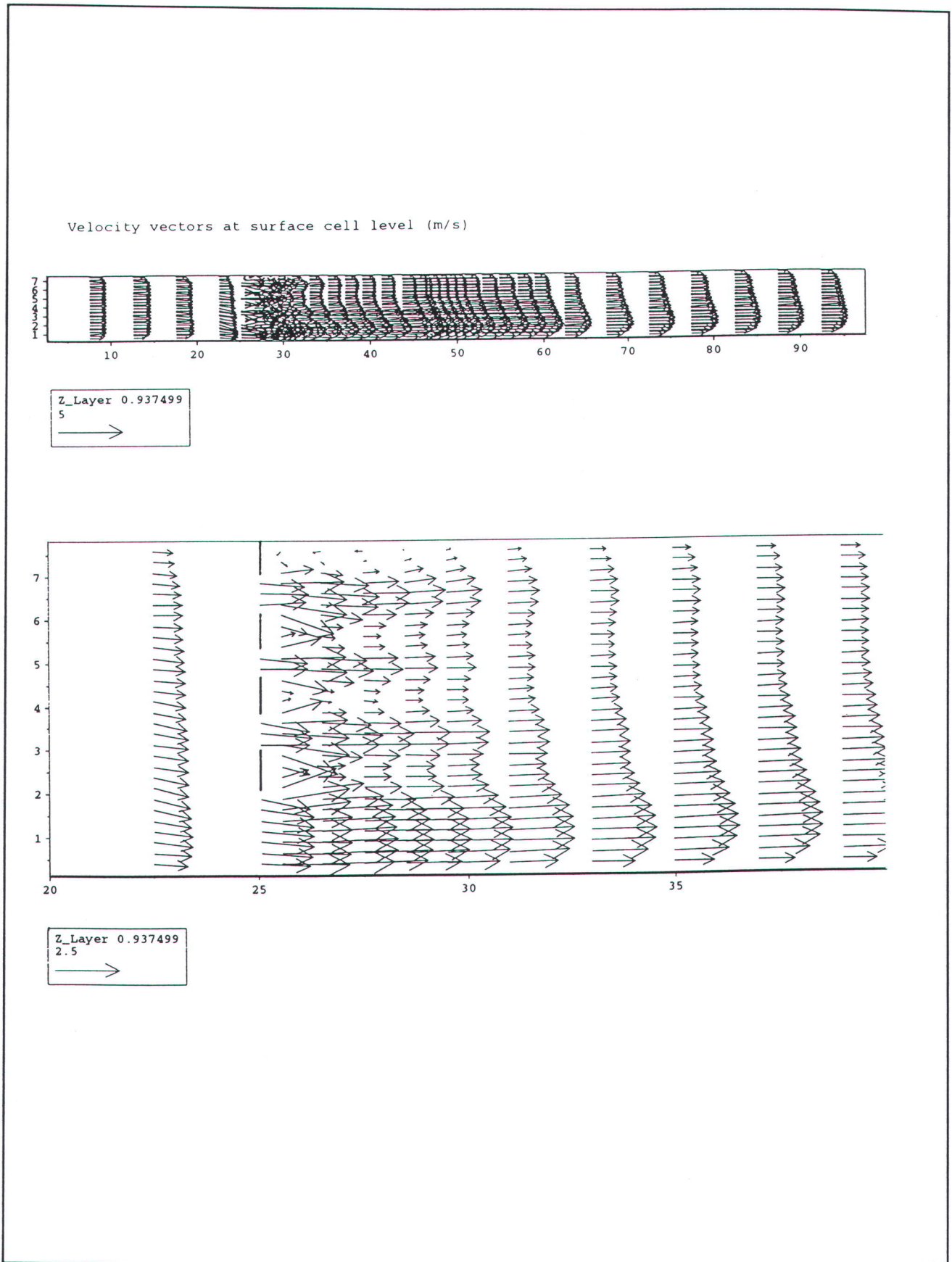
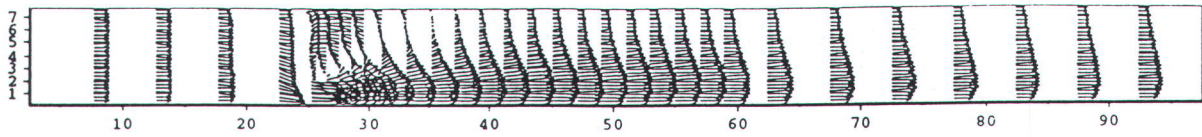


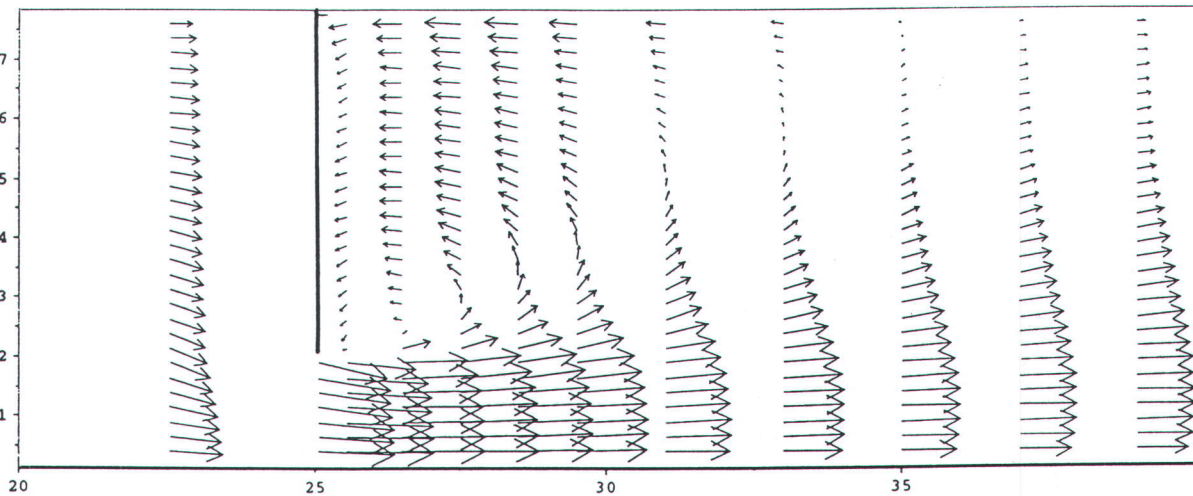
Figure 5.18 Test EW-2 : Porous groyne (3 vertical slots) - Surface layer



Velocity vectors at bed cell level (m/s)



Z\_Layer 0.0625  
5  
→

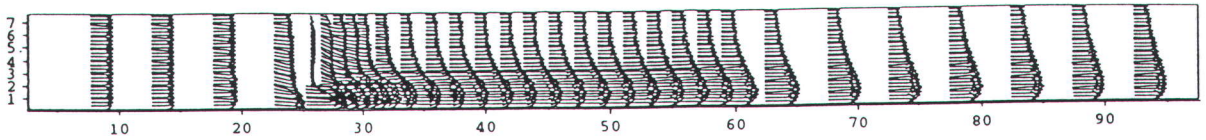


Z\_Layer 0.0625  
2,5  
→

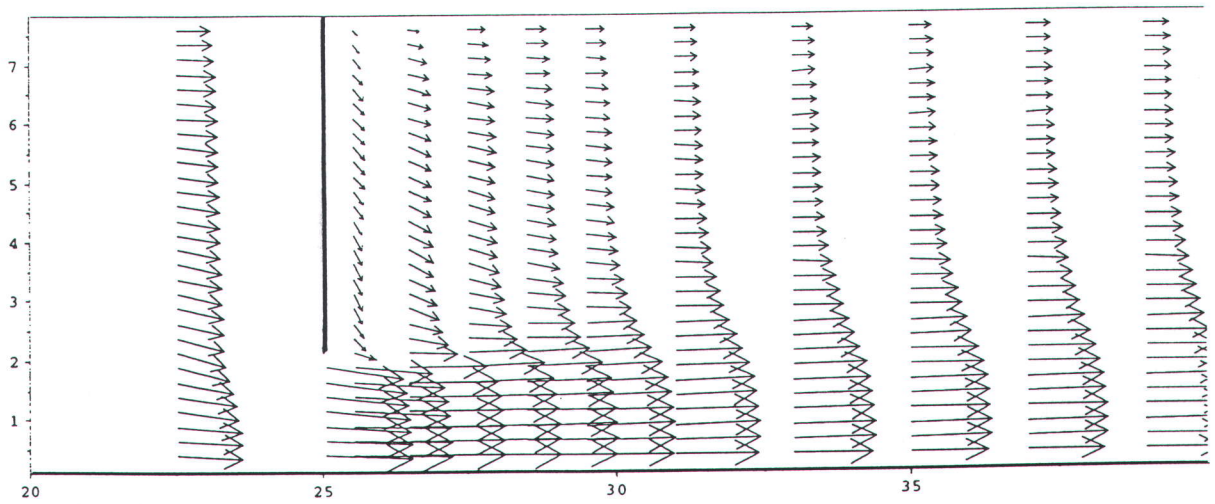
Figure 5.19 Test EW-3 : Porous groyne (submerged) - Bed layer



Velocity vectors at approx. half depth cell level (m/s)



Z\_Layer 0.5625  
5  
→

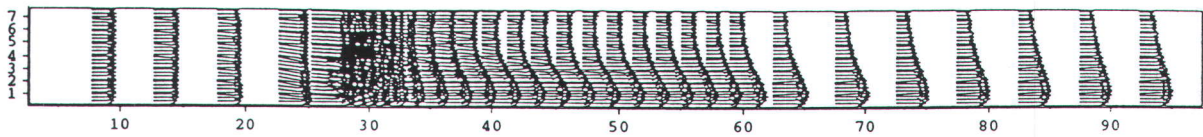


Z\_Layer 0.5625  
2.5  
→

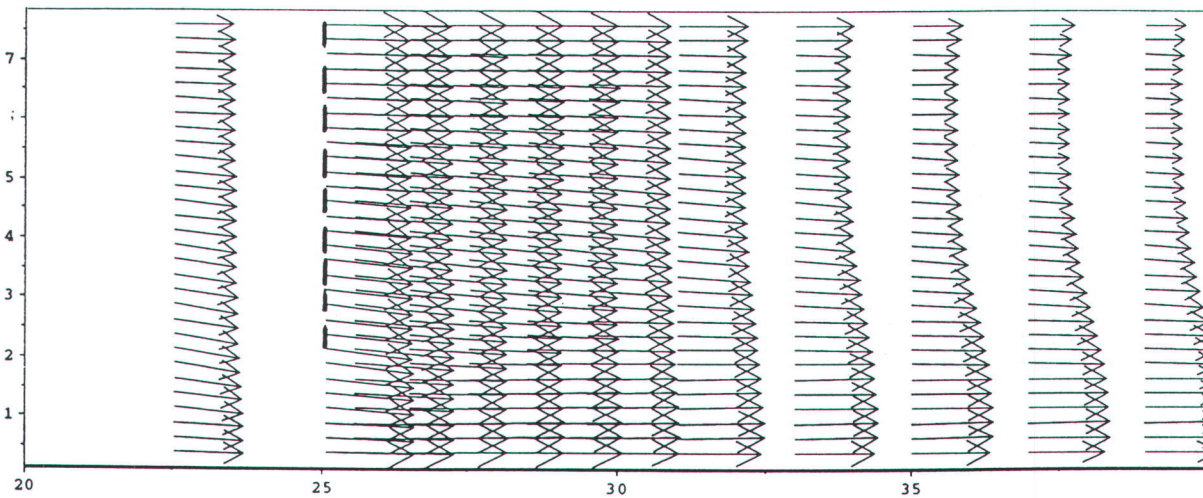
Figure 5.20 Test EW-3 : Porous groyne (submerged) - Mid layer



Velocity vectors at surface depth cell level (m/s)



Z\_Layer 0.9375  
5  
→



Z\_Layer 0.9375  
2:5  
→

--- location of groyne  
below current level

Figure 5.21 Test EW-3 : Porous groyne (submerged) - Surface layer

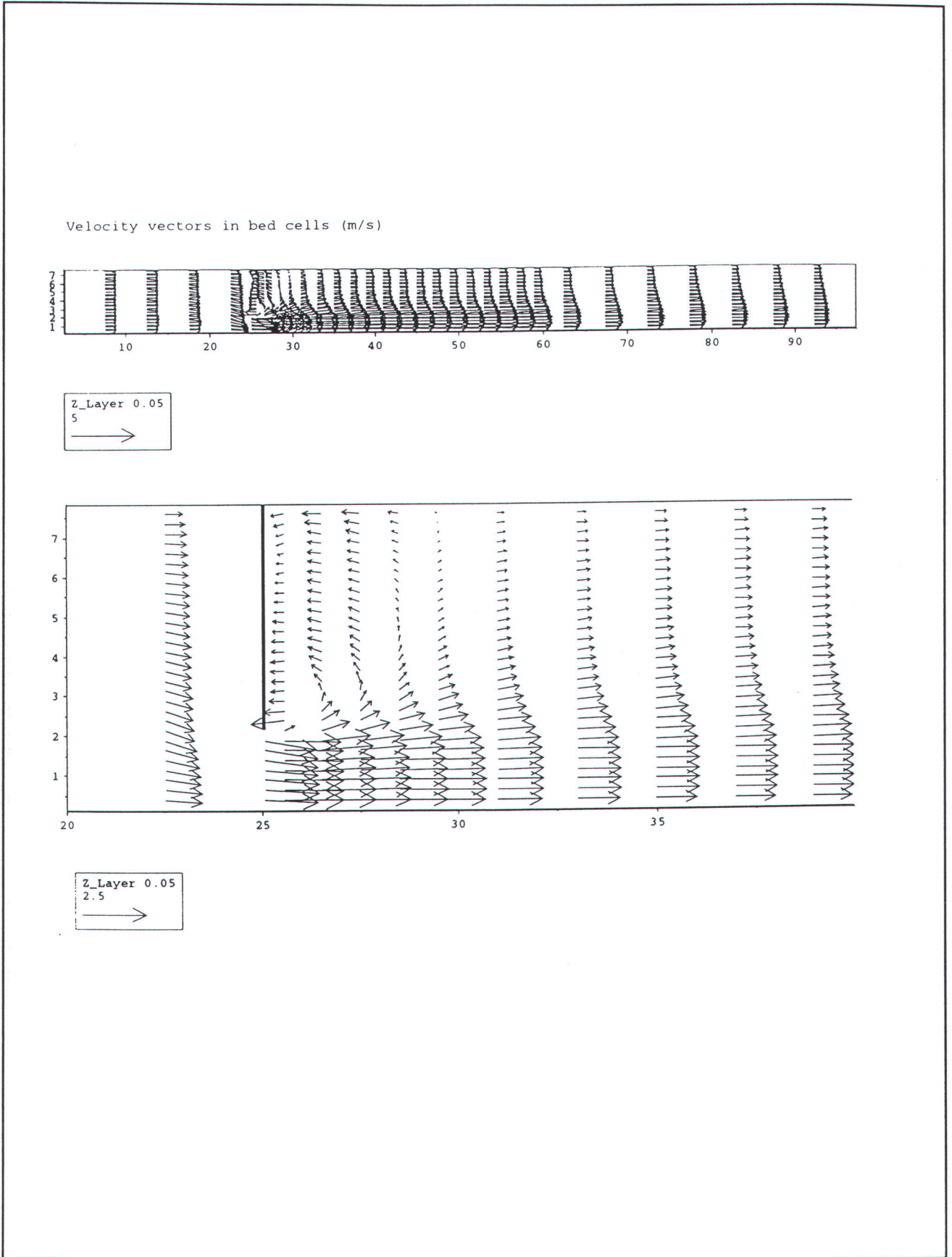
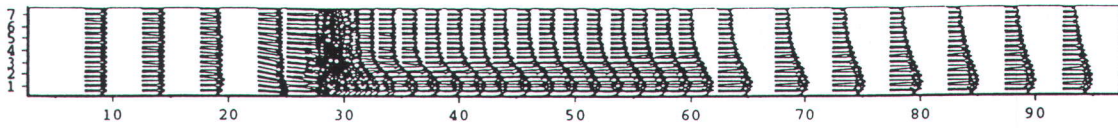


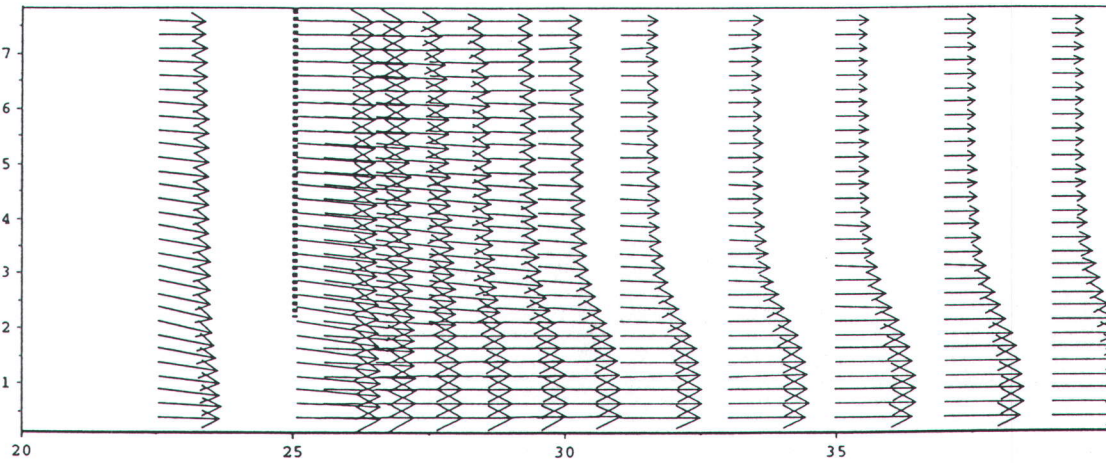
Figure 5.22 Test EW-4 : Porous groyne (horizontal slot) - Bed layer



Velocity vectors in cells at single jet at approx. half water depth(m/s)



Z\_Layer 0.45  
5  
→



Z\_Layer 0.45  
2.5  
→

..... location of groyne above  
and below this level

Figure 5.23 Test EW-4 : Porous groyne (horizontal slot) - Mid layer

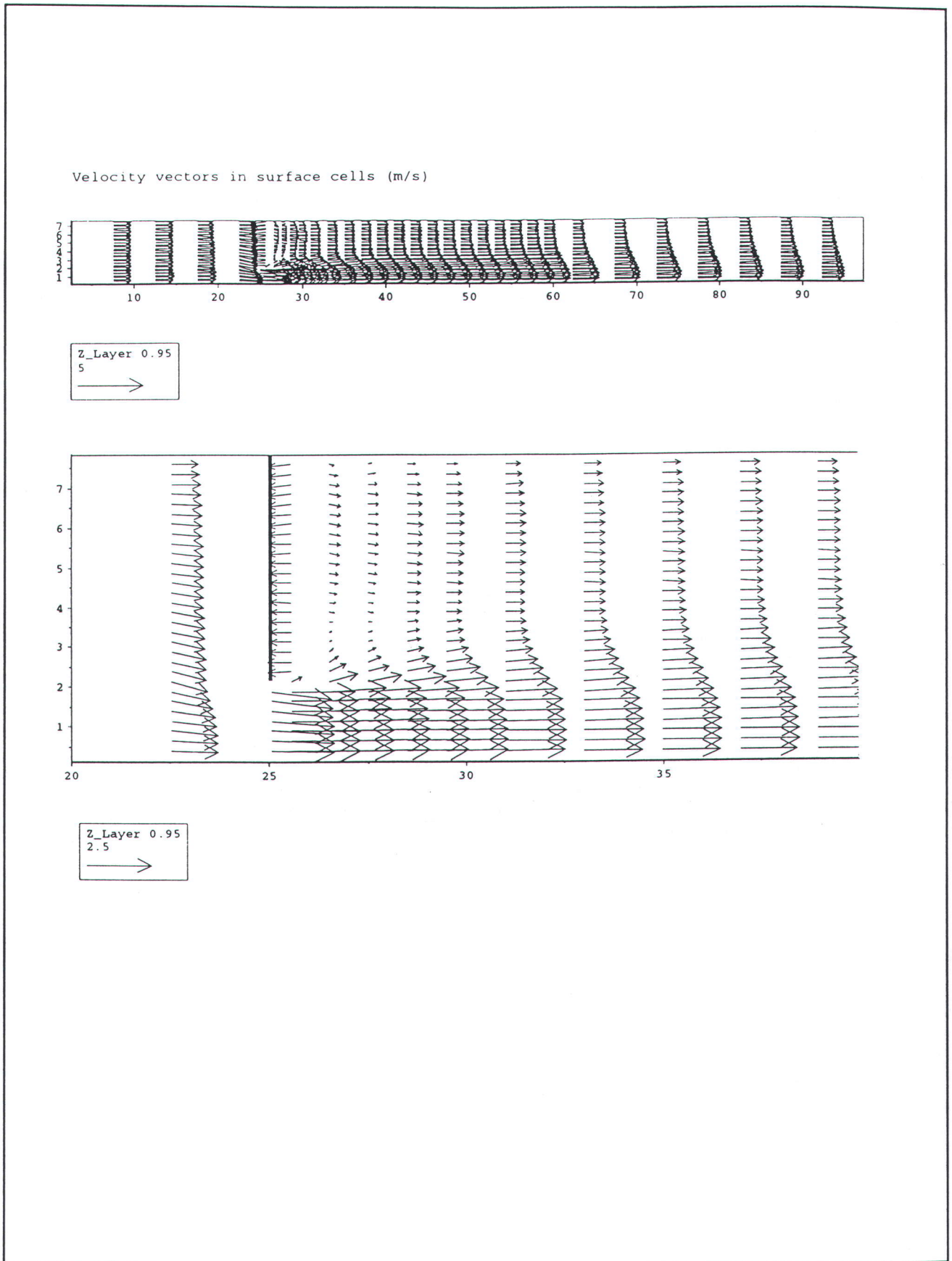
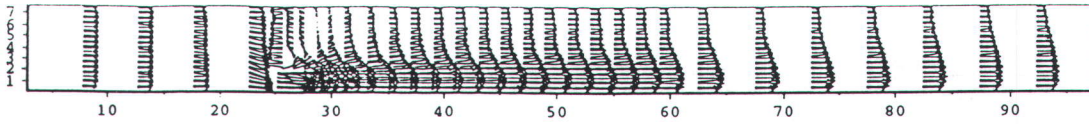


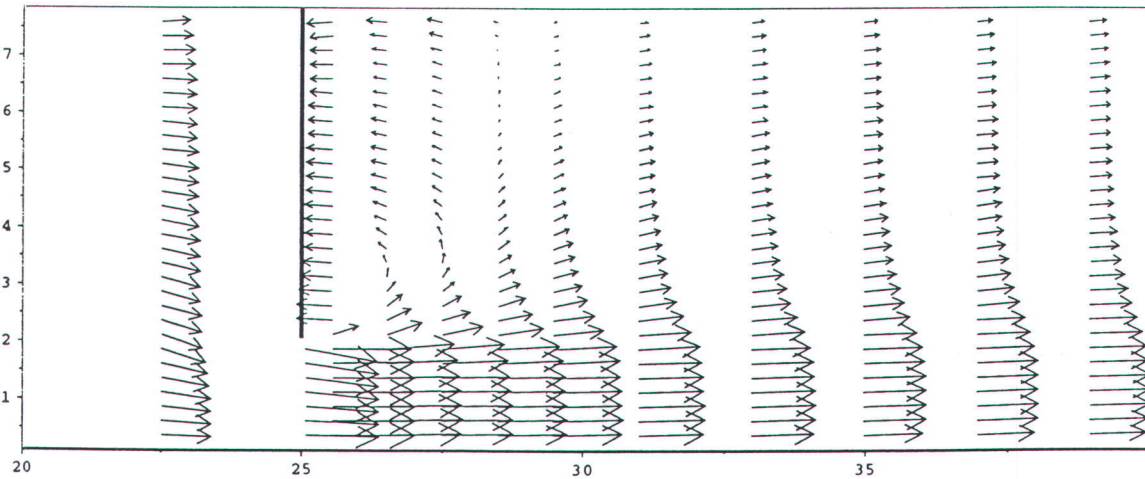
Figure 5.24 Test EW-4 : Porous groyne (horizontal slot) - Surface layer



Velocity vectors at bed level (m/s)



Z\_Layer 0.05  
5  
→



Z\_Layer 0.05  
2.5  
→

Figure 5.25 Test EW-5 : Porous groyne (two horizontal slots) - Bed layer

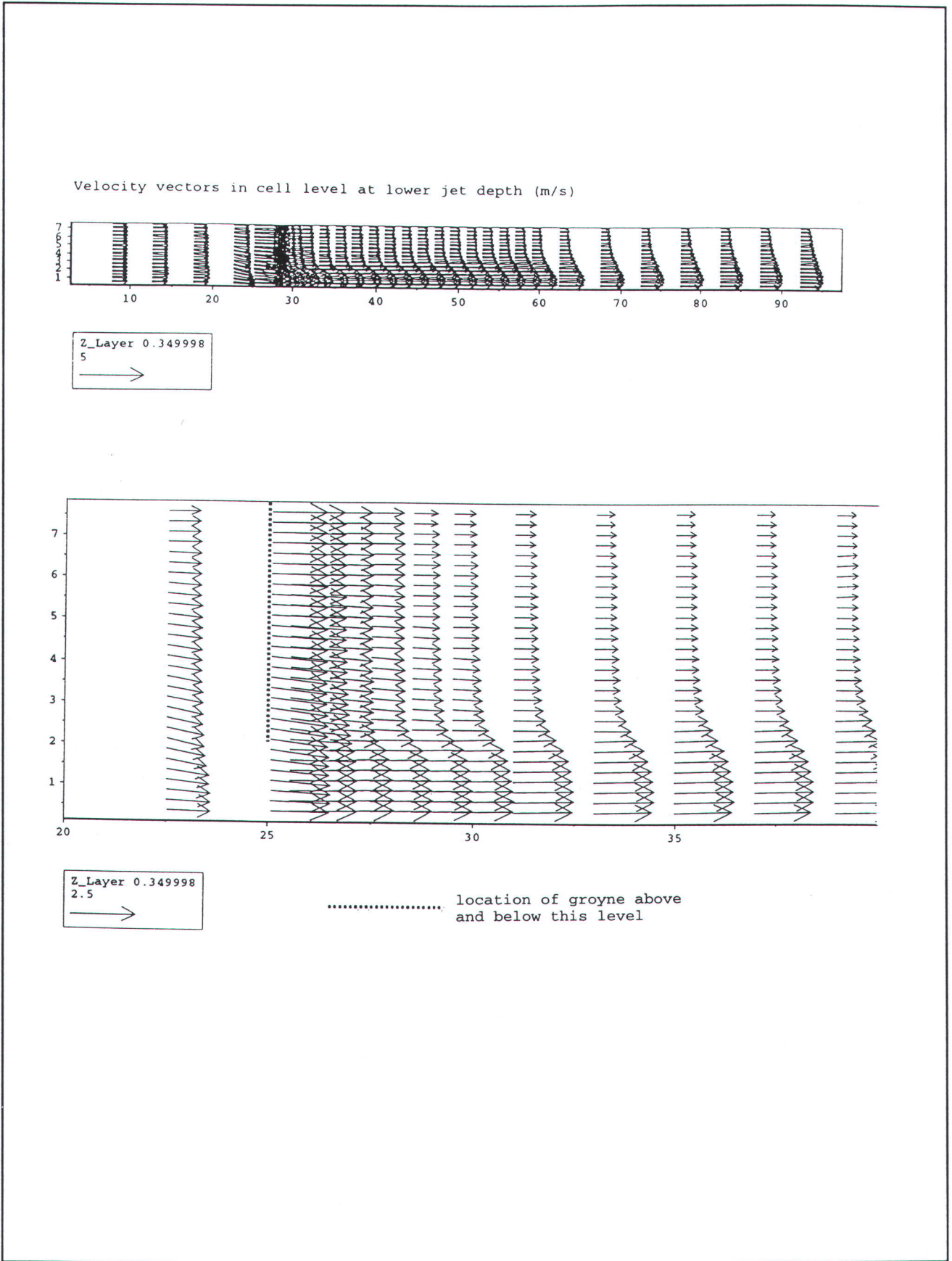
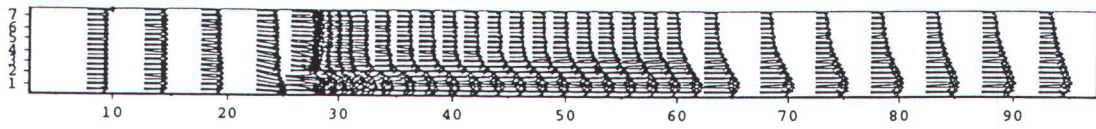


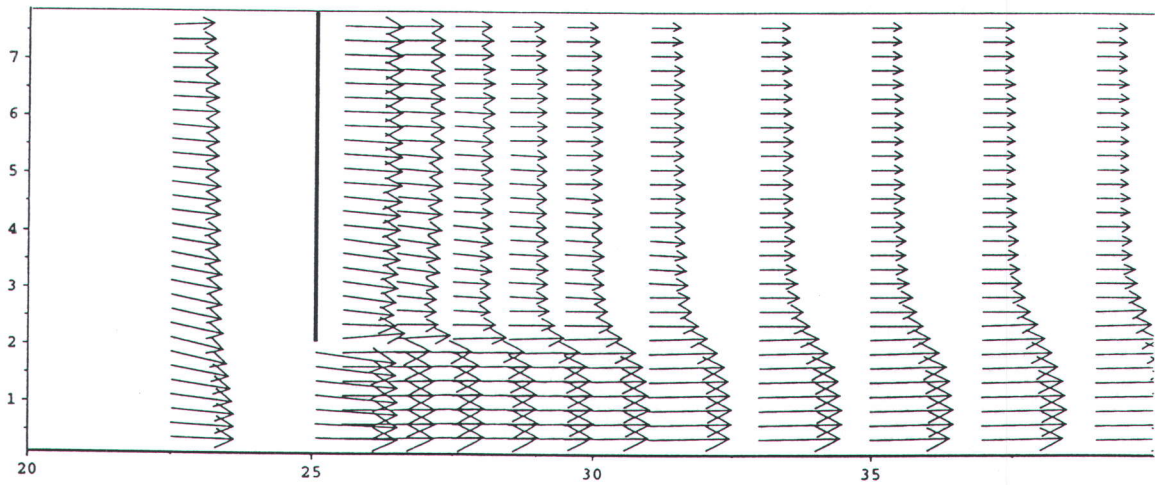
Figure 5.26 Test EW-5 : Porous groyne (two horizontal slots) - Lower jet



Velocity vectors in cells at approx. half water depth (m/s)



Z\_Layer 0.45  
5  
→



Z\_Layer 0.45  
2.5  
→

Figure 5.27 Test EW-5 : Porous groyne (two horizontal slots) - Mid layer

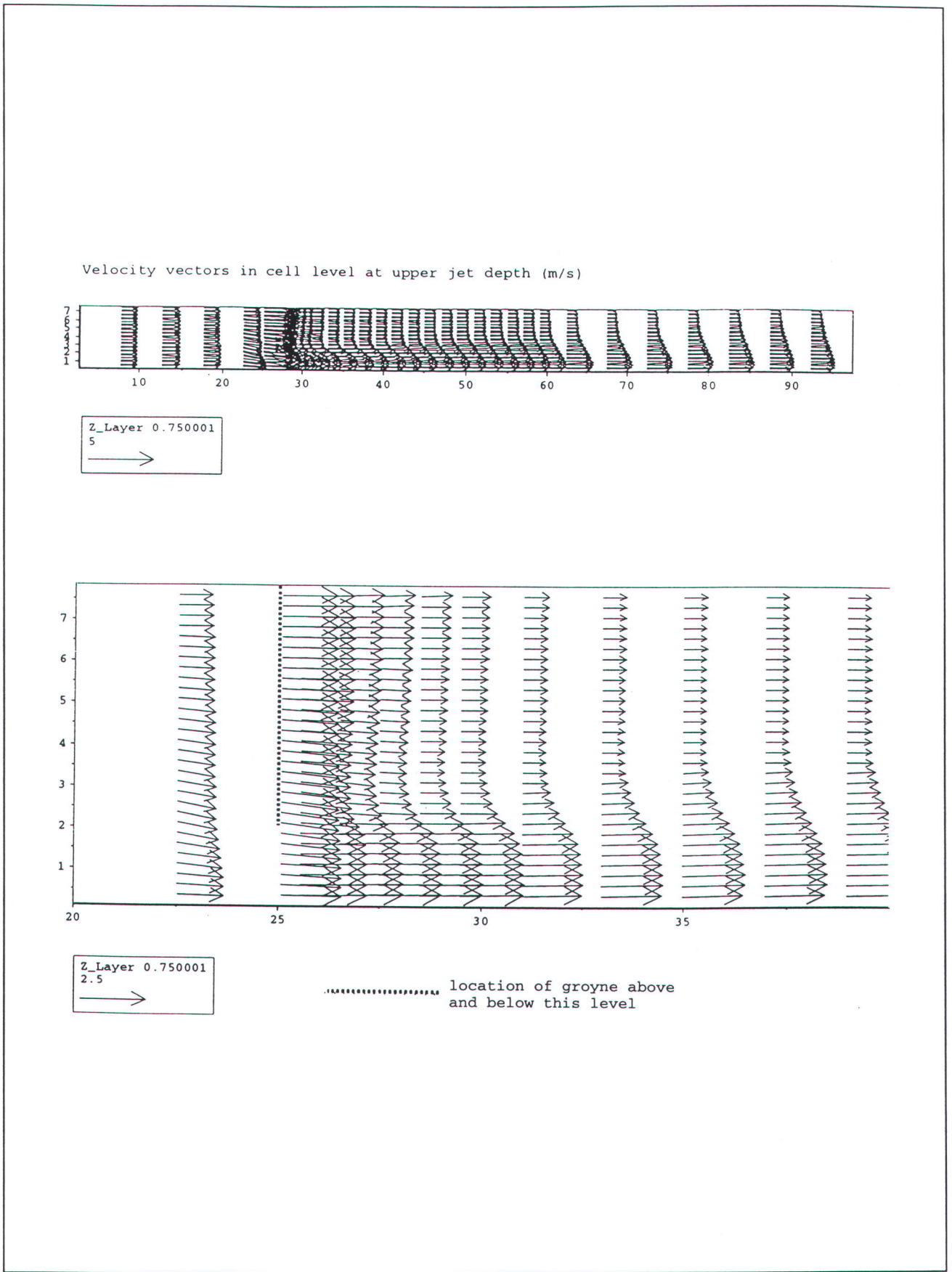
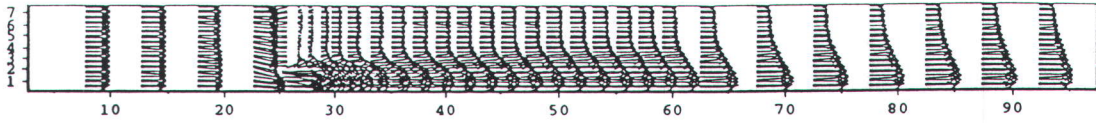


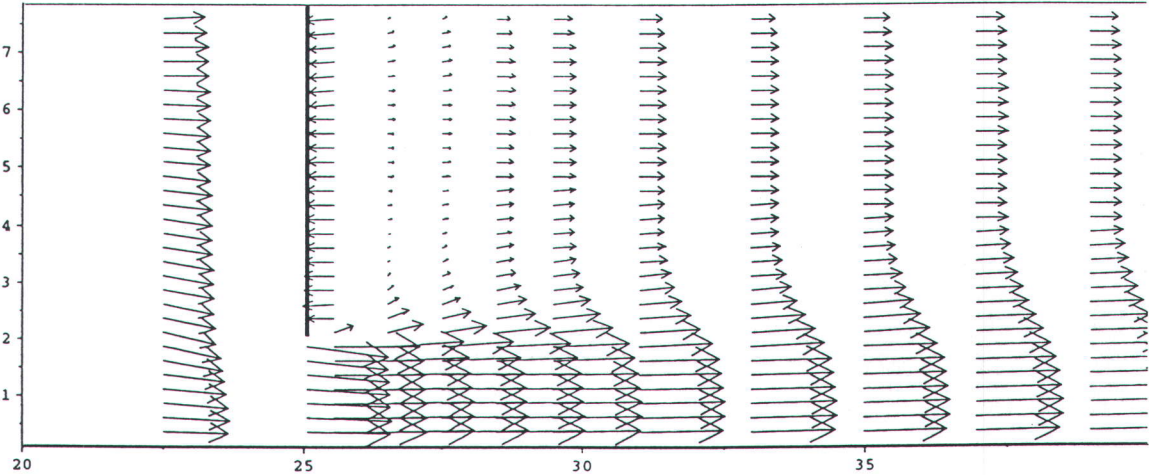
Figure 5.28 Test EW-5 : Porous groyne (two horizontal slots) - Upper jet



Velocity vectors in surface cells (m/s)



Z\_Layer 0.95  
5  
→



Z\_Layer 0.95  
2.5  
→

Figure 5.29 Test EW-5 Porous groyne (two horizontal slots) - Surface layer

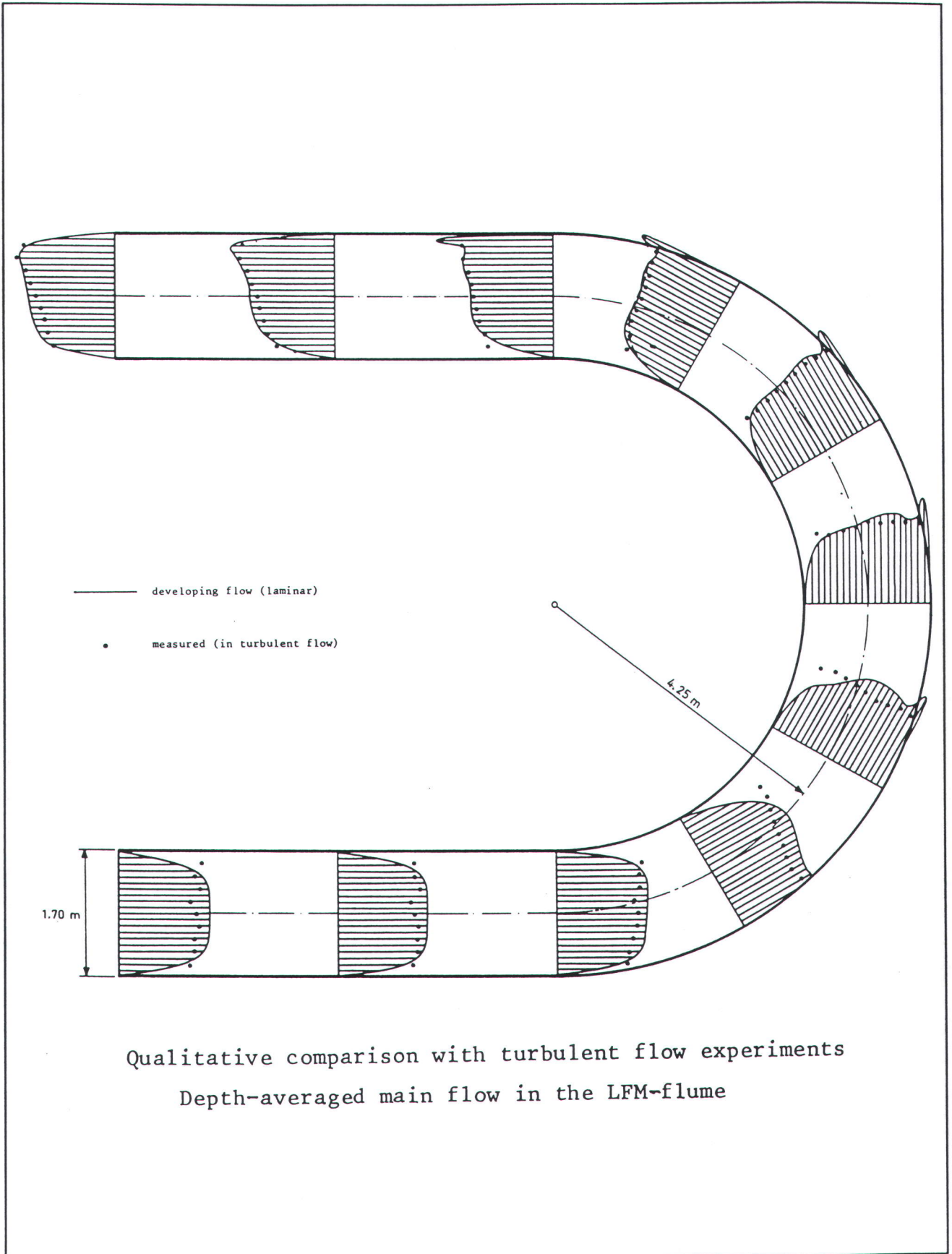


Figure 6.1 Test U0 : Velocity profiles in a U-shaped Channel (de Vriend)

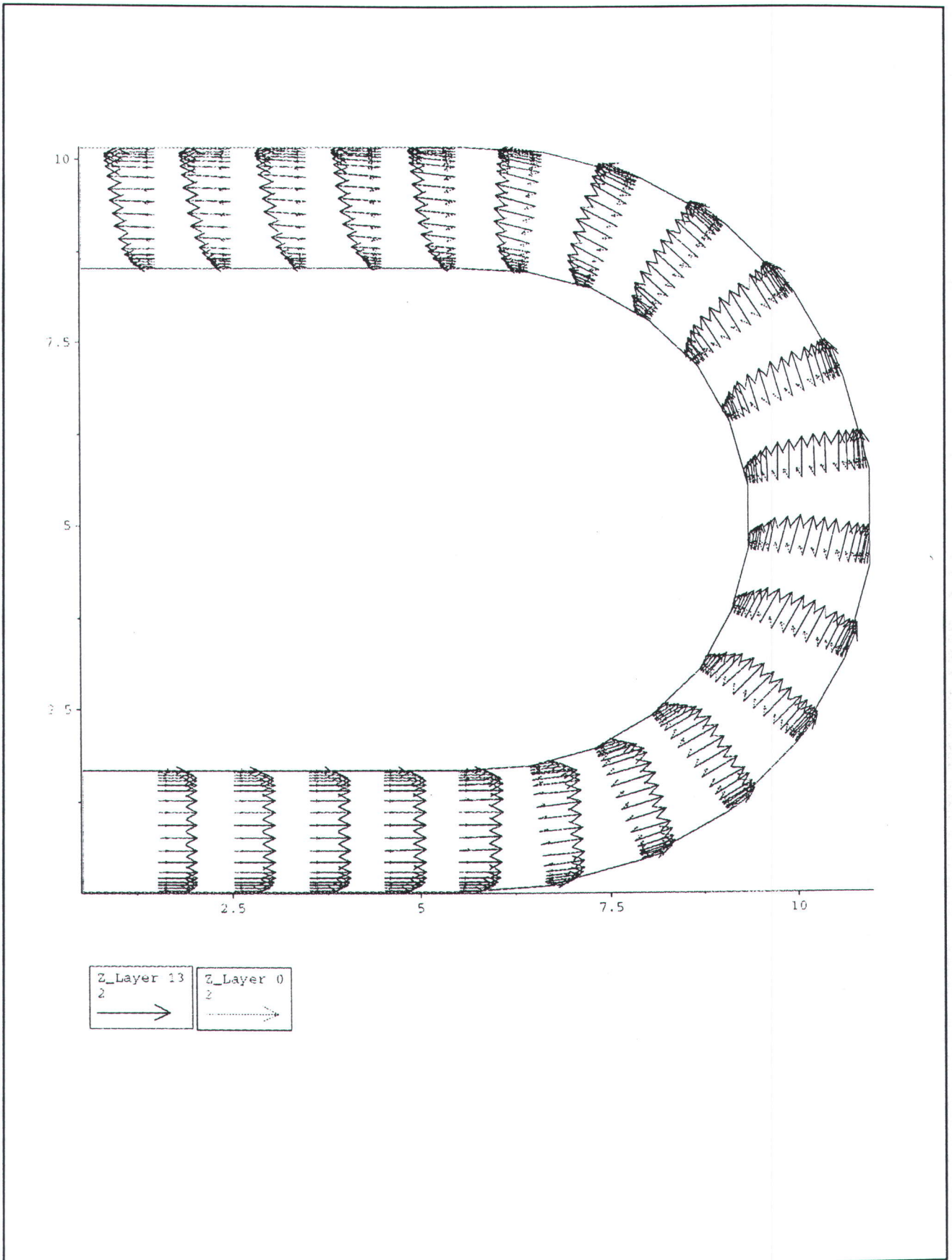


Figure 6.2 Test U0 : velocity profiles in a U-shaped Channel (SSIM)

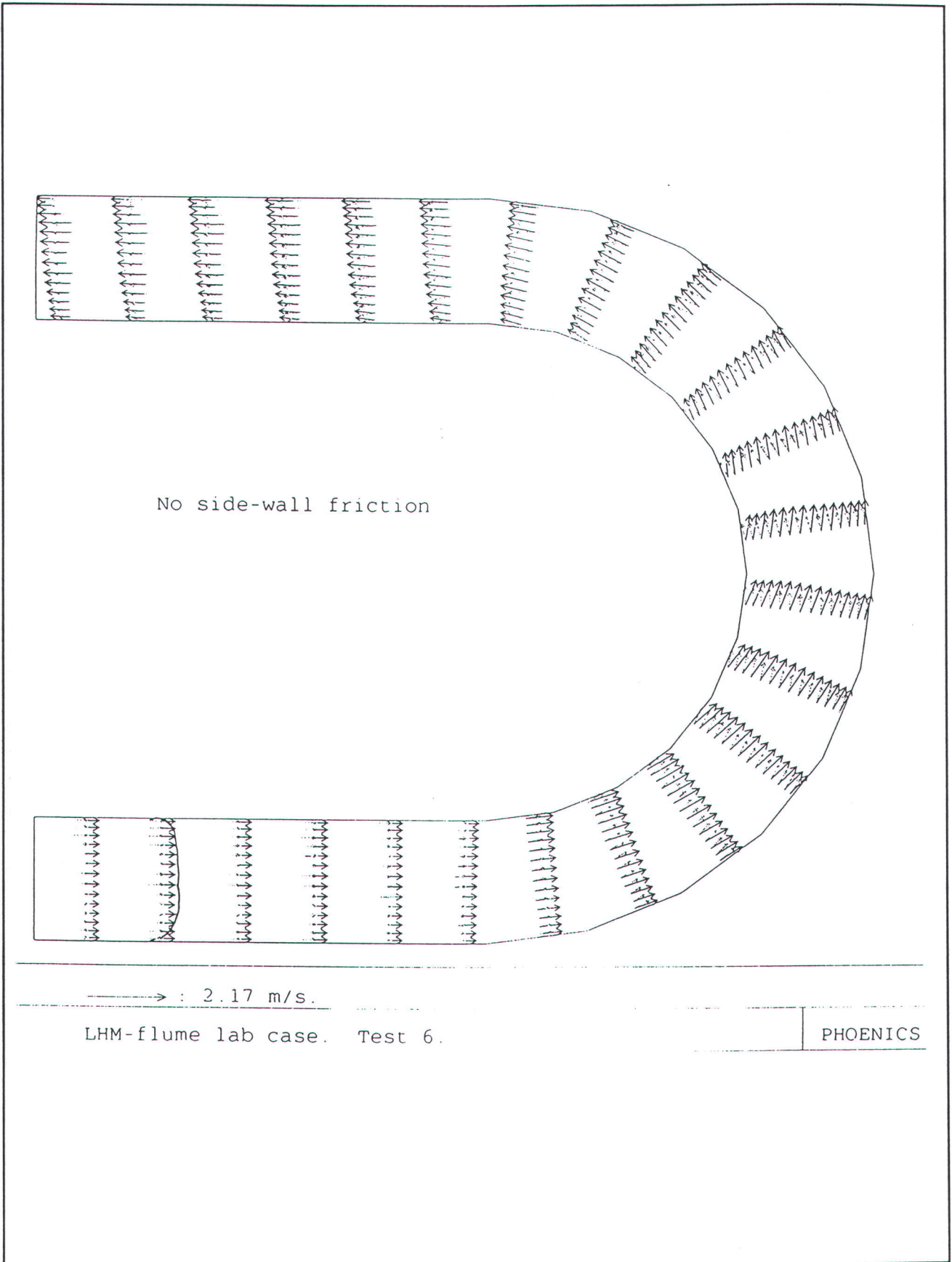


Figure 6.3 Test U0 : velocity profiles in a U-shaped Channel (Pheonics)

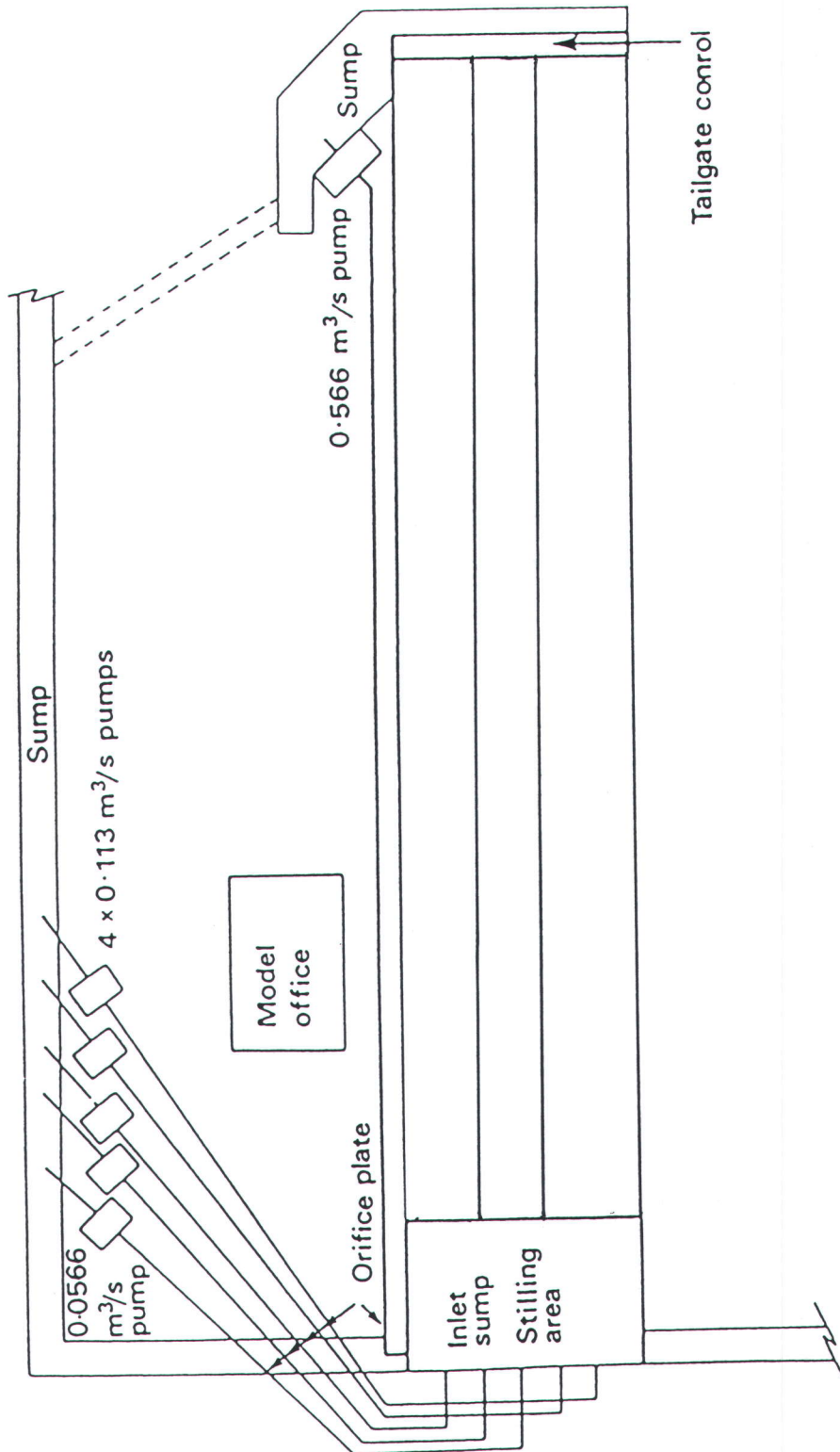
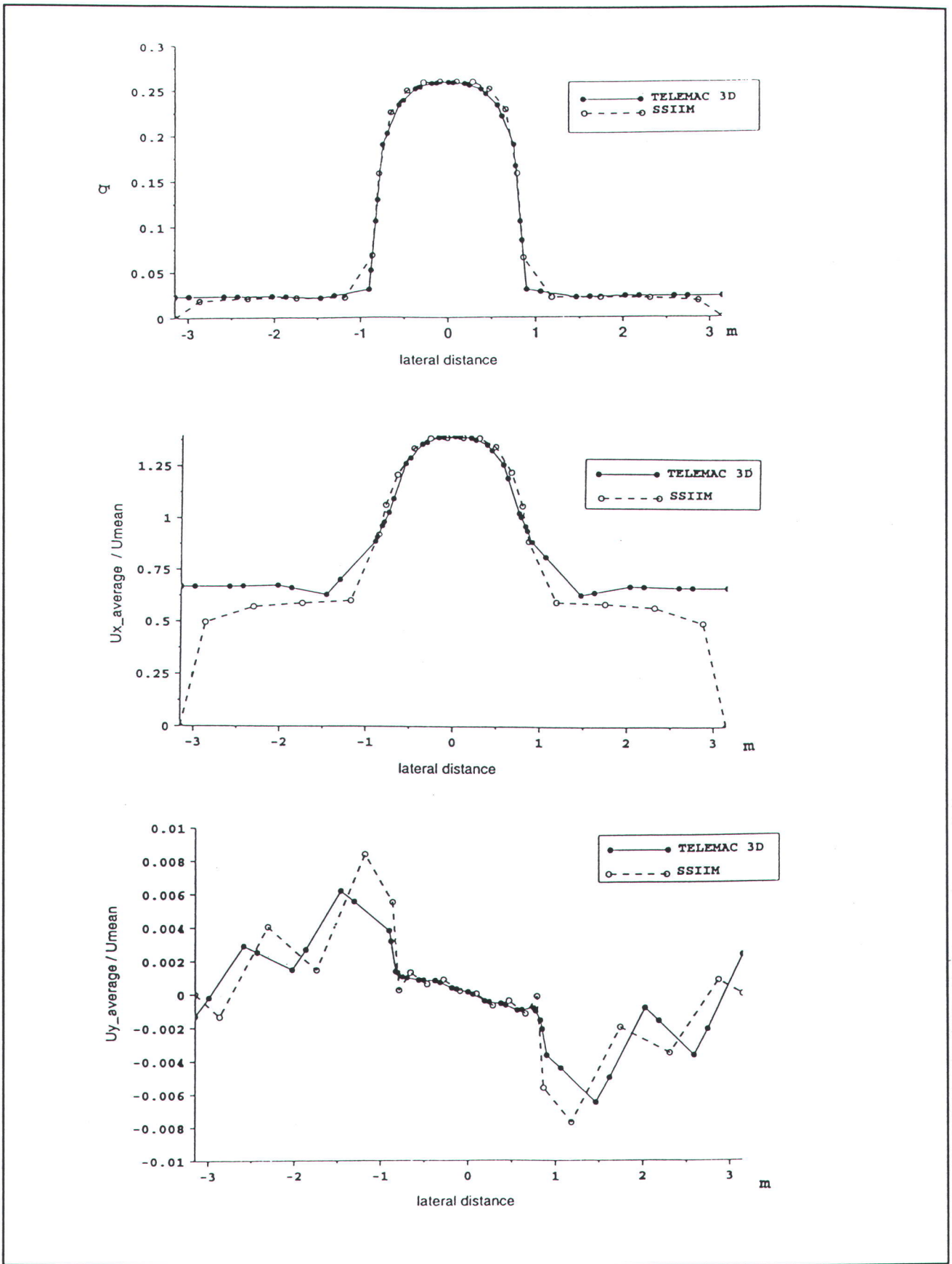
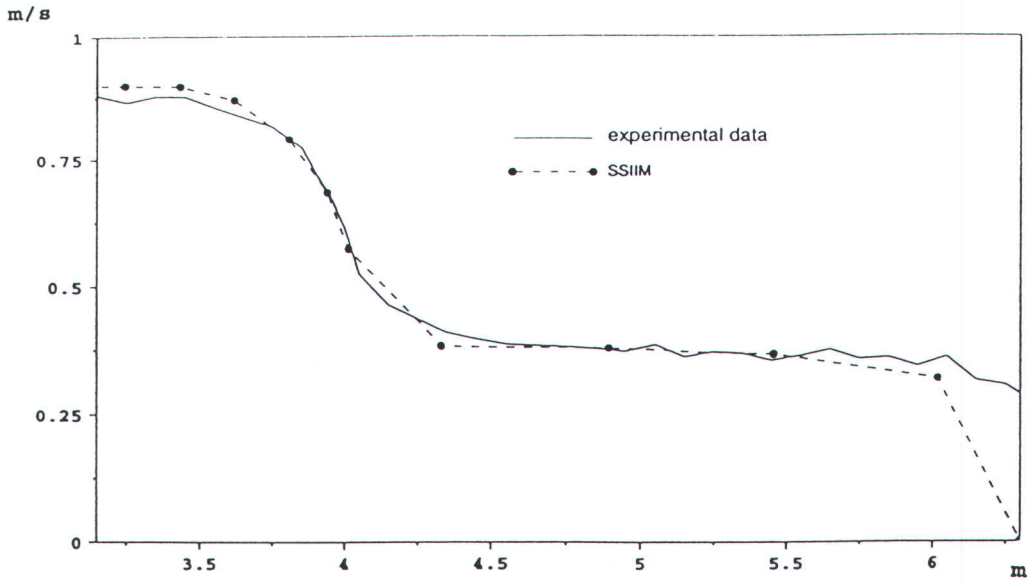


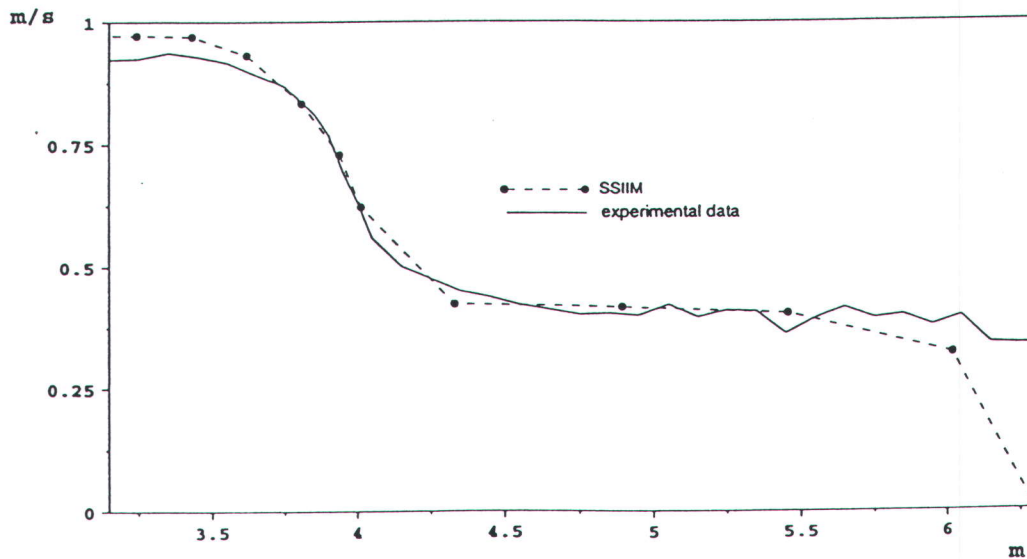
Figure 6.4 Test P0 : Straight out-of-bank flow, Layout of the F.C.F flume



**Figure 6.5 Test P0 : Straight out-of-bank flow, comparison of Telemac and SSIIM**



Depth-averaged velocity in the cross-section x=36m



Plan velocity at the surface layer in the cross-section x=36m

Figure 6.6 Test P0 : Straight out-of-bank flow, comparison of SSIIM with experiment

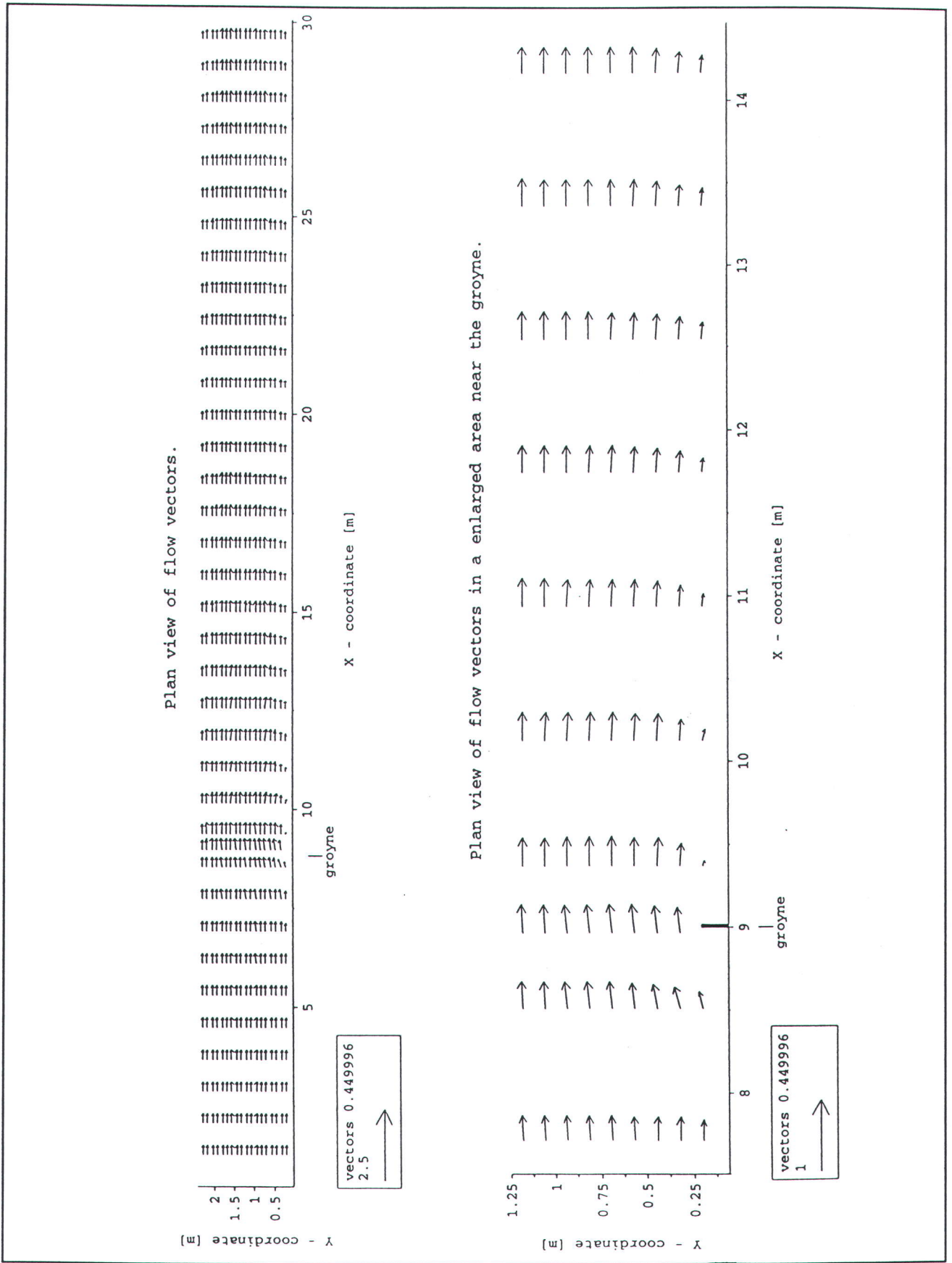


Figure 6.7 Test RAa-1 : Hanover flume results from original grid

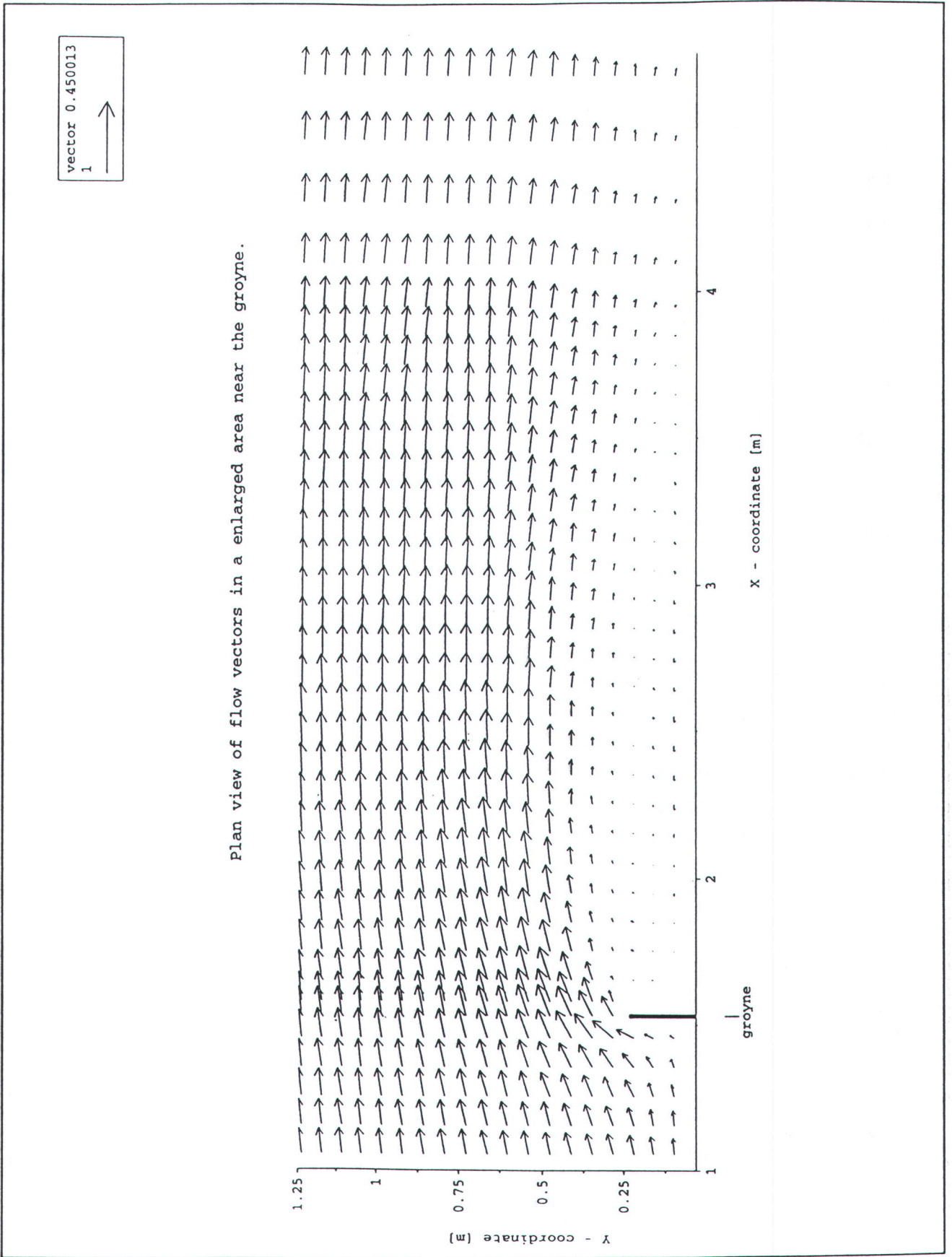


Figure 6.8 Test RAa-4 : Hanover flume results from non uniform grid

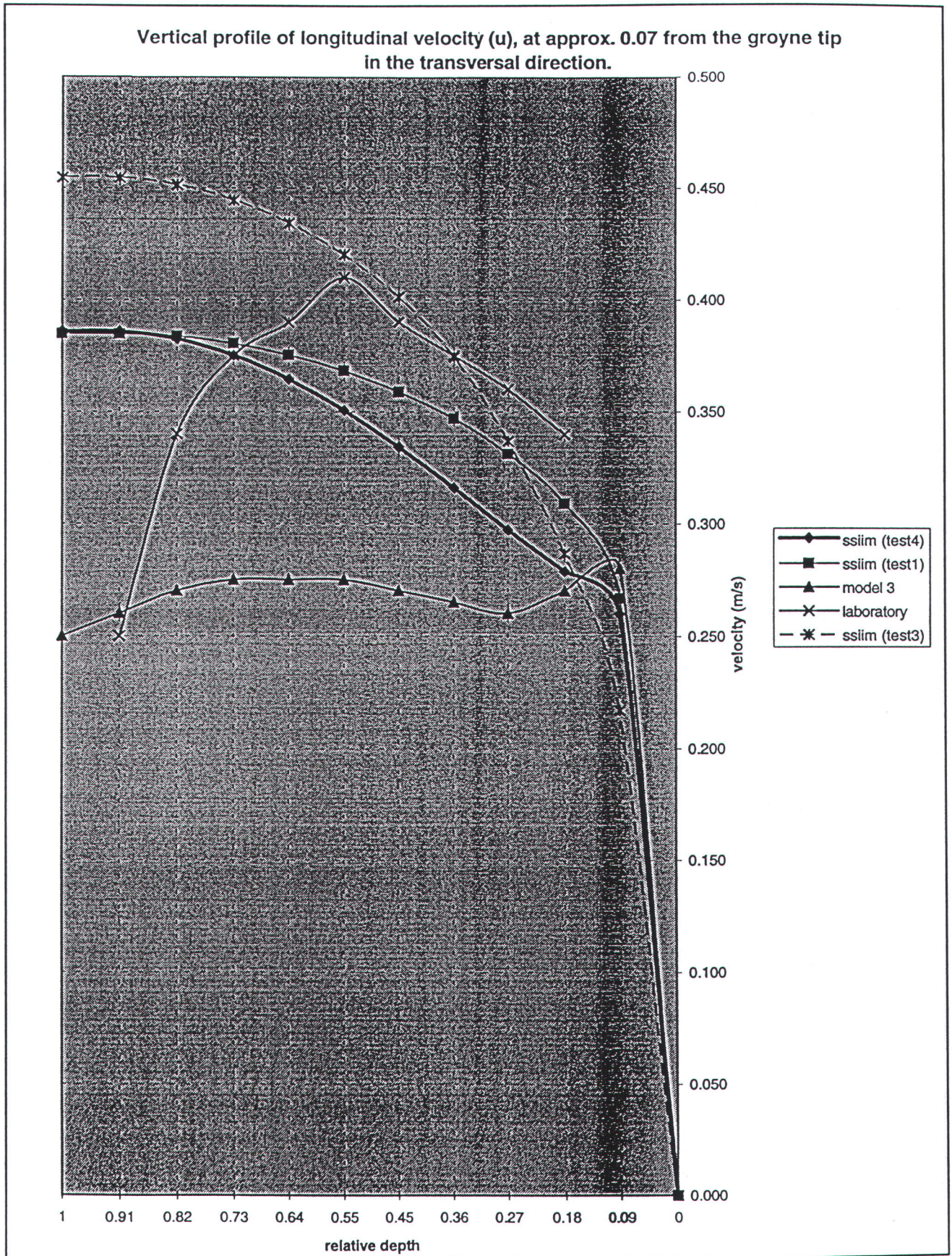


Figure 6.9 Test RAa : Hanover flume comparison of methods (longitudinal velocity)



Vertical profile of transversal velocity ( $v$ ), at approx 0.07 from the groyne tip in the transversal direction.

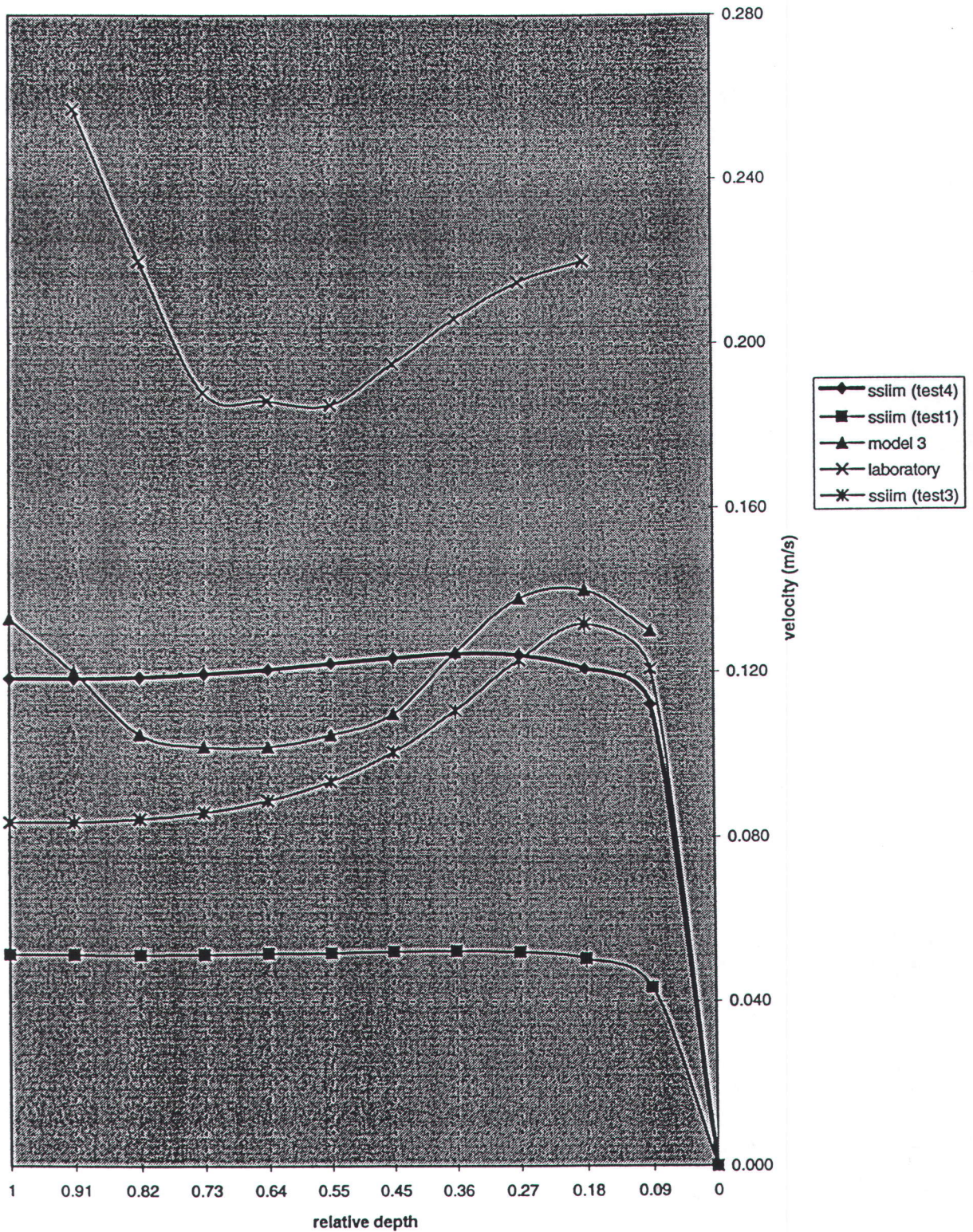


Figure 6.10 Test RAa : Hanover flume comparison of methods (transverse velocity)

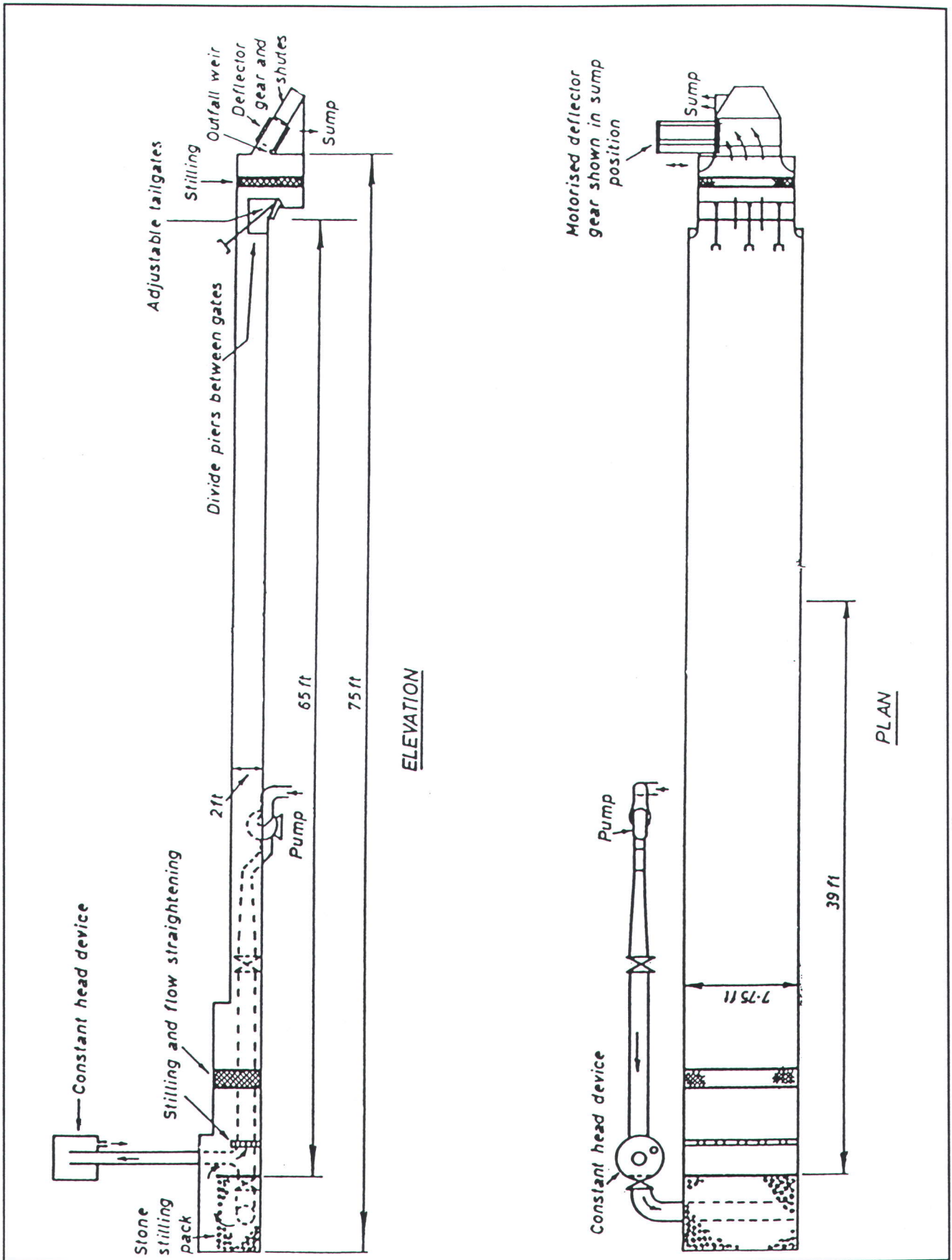
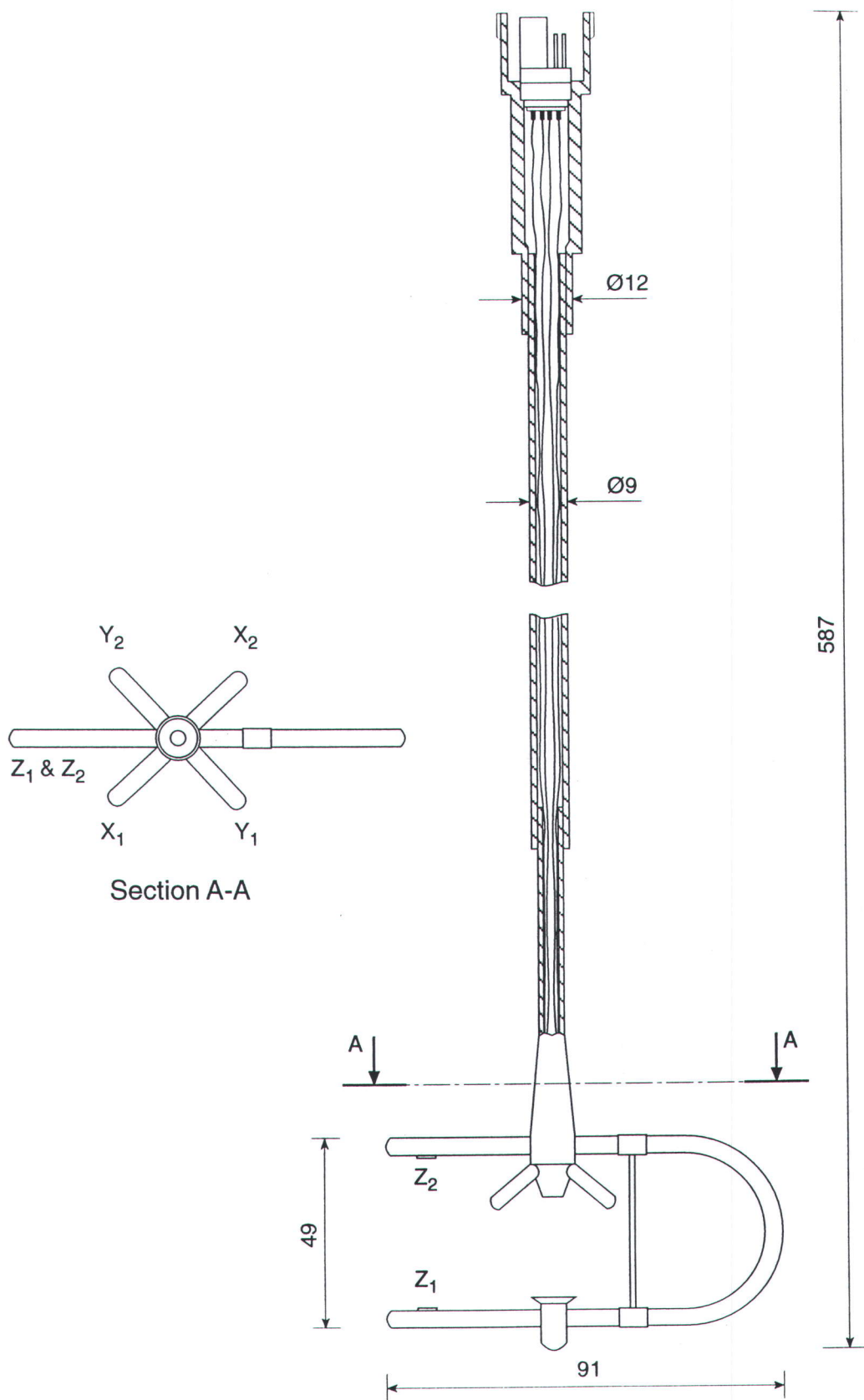
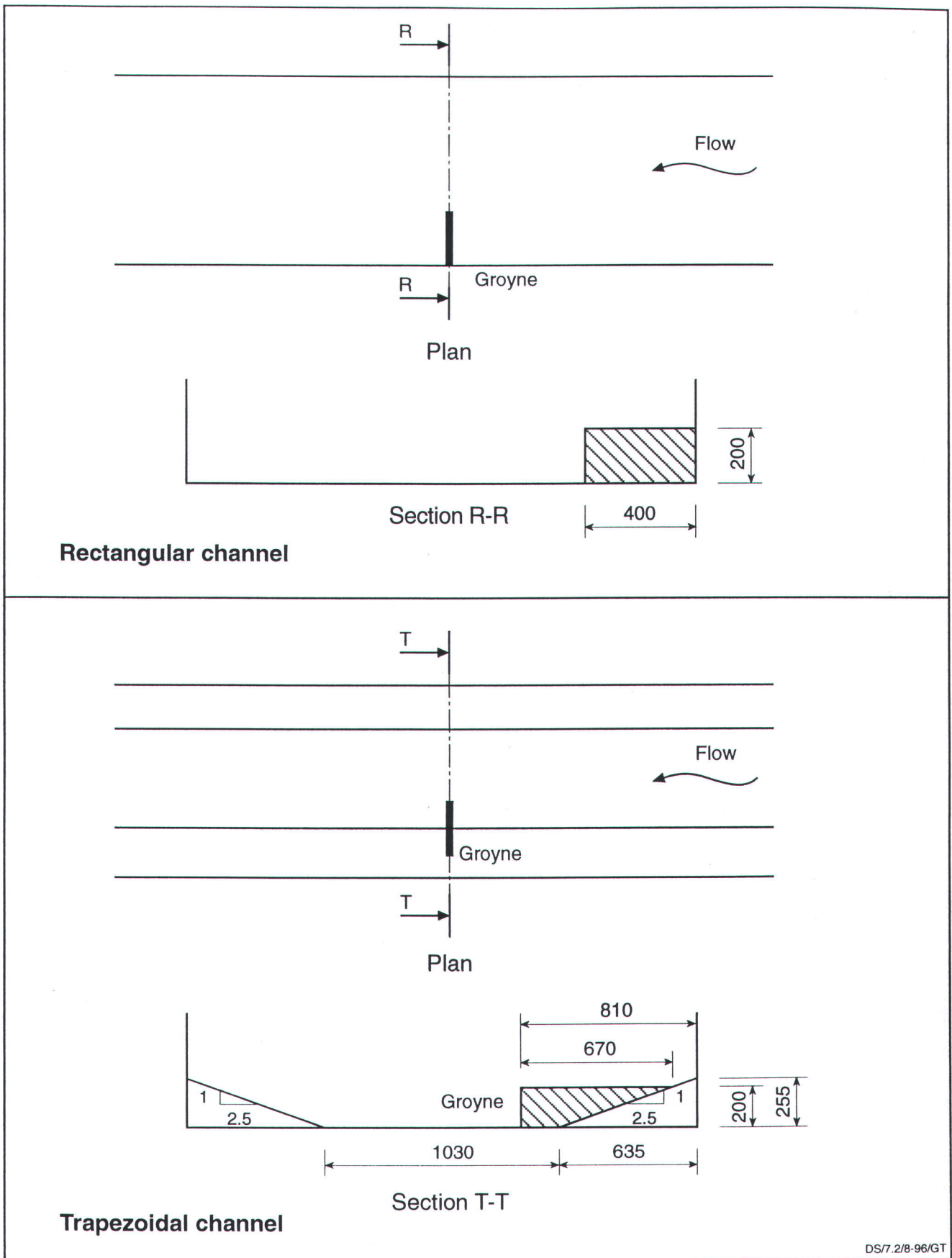


Figure 7.0 Layout of General Purpose flume(GP flume)



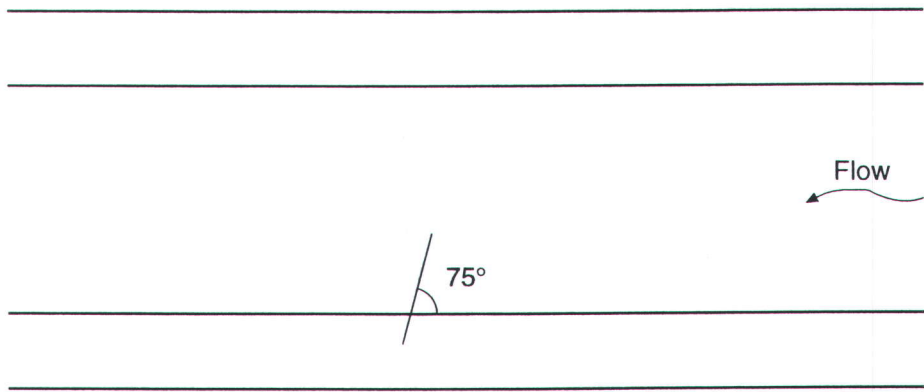
DS/7.1/8-96/GT

Figure 7.1 Minilab probe

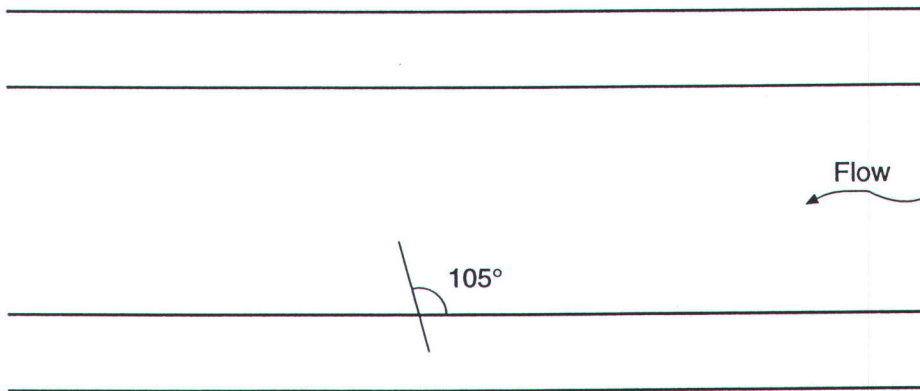


DS/7.2/8-96/GT

Figure 7.2 Types of channel used for the laboratory tests in the GP flume



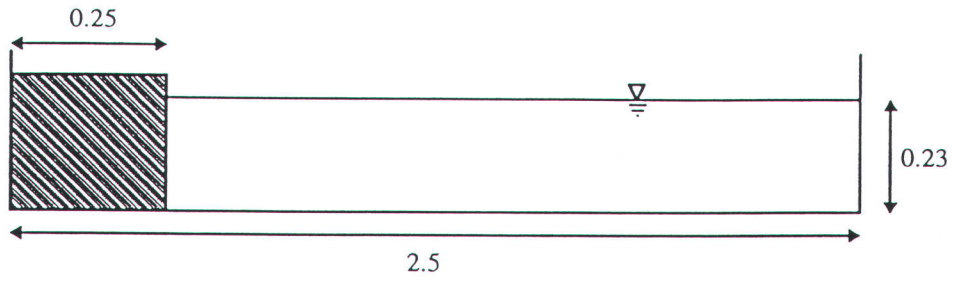
**Upstream facing groyne (Test TC)**



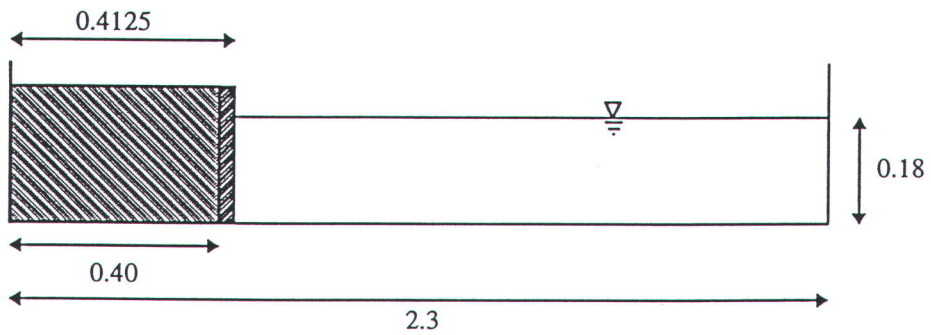
**Downstream facing groyne (Test TD)**

DS/7.3/8-96/GT

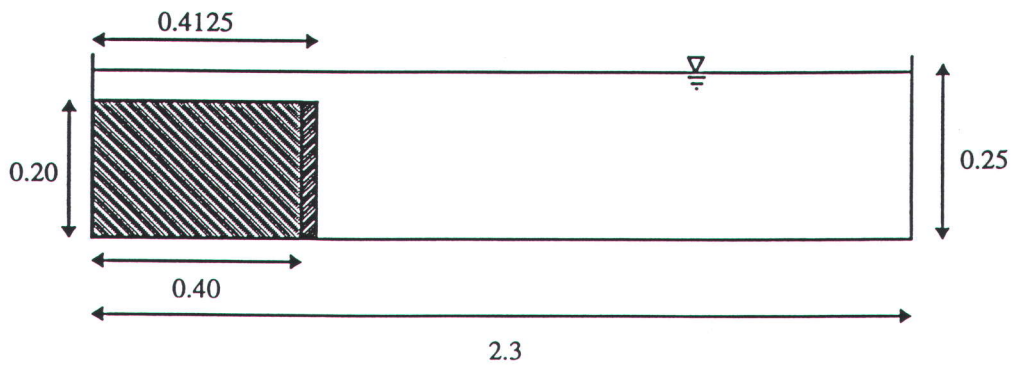
**Figure 7.3 Orientation of groynes in Tests TC and TD**



HANOVER FLUME: Test RAa

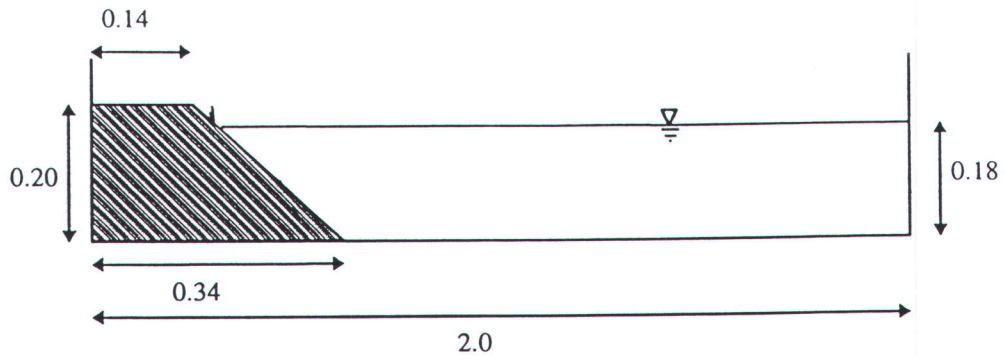


G.P. FLUME: Test RAb

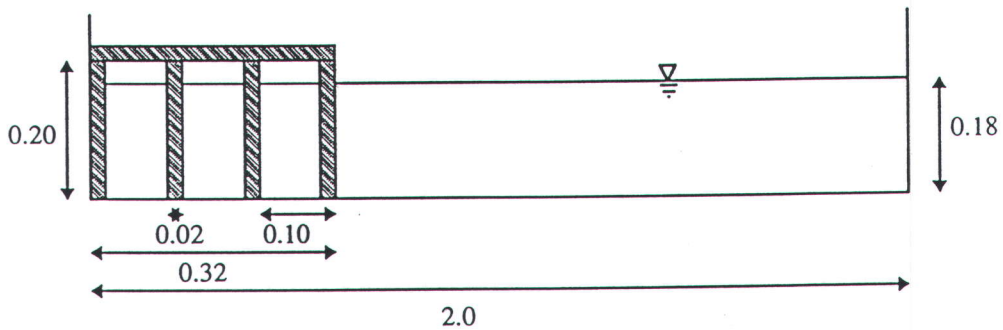


G.P. FLUME: Test RB

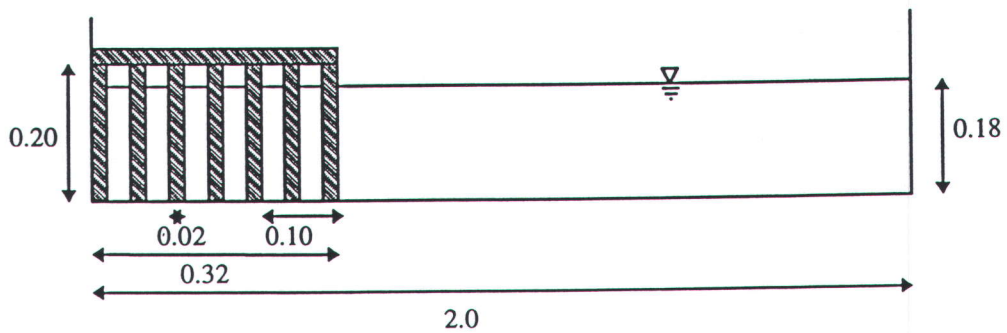
Figure 7.4 Dimensions of rectangular groynes in rectangular channel



G.P. FLUME: Test RM



G.P. FLUME: Test RX



G.P. FLUME: Test RY

Figure 7.5 Dimensions of permeable and tapered groynes in rectangular channel

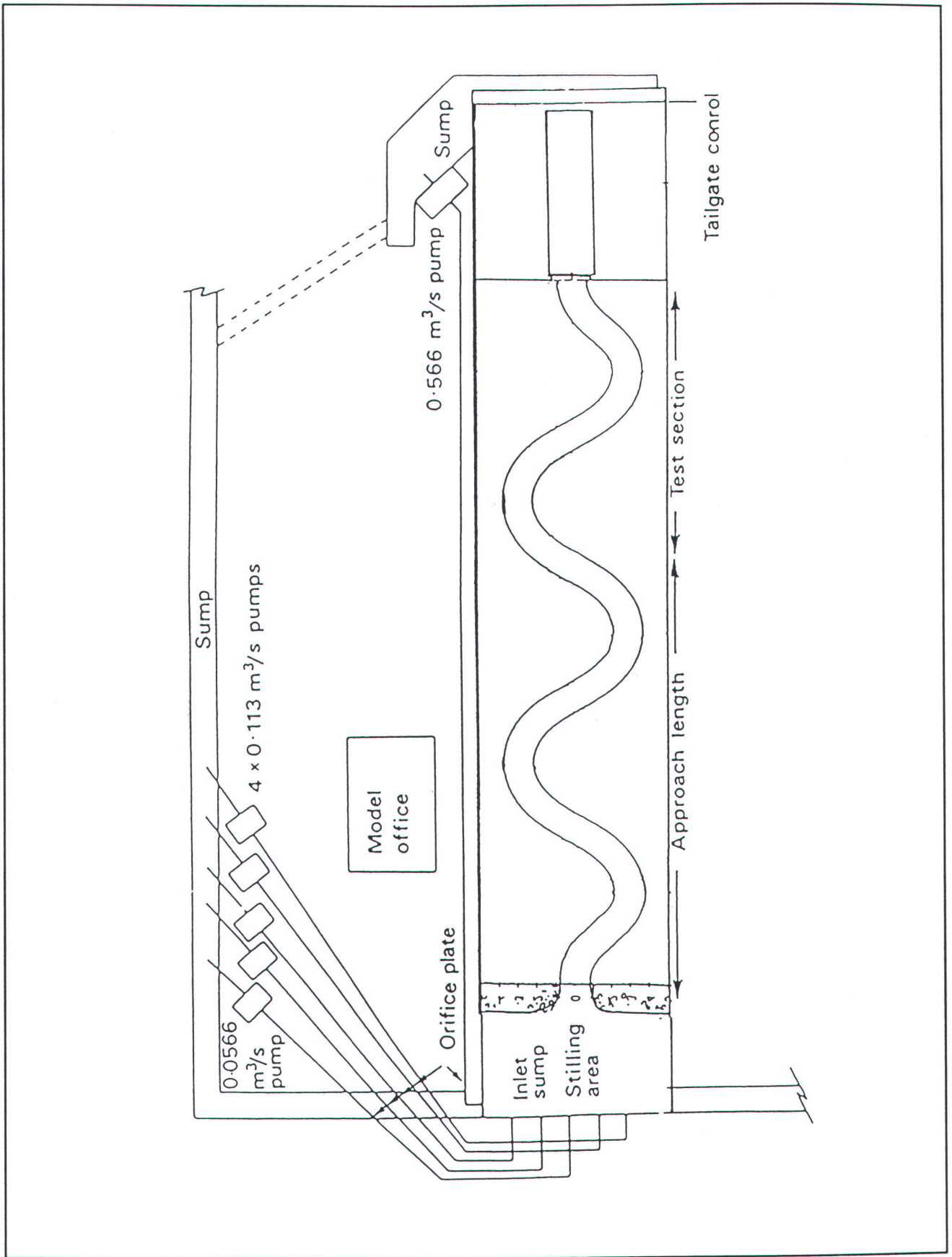
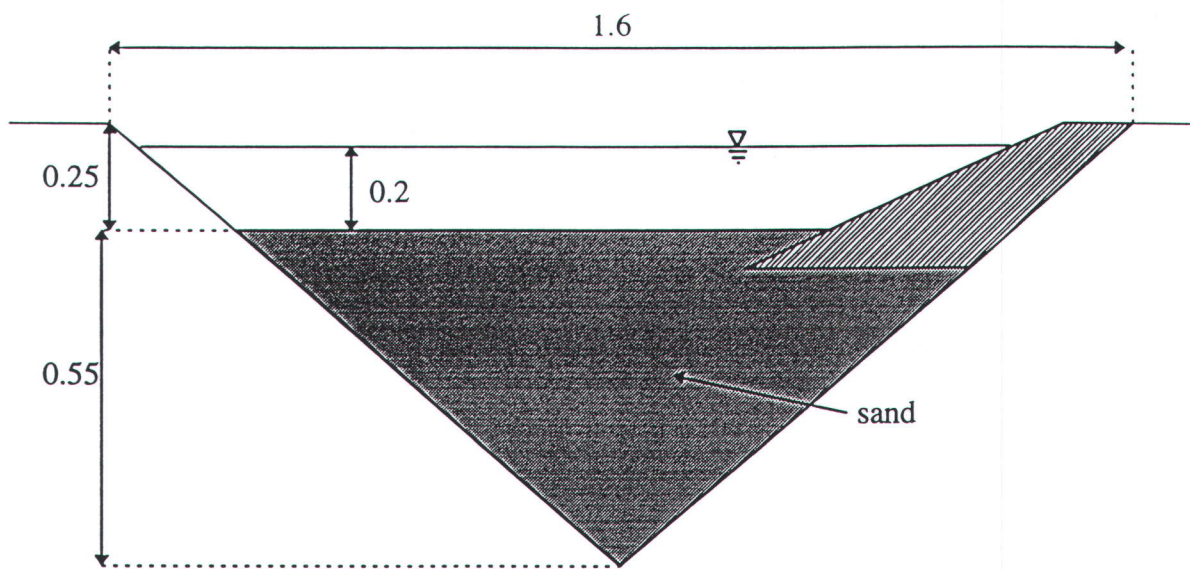


Figure 7.6 Layout of Flood Channel Facility (FCF) - Series C



CROSS-SECTION OF THE CHANNEL

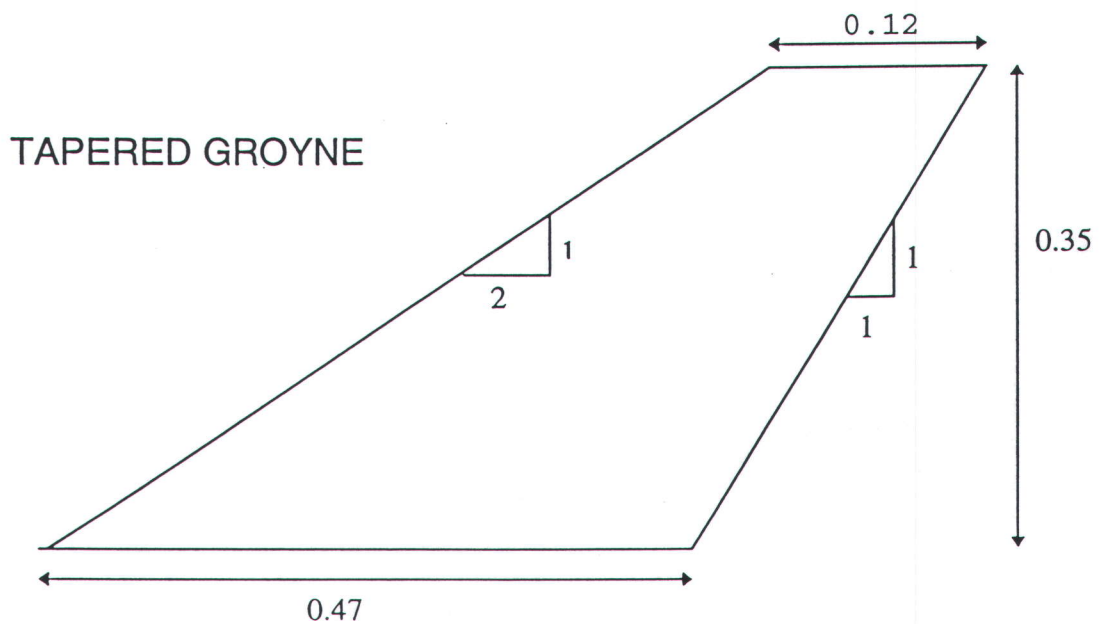
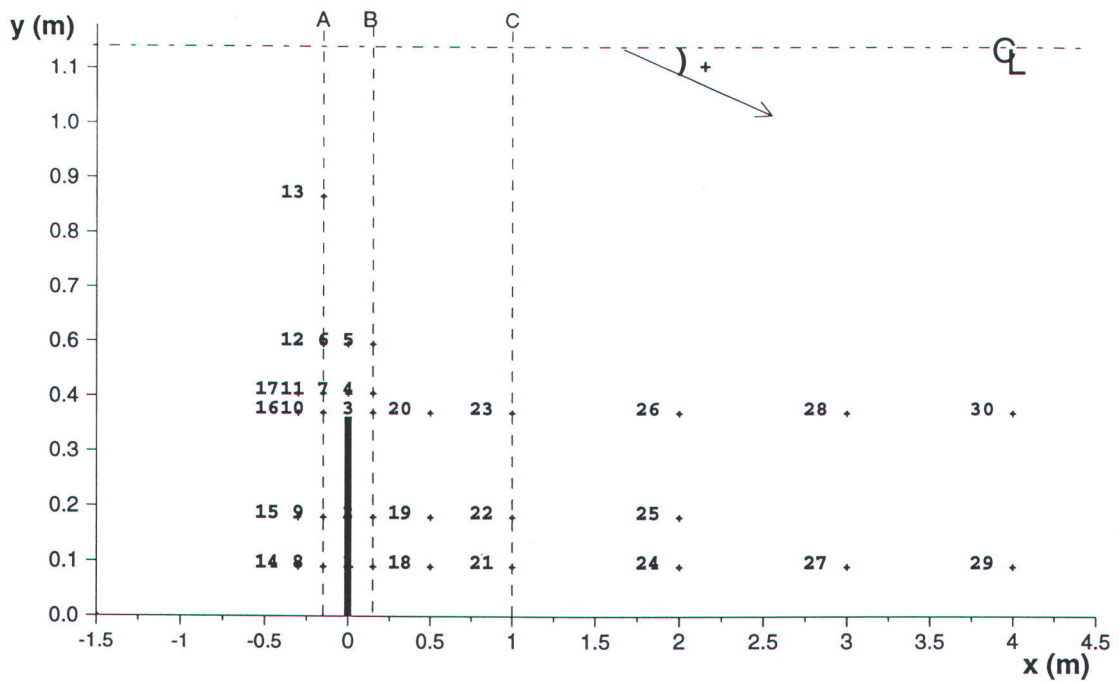
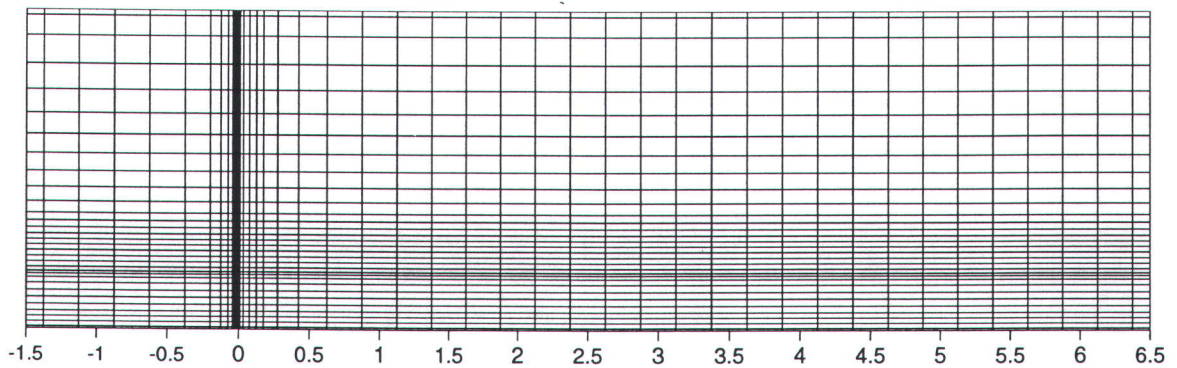


Figure 7.7 Dimensions of groynes in FCF

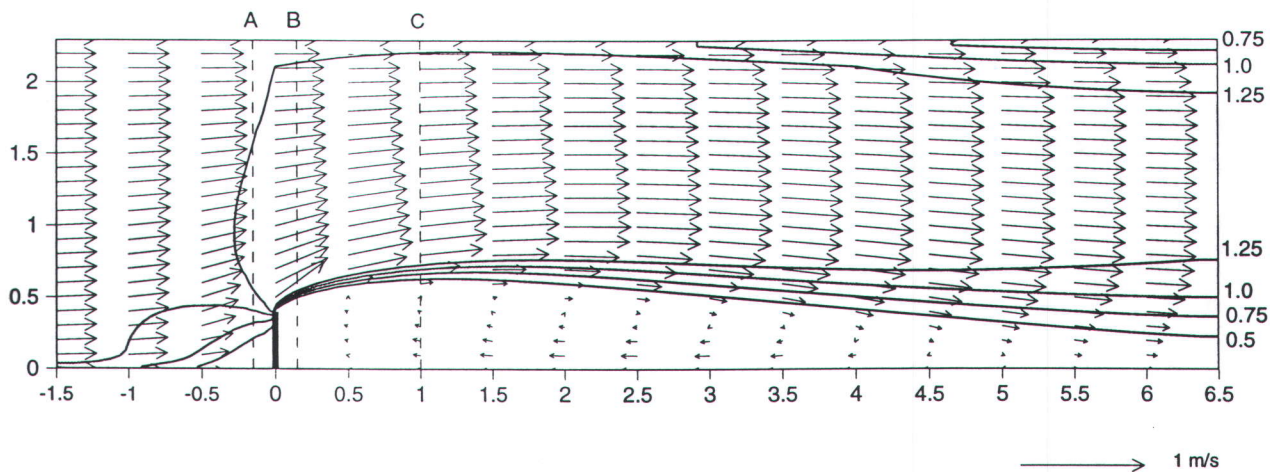


Experimental points and sections

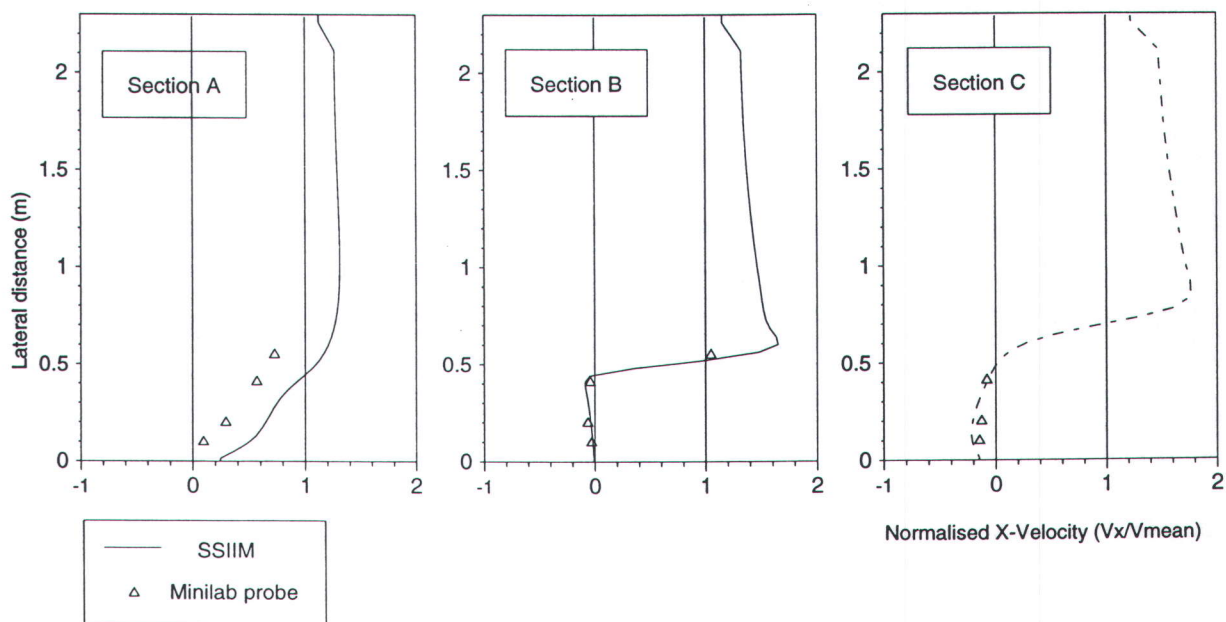


Plan view of the grid  $(x,y,z) = (45,31,13) = 18135$  cells

Figure 8.1 Experimental points and numerical grid for Test RAb

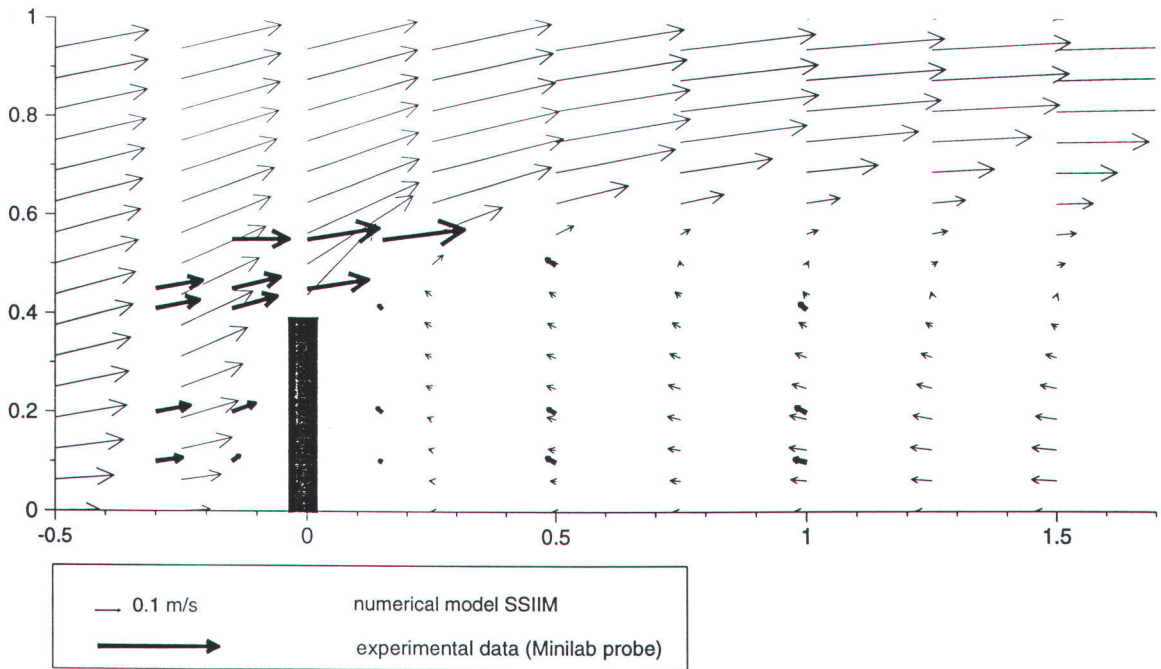


Velocity vectors and normalised velocity contours at mid-depth

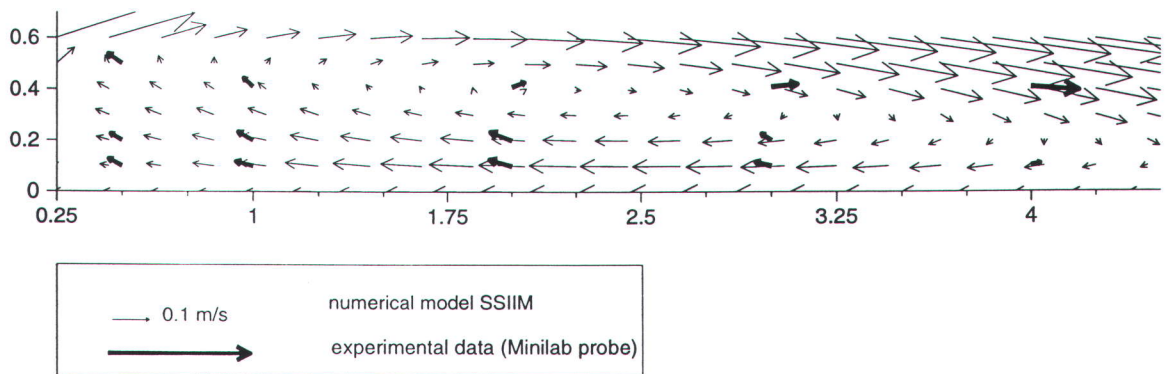


Normalised X-Velocity profiles at 66.6% from the bed (12cm)

Figure 8.2 Test RAb - Unsubmerged groyne in a rectangular channel  
Mid depth velocities and cross-section profiles of X velocity

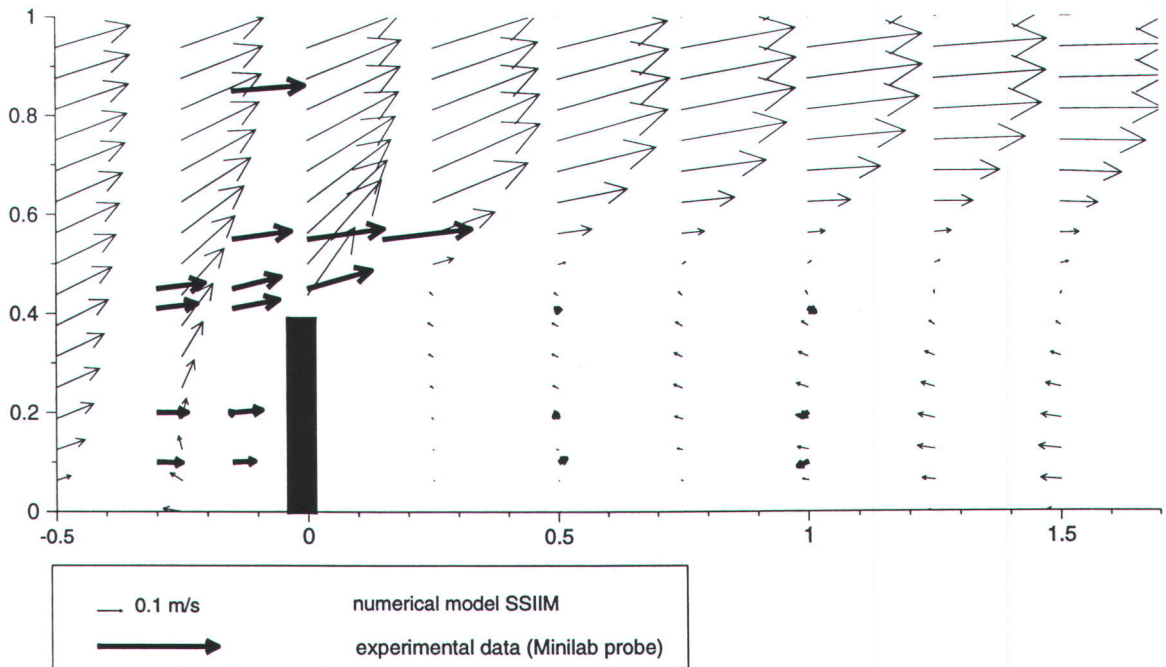


Plan velocity vectors close to the groyne at 66.6% from the bed

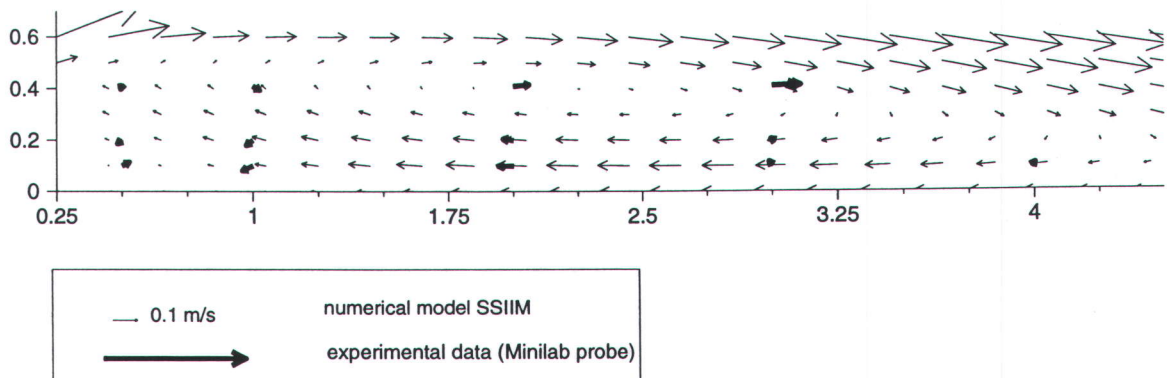


Plan velocity vectors in the recirculation zone at 66.6% from the bed

Figure 8.3 Test RAb - Unsubmerged groyne in a rectangular channel  
Plan velocity vectors near groyne and in the recirculation zone



**Plan velocity vectors close to the groyne at 20% from the bed**



**Plan velocity vectors in the recirculation zone at 20% from the bed**

**Figure 8.4 Test RAb - Unsubmerged groyne in a rectangular channel  
Plan velocity vectors (near bed)**

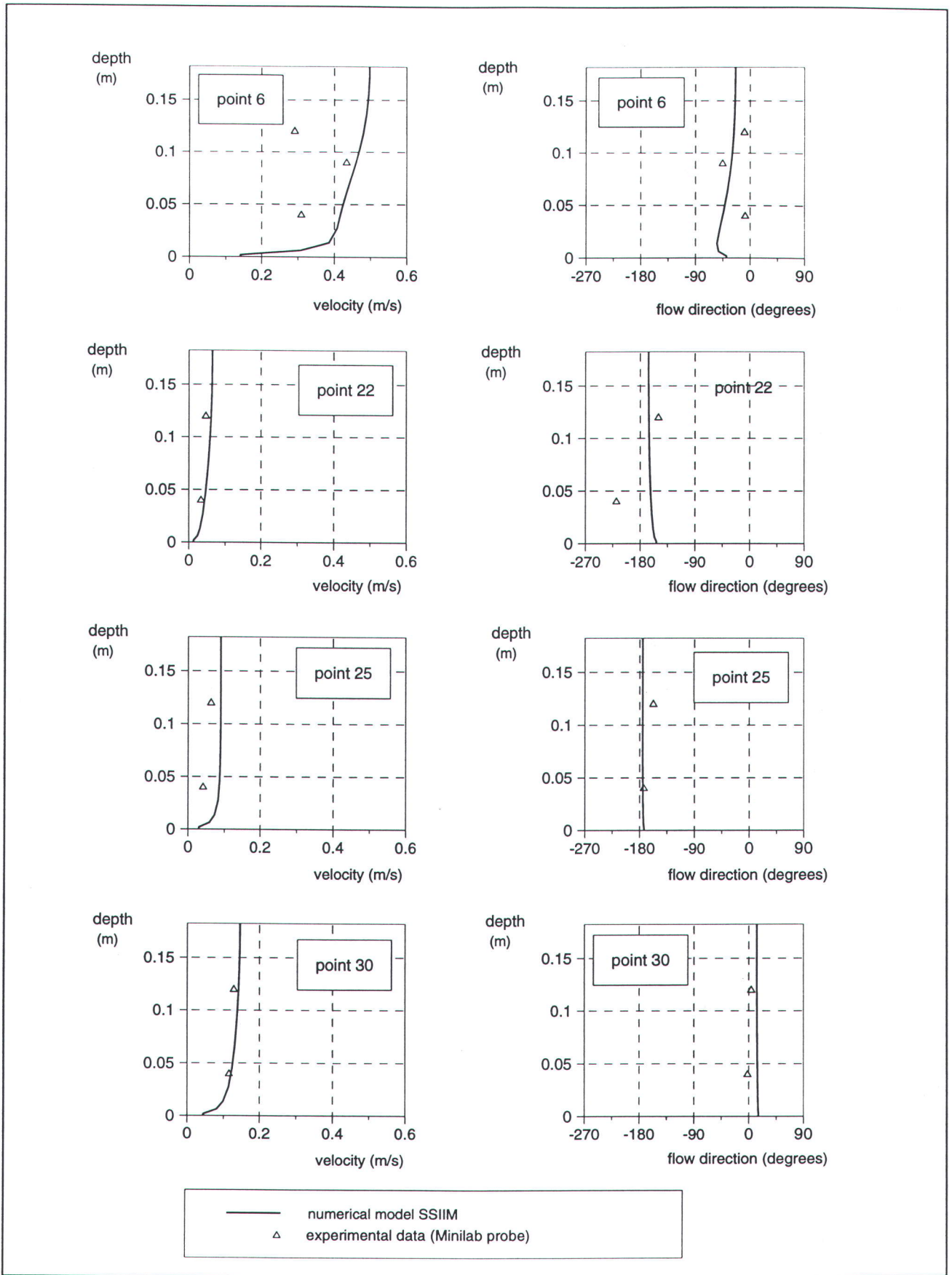


**Figure 8.5 Test RA**b** - Comparison between SSIM and experimental data  
Vertical profiles of plan velocity and flow direction**

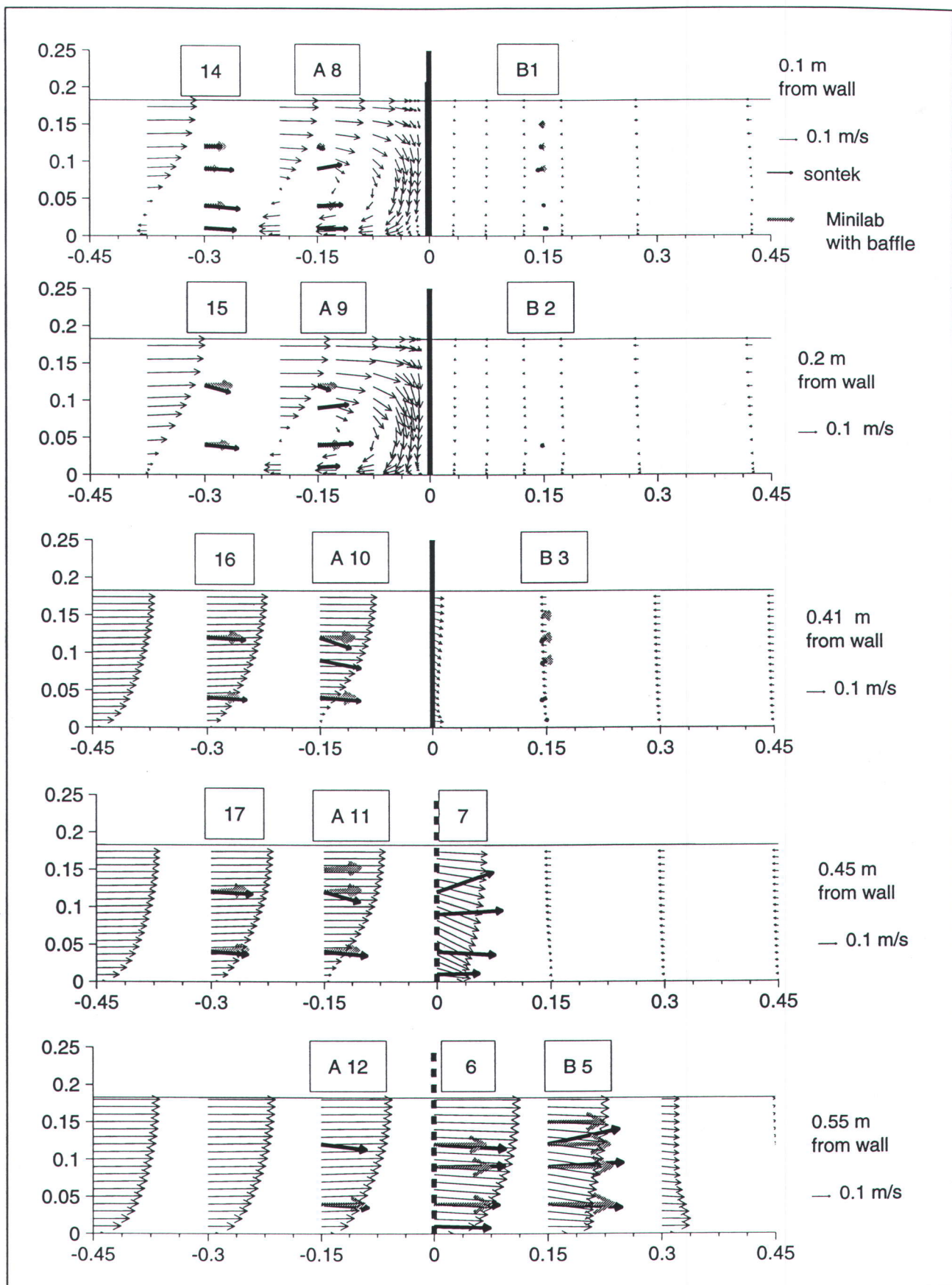


**Figure 8.6 Test RAb - Unsubmerged groyne in rectangular channel**  
**Long section view of velocity vectors (near groyne)**

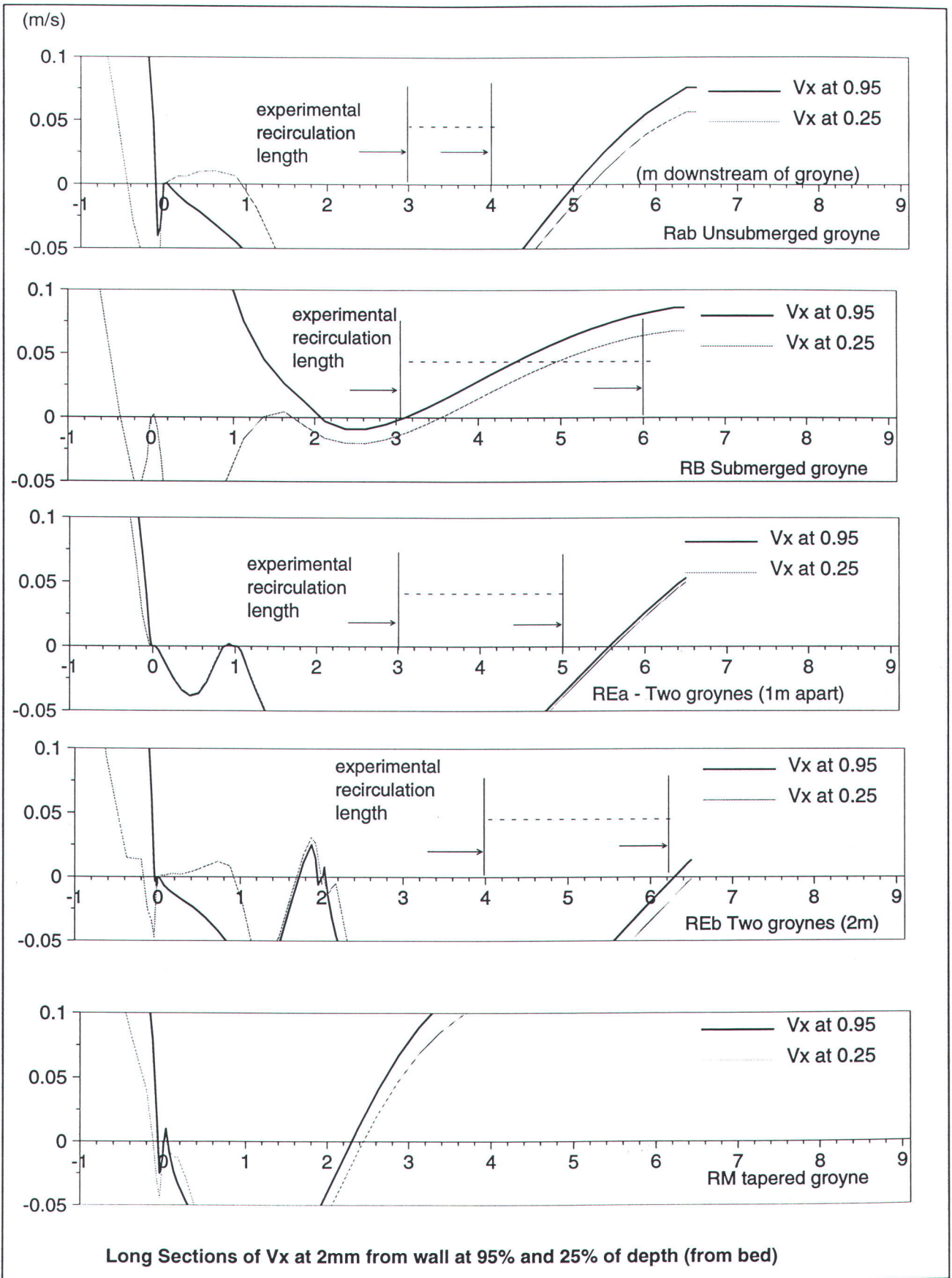


Figure 8.7 Recirculation lengths in rectangular channel

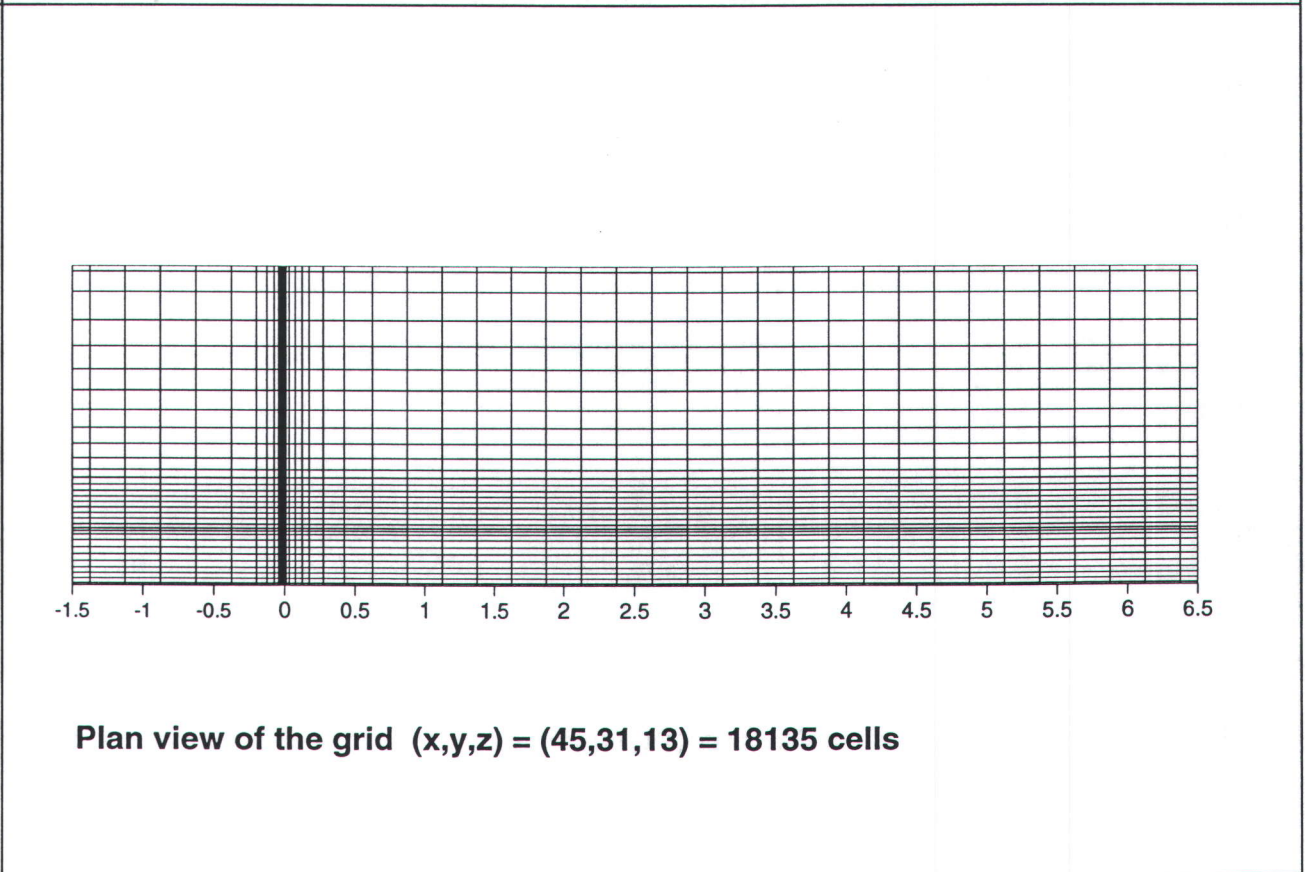
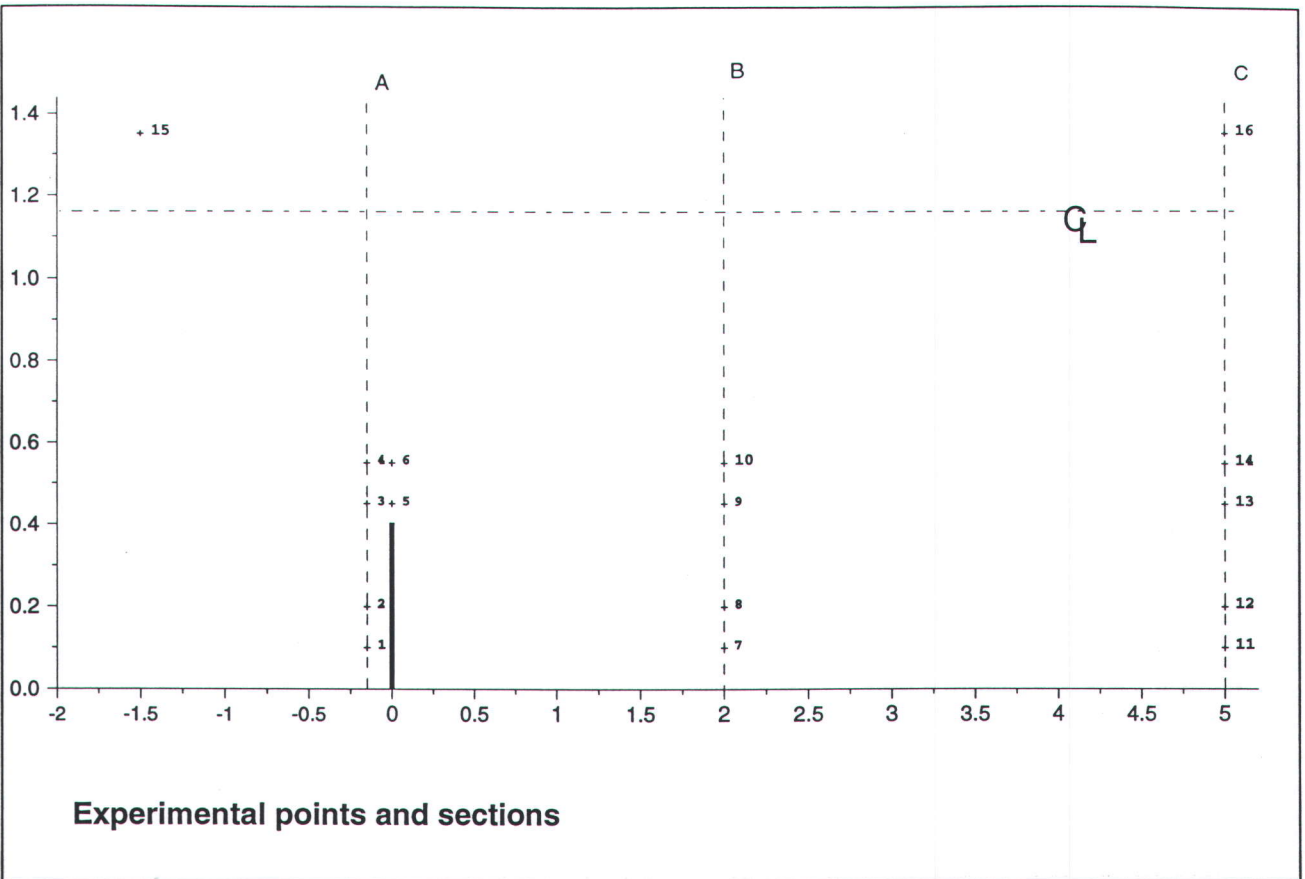
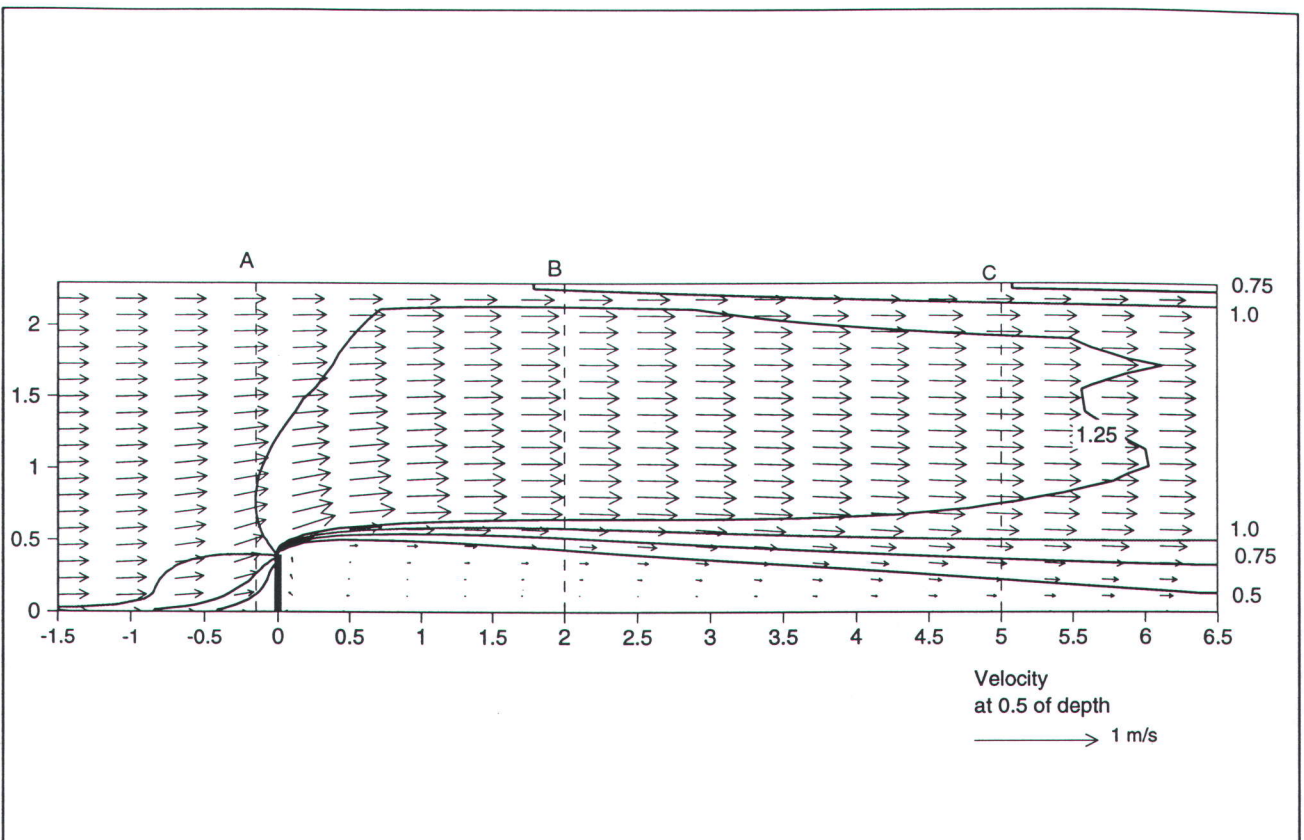
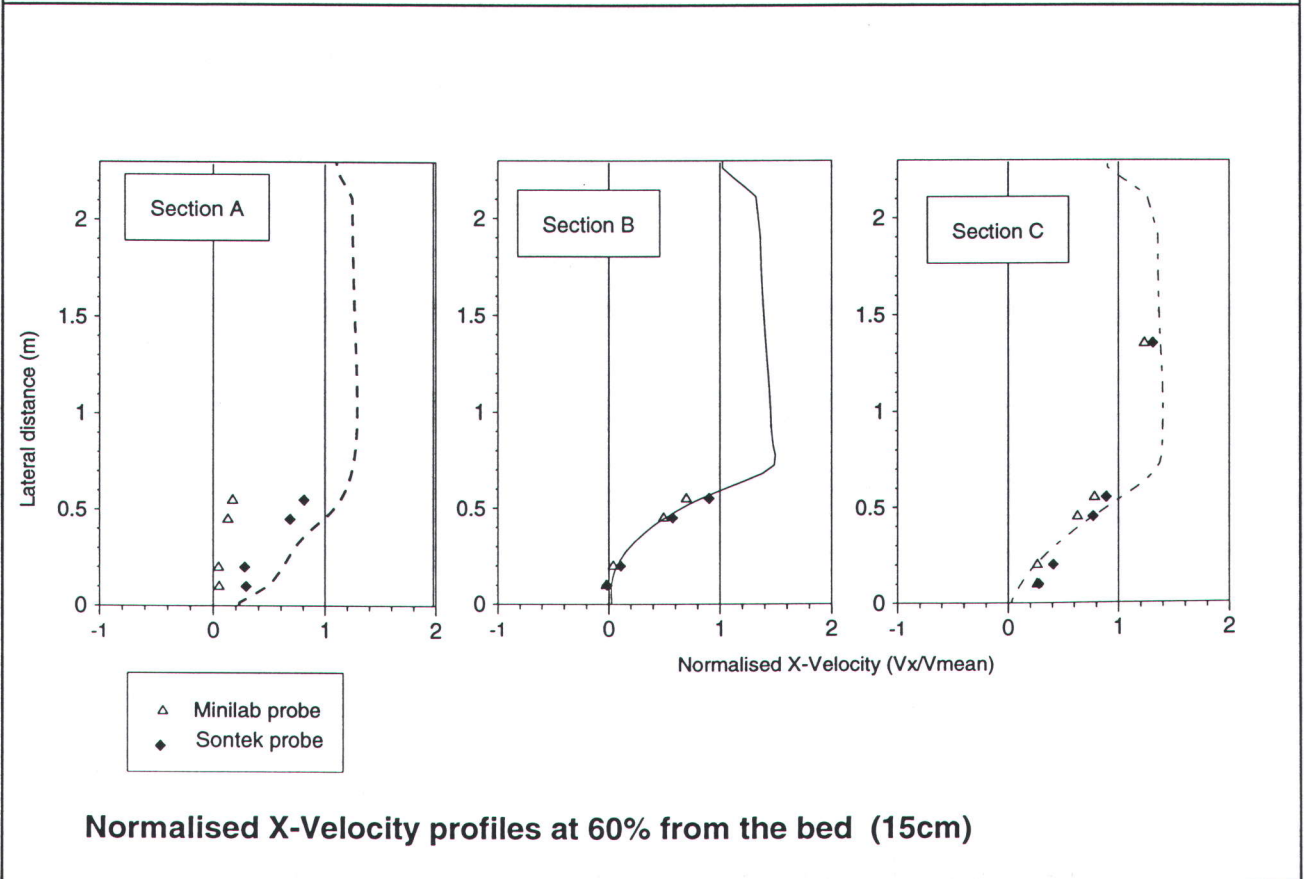


Figure 8.8 Experimental points and numerical grid for Test RB-1

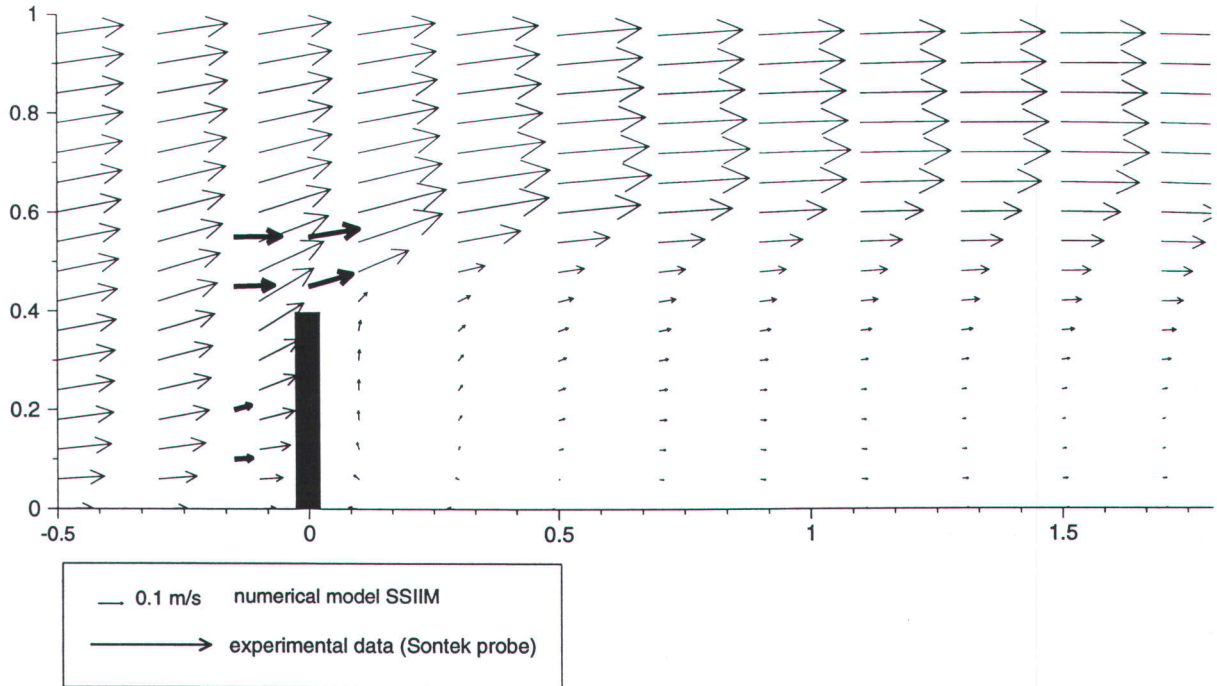


Mid-depth velocity vectors and normalised velocity contours

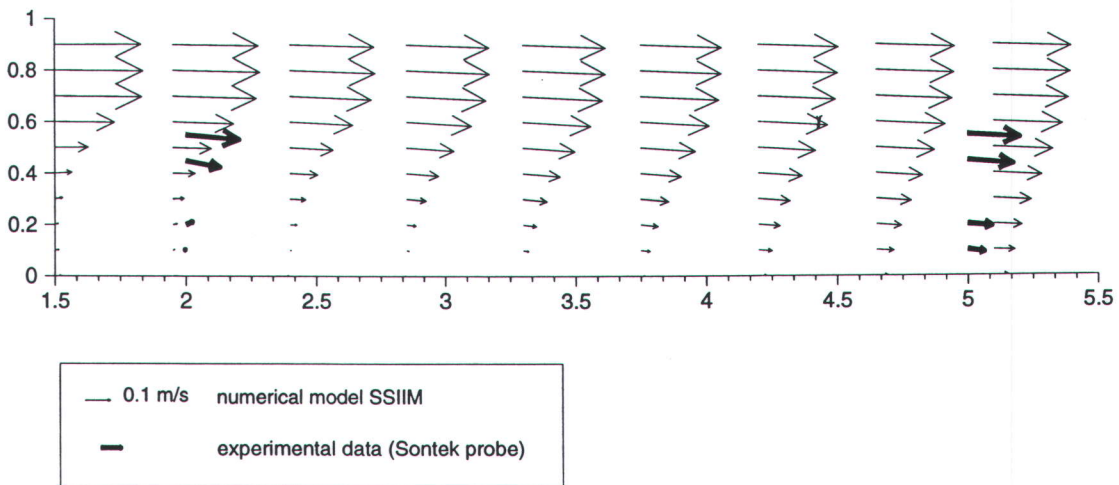


Normalised X-Velocity profiles at 60% from the bed (15cm)

Figure 8.9 Test RB - Submerged groyne in a rectangular channel  
Mid-depth velocities and cross-section profiles of X-velocity

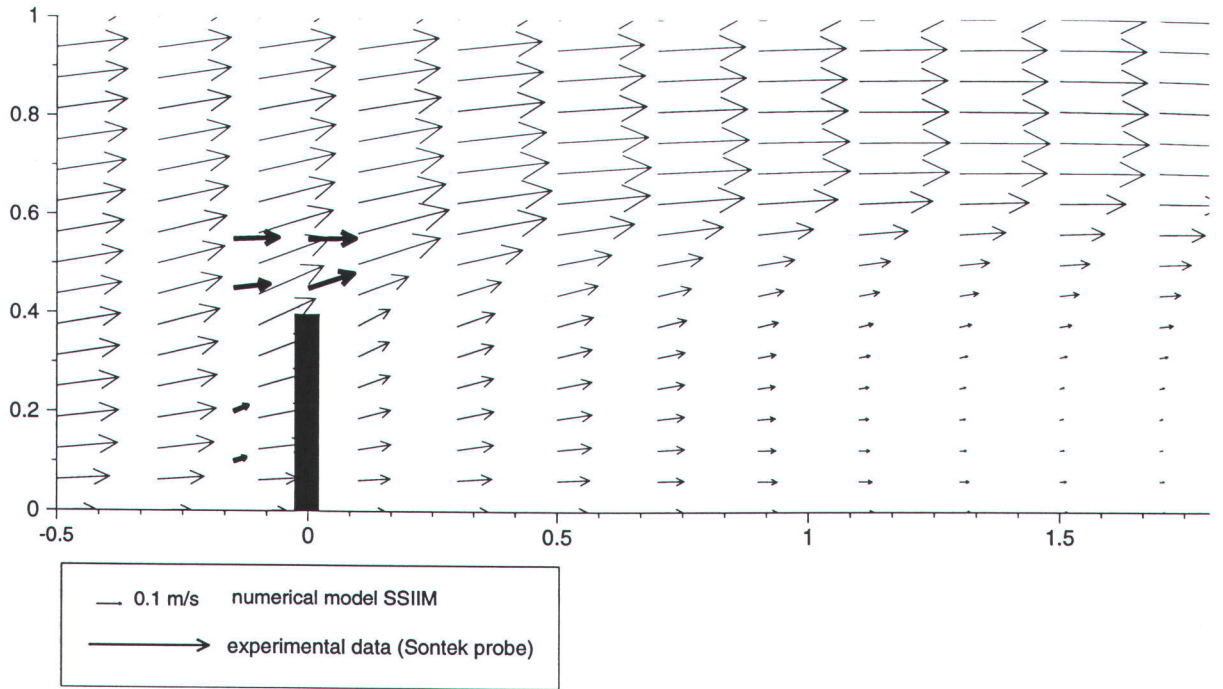


Plan velocity vectors close to the groyne at 60% from the bed

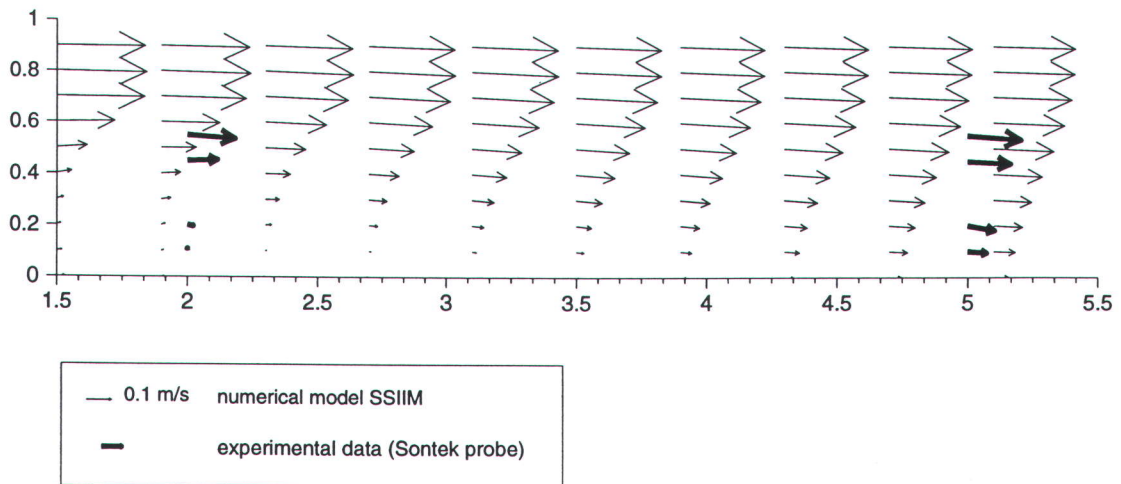


Plan velocity vectors in the recirculation zone at 60% from the bed

Figure 8.10 Test RB - Submerged groyne in rectangular channel  
Plan velocity vectors above mid depth



**Plan velocity vectors close to the groyne at 80% from the bed**



**Plan velocity vectors in the recirculation zone at 80% from the bed**

**Figure 8.11 Test RB - Submerged groyne in rectangular channel  
Plan velocity vectors (near surface)**

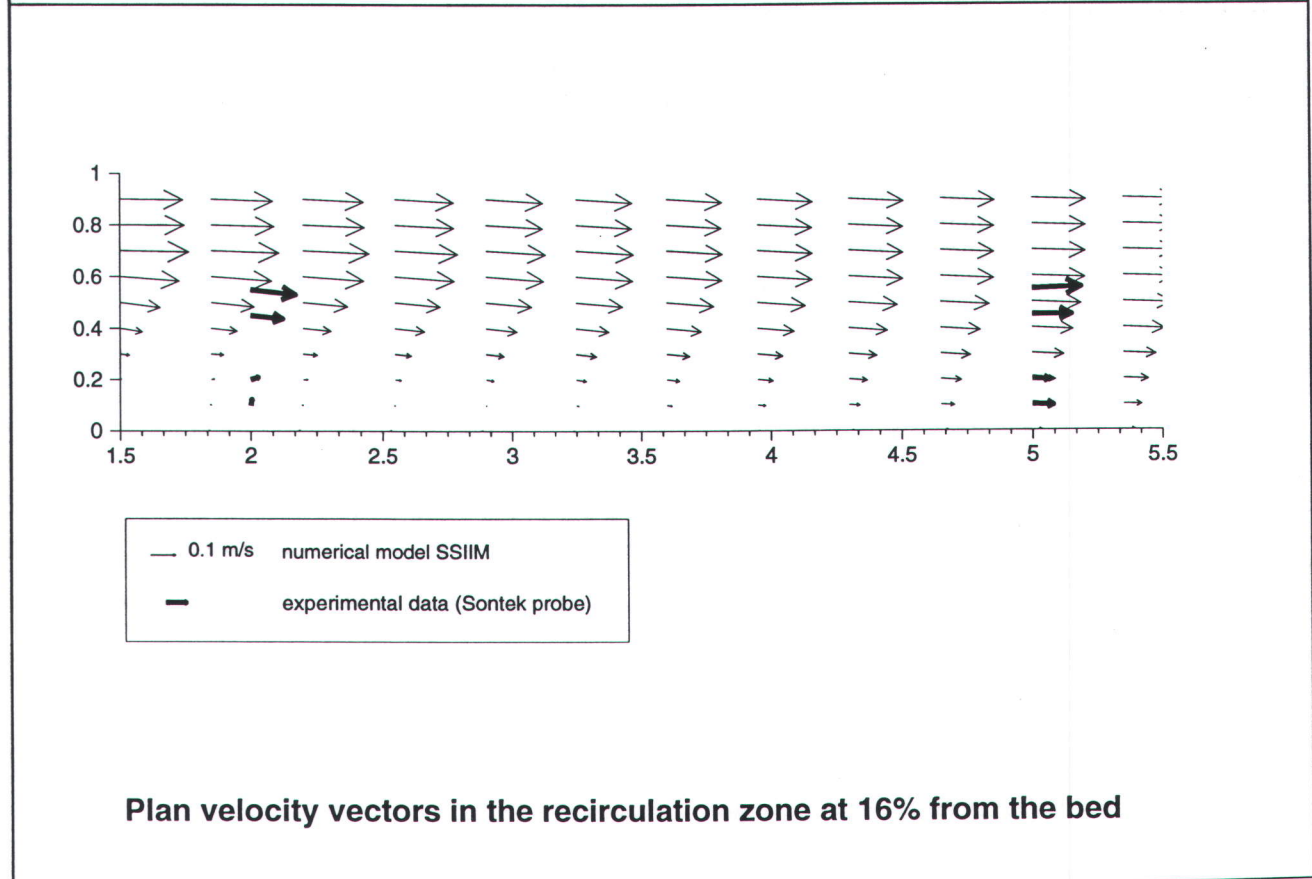
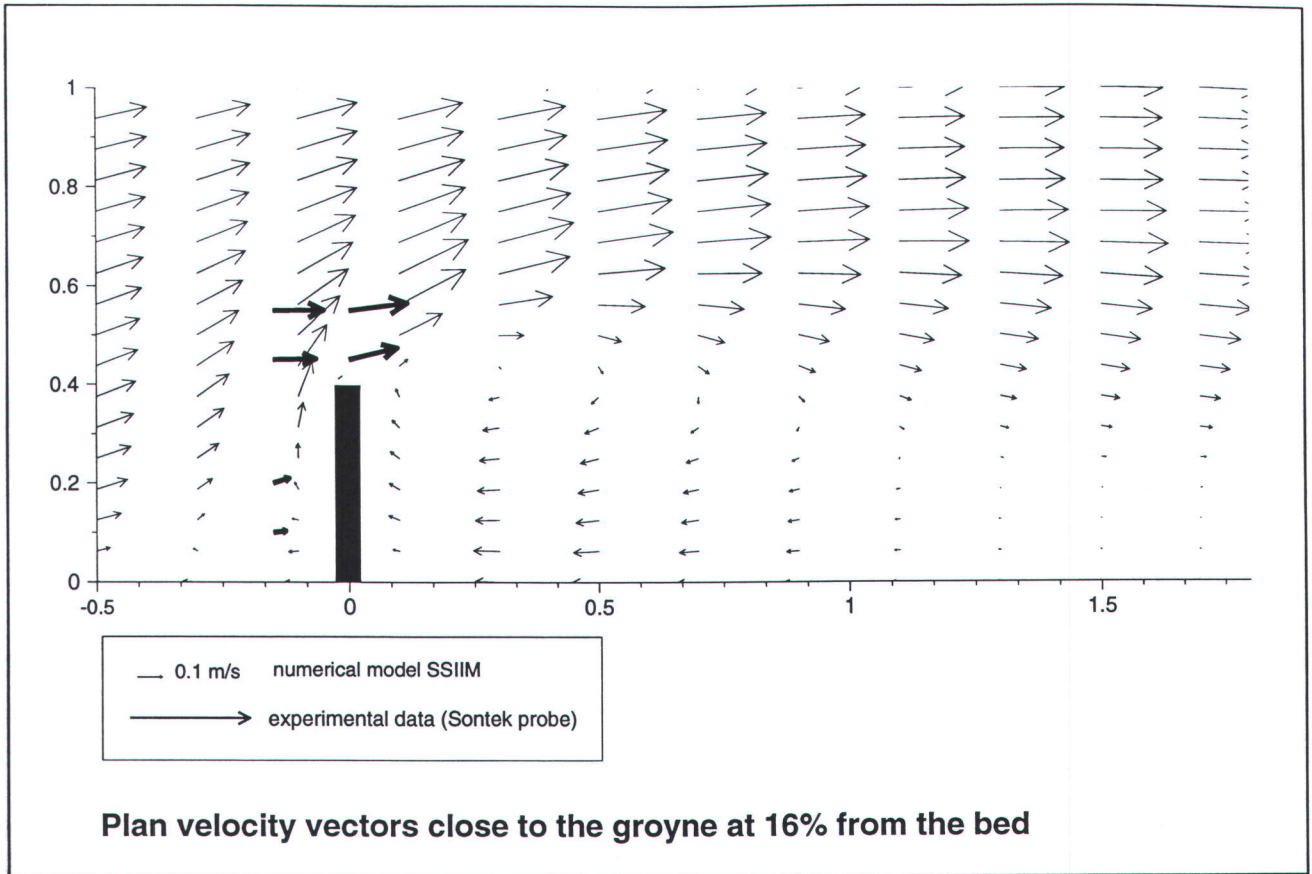


**Figure 8.12 Test RB - Submerged groyne in rectangular channel  
Plan velocity vectors (near bed)**

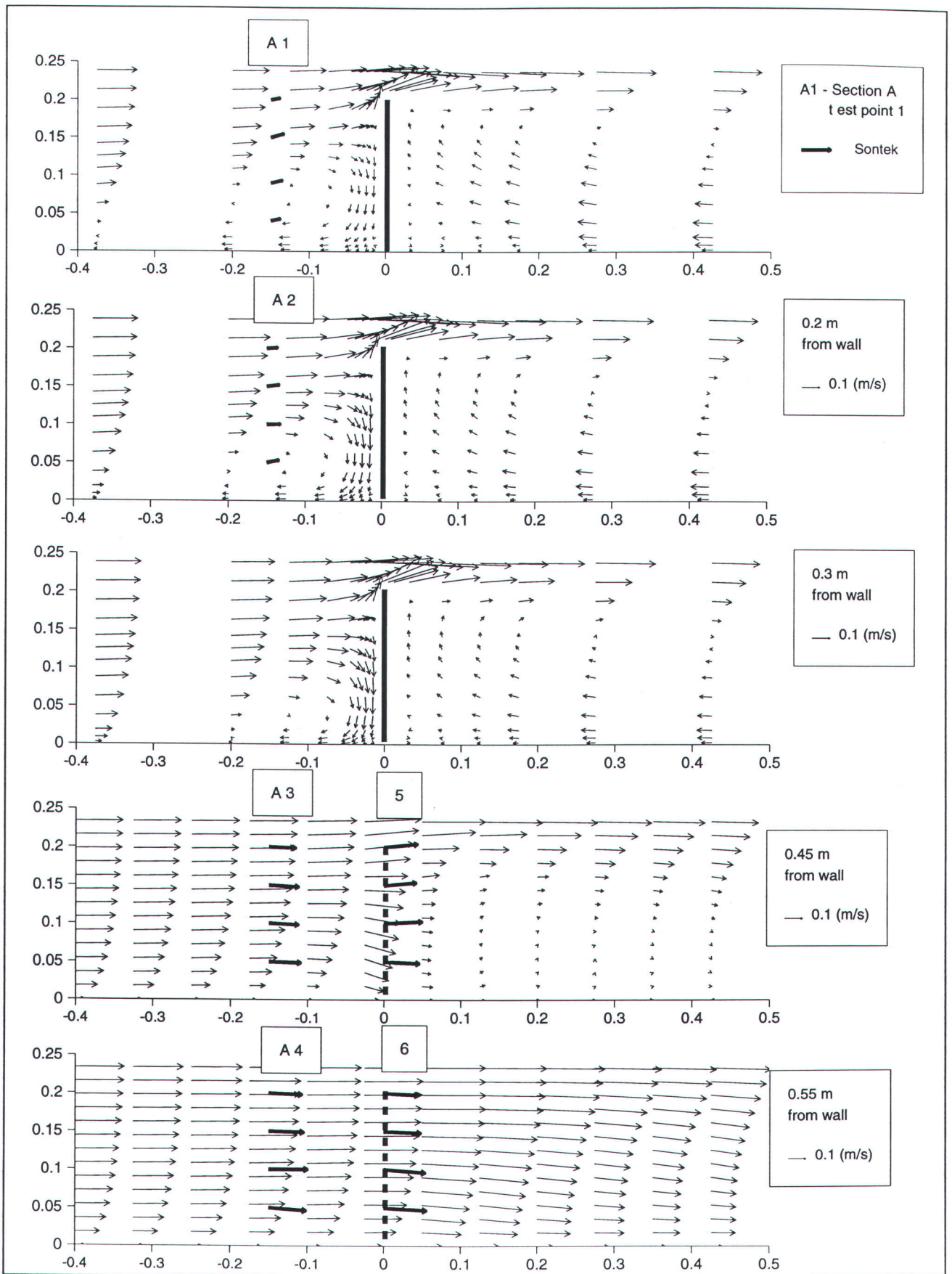


**Figure 8.13 Test RB - Submerged groyne in rectangular channel  
Long section - velocity vectors near groyne**

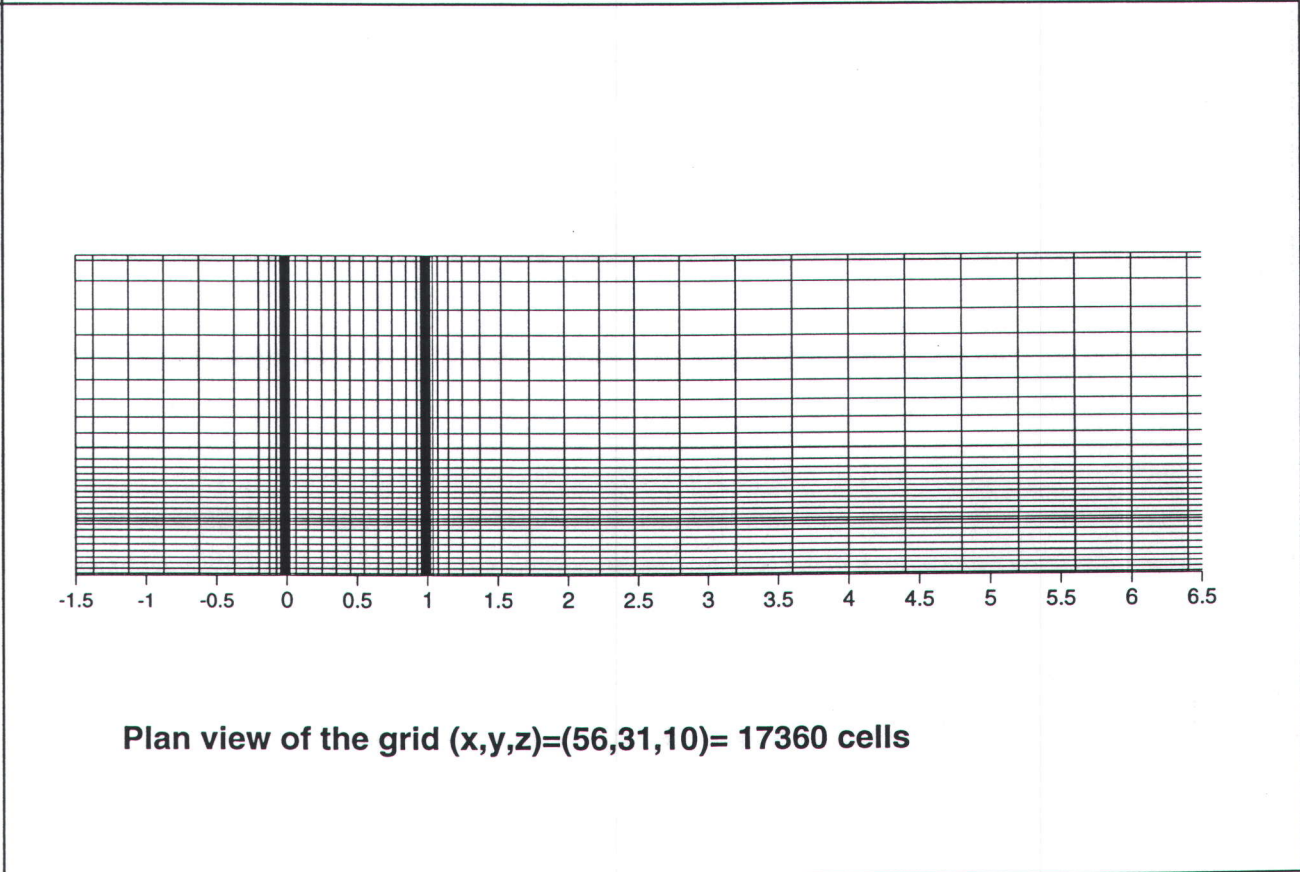
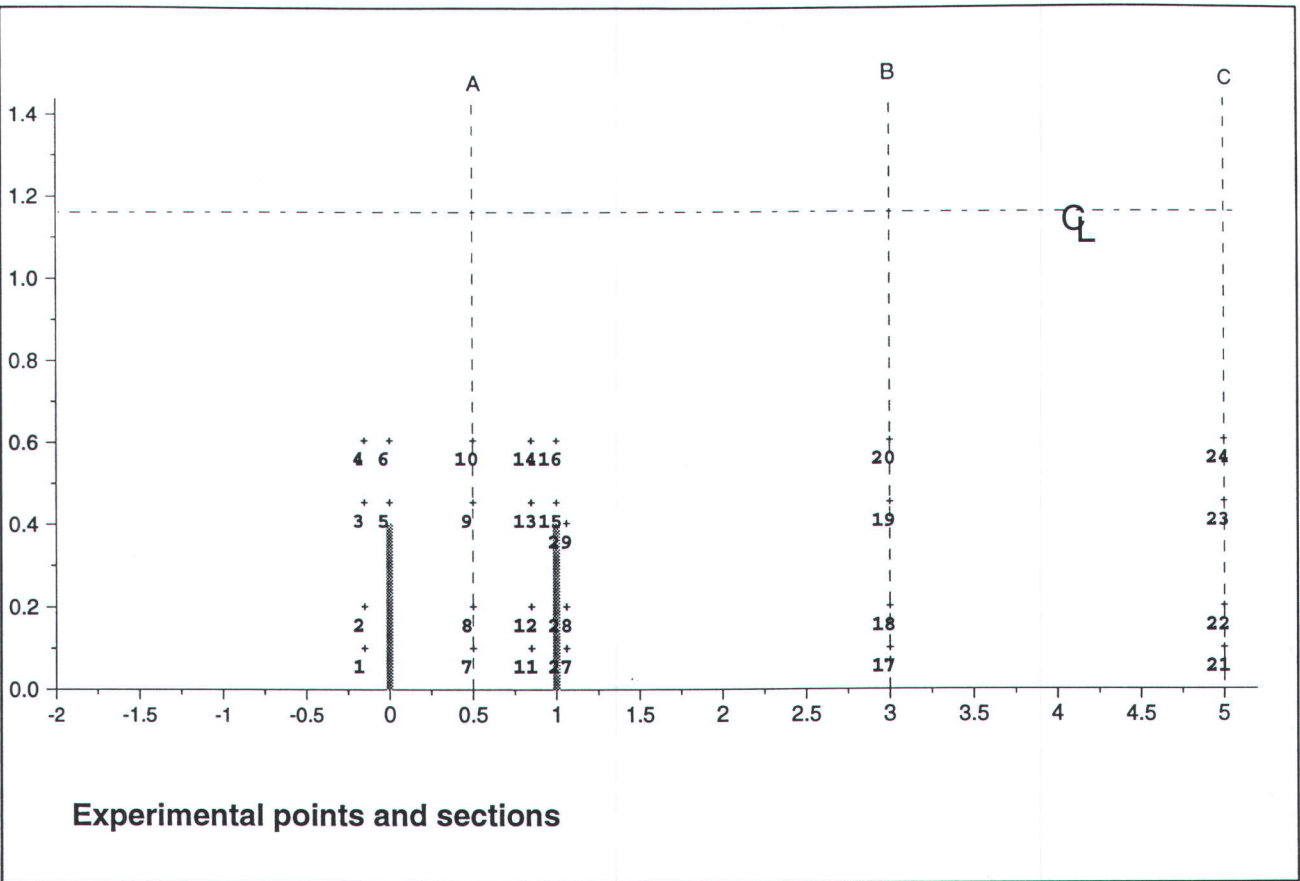
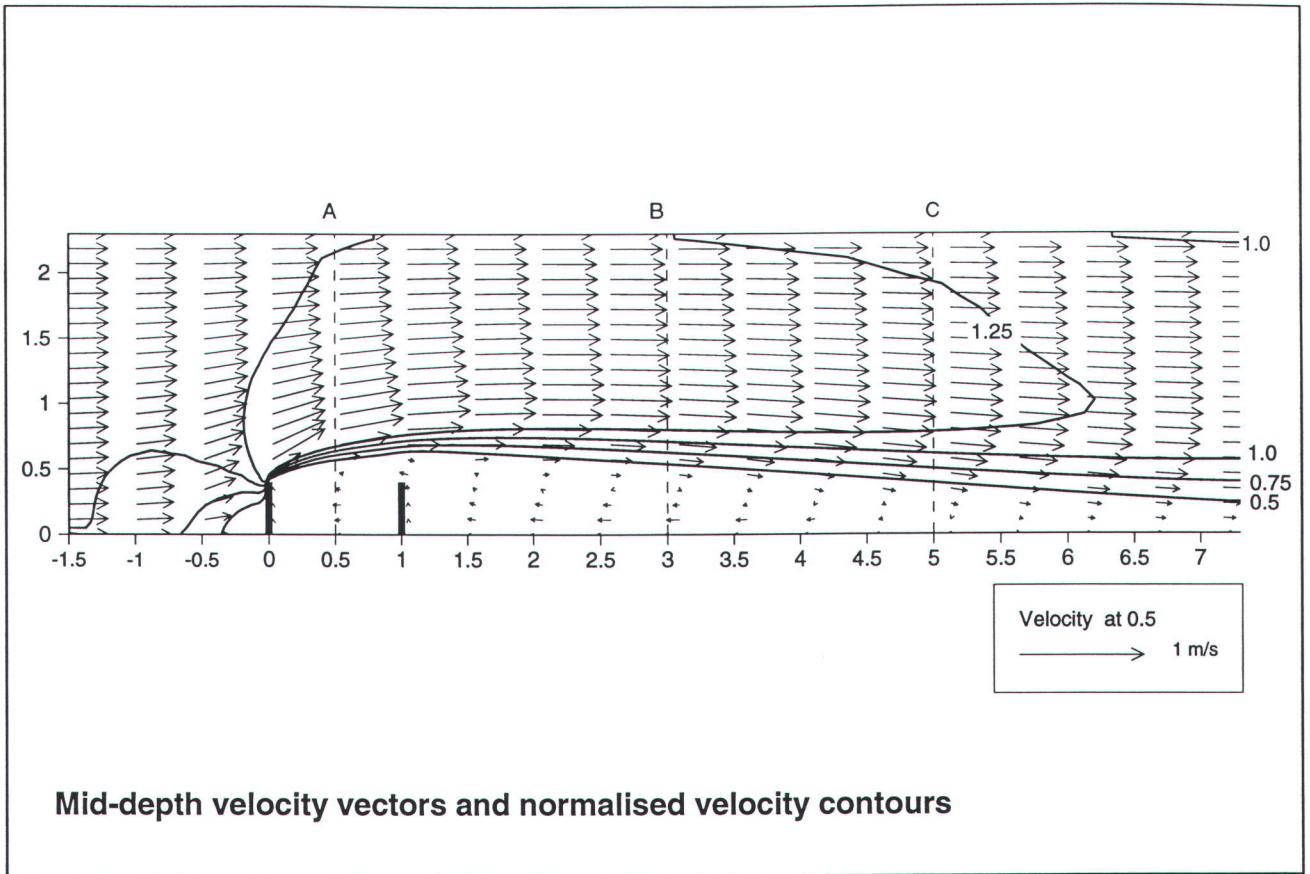
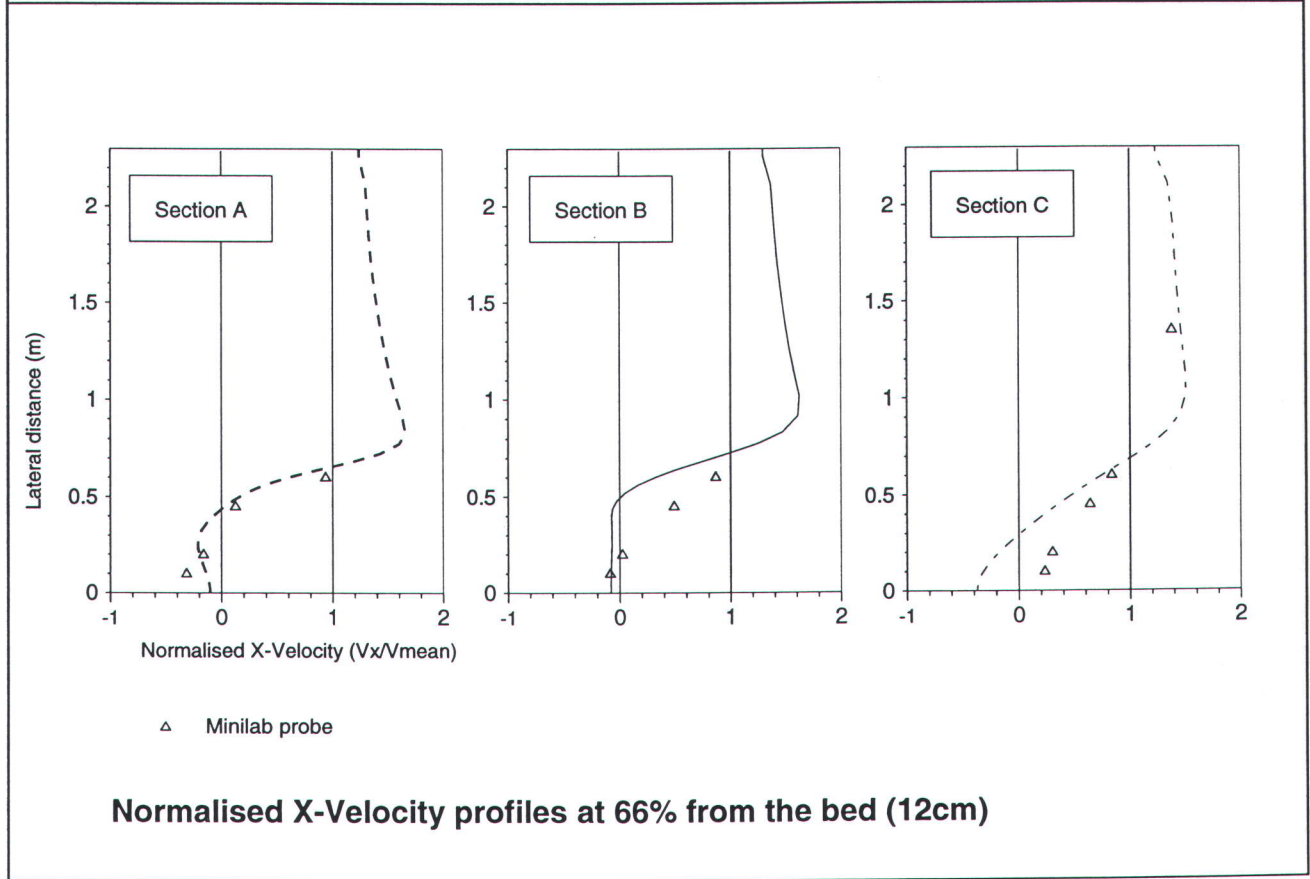


Figure 8.14 Experimental points and numerical grid for Test REa-1

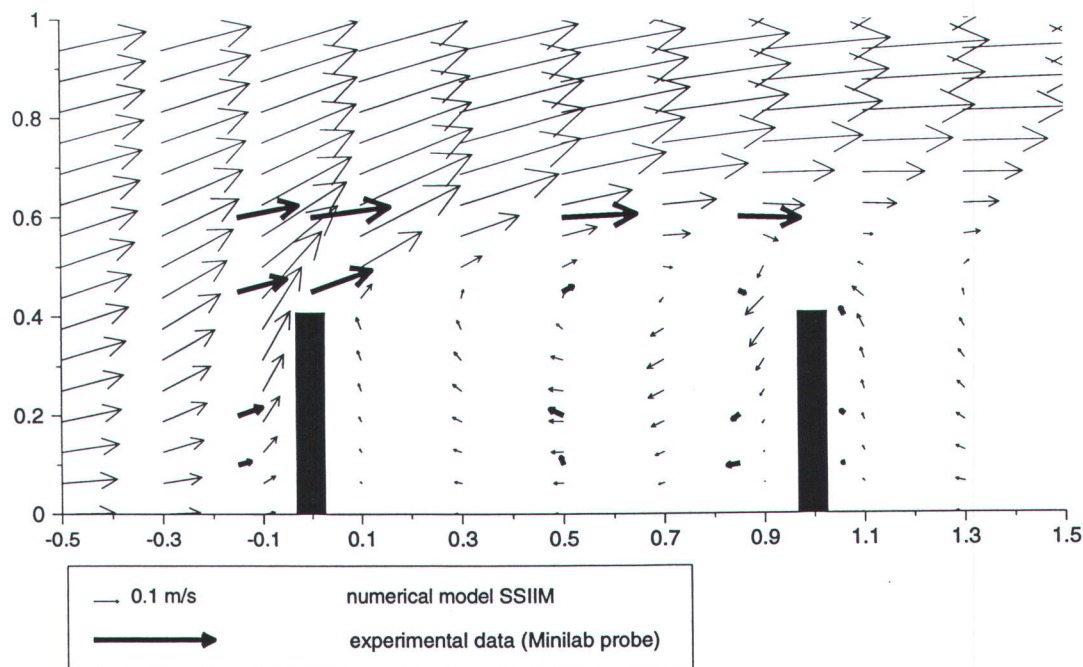


Mid-depth velocity vectors and normalised velocity contours

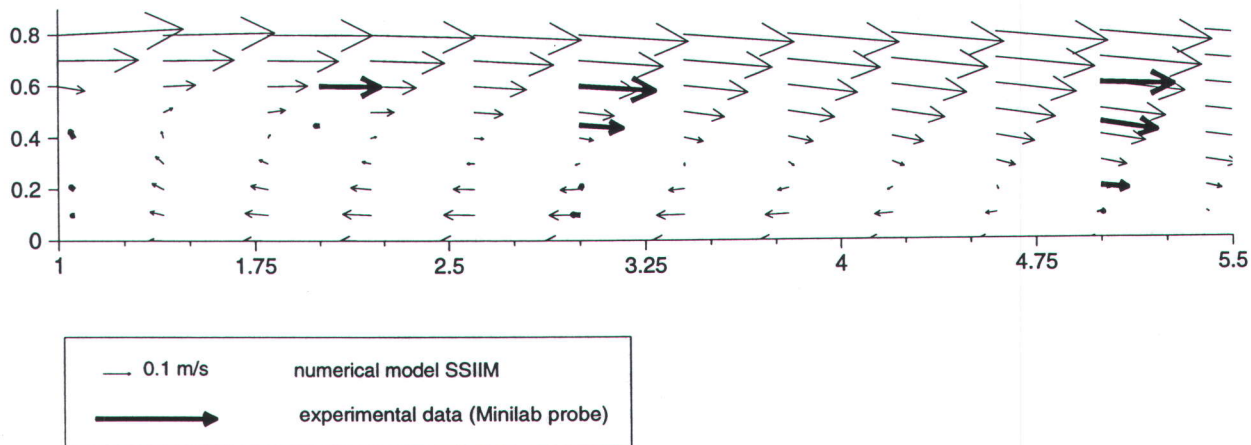


Normalised X-Velocity profiles at 66% from the bed (12cm)

Figure 8.15 Test REa - Two groynes 1m apart in a rectangular channel  
Mid-depth velocities and cross-section profiles of X-velocity



Plan velocity vectors close to the groyne at 66% from the bed



Plan velocity vectors in the recirculation zone at 66% from the bed

Figure 8.16 Test REa - Two groynes 1m apart in a rectangular channel  
Plan velocity vectors near groyne and in recirculation zone

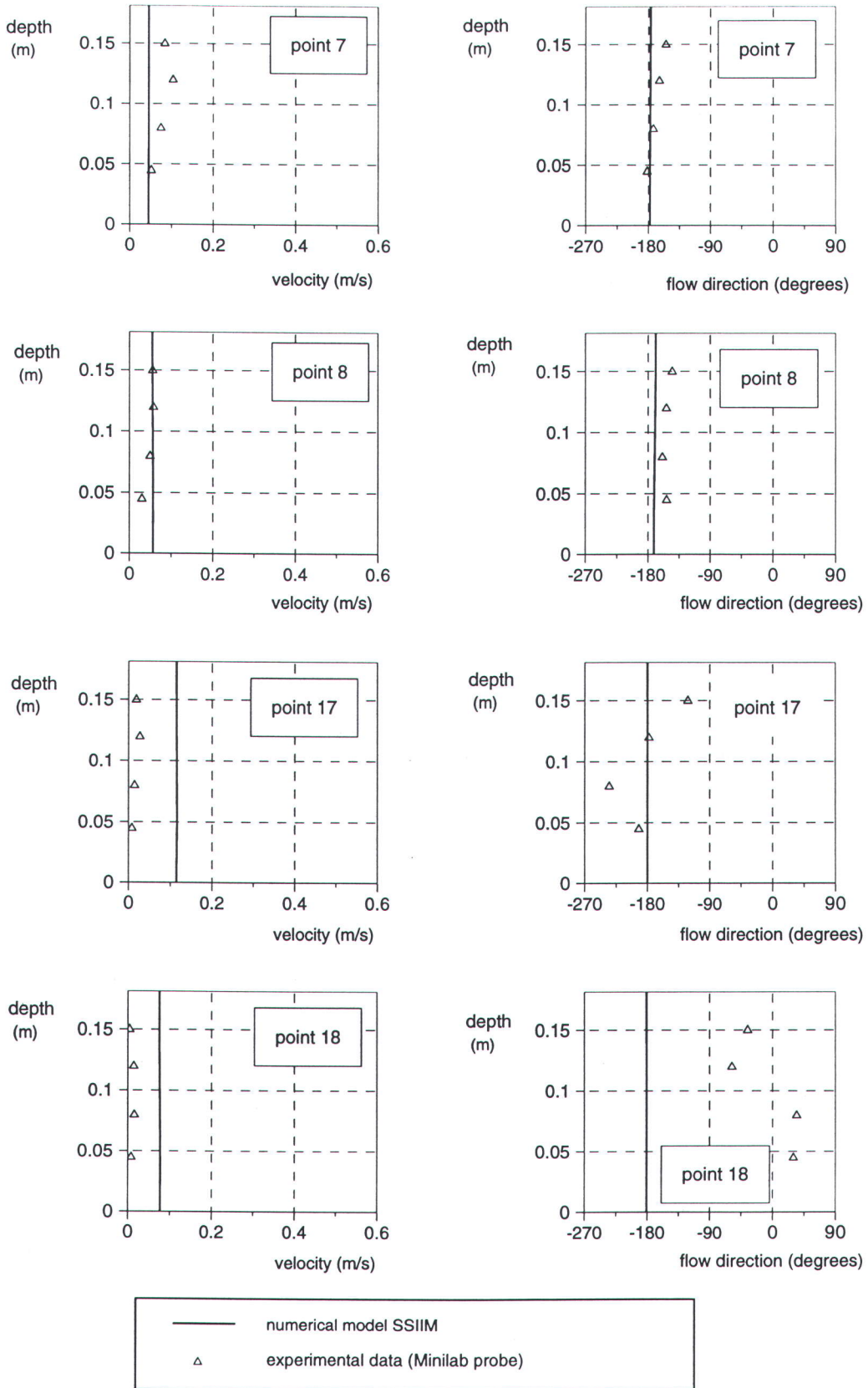


**Figure 8.17 Test REa - Two groynes (1m apart) in a rectangular channel  
Vertical profiles of plan velocity and flow direction**

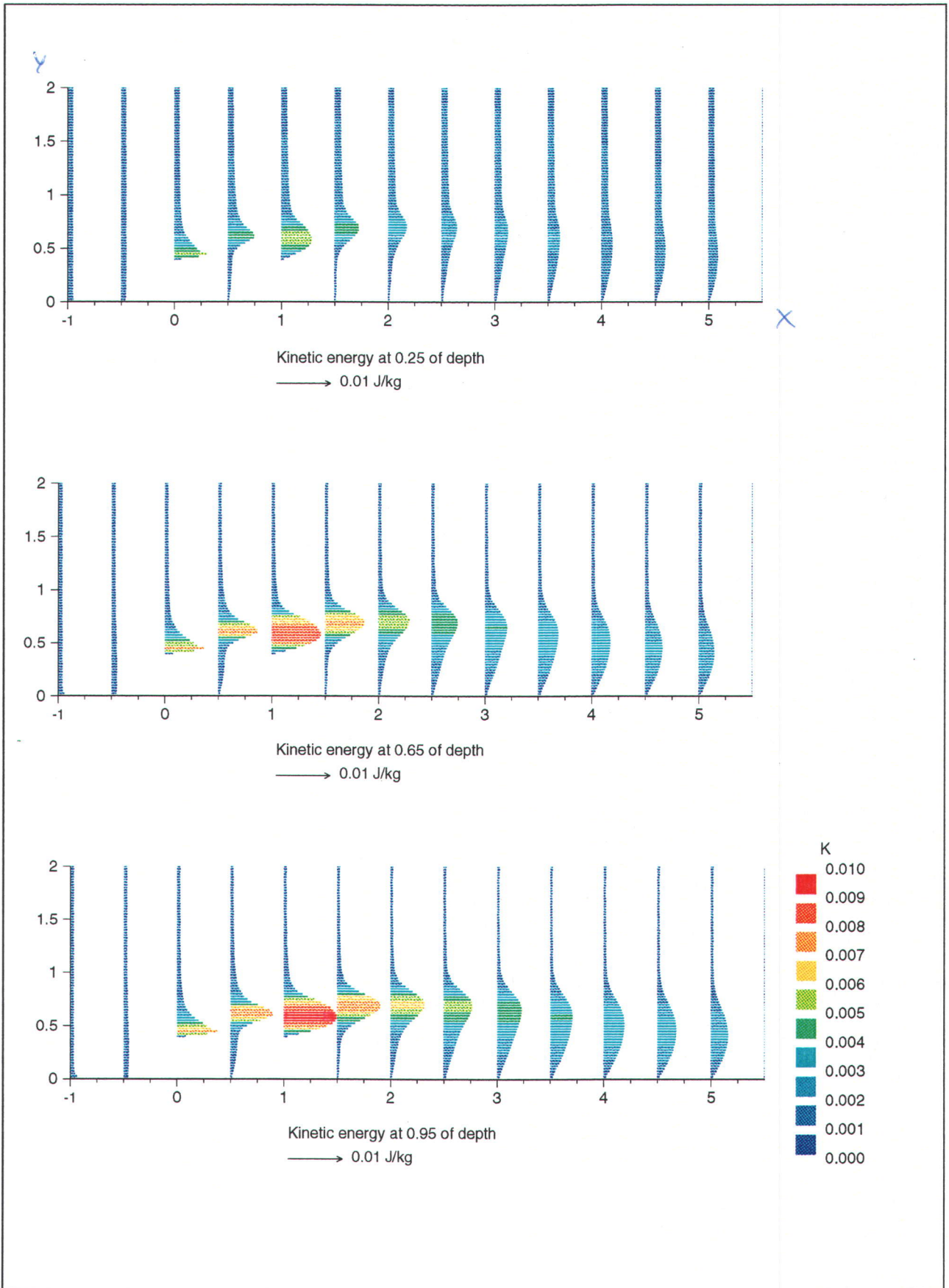


**Figure 8.18 Test REa Two groynes (1m apart ) in rectangular channel  
Turbulent kinetic energy at three depths**

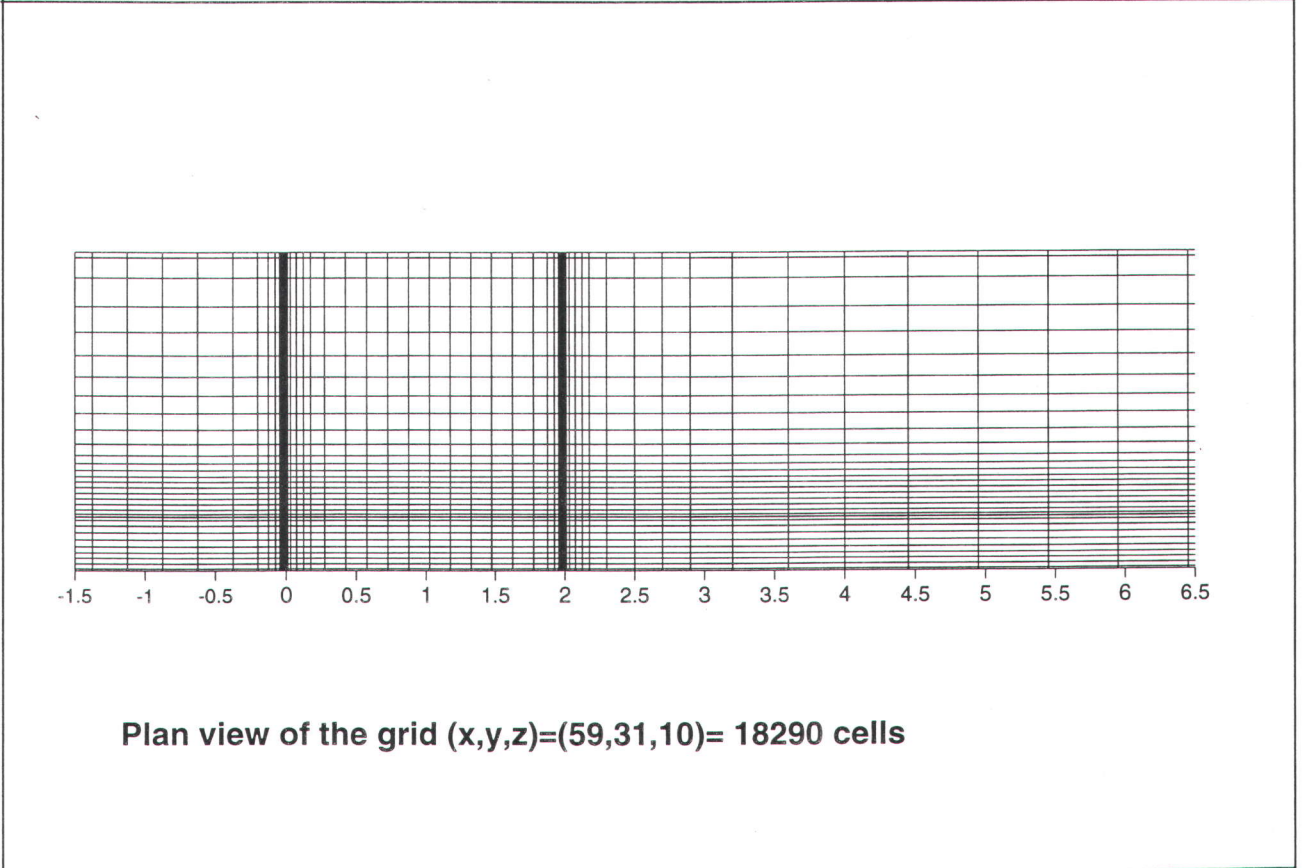
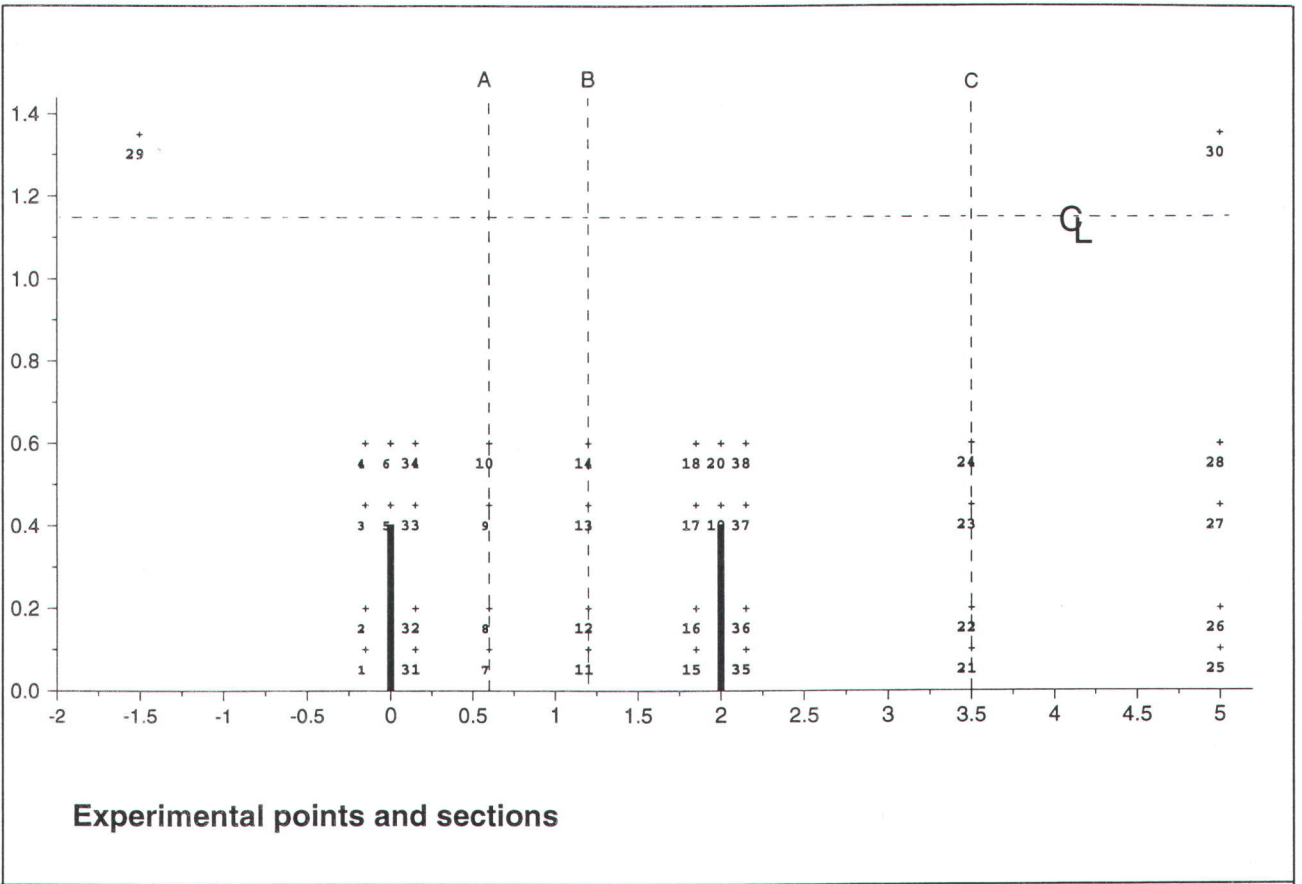
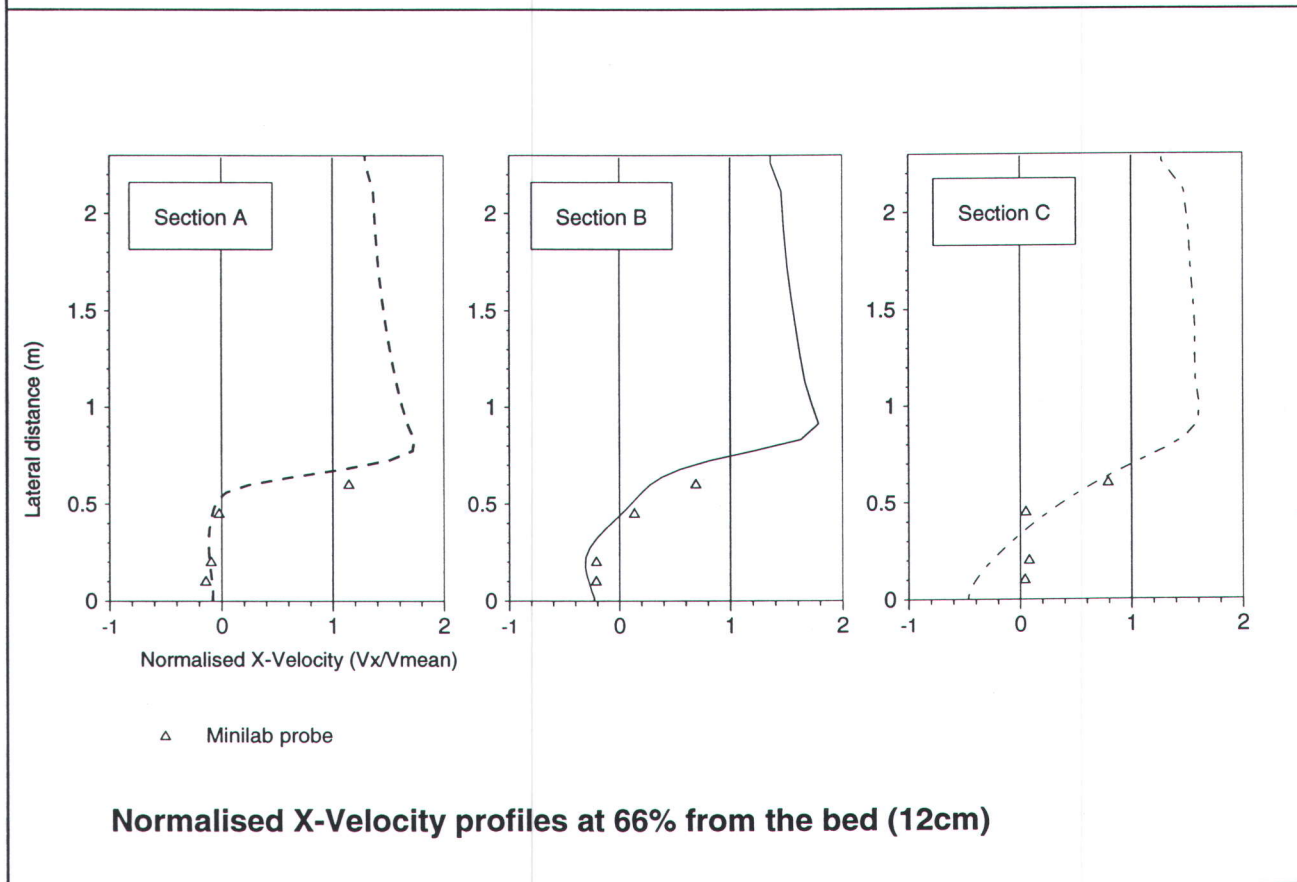
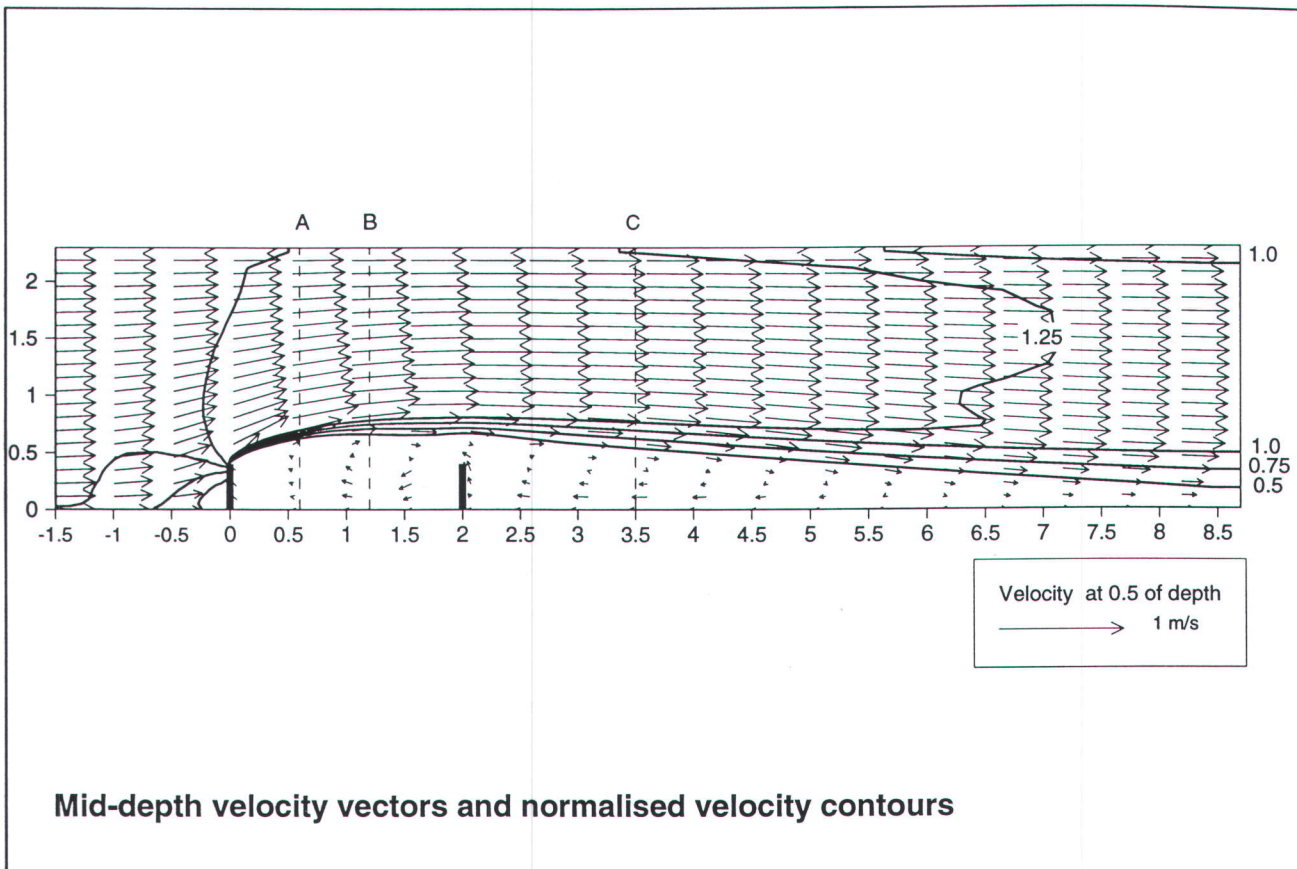
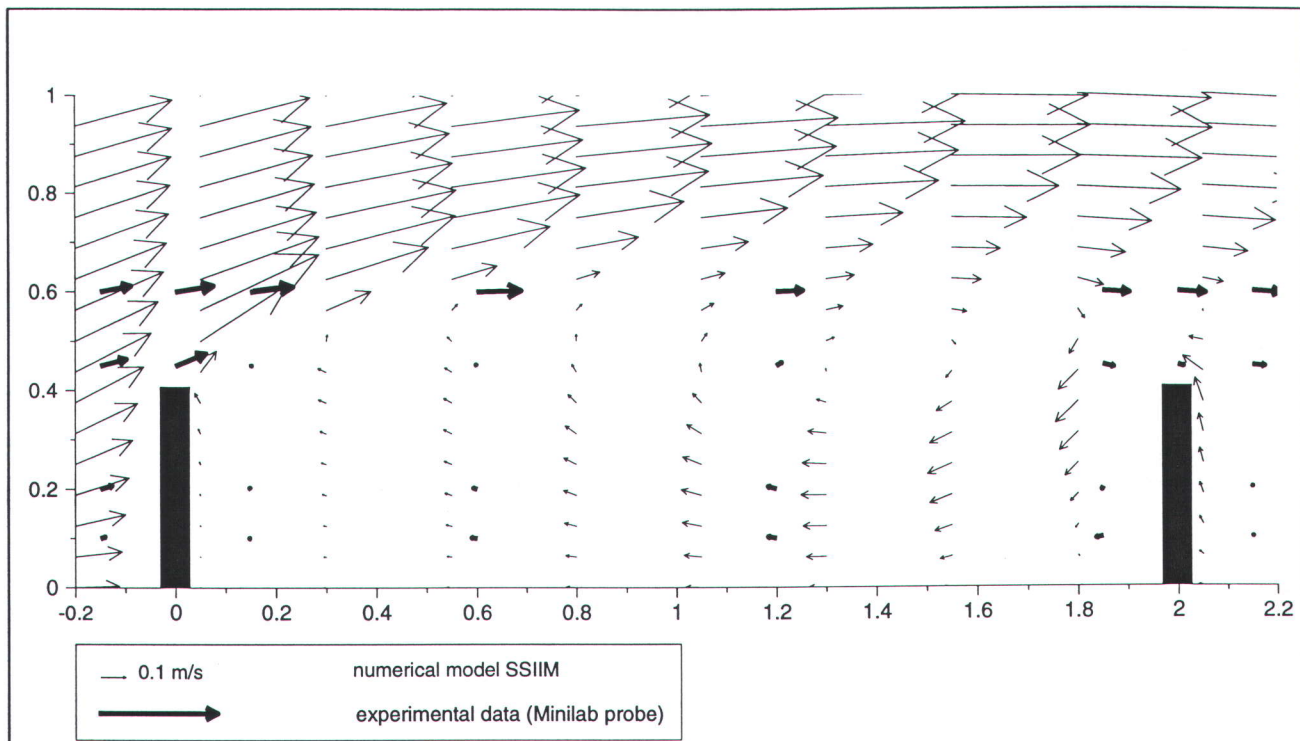


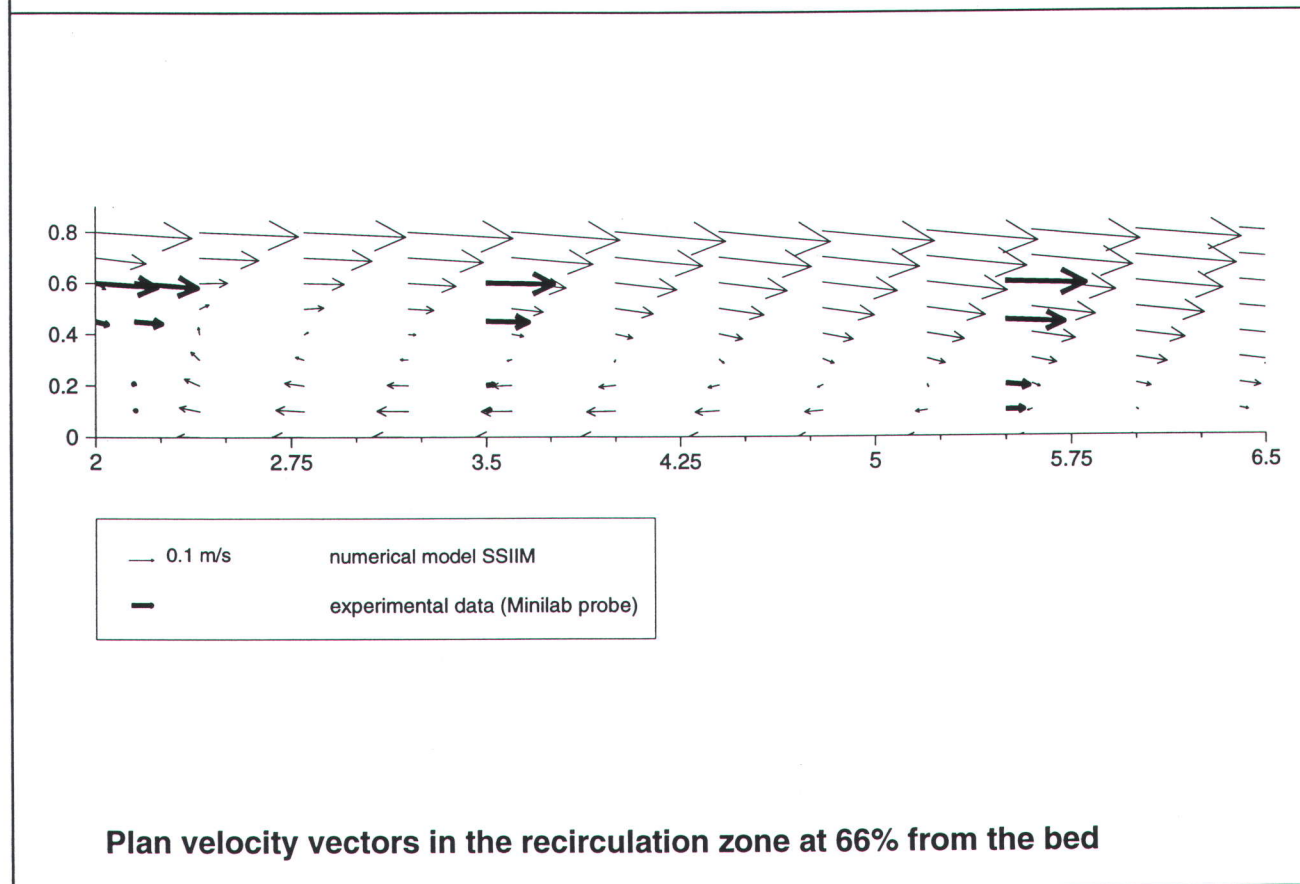
Figure 8.19 Experimental points and numerical grid for Test REb-1



**Figure 8.20 Test REb - Two groynes 2m apart in a rectangular channel  
Mid-depth velocities and cross-section profiles of X-velocity**



Plan velocity vectors close to the groyne at 66% from the bed



Plan velocity vectors in the recirculation zone at 66% from the bed

**Figure 8.21 Test REb - Two groynes 2m apart in a rectangular channel  
Plan velocity vectors near groyne and in recirculation zone**

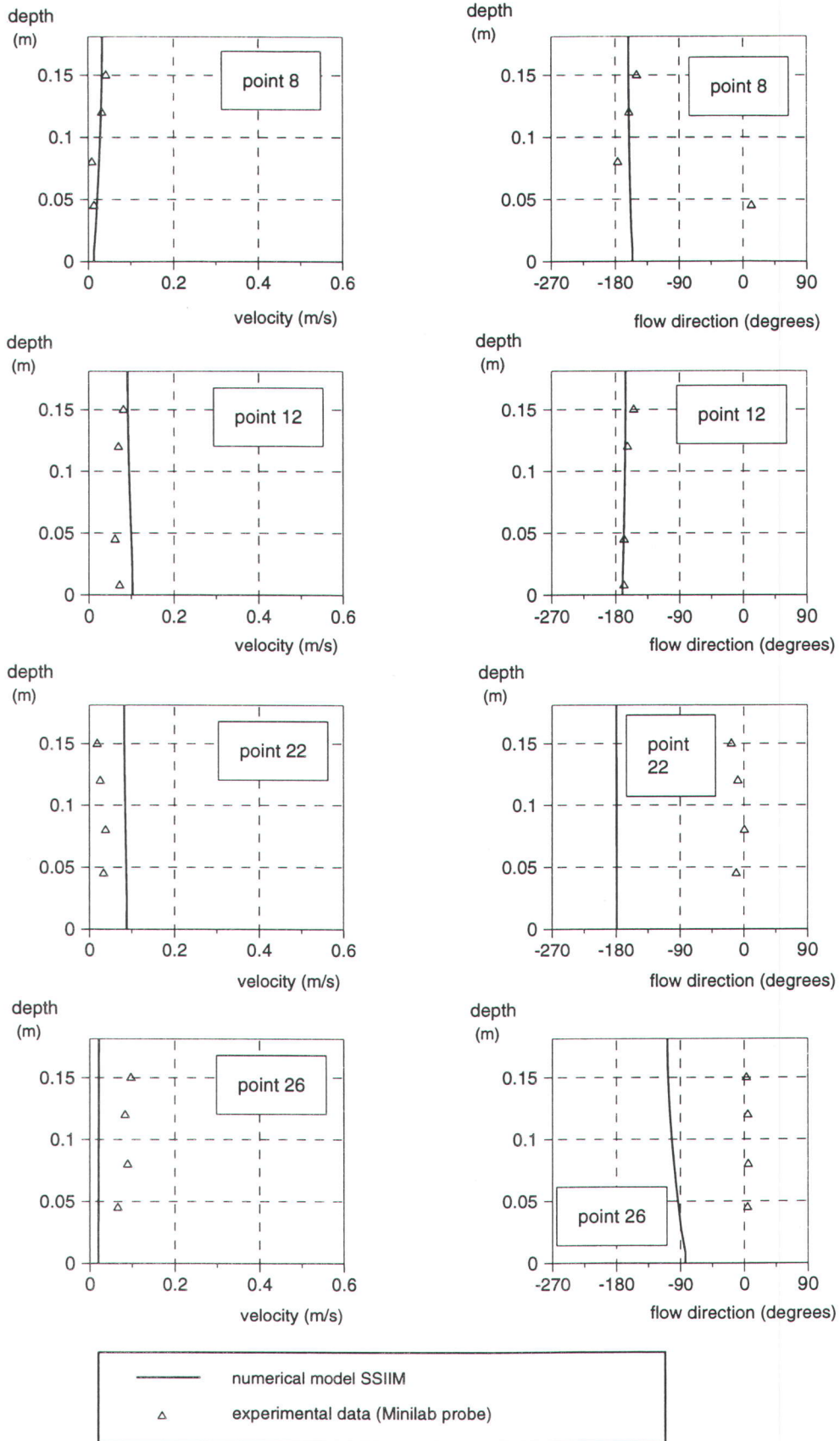


**Figure 8.22 Test REb - Two groynes (2m apart) in a rectangular channel**  
**Vertical profiles of plan velocity and flow direction**

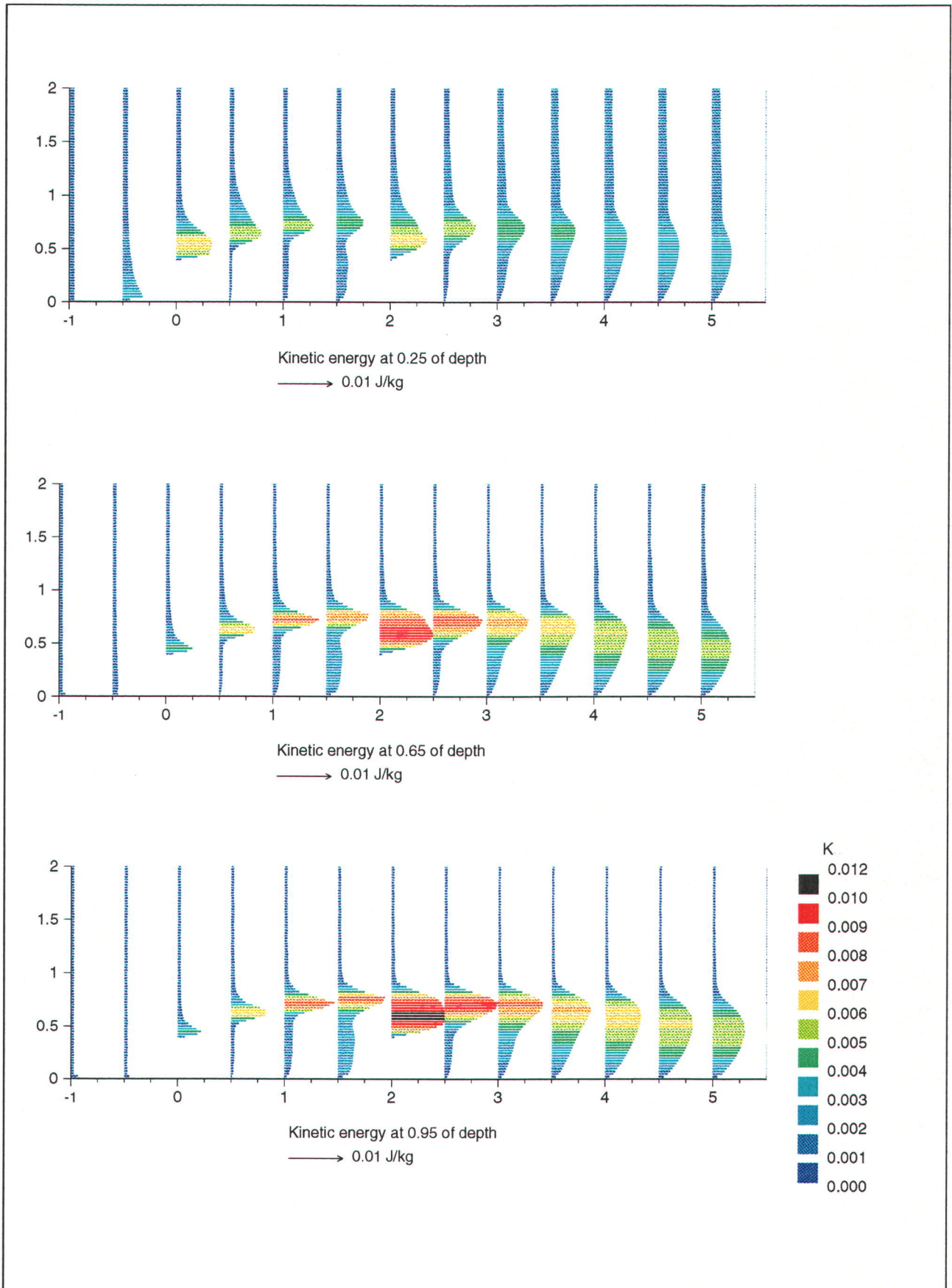
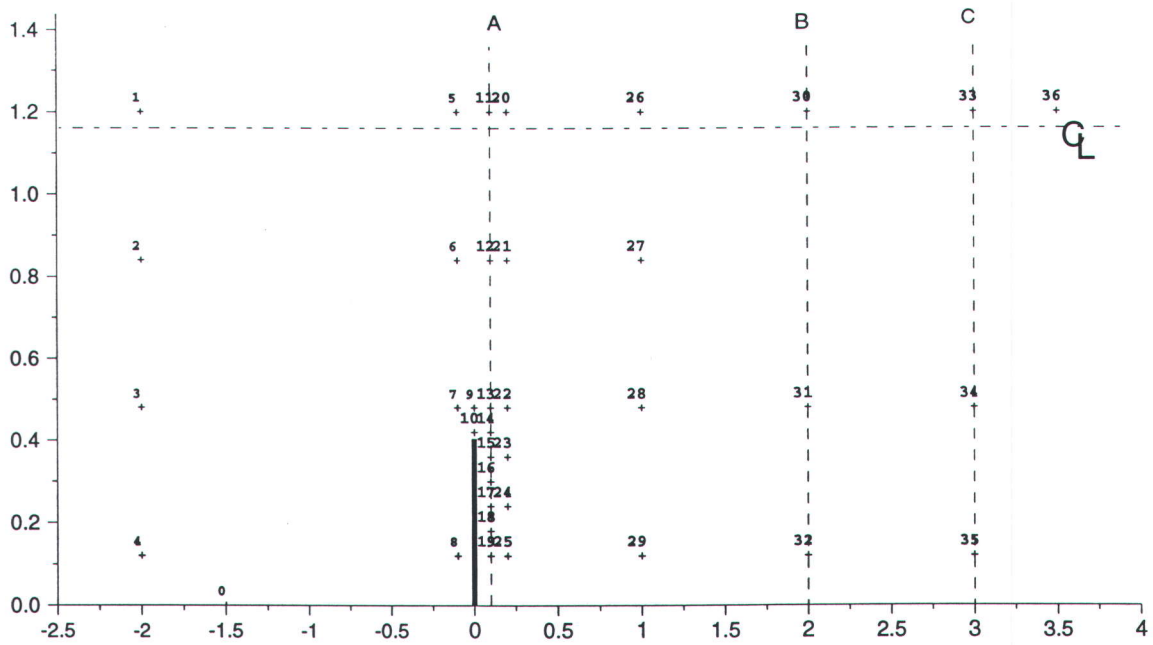
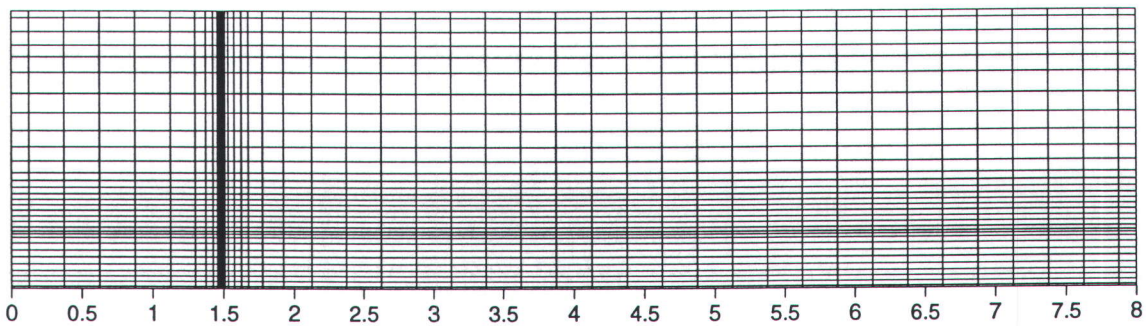


**Figure 8.23** Test REb Two groynes (2m apart) in rectangular channel  
Turbulent kinetic energy at three depths



Experimental points and sections



Plan view of the grid  $(x,y,z) = (45,31,10) = 13950$  cells

Figure 8.24 Experimental points and numerical grid for Tests RX and RY

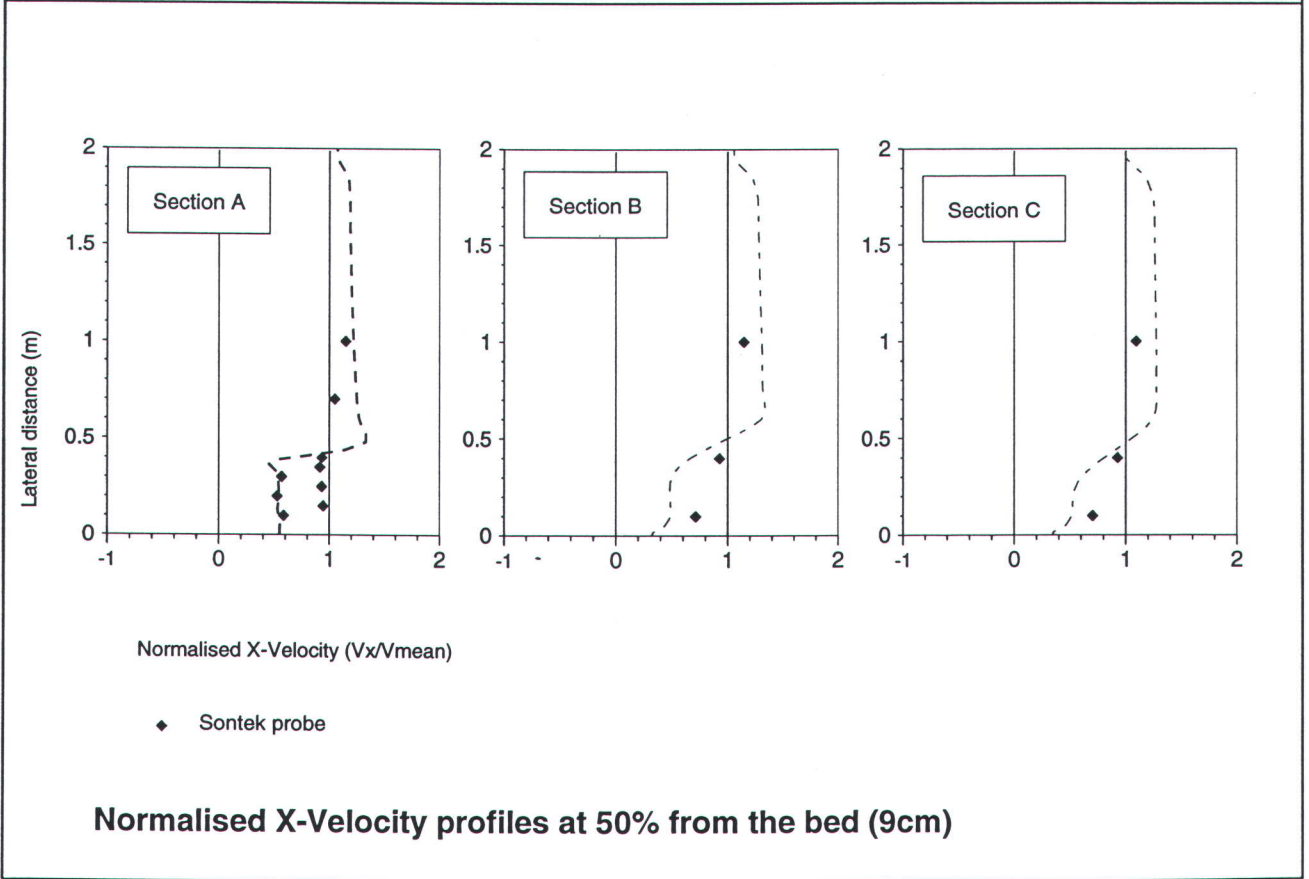
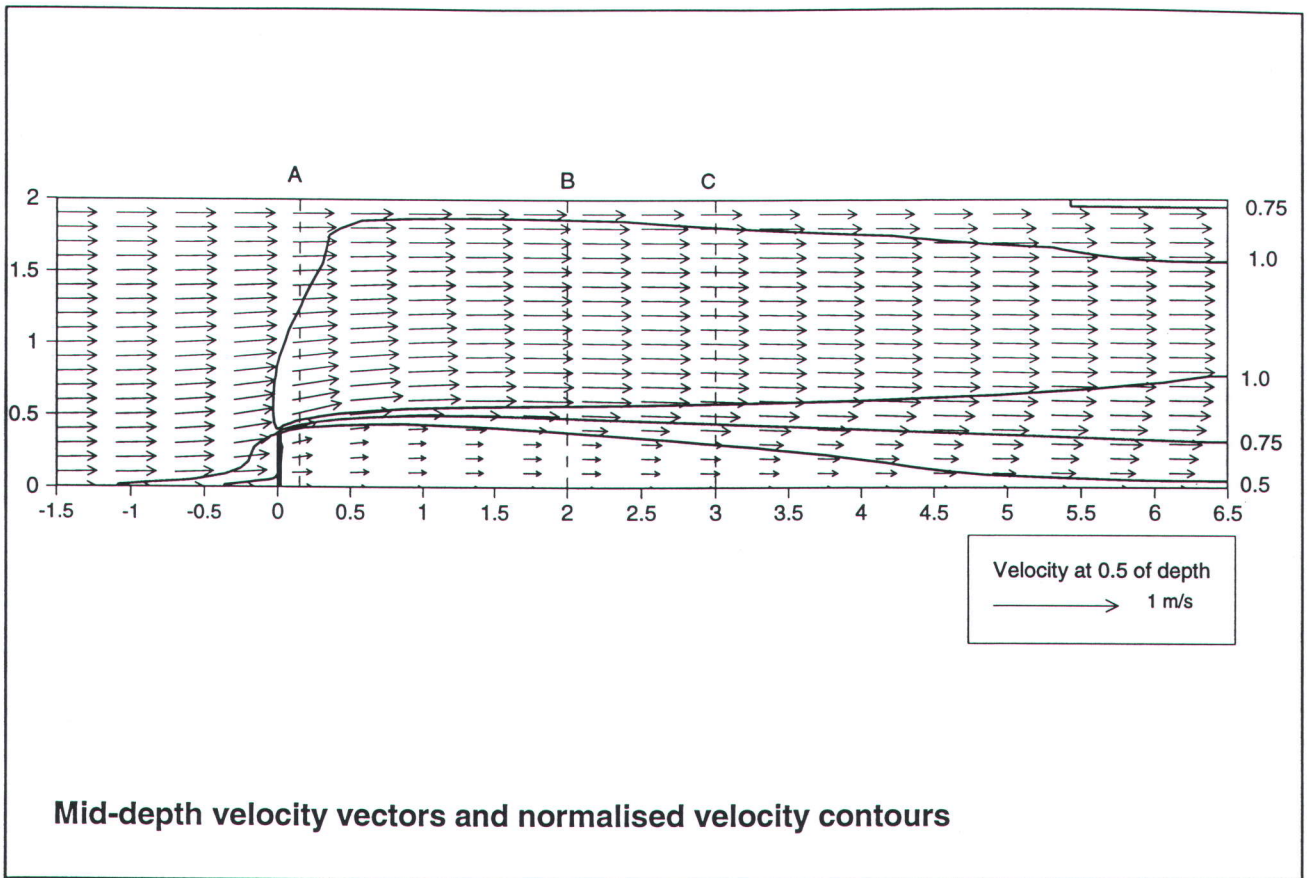


**Figure 8.25 Test RX - Permeable groyne with 25% obstruction  
Mid-depth velocities and cross-section profiles of X-velocity**

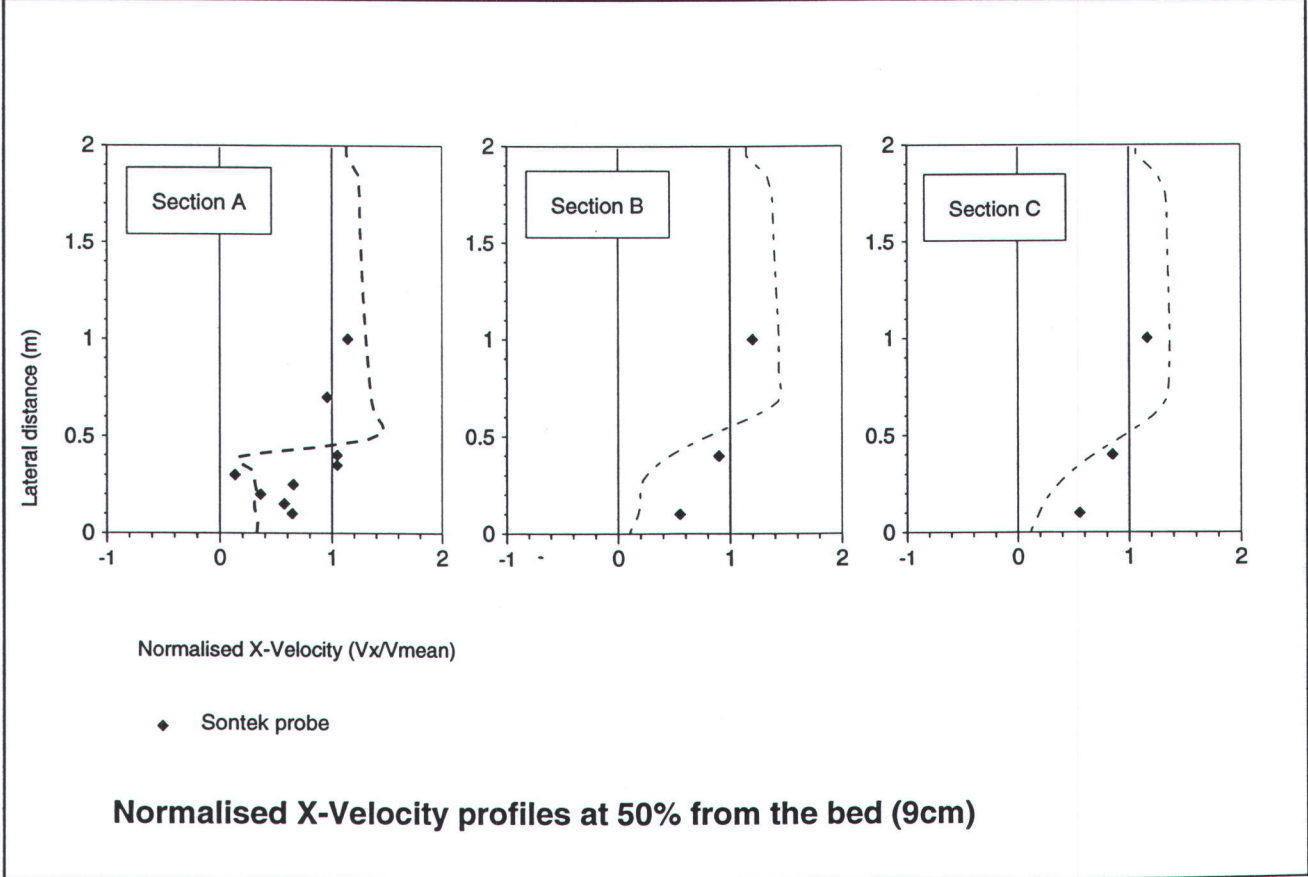
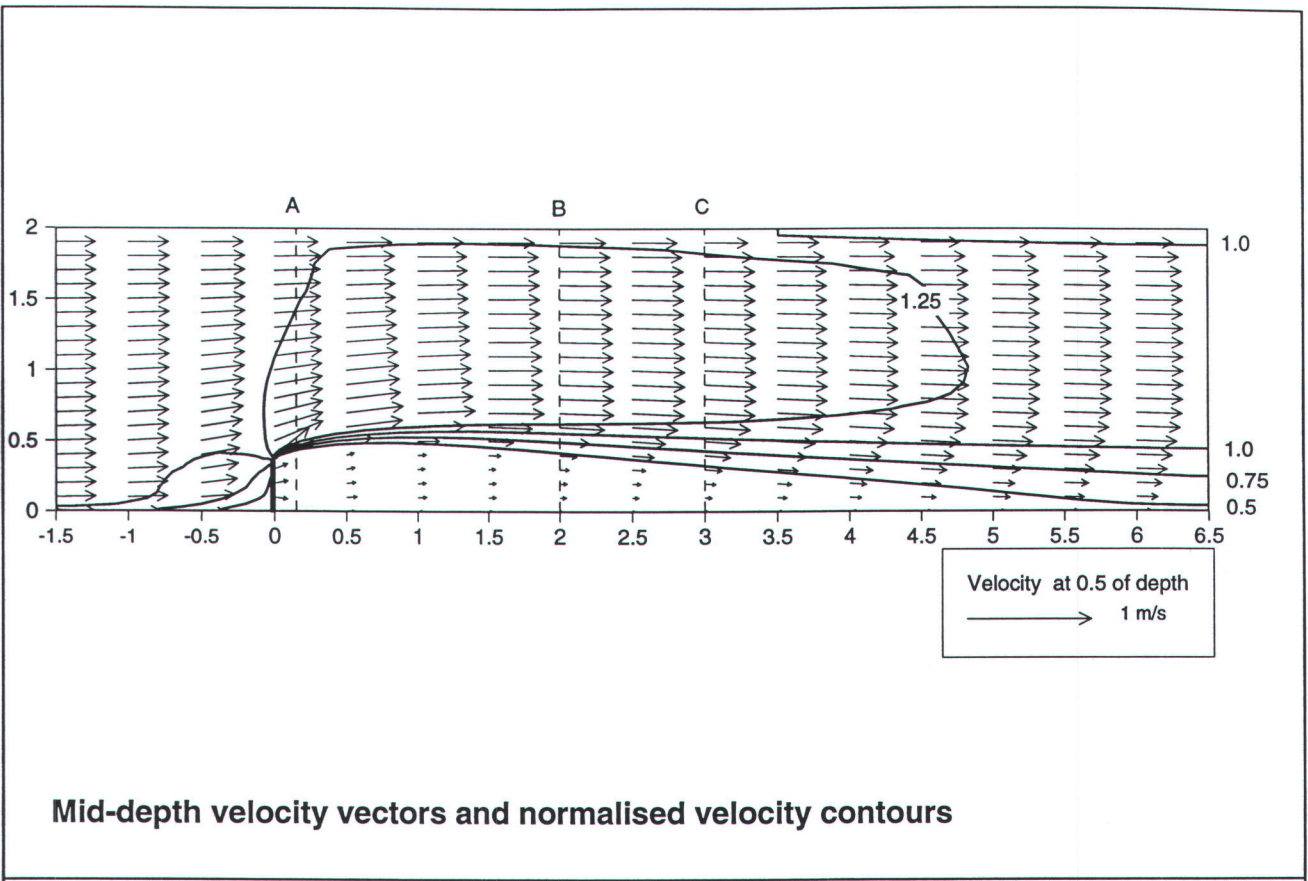
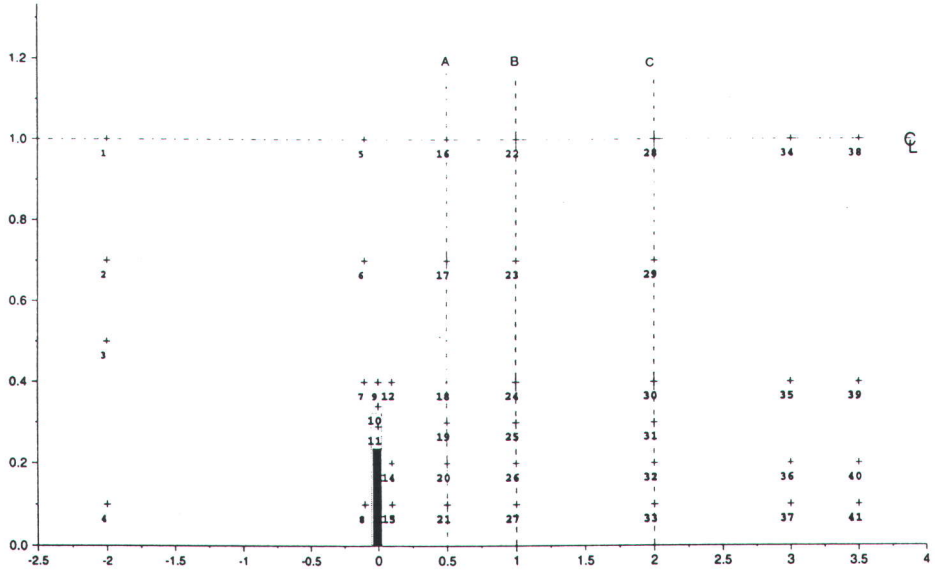
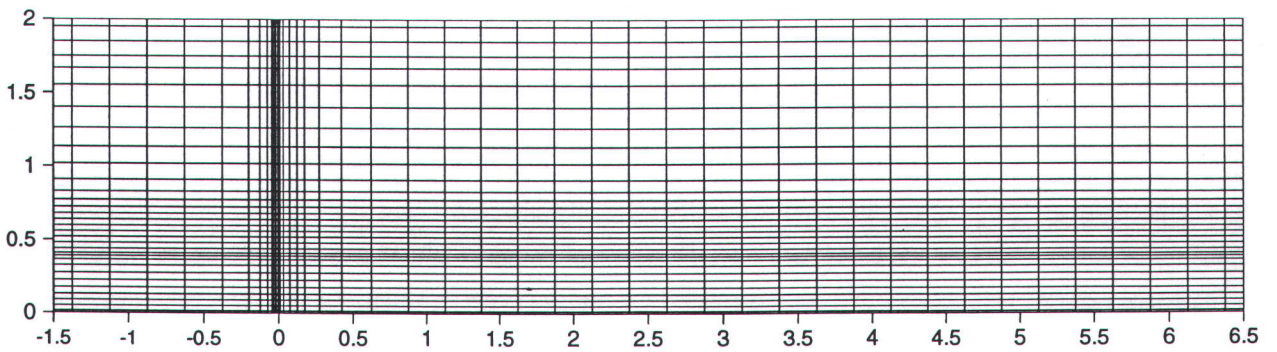


Figure 8.26 Test RY - Single permeable groyne with 44% obstruction  
Mid-depth velocities and cross-section profiles of X-velocity

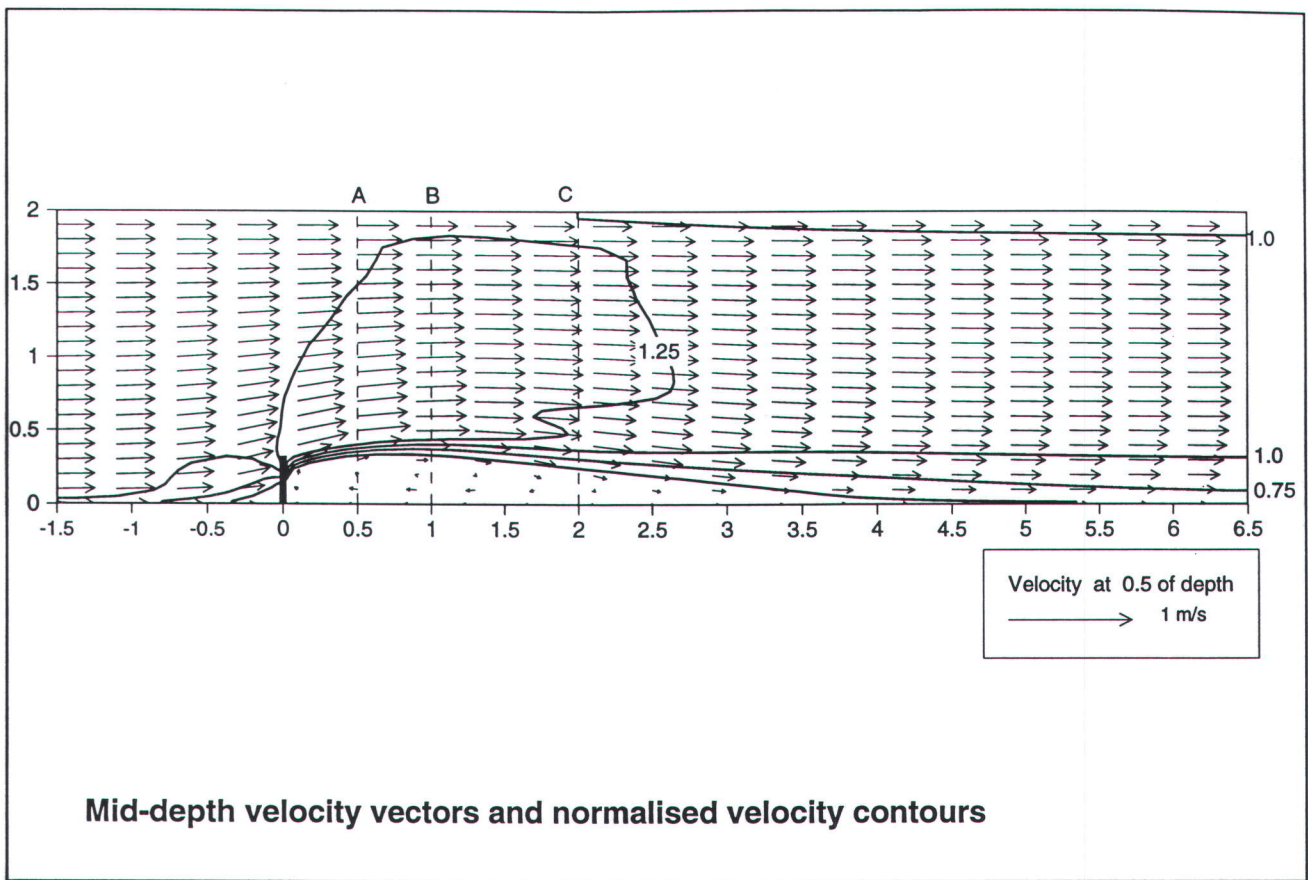


**Experimental points and sections**



**Plan view of the grid  $(x,y,z)=(45,31,10)= 13950$  cells**

**Figure 8.27 Experimental points and numerical grid for Test RM**



Mid-depth velocity vectors and normalised velocity contours

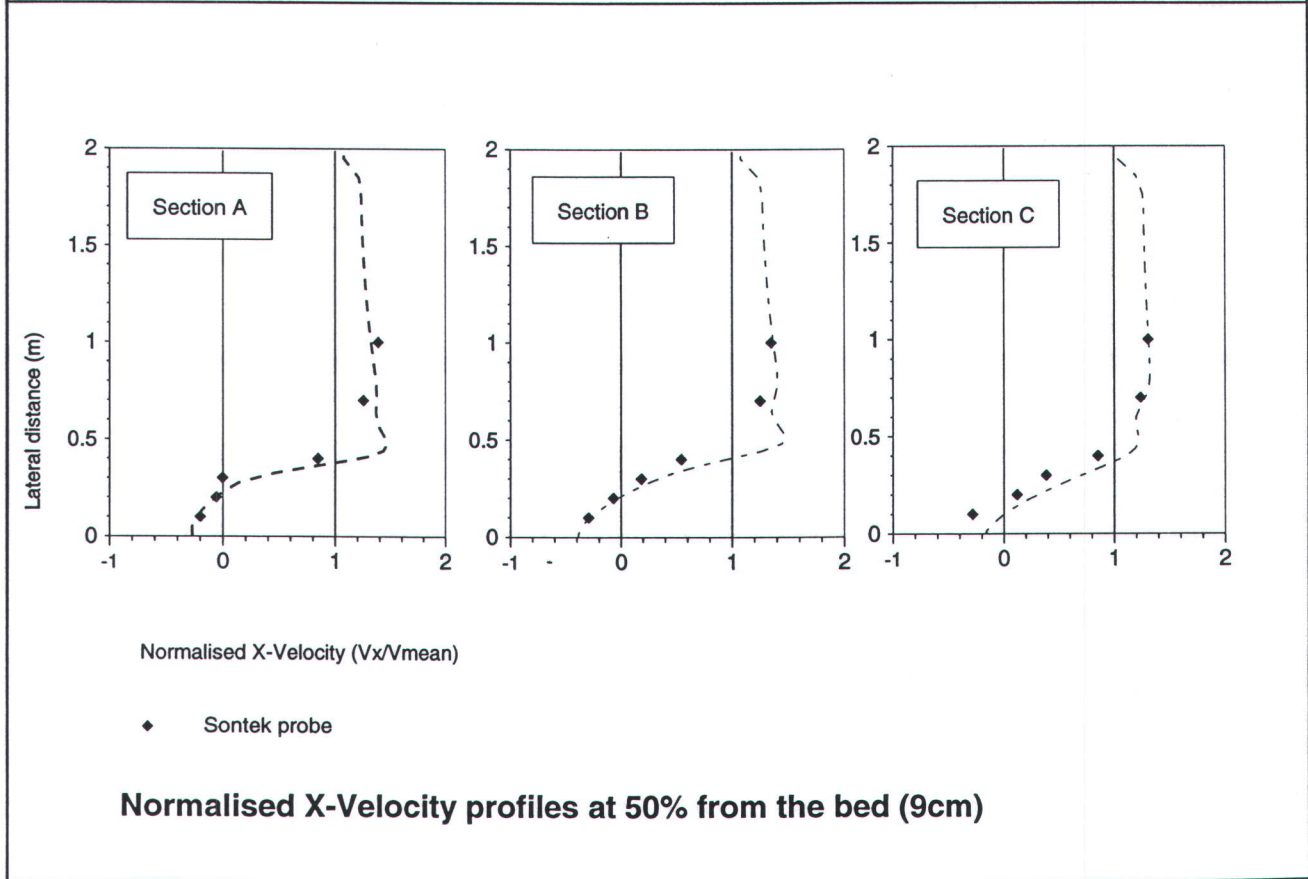
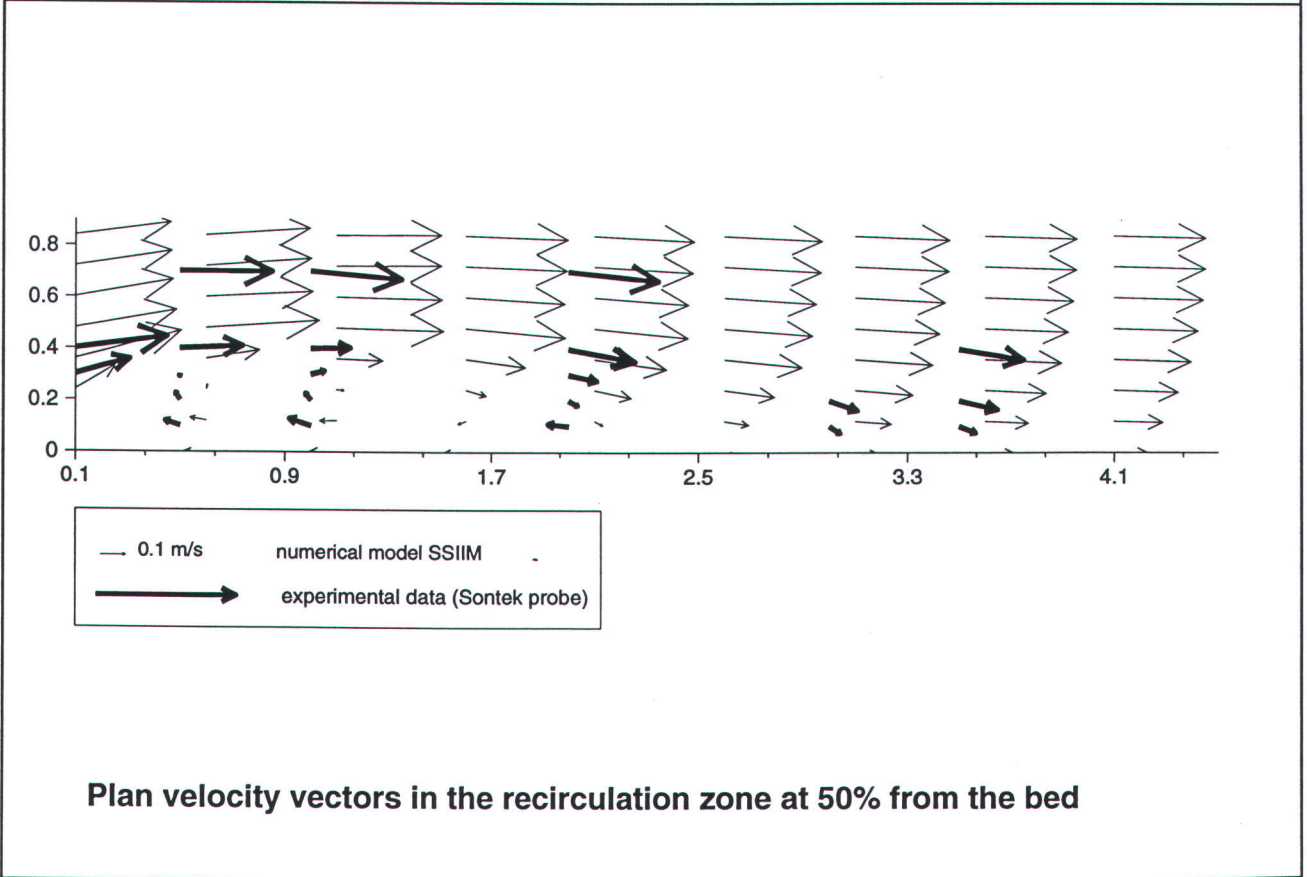
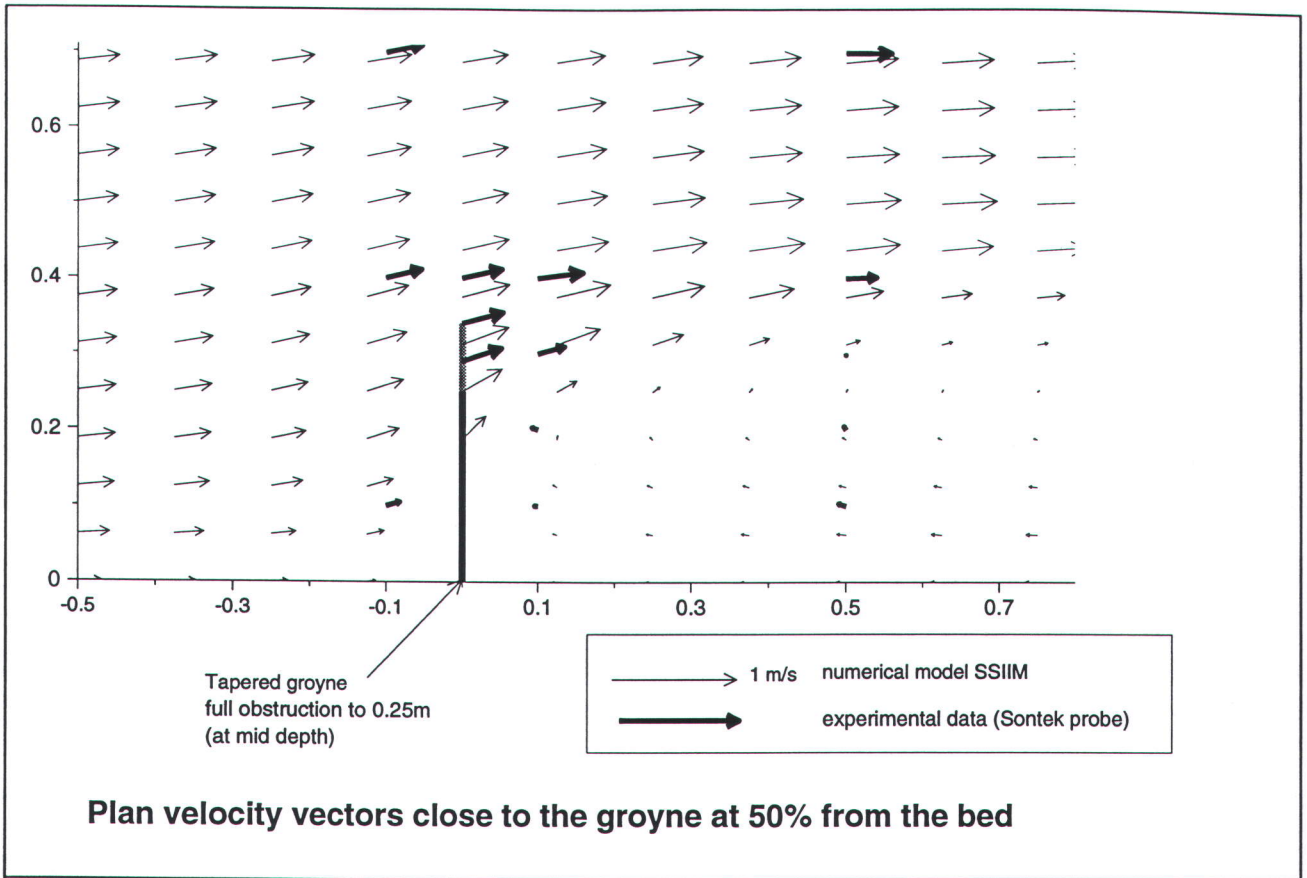
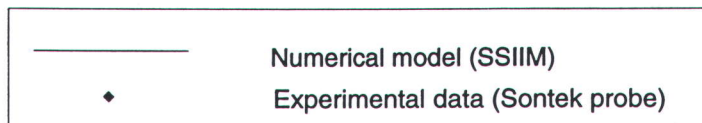
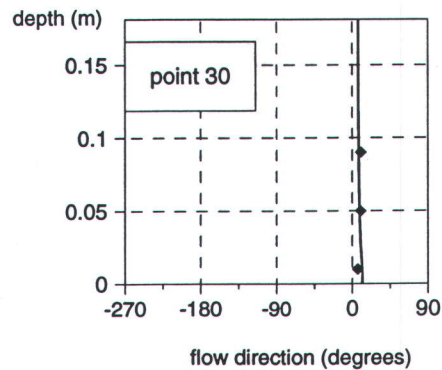
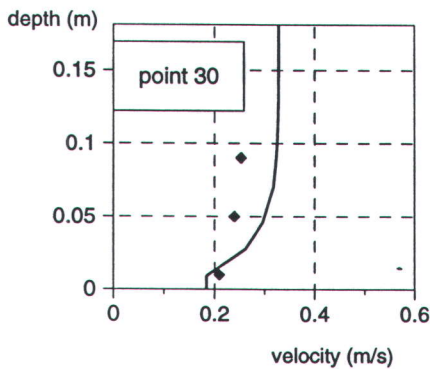
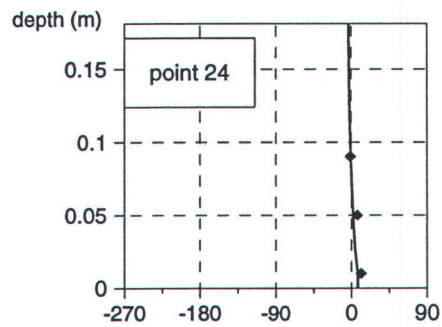
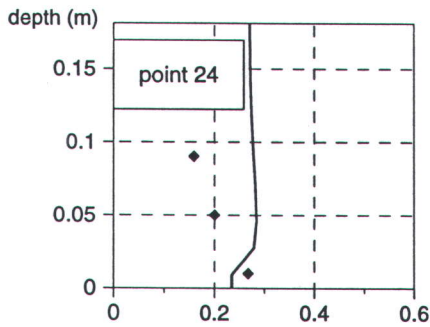
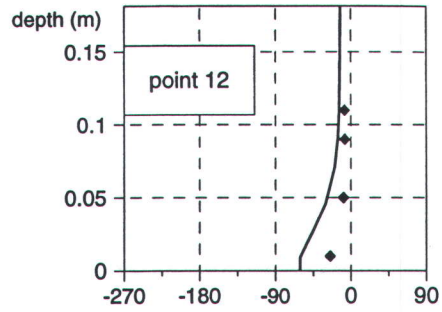
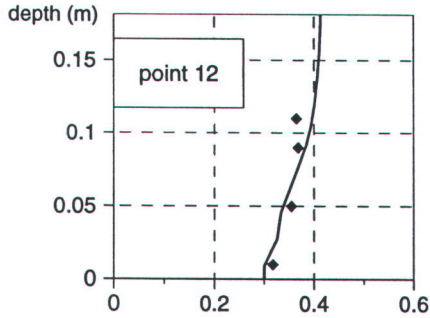
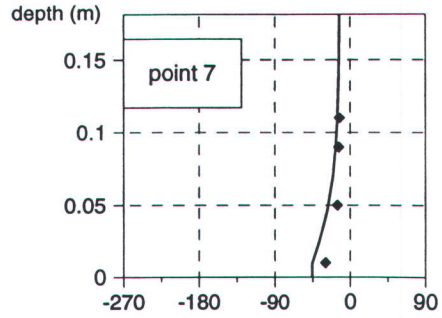
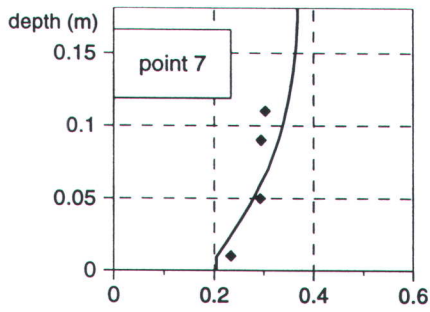


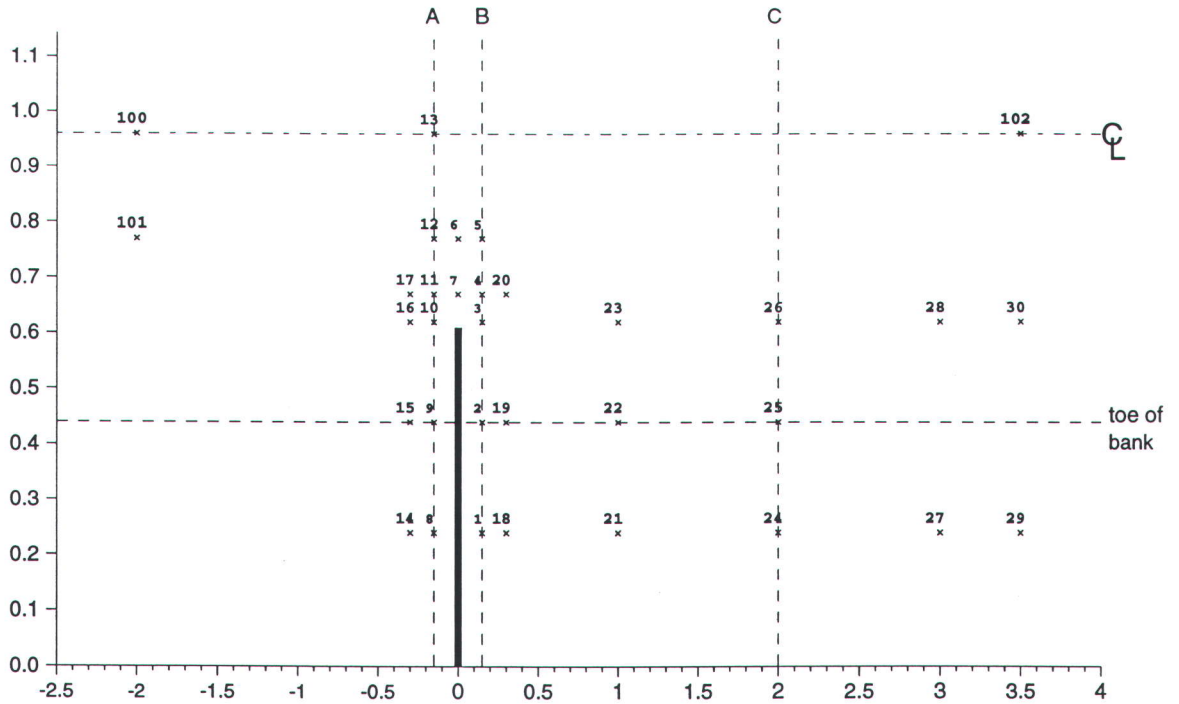
Figure 8.28 Test RM - Tapered groyne in a rectangular channel  
Mid-depth velocities and cross-section profiles of X-velocity



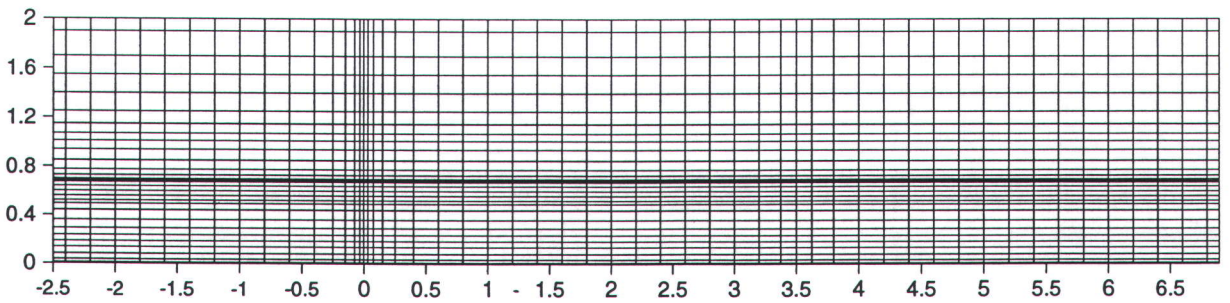
**Figure 8.29 Test RM - Tapered groyne in a rectangular channel  
Plan velocity vectors near groyne and in recirculation zone**



**Figure 8.30 Test RM - Tapered groyne in rectangular channel  
Vertical profiles of plan velocity and flow direction**

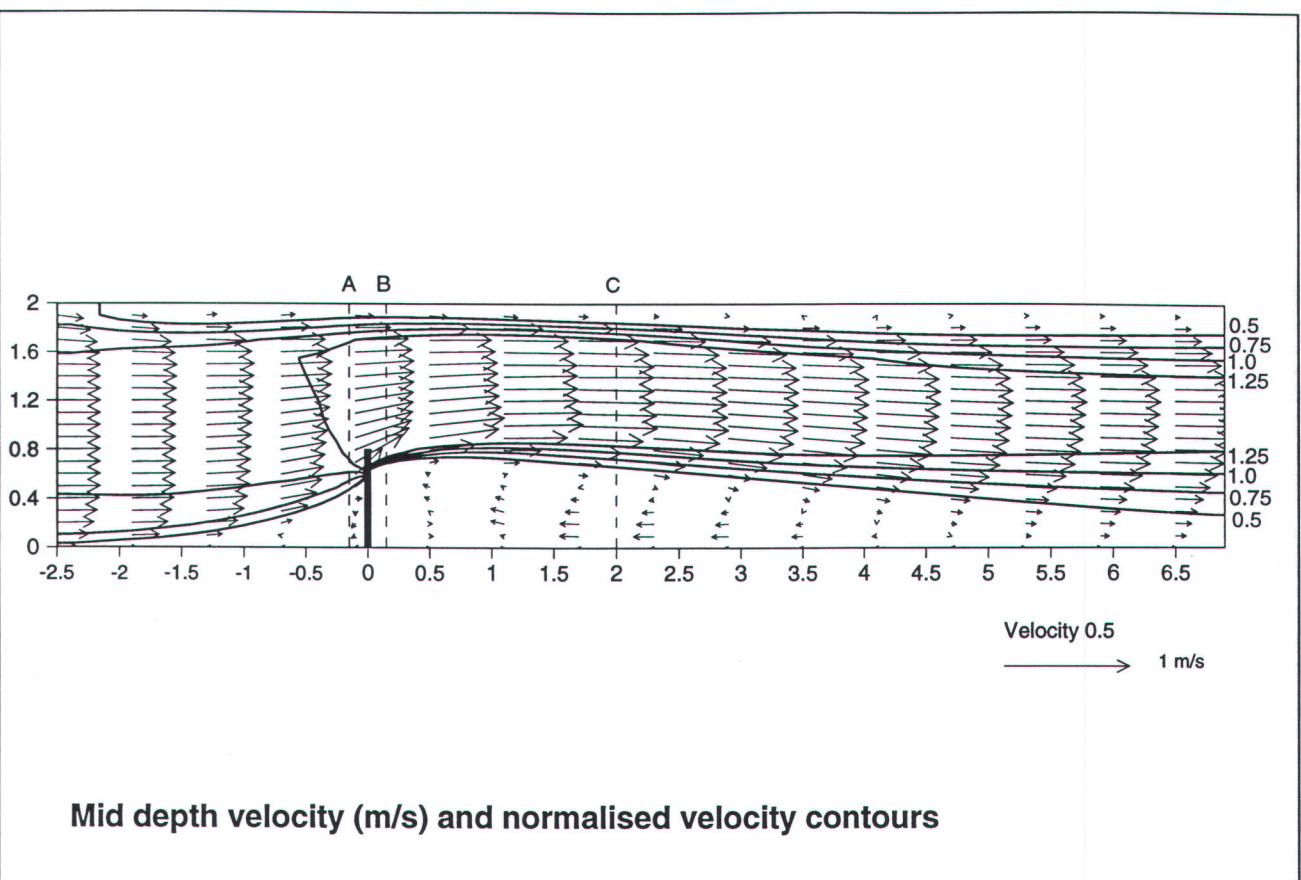


Experimental points and sections

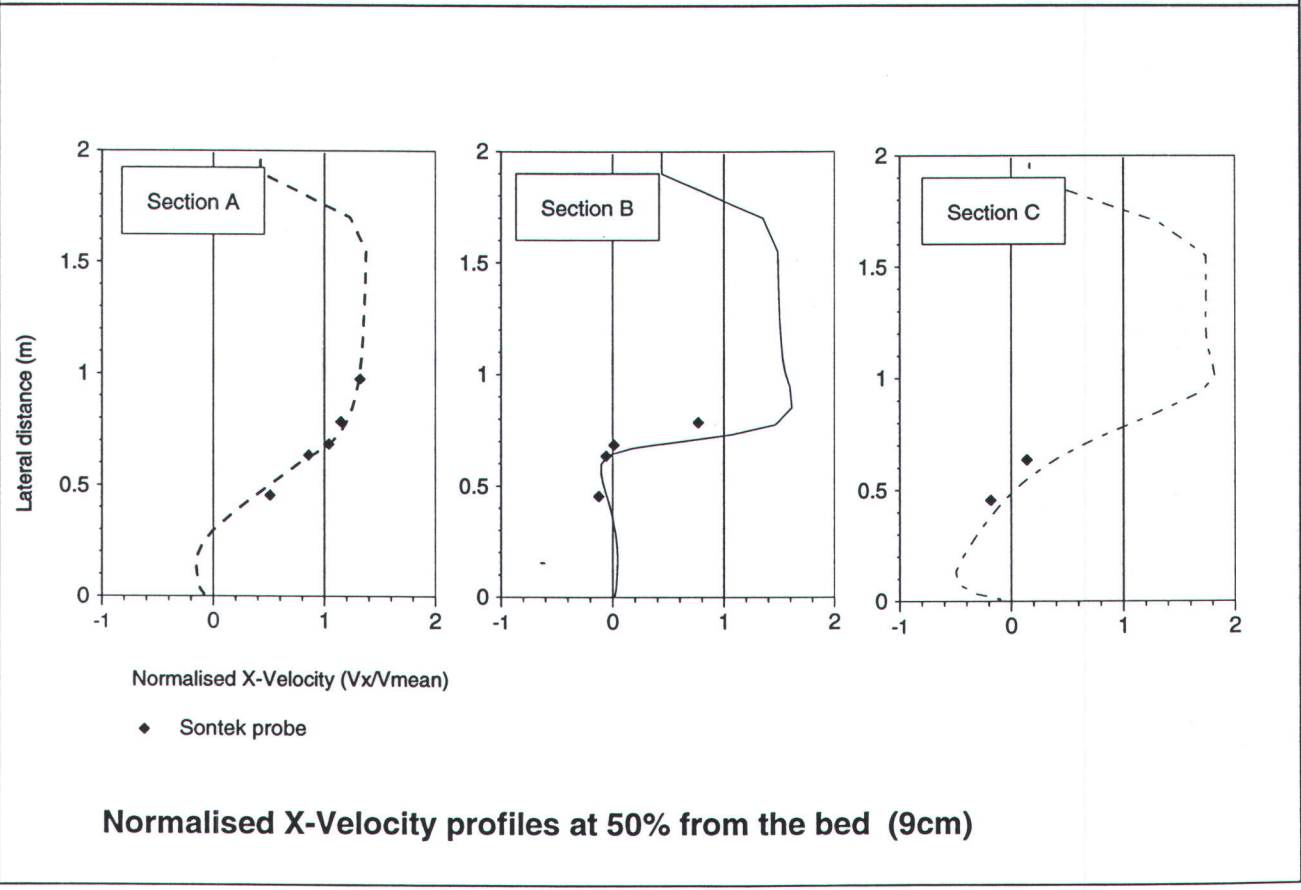


Plan view of the grid  $(x,y,z)=(54,29,12)= 18792$  cells

Figure 9.1 Experimental points and numerical grid for Test TA-9

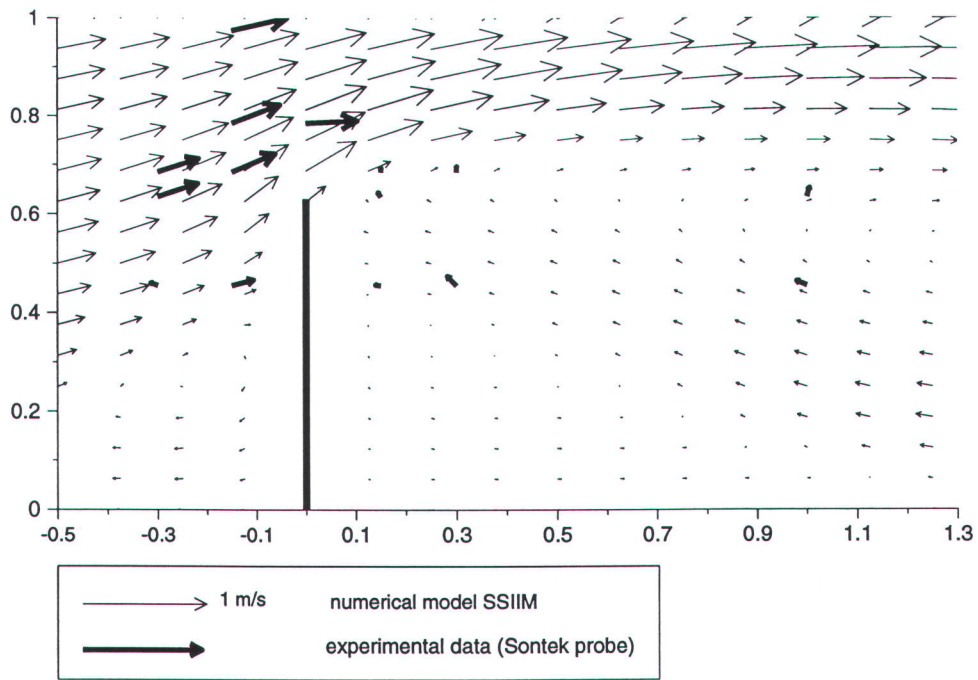


Mid depth velocity (m/s) and normalised velocity contours

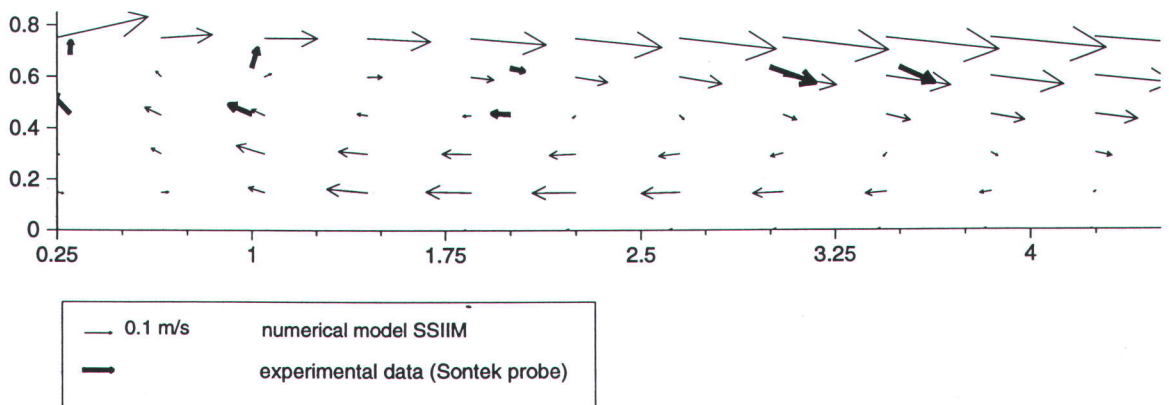


Normalised X-Velocity profiles at 50% from the bed (9cm)

Figure 9.2 Test TA - Unsubmerged groyne in a trapezoidal channel  
Mid-depth velocity vectors and cross-section profiles of X-velocity



**Plan velocity vectors close to the groyne at 50% from the bed**



**Plan velocity vectors in the recirculation zone at 50% from the bed**

**Figure 9.3 Test TA - Unsubmerged groyne in a trapezoidal channel  
Plan velocity vectors near groyne and in the recirculation zone**

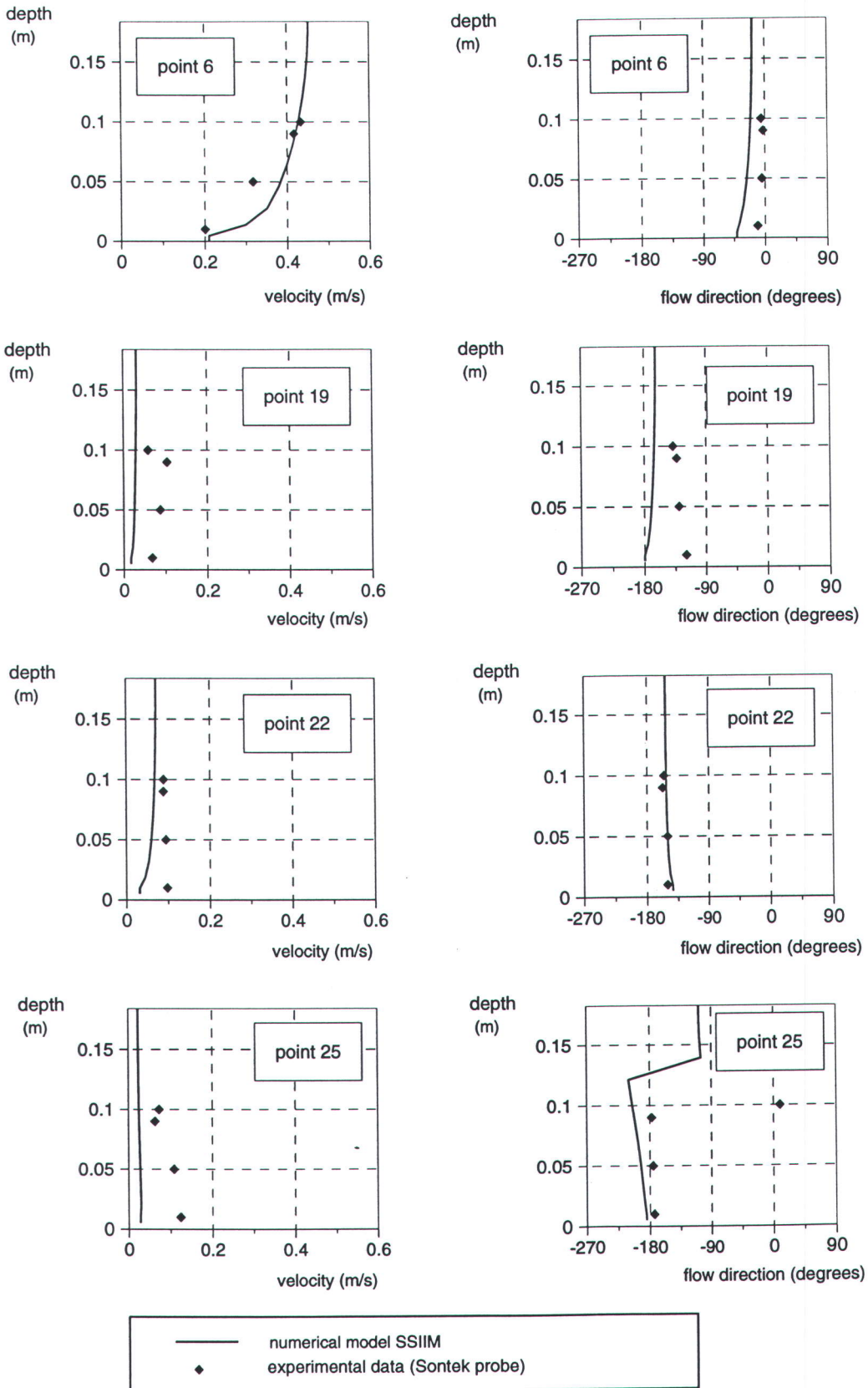


**Figure 9.4 Test TA - Rectangular groyne in a trapezoidal channel  
Vertical profiles of plan velocity and flow direction**

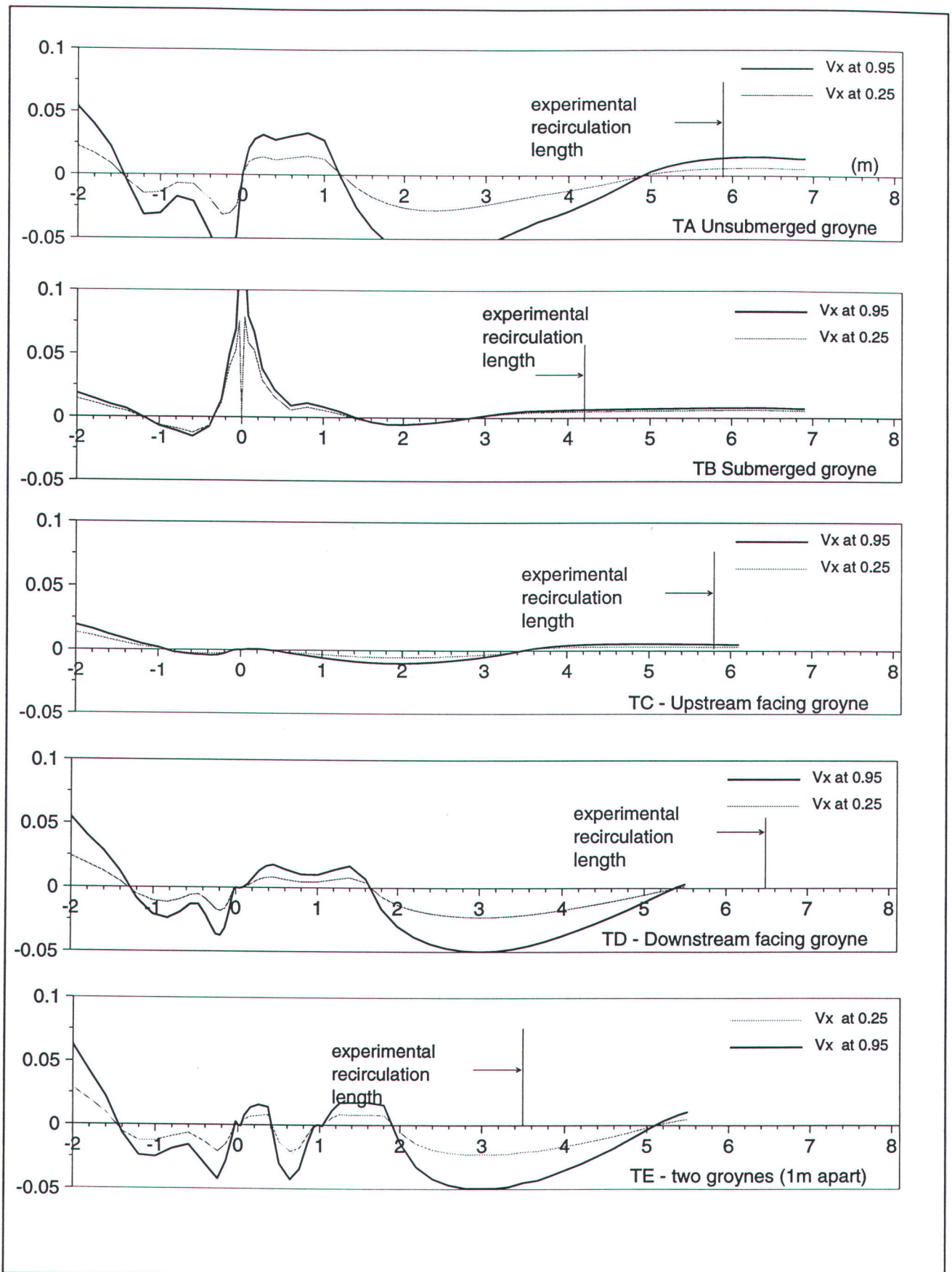
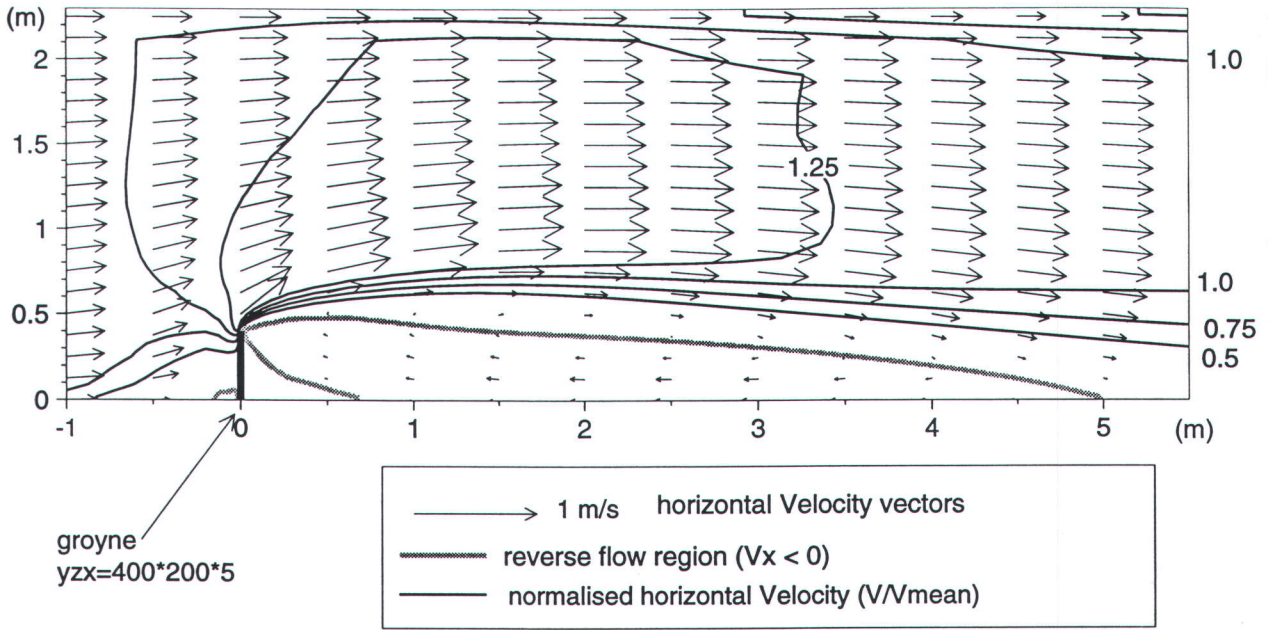
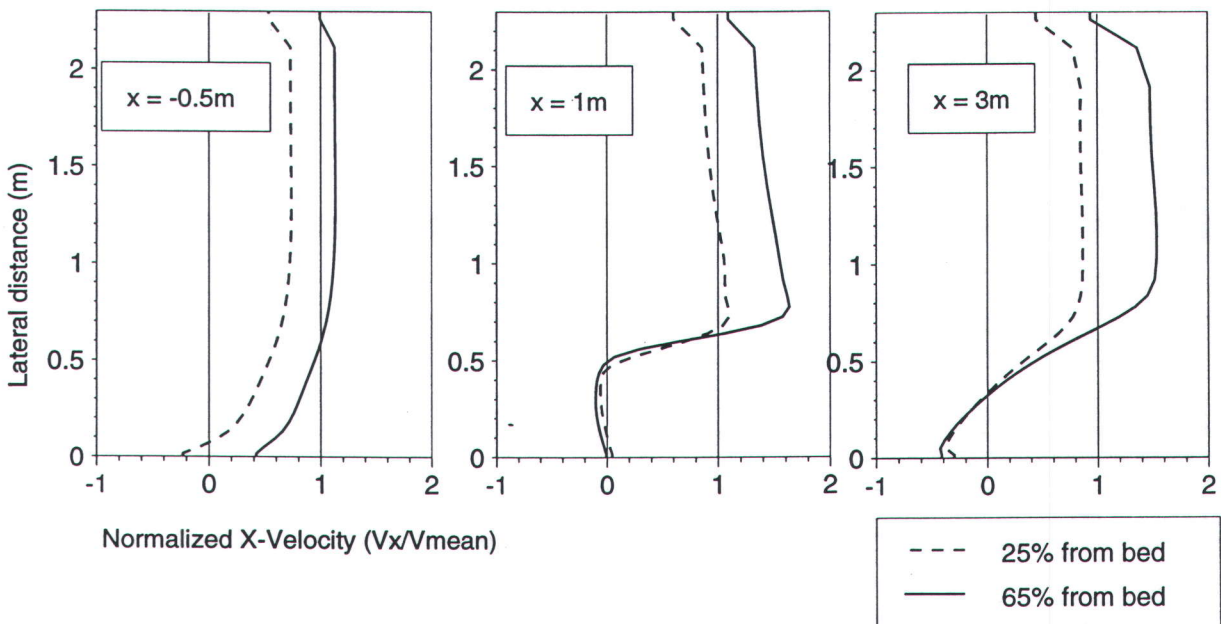


Figure 9.5 Recirculation lengths in trapezoidal channel



Velocity vectors and contours at 65% from the bed



Normalized X-Velocity profiles at 25% and 65% from the bed

Figure 9.6 Test RA6 Rectangular groyne in rectangular channel  
Plan velocities

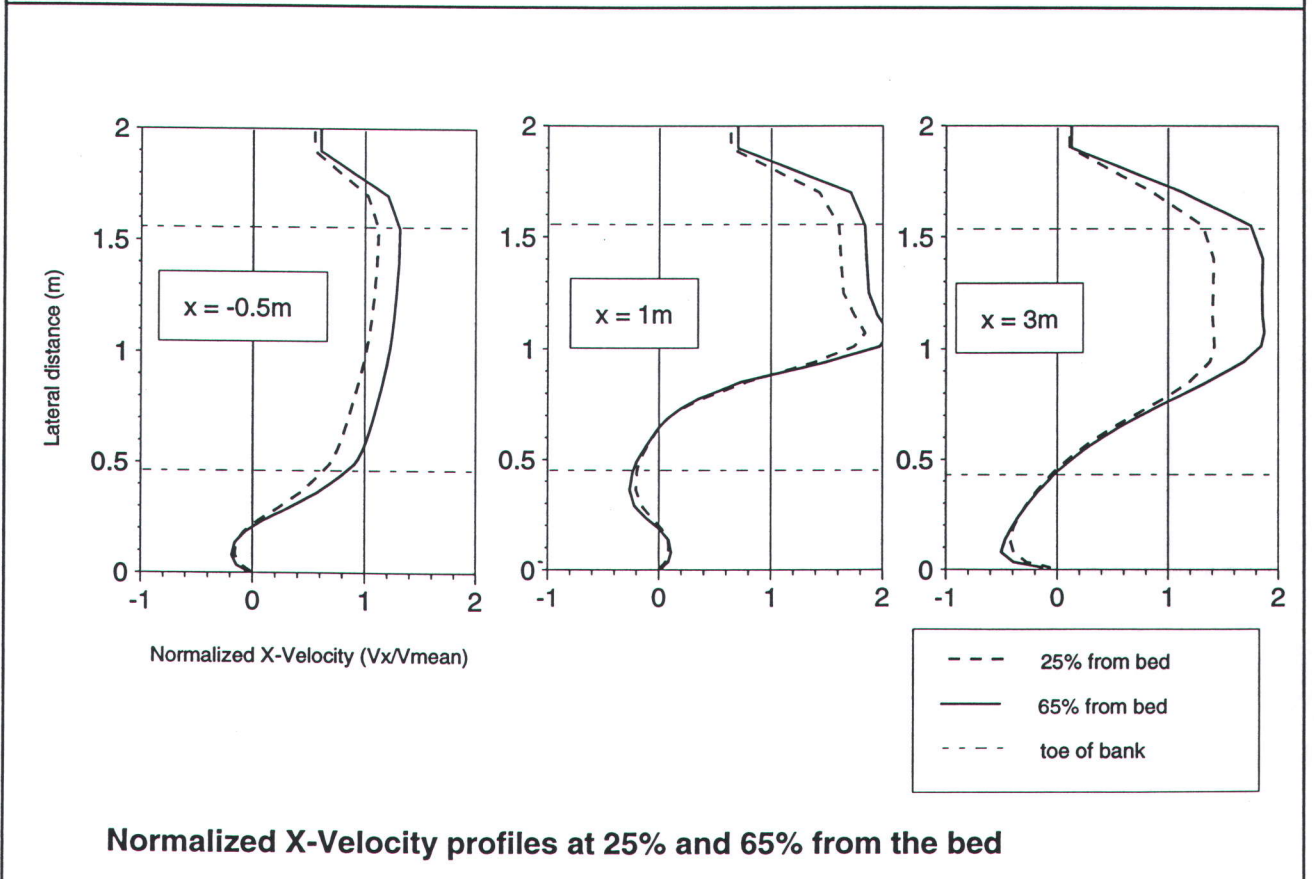
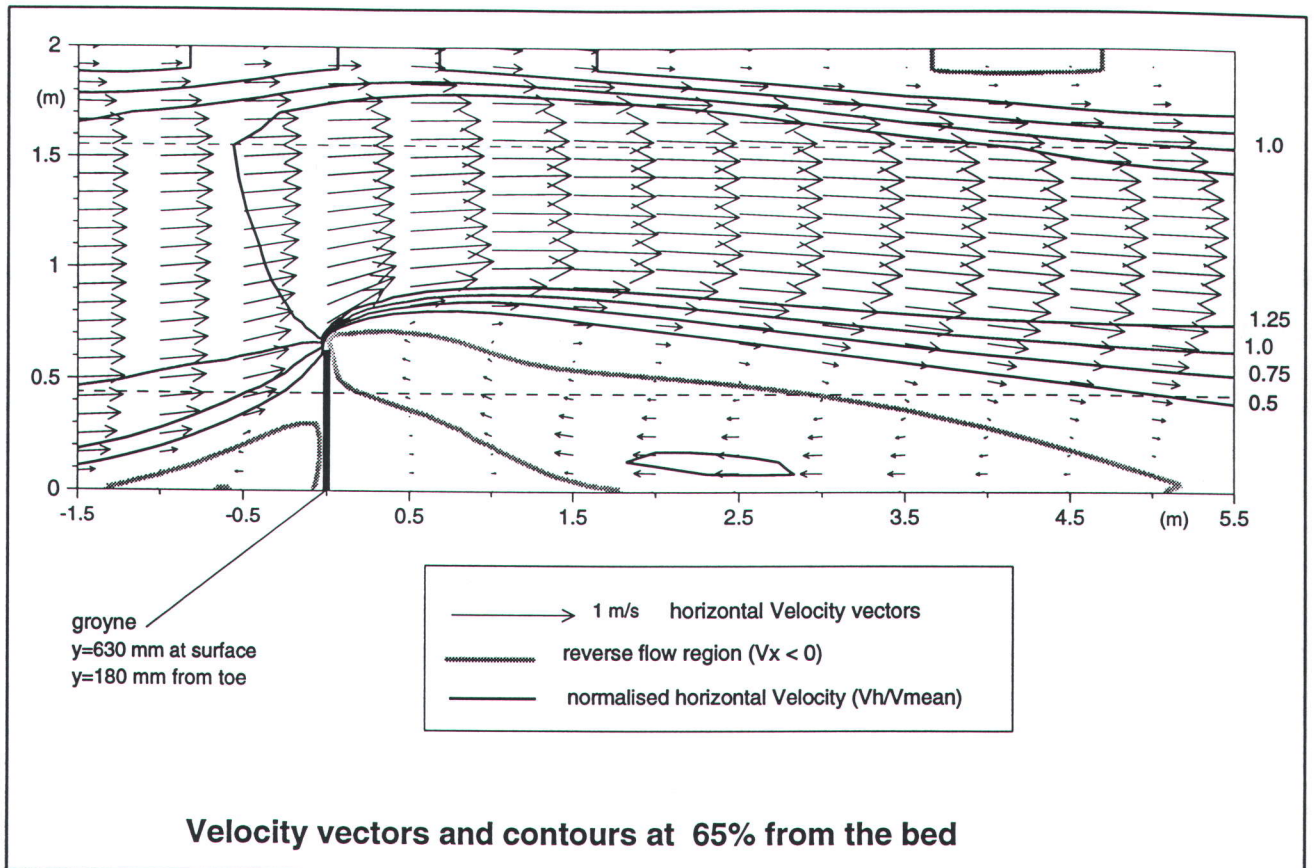


**Figure 9.7 Test TA - Rectangular groyne in trapezoidal channel  
Plan velocities**

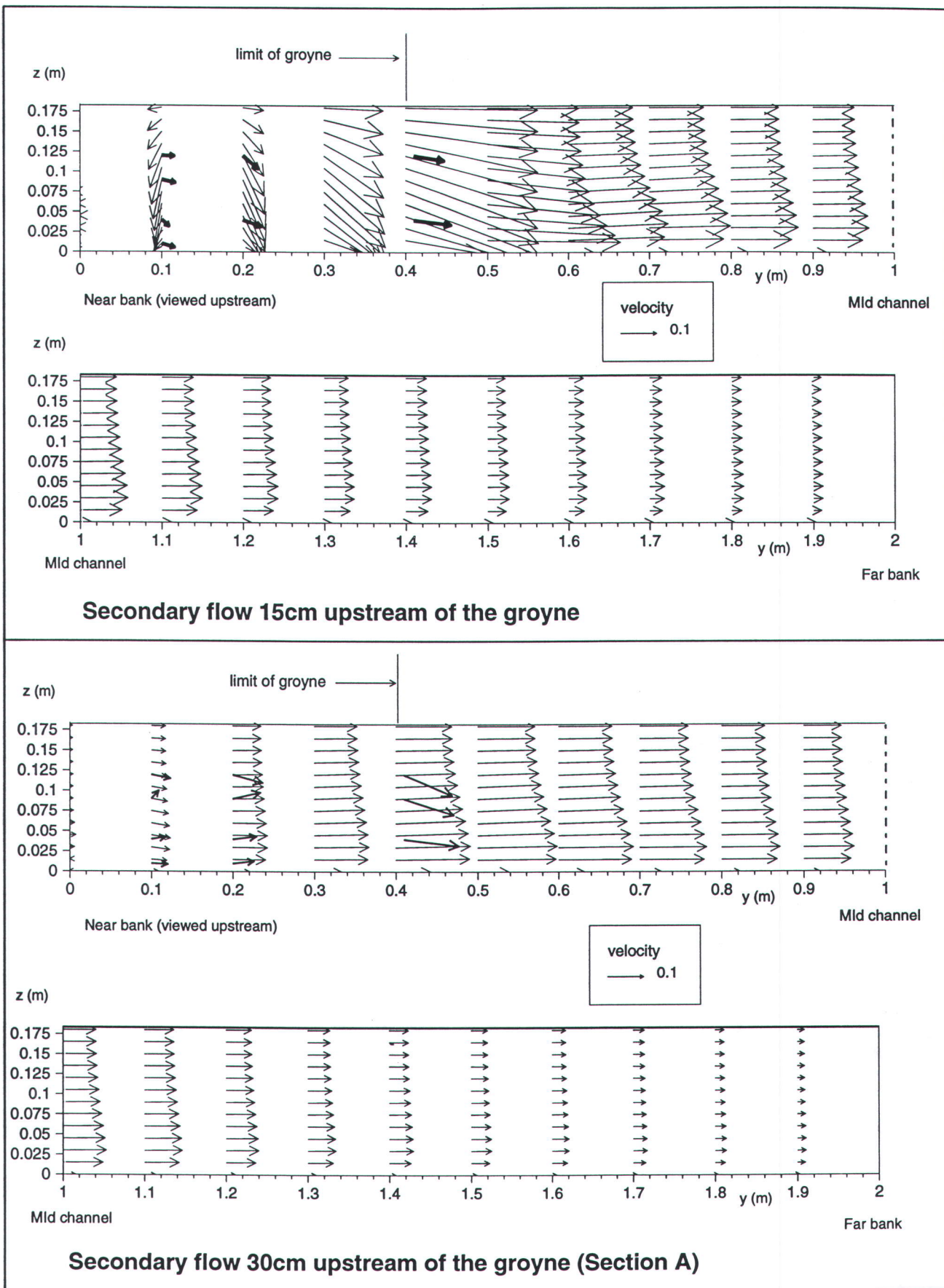


**Figure 9.8 Test RAb - Rectangular groyne in a rectangular channel  
Secondary flows upstream of the groyne**

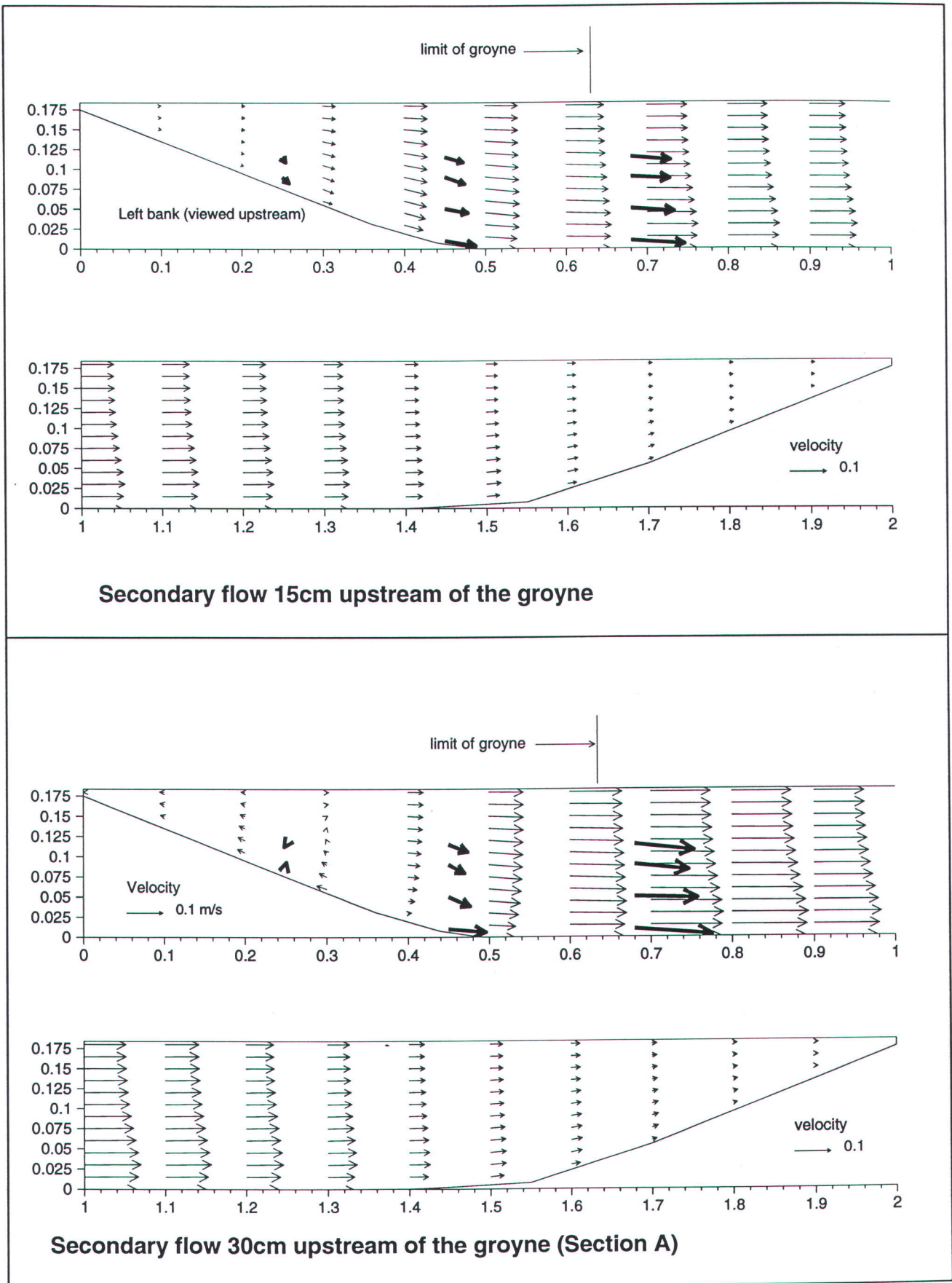


**Figure 9.9 Test TA - Rectangular groyne in a trapezoidal channel  
Secondary flows upstream of the groyne**

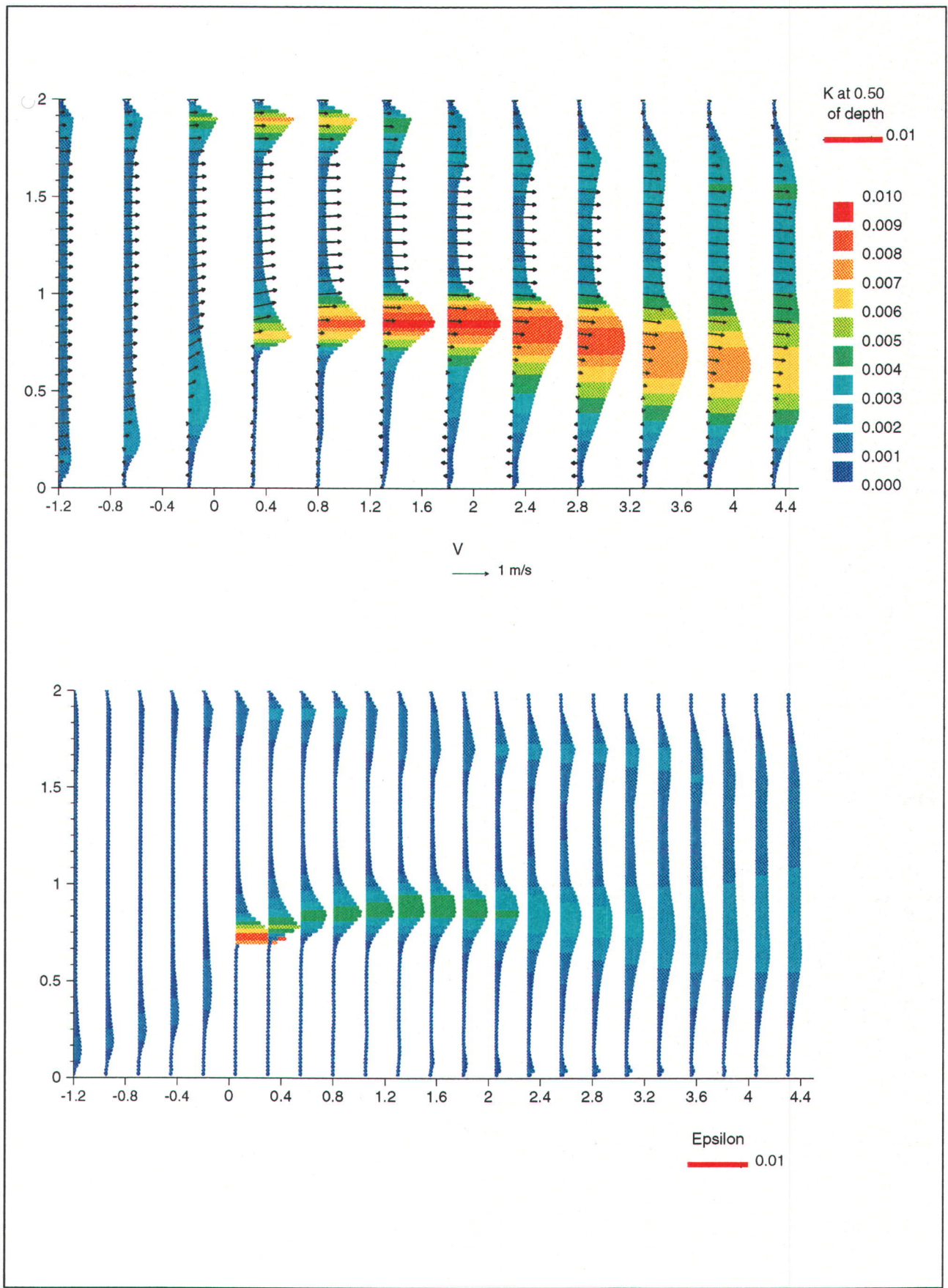


**Figure 9.10** Test TA rectangular groyne in trapezoidal channel  
Plan profiles velocity,  $k$  and epsilon at mid-depth

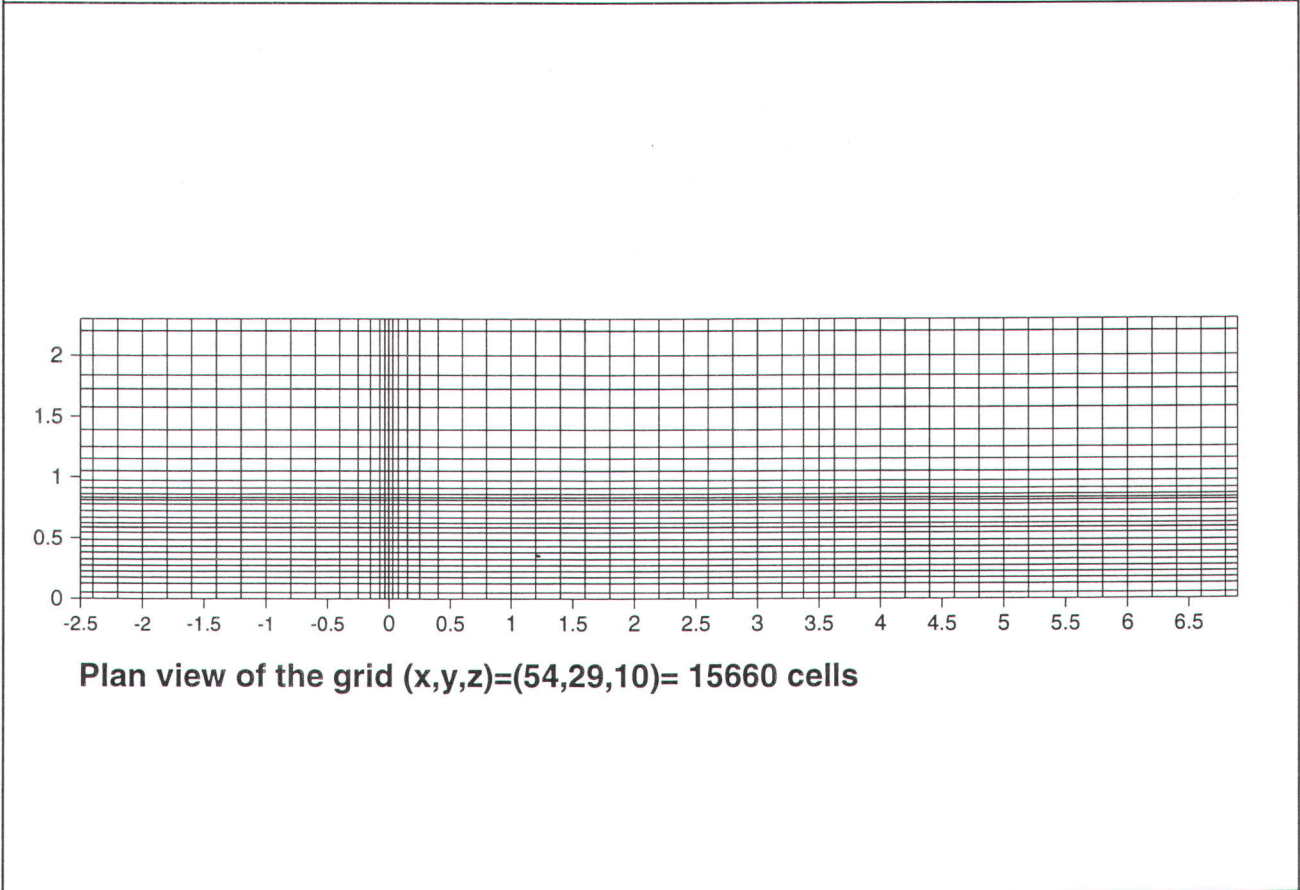
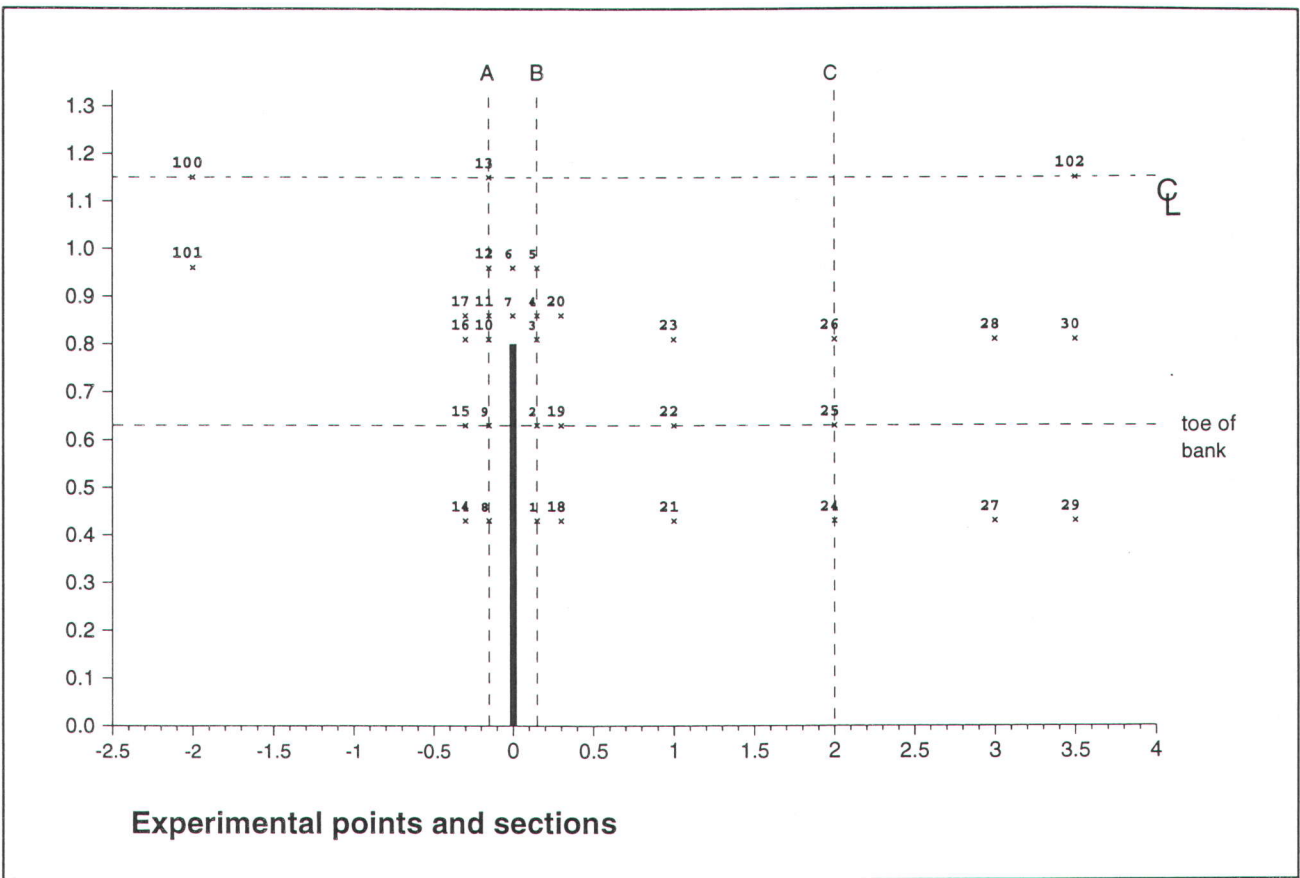


**Figure 9.11 Experimental points and numerical grid for Test TB-1**

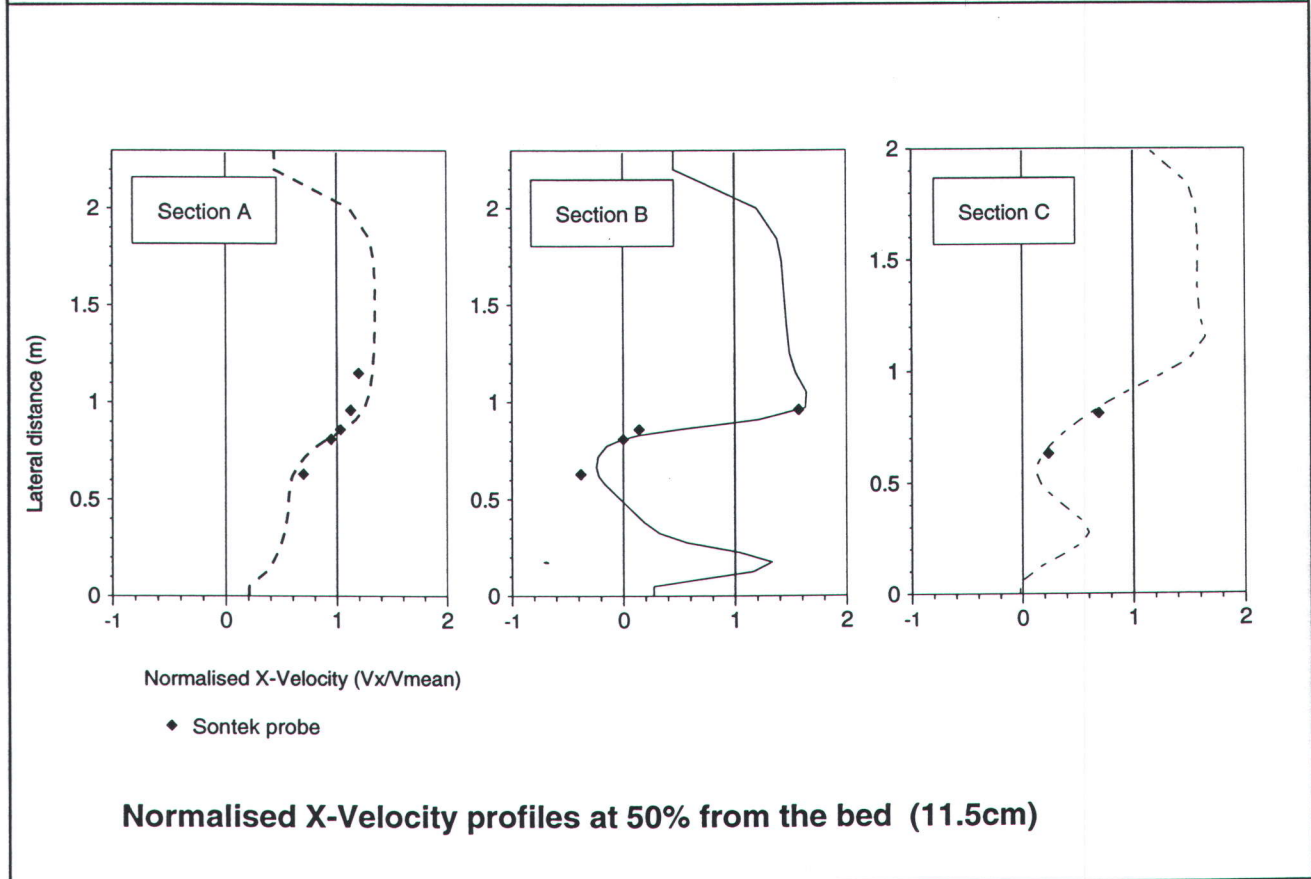
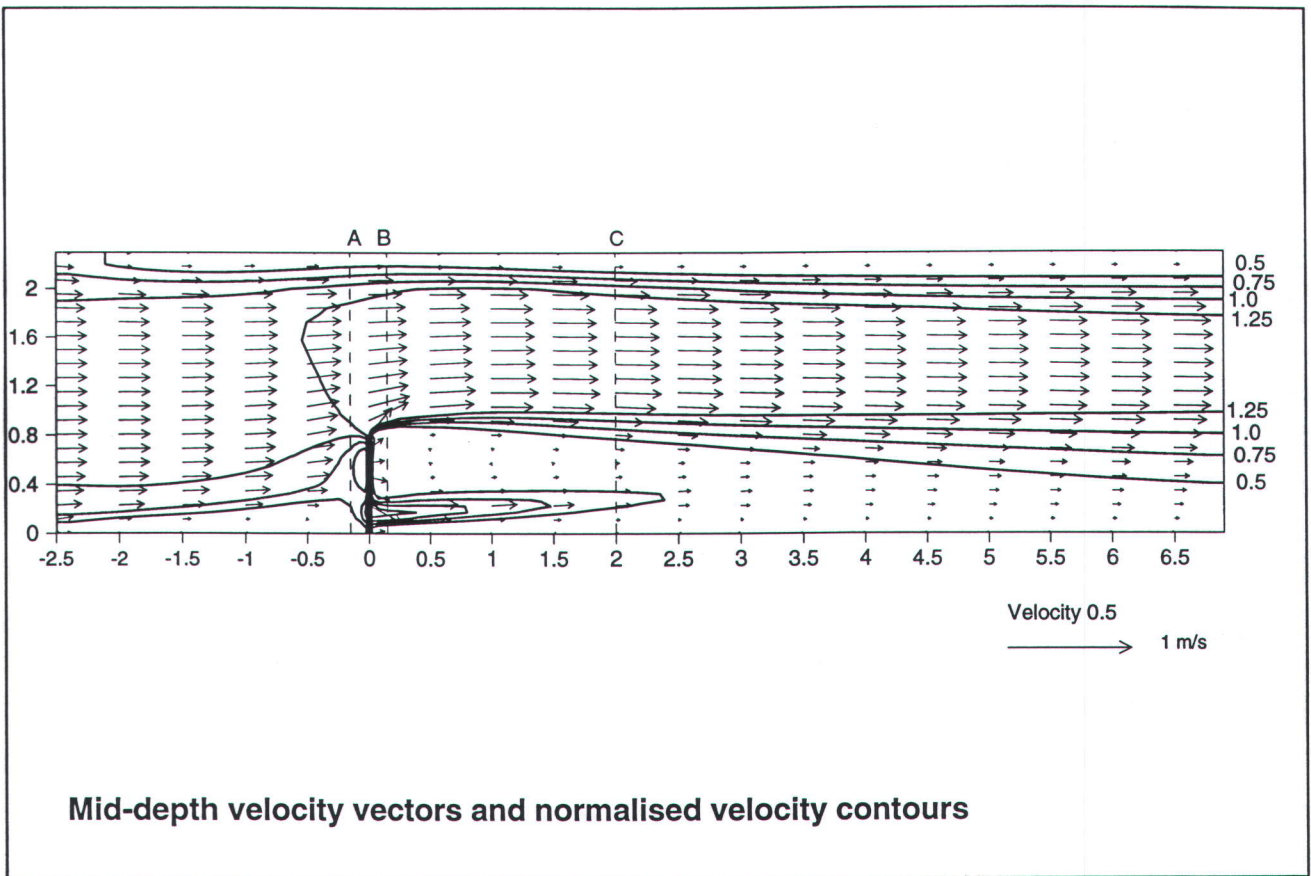


**Figure 9.12 Test TB - Submerged groyne in a trapezoidal channel**  
**Mid-depth velocities and cross-section profiles of X-velocity**

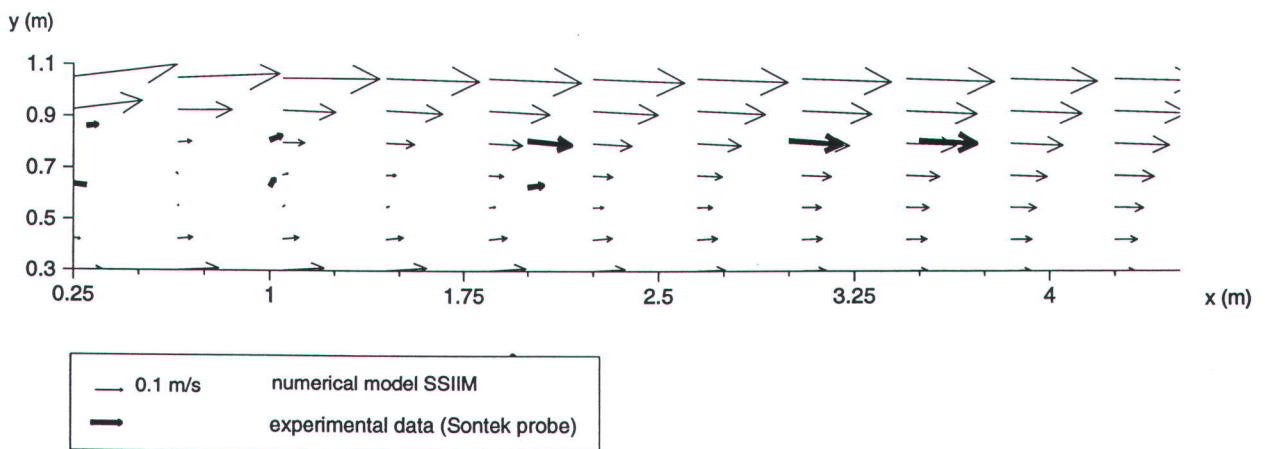
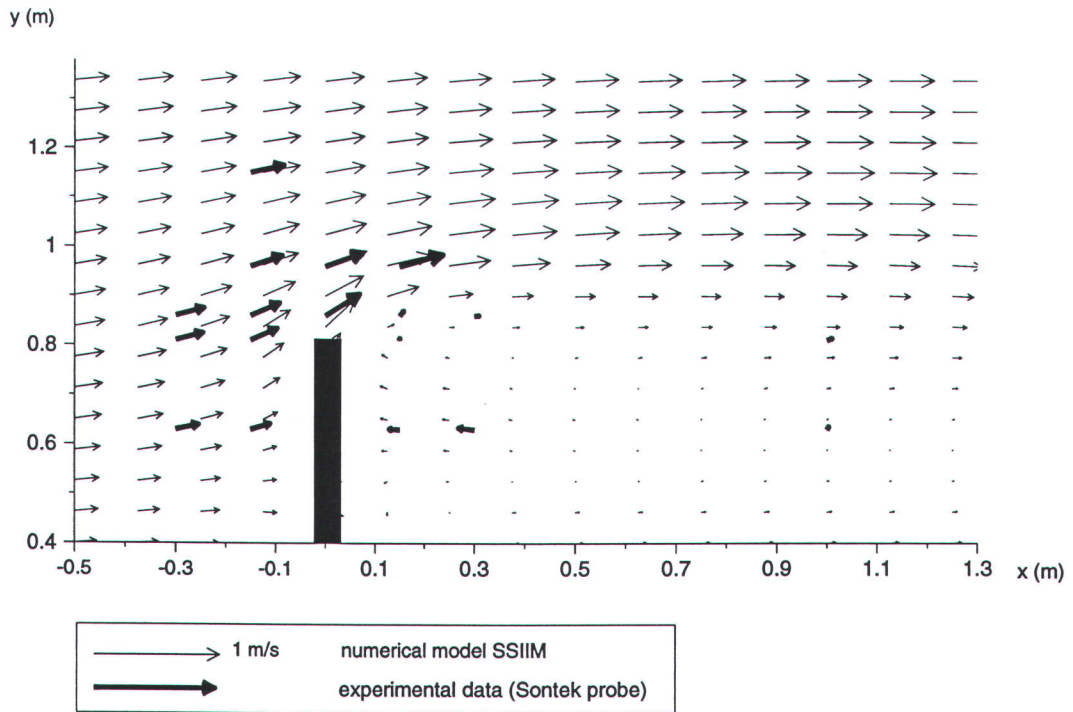


**Figure 9.13 Test TB - Submerged groyne in a trapezoidal channel**  
**Plan velocity vectors near groyne and in the recirculation zone**

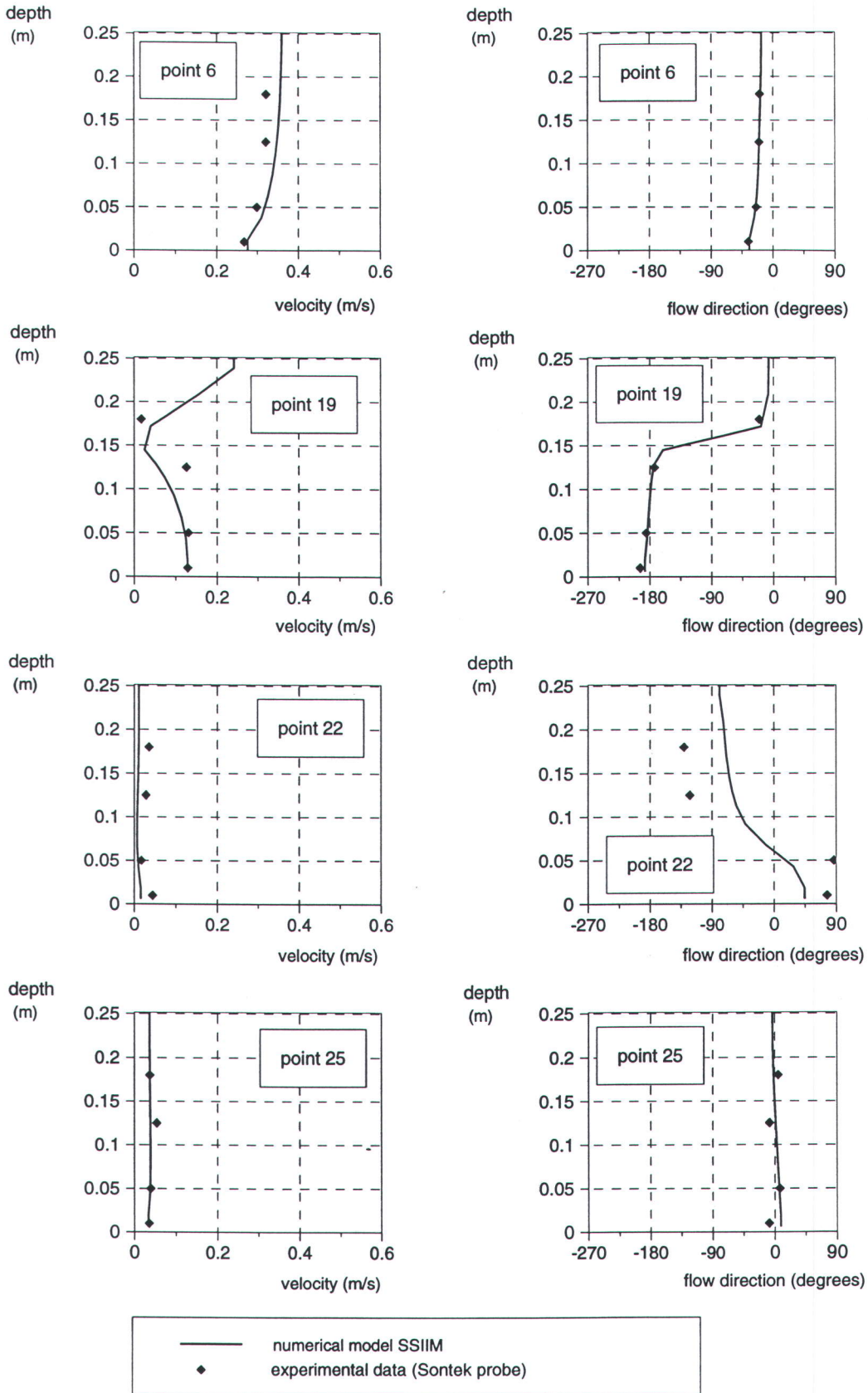


**Figure 9.14 Test TB - Submerged groyne in a trapezoidal channel**  
**Vertical profiles of plan velocity and flow direction**

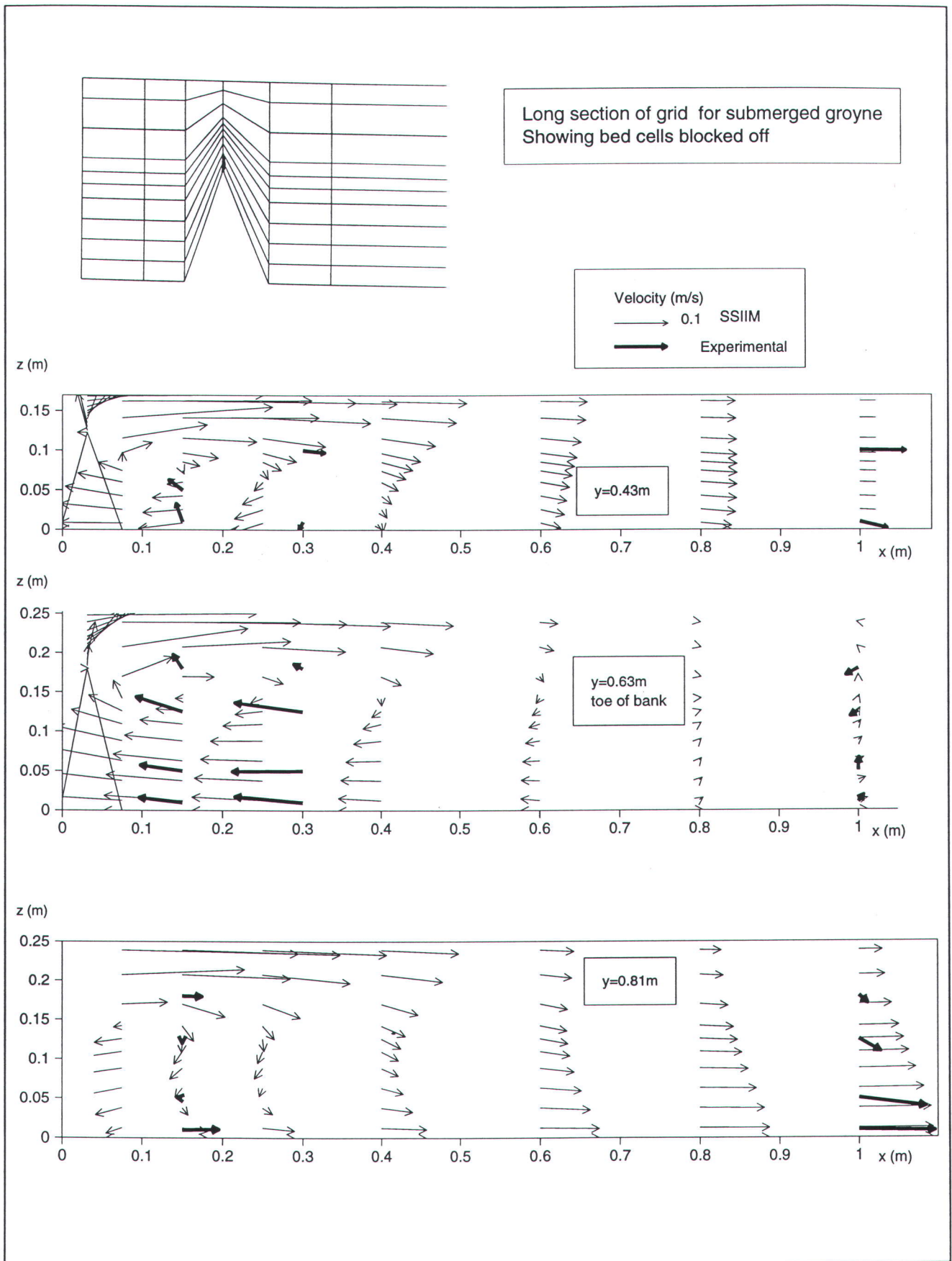
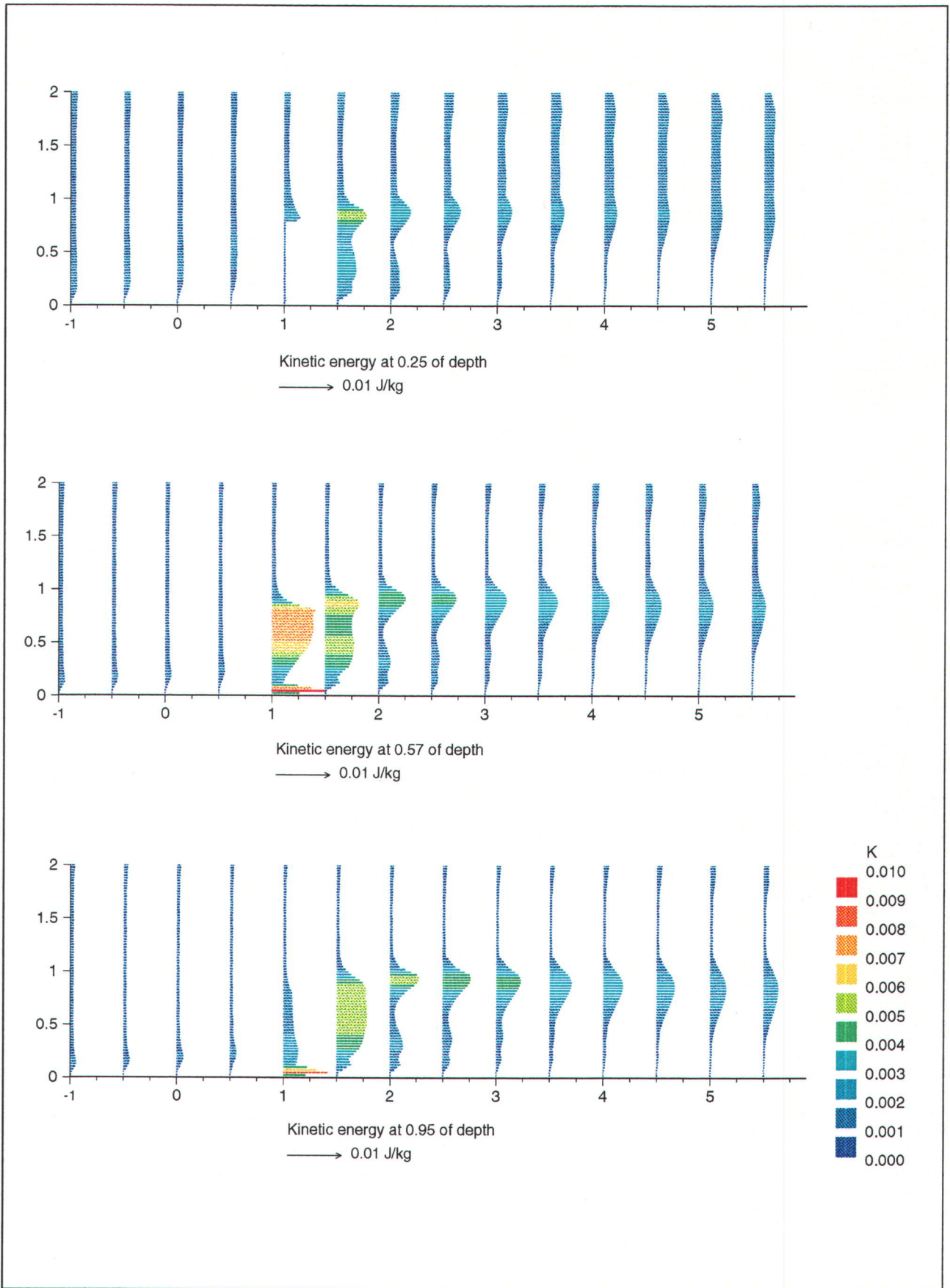


Figure 9.15 Test TB - Long section for submerged groyne



**Figure 9.16** Test TB Submerged groyne in a triangular channel  
Turbulent kinetic energy at three depths

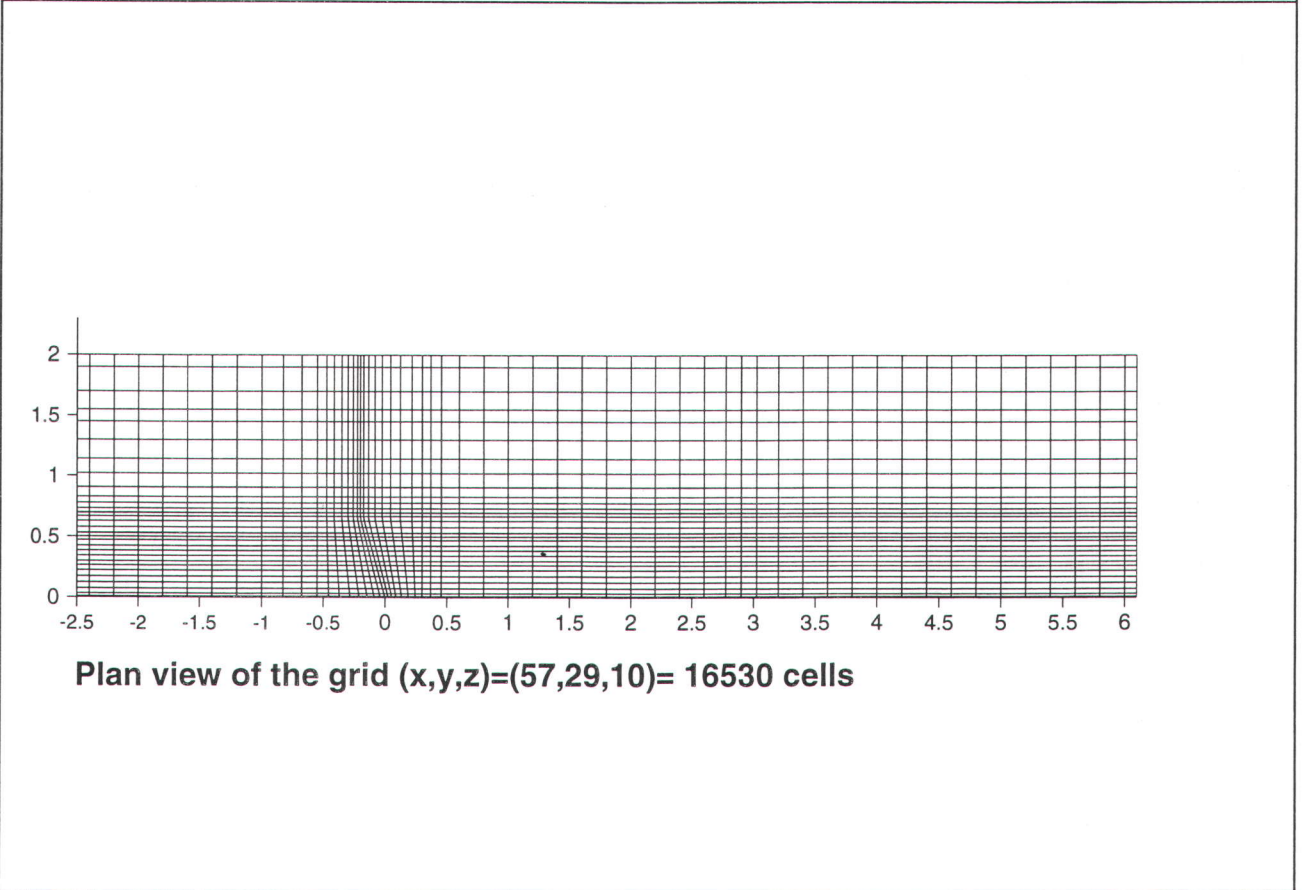
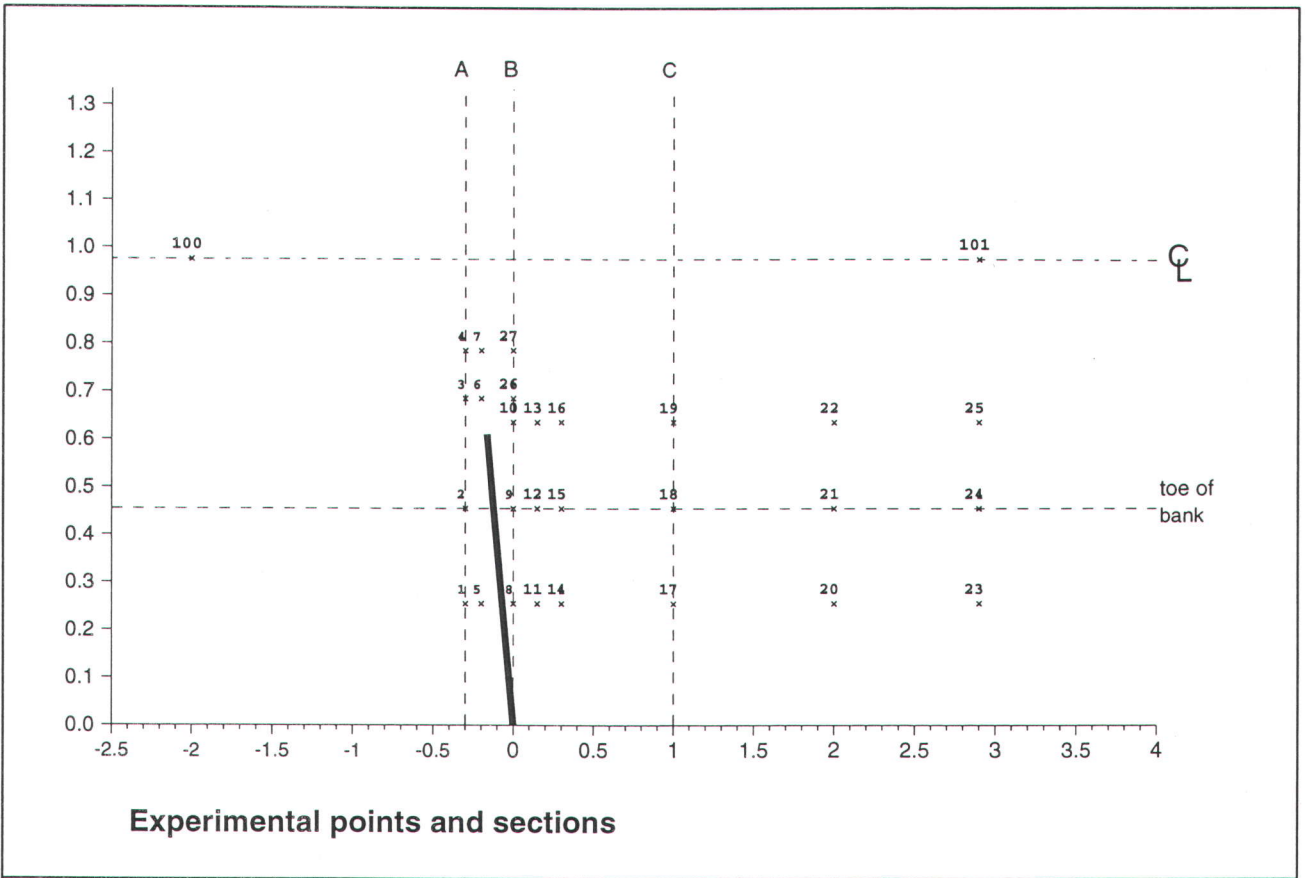
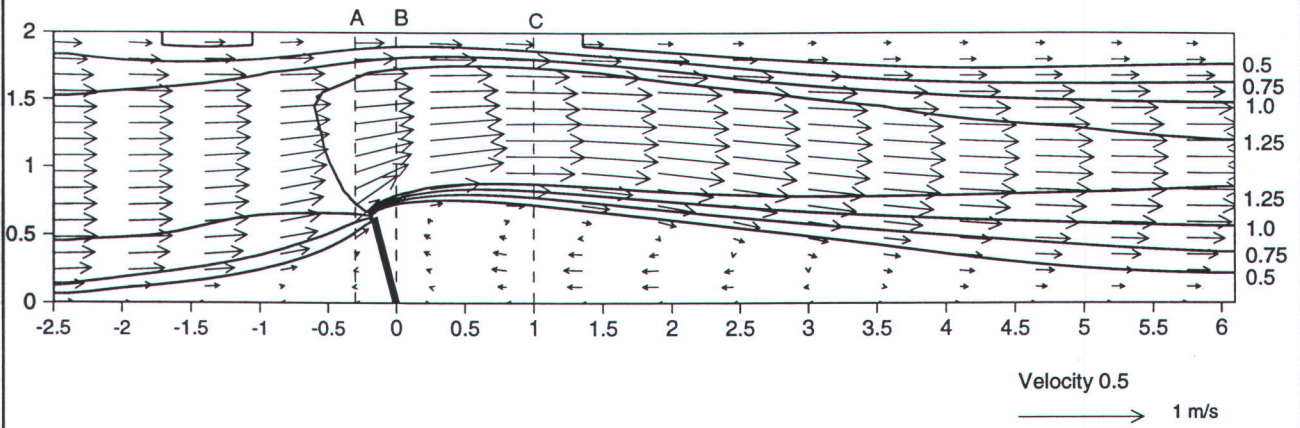
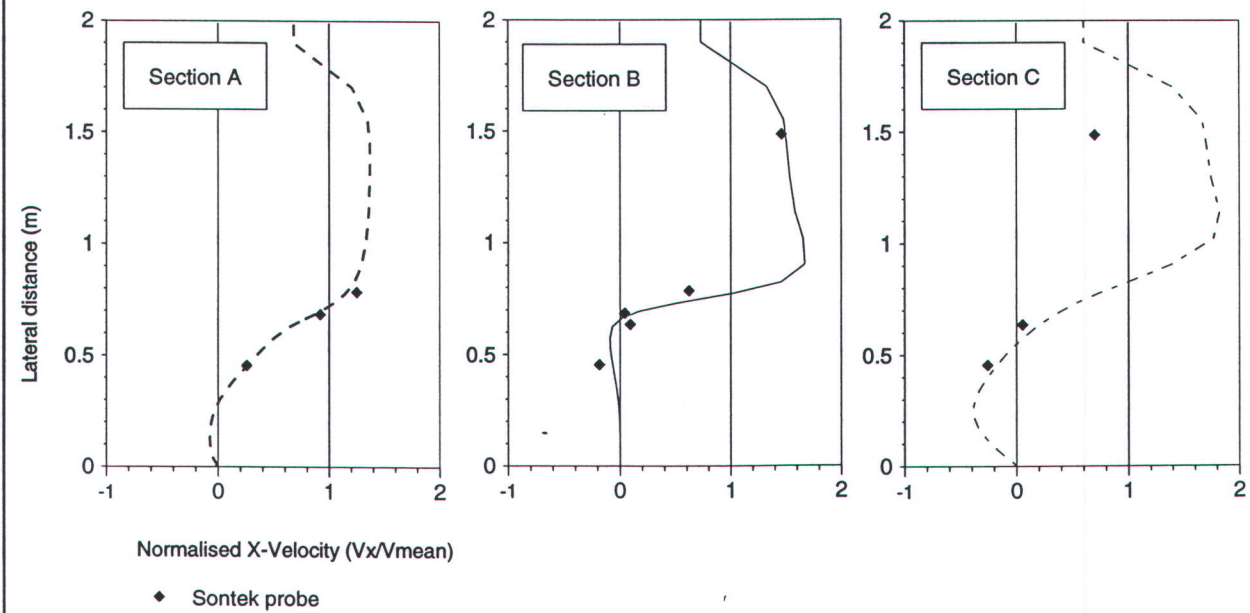


Figure 9.17 Experimental points and numerical grid for Test TC-1

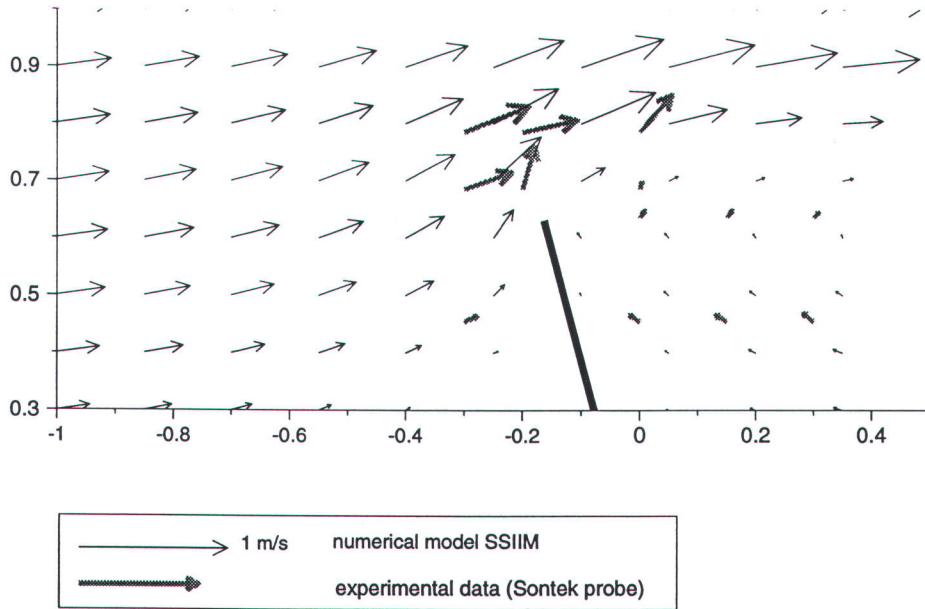


Mid depth velocity (m/s) and normalised velocity contours

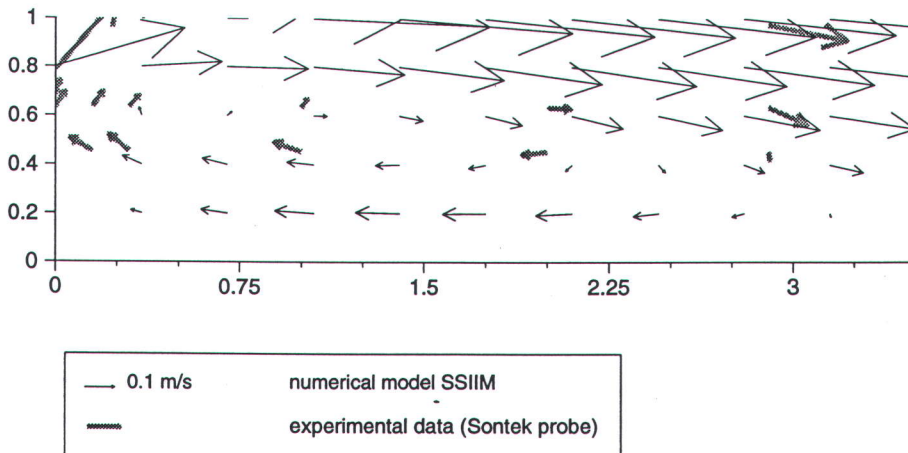


Normalised X-Velocity profiles at 50% from the bed (9cm)

Figure 9.18 Test TC - A 75° angled unsubmerged groyne in a trapezoidal channel



Plan velocity vectors close to the groyne at 50% from the bed



Plan velocity vectors in the recirculation zone at 50% from the bed

Figure 9.19 Test TC - A 75° angled groyne in a trapezoidal channel  
Plan velocity vectors near groyne and in the recirculation zone

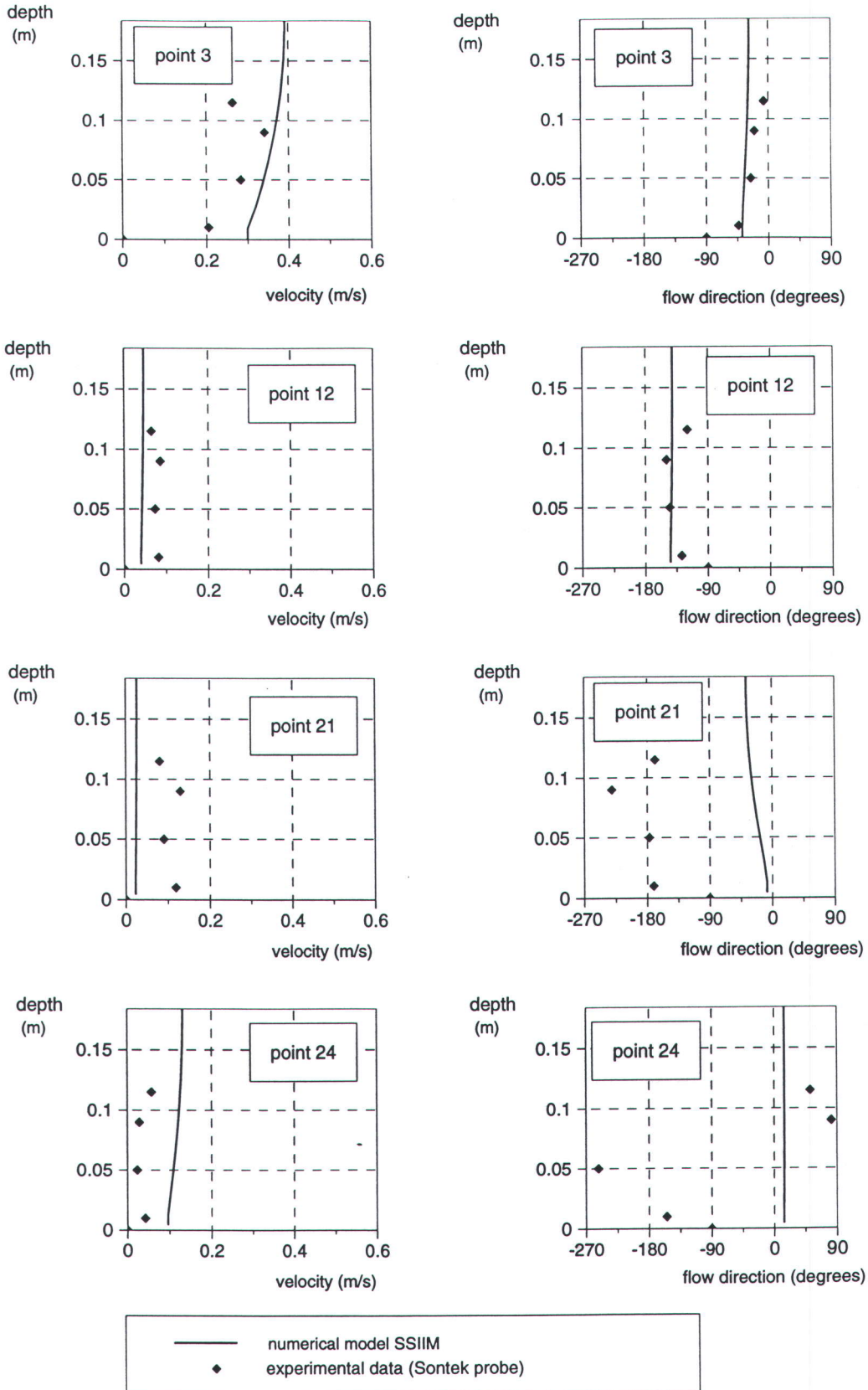
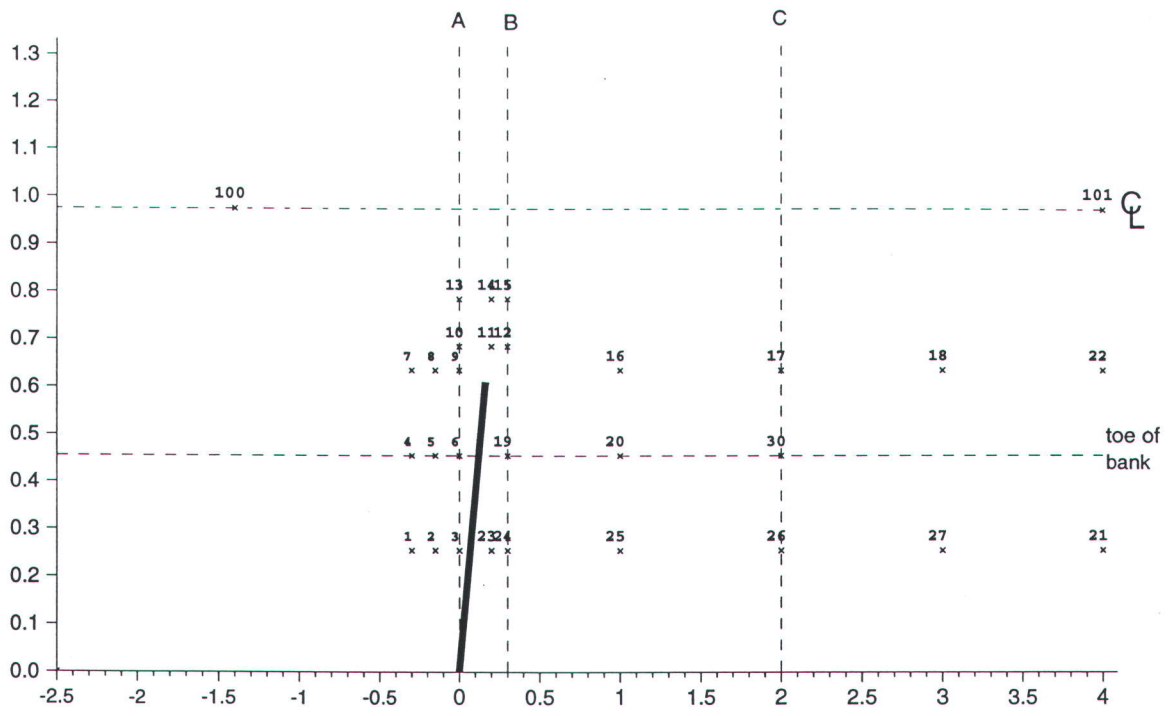
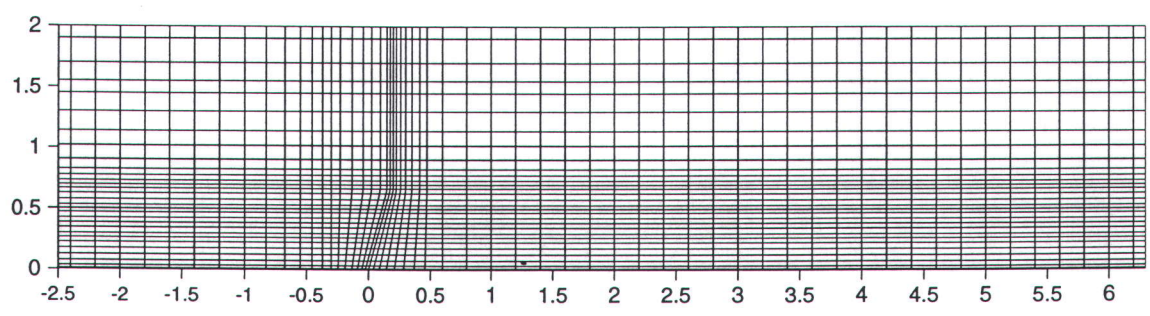


**Figure 9.20 Test TC - Upstream angled groyne in trapezoidal channel**  
**Vertical profiles of plan velocity and flow direction**

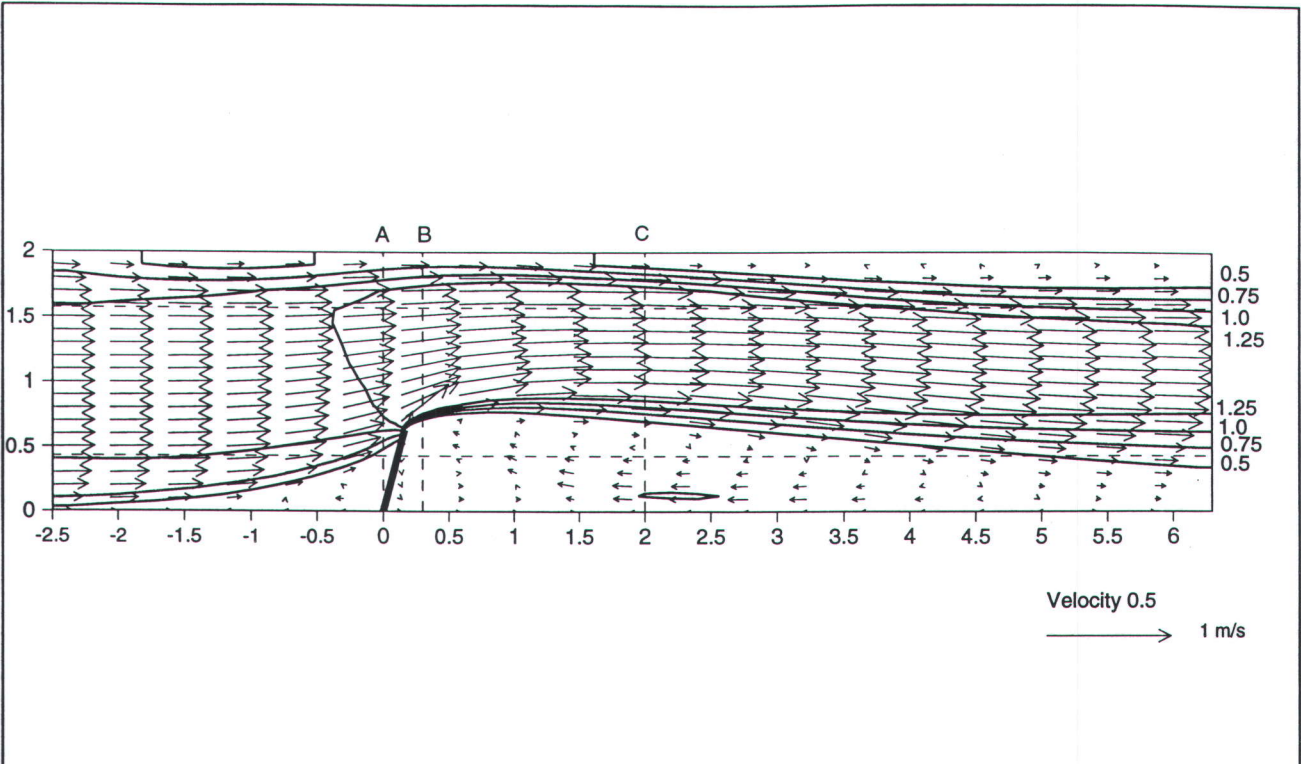


Experimental points and sections

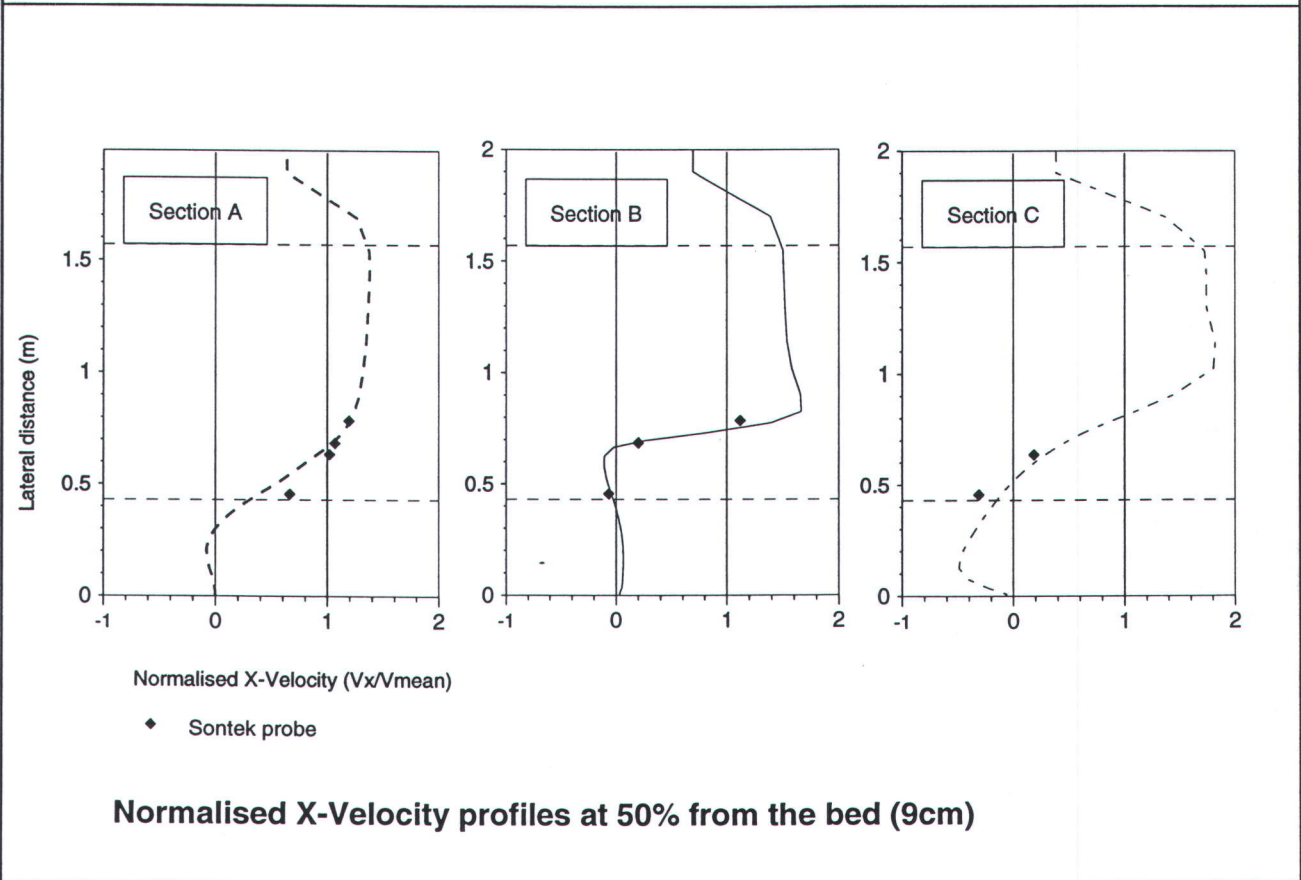


Plan view of the grid  $(x,y,z)=(57,29,10)= 16530$  cells

Figure 9.21 Experimental points and numerical grid for Test TD-1

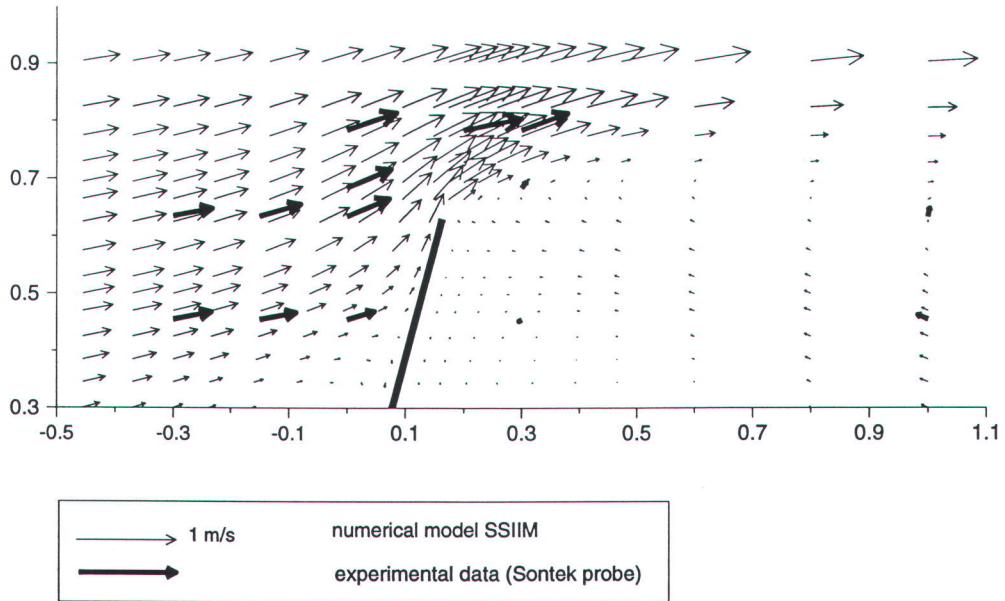


Mid depth velocity vectors (m/s) and normalised velocity contours

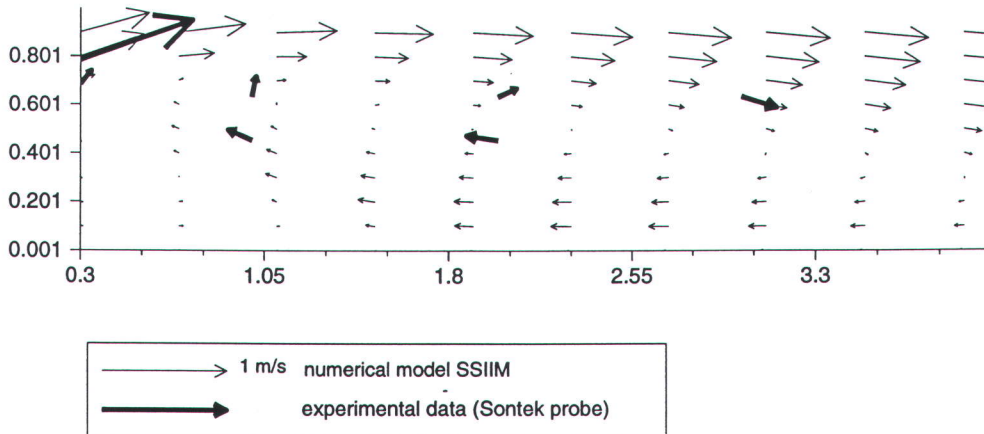


Normalised X-Velocity profiles at 50% from the bed (9cm)

Figure 9.22 Test TD - A 105° angled groyne in a trapezoidal channel  
Plan velocities



Plan velocity vectors close to the groyne at 50% from the bed



Plan velocity vectors in the recirculation zone at 50% from the bed

Figure 9.23 Test TD - A  $105^\circ$  angled groyne in a trapezoidal channel  
Plan velocity vectors near the groyne and in recirculation zone

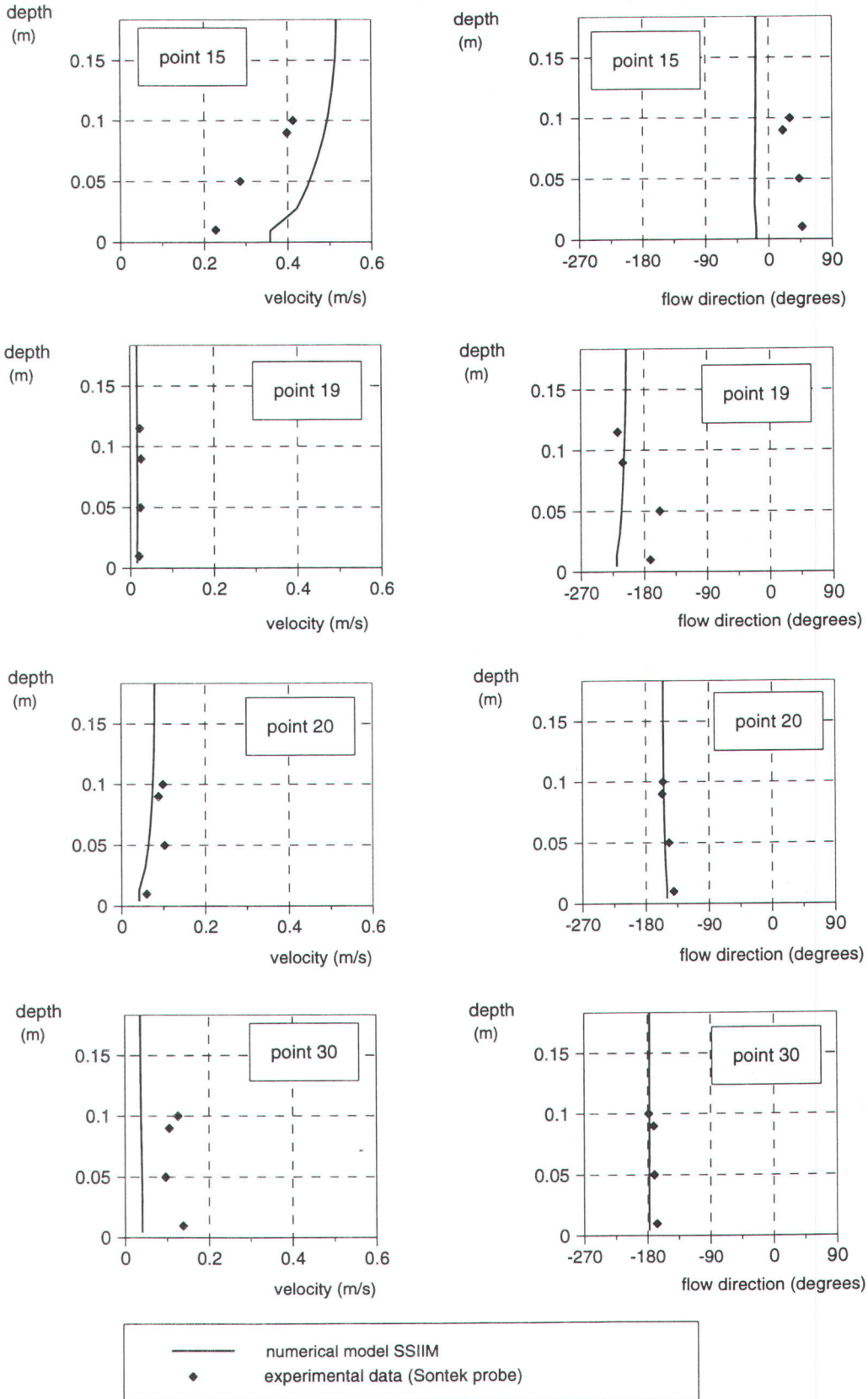


**Figure 9.24 Test TD - Downstream angled groyne in a trapezoidal channel**  
**Vertical profiles of plan velocity and flow direction**

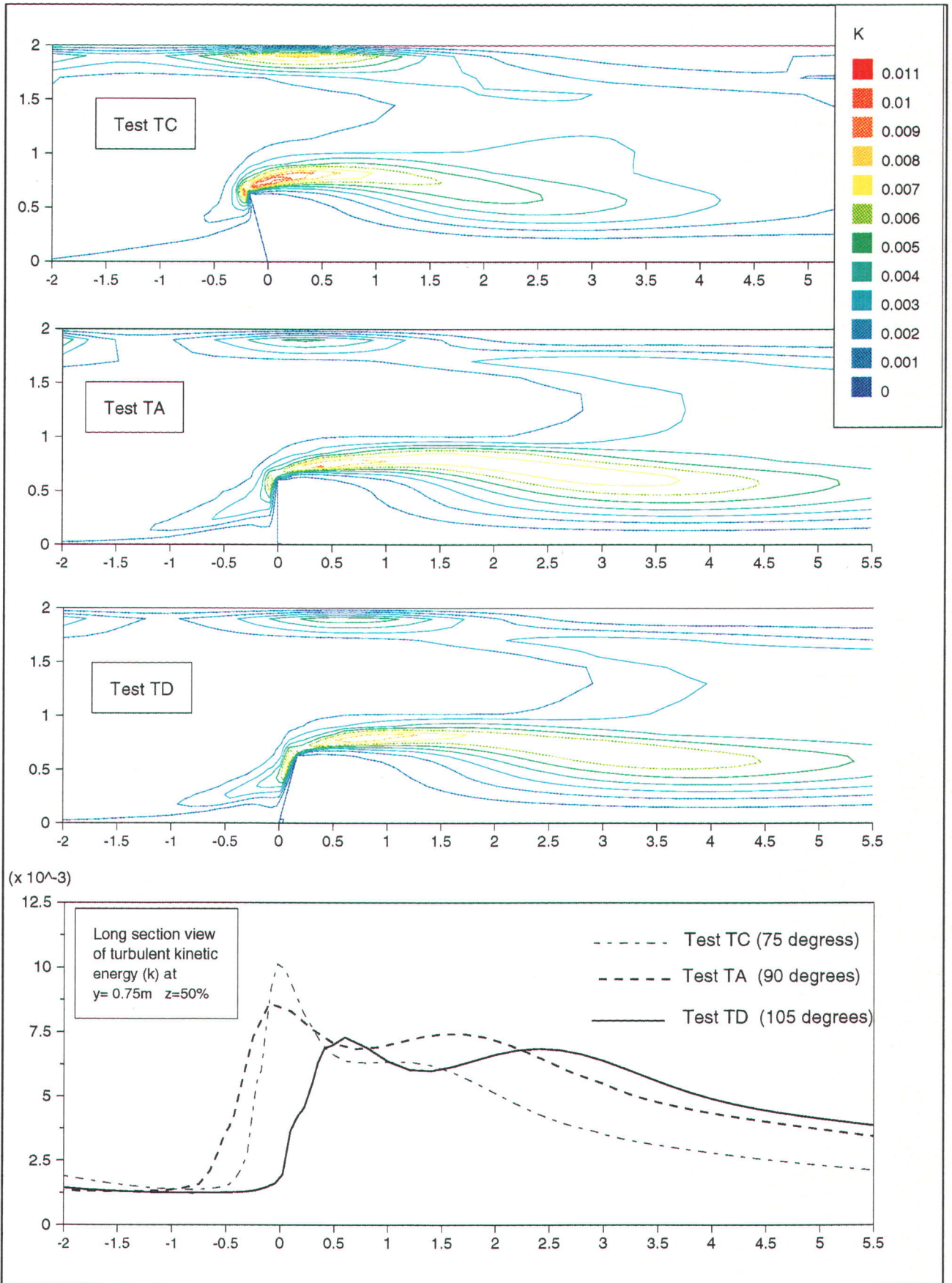
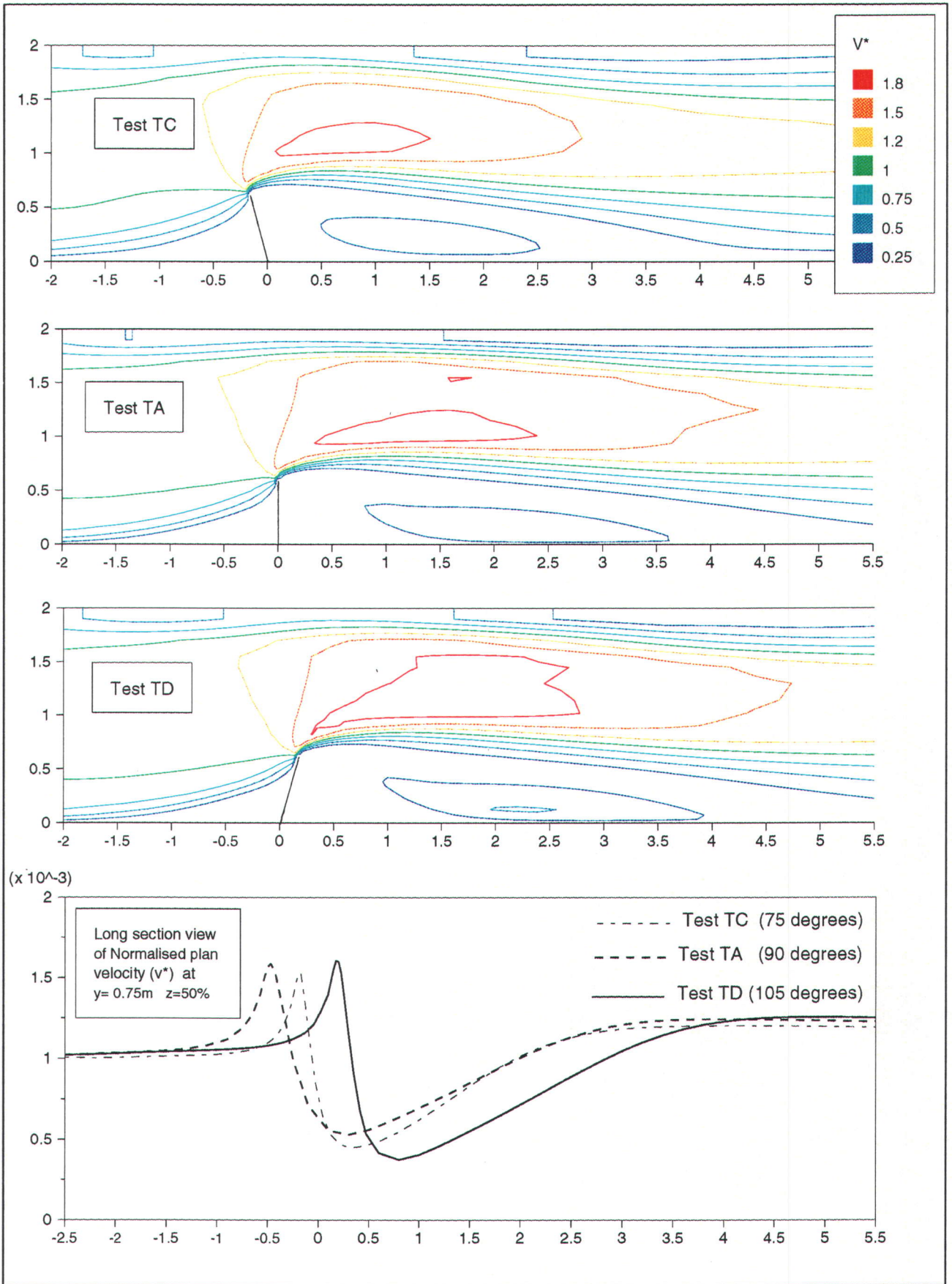
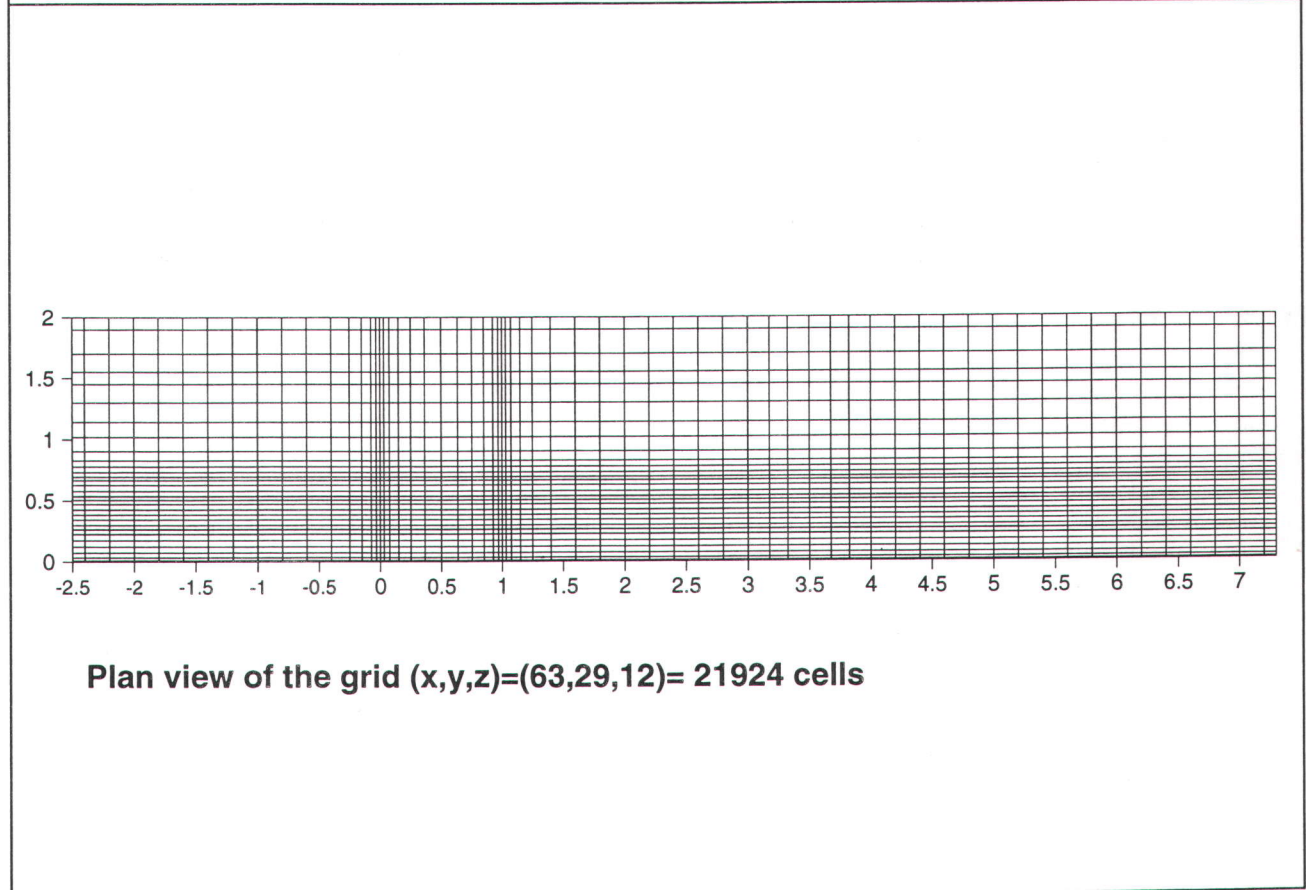
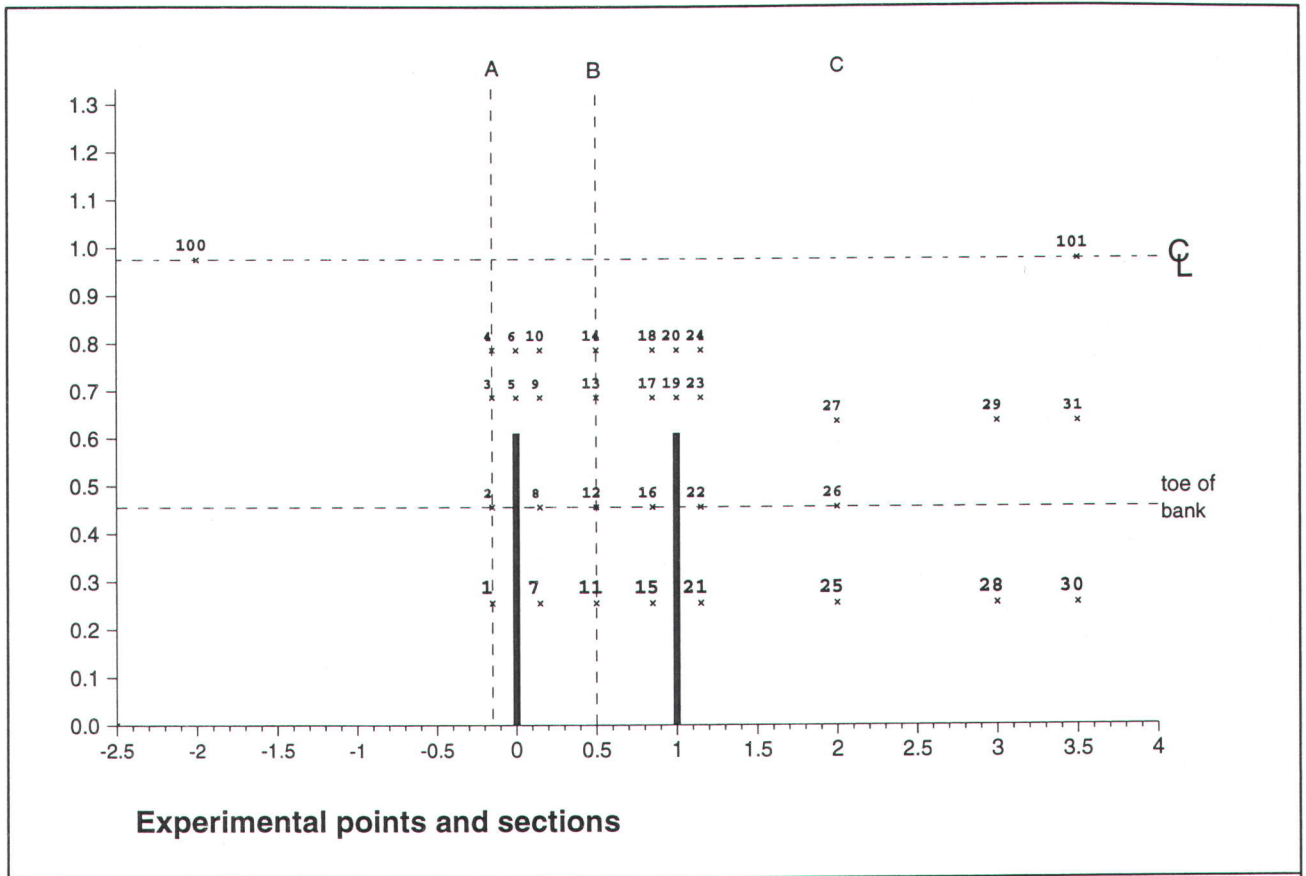


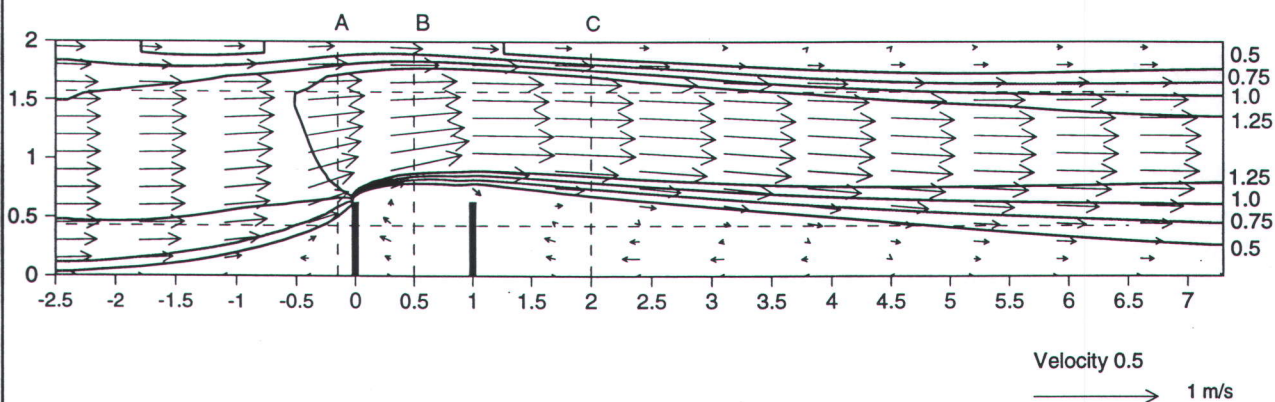
Figure 9.25 Dependence of  $k$  on groyne angle in a trapezoidal channel



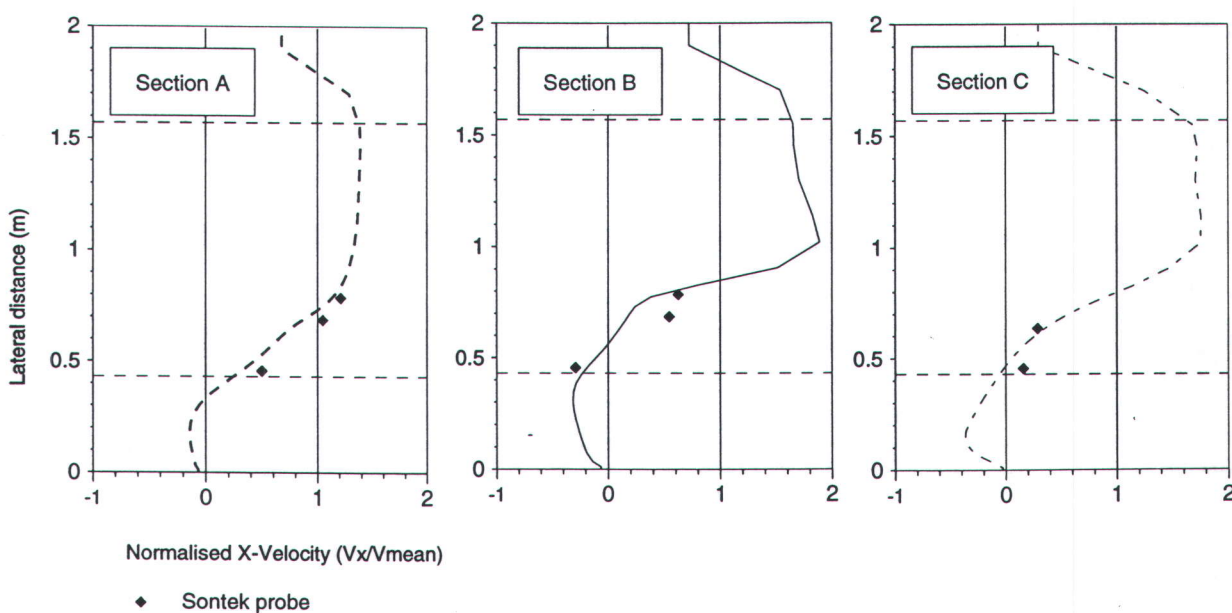
**Figure 9.26 Dependence of mid-depth velocity on groyne angle in a trapezoidal channel**



**Figure 9.27 Experimental points and numerical grid for Test TE-1**

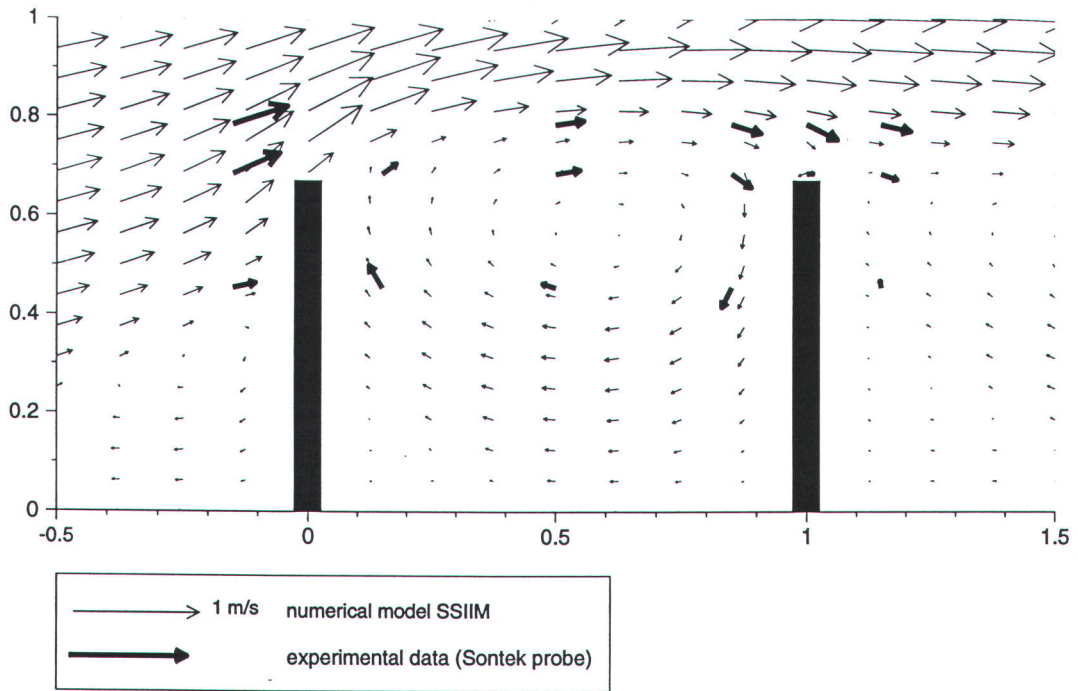


Mid depth velocity vectors (m/s) and normalised velocity contours

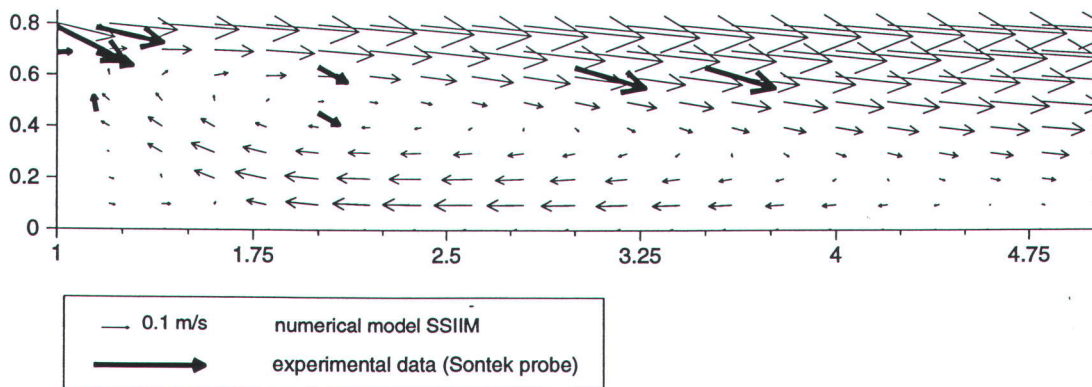


Normalised X-Velocity profiles at 50% from the bed (9cm)

Figure 9.28 Test TE - Two unsubmerged groynes 1m apart  
Plan velocities at mid depth



Plan velocity vectors close to the groynes at 50% from the bed



Plan velocity vectors in the recirculation zone at 50% from the bed

**Figure 9.29** Test TE Two unsubmerged groynes 1m apart  
Plan velocity vectors near the groyne and in recirculation zone

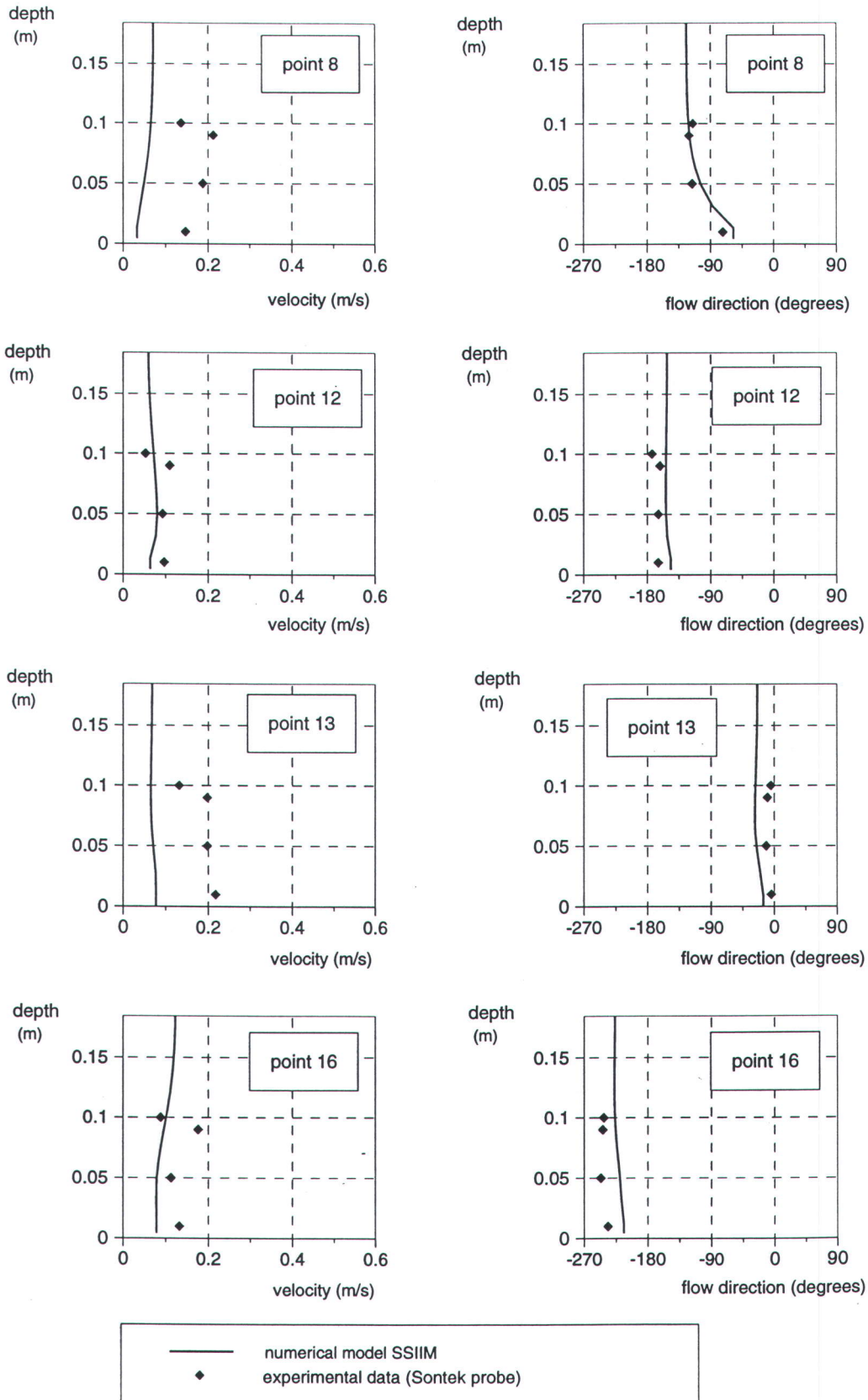


**Figure 9.30 Test TE - Two groynes 1m apart in a trapezoidal channel  
Vertical profiles of plan velocity and flow direction**

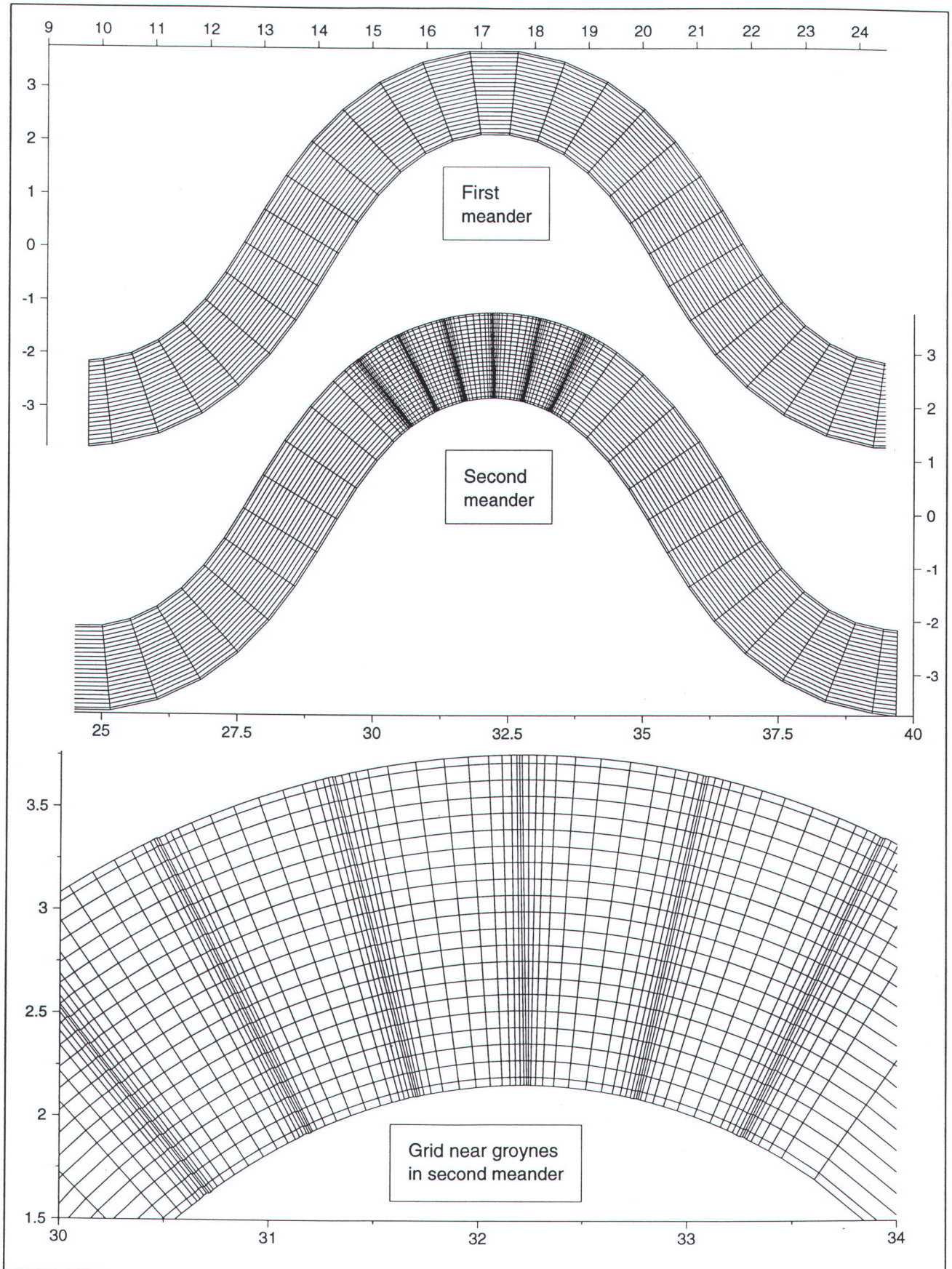
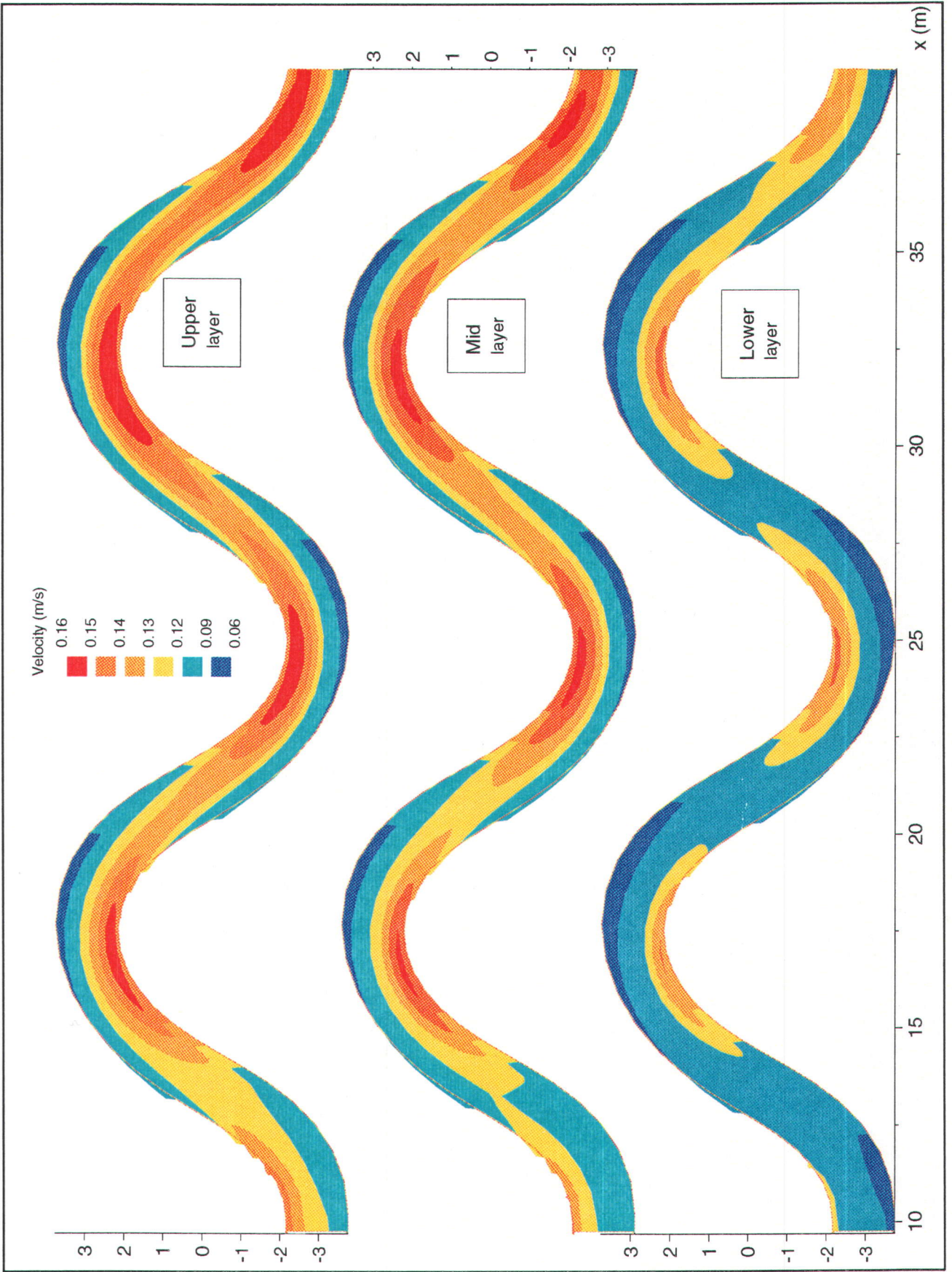
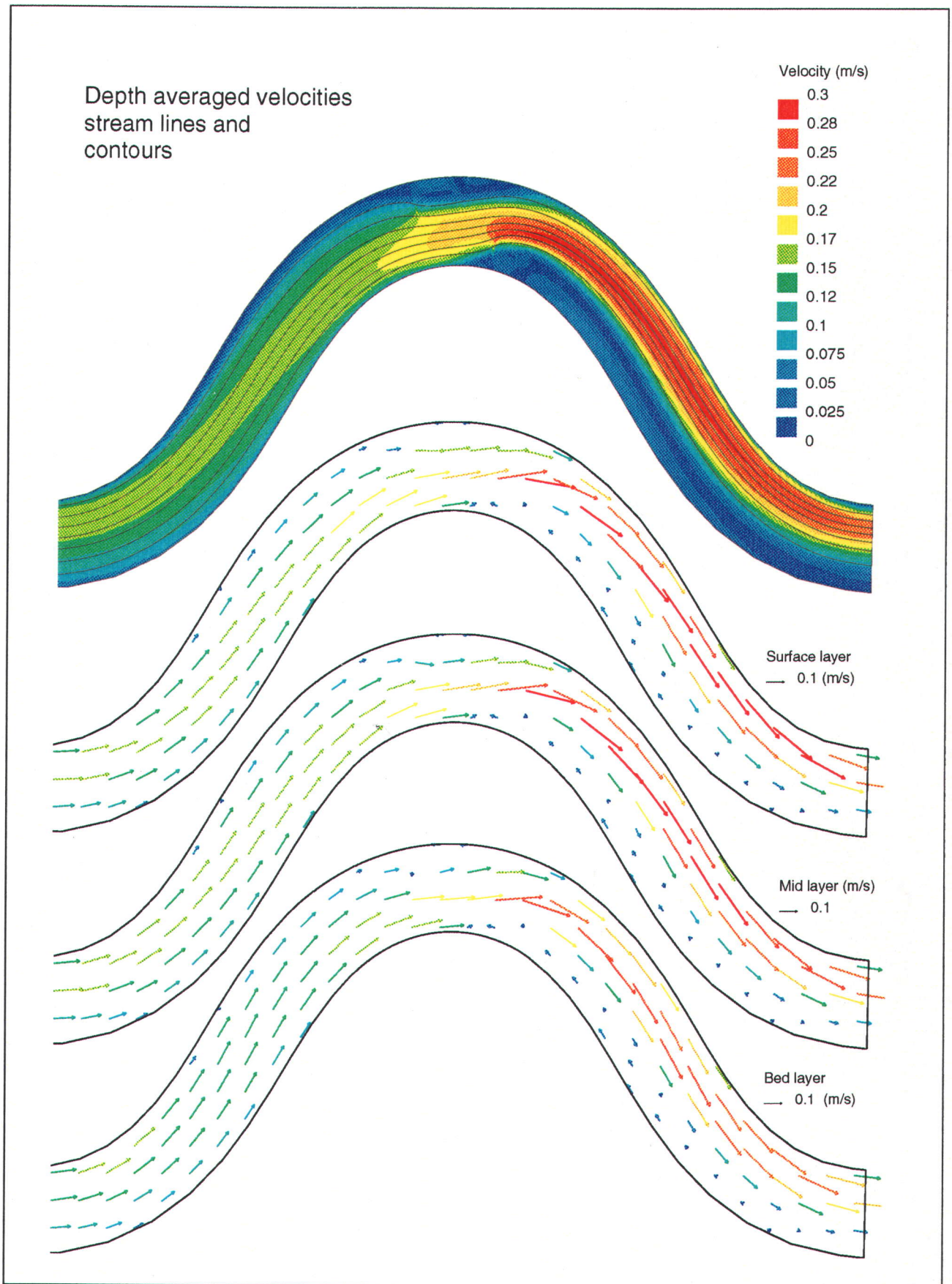


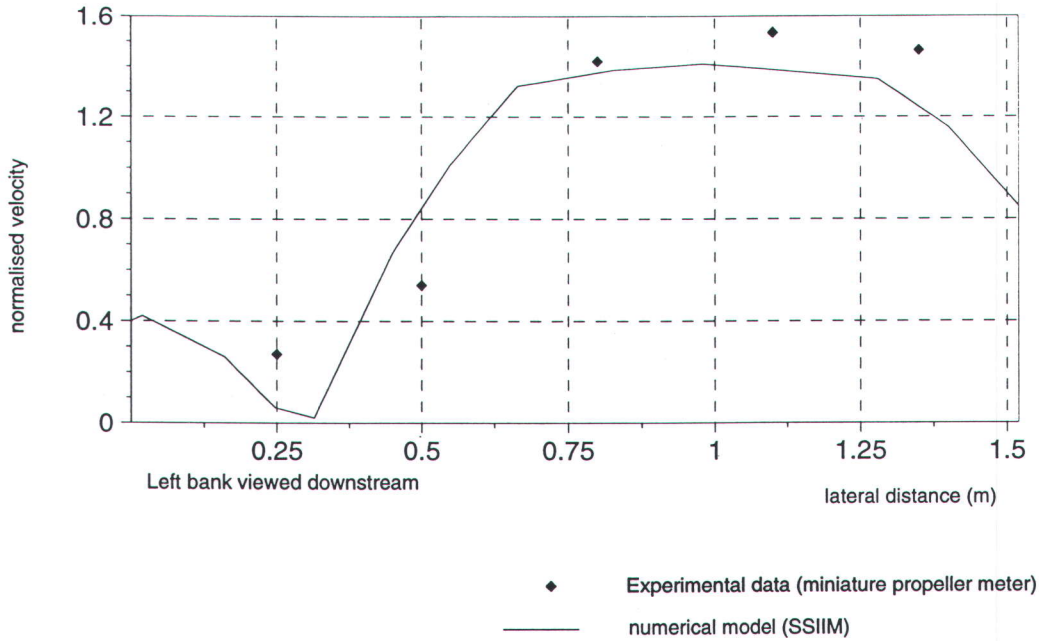
Figure 10.1 Test SPb-2 FCF flume - numerical grid



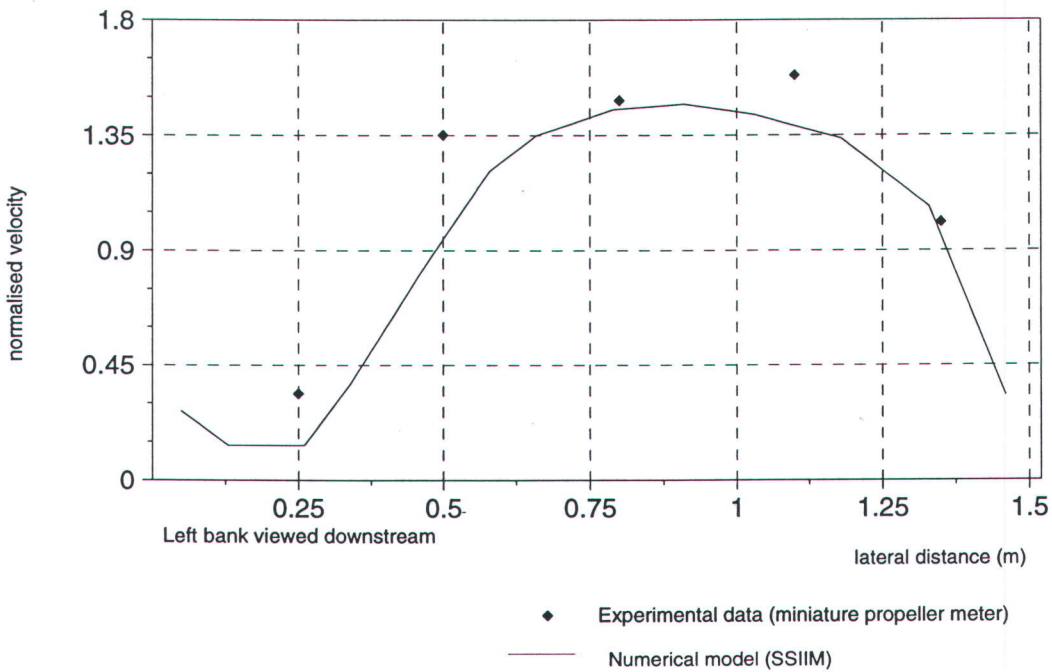
**Figure 10.2 Test SP0-1 Unobstructed sinuous channel Velocity contours at three depths**



**Figure 10.3 Test SPb-1 Four groynes in a sinuous channel  
Velocities at three depths and depth averaged streamlines**



**Normalised velocity in the section between groyne 1 and 2**



**Normalised velocity in the section between groyne 2 and 3**

**Figure 10.4 Test SP - Four groynes in a sinuous channel  
Cross-section profiles of plan velocity**

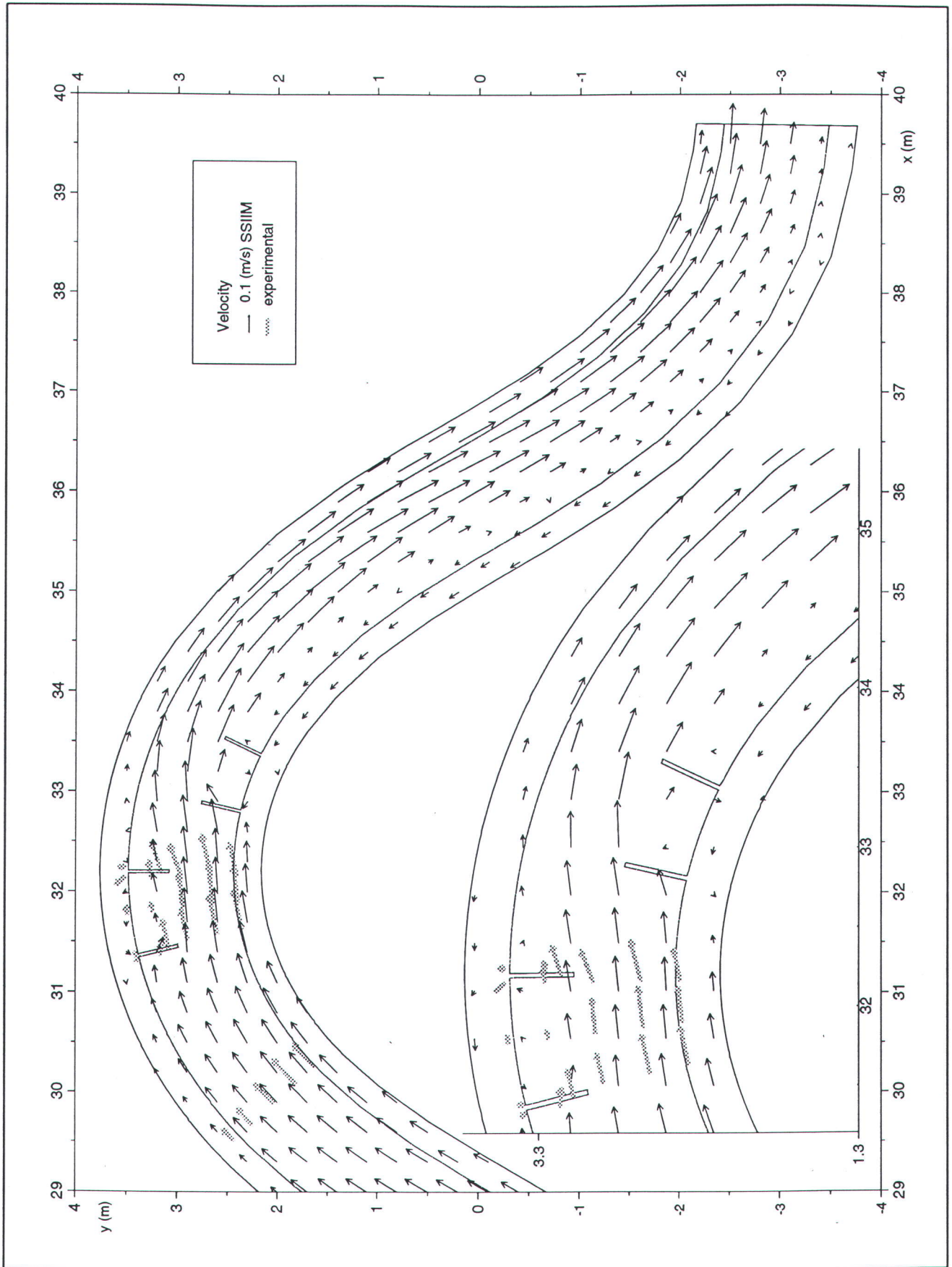


**Figure 10.5 Test SPb-1 Four groynes in a sinuous channel  
Comparison of near bed velocities**

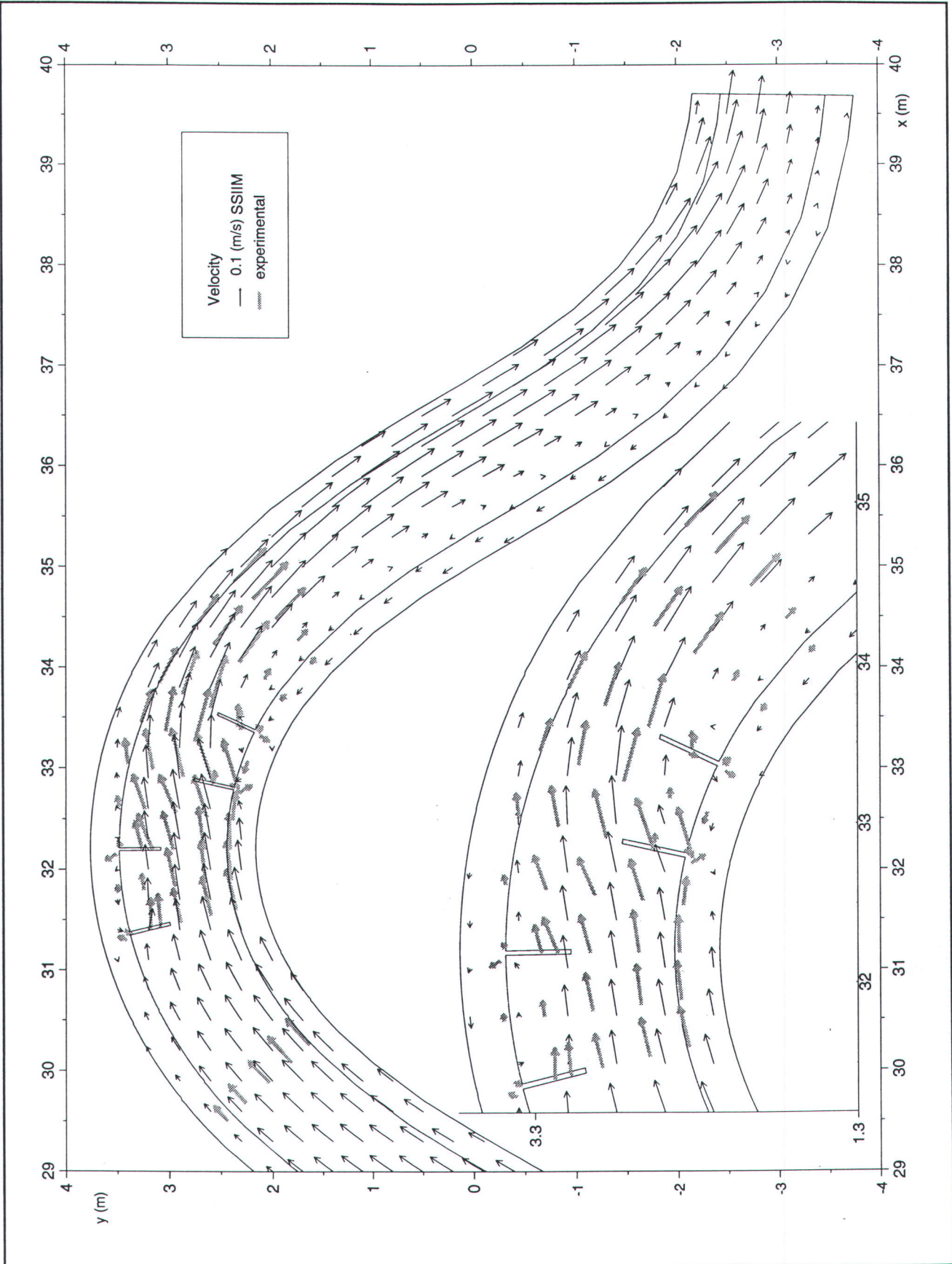


Figure 10.6 Test SPb - Sinuous channel with 4 groynes mid-depth velocities





## Plates



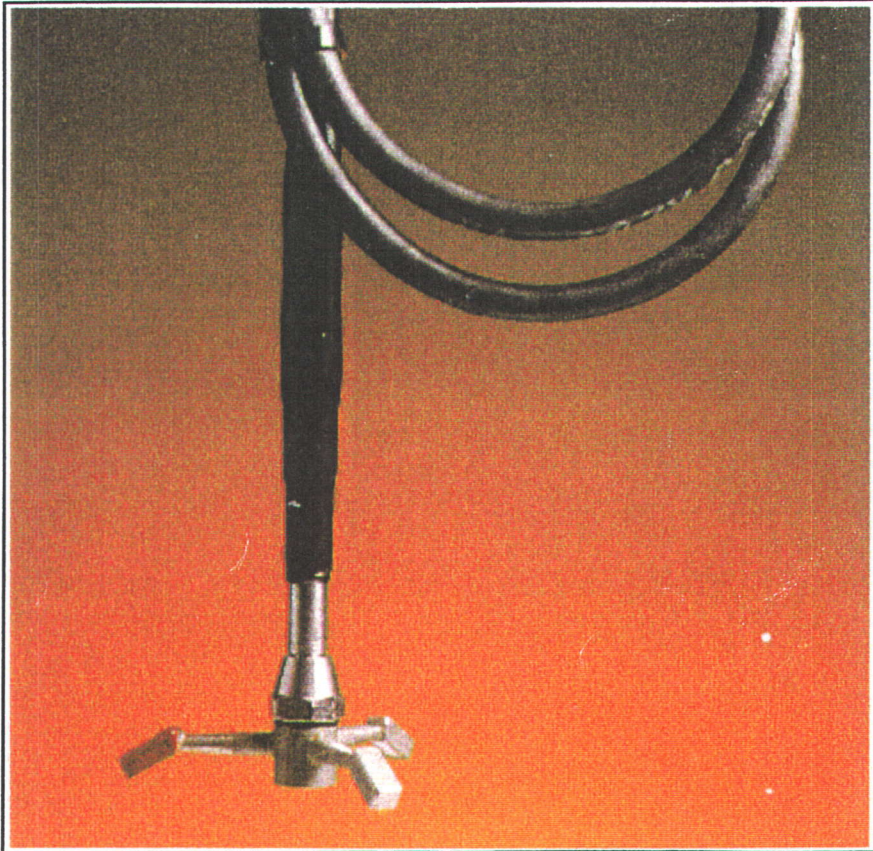
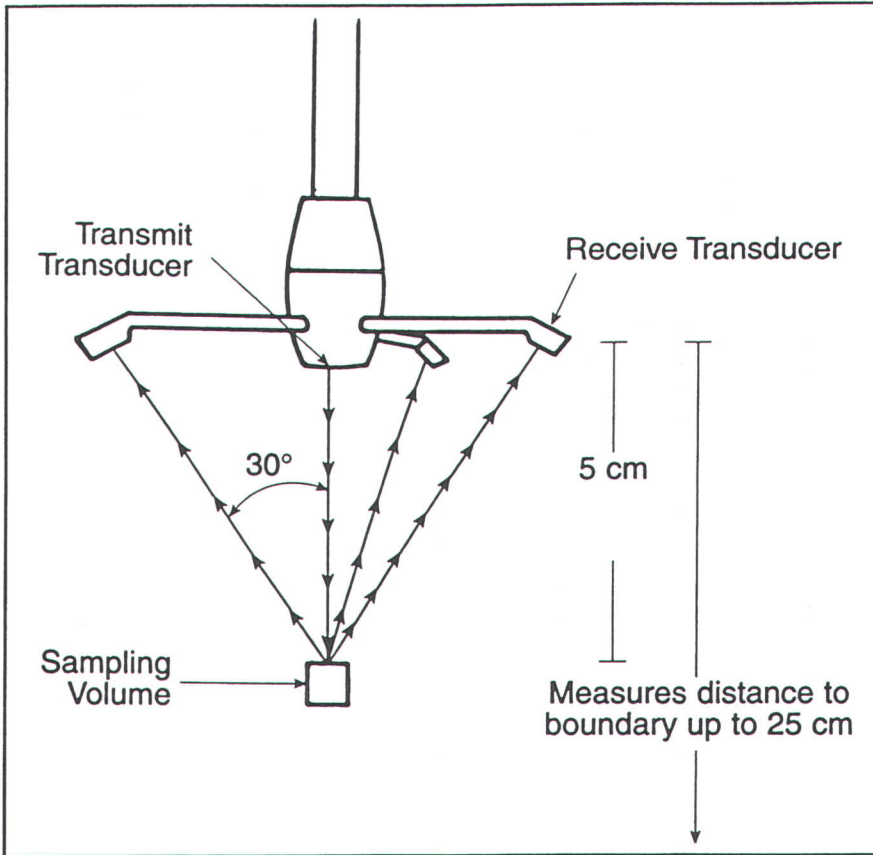
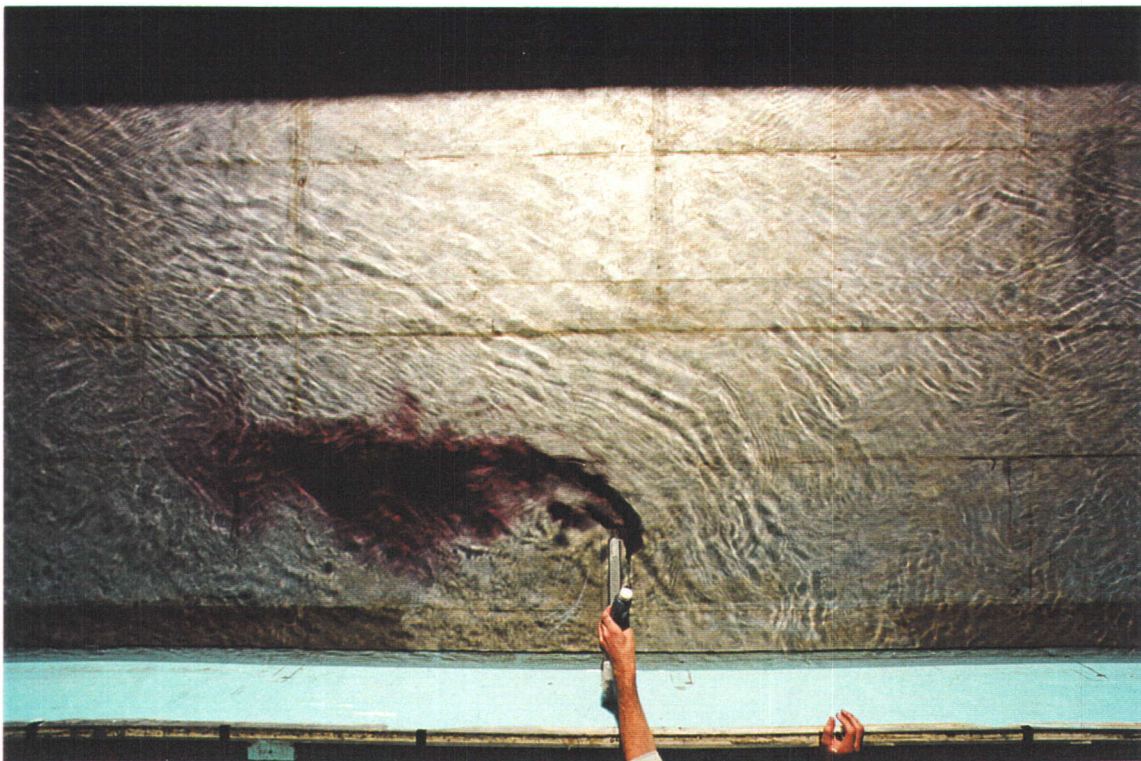
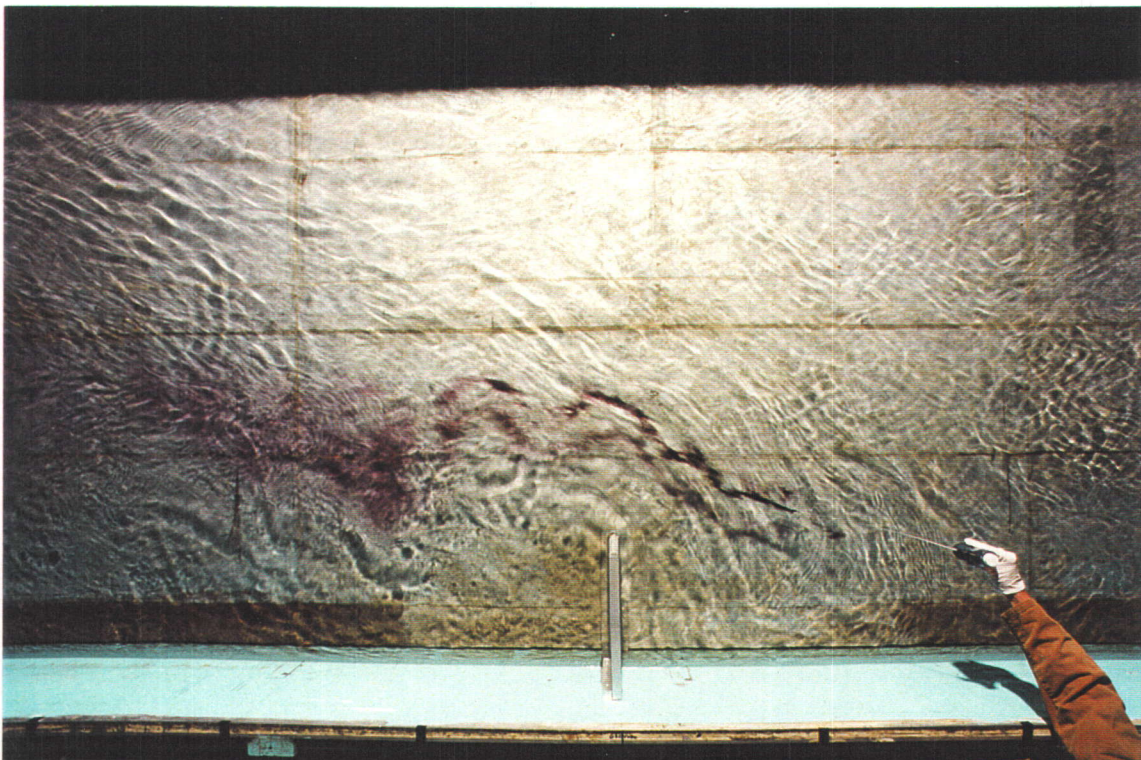


Plate 1 Sontek Probe





**Plate 2**      **Unsubmerged groyne - Vortex shedding**



**Plate 3**      **Unsubmerged groyne - Recirculation zone**



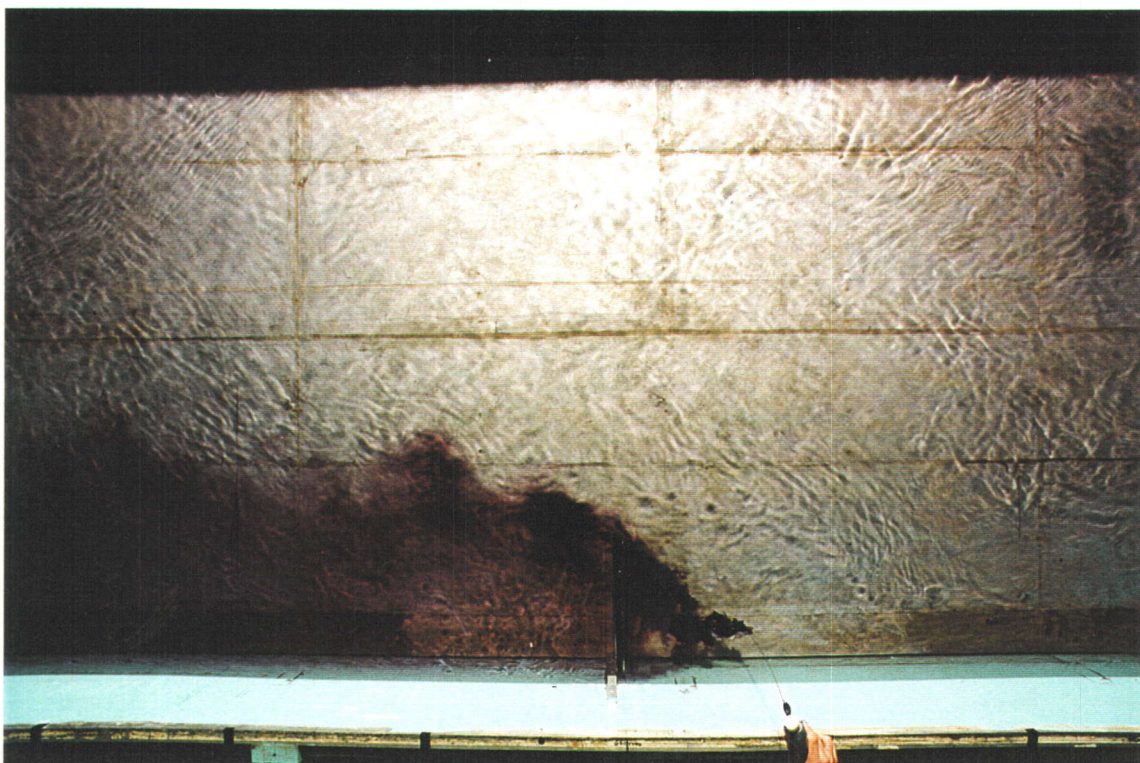


**Plate 4**      **Submerged groyne - Surface flow**



**Plate 5**      **Submerged groyne - Near bed flow**





## **Appendices**





## **Appendix 1**

### **Introduction to Three Dimensional Modelling Theory**





## Appendix 1 Introduction to Three Dimensional Modelling Theory

The computer modelling package used in this work solves the Navier Stokes conservation of momentum equations for turbulent flow in a general three-dimensional geometry to obtain the water velocity. The turbulence modelling is controlled by the standard k-ε set of equations. The following description, based on the description by Rodi (1980), makes use of the tensor notation.

In tensor notation, repeated subscripts imply summation. Thus equation (1) below may be read as

$$\frac{\partial U_i}{\partial x_i} = \frac{\partial U_1}{\partial x_1} + \frac{\partial U_2}{\partial x_2} + \frac{\partial U_3}{\partial x_3} = 0$$

The subscripts 1, 2 and 3 refer to values in the x, y and z directions and thus the above can be conventionally written as

$$\frac{\partial u}{\partial x} + \frac{\partial v}{\partial y} + \frac{\partial w}{\partial z} = 0$$

Summation on repeated subscripts refers to separate equations. Thus equation 2 below describes the three momentum equations in the x, y and z directions corresponding to  $j = 1, 2, 3$

### 5.1 The Navier-Stokes Equation

For incompressible flows, the governing equations, expressed in tensor notation, are:

for mass conservation, the continuity equation

$$\frac{\partial U_i}{\partial x_i} = 0 \tag{1}$$

and for momentum conservation, the Navier Stokes equation

$$\frac{\partial U_i}{\partial t} + U_j \frac{\partial U_i}{\partial x_j} = - \frac{1}{\rho_r} \frac{\partial P}{\partial x_i} + \nu \frac{\partial^2 U_i}{\partial x_j^2} + g \frac{\rho - \rho_r}{\rho_r} \tag{2}$$

where  $U_i$  is the instantaneous velocity component in the direction  $x_i$ .

The Boussinesq approximation has been made in the above equations so that the influence of variable density appears only in the buoyancy term (last term on the right-hand side of equation (2)). This effect is not significant in most river flows and is excluded from further consideration.

However, equations 1 and 2 cannot be solved for complex turbulent flows. Therefore a statistical approach is taken and the instantaneous values of  $U_i$  and  $P$  are separated into mean and fluctuating quantities:

$$U_i = \bar{U}_i + u_i \tag{3}$$



$$P = \bar{P} + p$$

where the mean quantities are defined as

$$\bar{U}_i = \frac{1}{t_2 - t_1} \int_{t_1}^{t_2} U_i dt$$

$$\bar{P} = \frac{1}{t_2 - t_1} \int_{t_1}^{t_2} P dt \tag{4}$$

and the averaging time  $t_2 - t_1$  is long compared with the time scale of the turbulent motion. For brevity, the overbars indicating averaged values will be dropped. Introducing (3) into (1) and (2) and subsequent averaging in the way indicated by (4) yields the following equations:

•Continuity equation:

$$\frac{\partial U_i}{\partial x_i} = 0 \tag{5}$$

•Momentum equation:

$$\frac{\partial U_i}{\partial t} + U_j \frac{\partial U_i}{\partial x_j} = - \frac{1}{\rho_r} \frac{\partial P}{\partial x_i} + \frac{\partial}{\partial x_j} (v \frac{\partial U_i}{\partial x_j} - \overline{u_i u_j}) \tag{6}$$

These are the equations governing the mean-flow quantities  $U_i$  and  $P$ .

The first and second terms on the left hand side of the equation represent unsteady flow and convection. The two terms on the right hand side are the pressure and Reynolds stress terms. The unsteady term is often neglected from river flow calculations. Although it is to be expected that the unsteady flows generated by vortex shedding at the tip of the groyne will create unsteadiness downstream of the groyne, this effect is thought to be not sufficiently large to justify the additional cost and complexity of an unsteady model.

### A1.2 Development of the Turbulence Model

Equations 4 and 5 are exact as no assumptions have been made to derive them. However, due to the non-linearity of equation (2), they do not form a closed set. This is because the averaging process has introduced unknown correlations which form the turbulent stresses, or Reynolds stresses:

$$\rho \overline{u_i u_j}$$

Exact equations can be derived for the quantity above, but they contain turbulence correlations of the next higher order. Closure of the problem can only be obtained by introducing a turbulence model which will make an approximation to these correlations.

An important concept in turbulence modelling is the Boussinesq eddy-viscosity theory which assumes that the turbulent stresses are proportional to the mean-velocity gradients. This concept may be expressed as:



$$-\overline{u_i u_j} = \nu_t \left( \frac{\partial U_i}{\partial x_j} + \frac{\partial U_j}{\partial x_i} \right) - \frac{2}{3} k \delta_{ij} \quad (7)$$

where  $\nu_t$  is the turbulent or eddy viscosity, and  $k$  is the kinetic energy of the turbulence. The first two terms on the right side of the equation form the diffusive term in the Navier-Stokes equation.

### A1.3 The k- $\epsilon$ Model

The eddy viscosity,  $\nu_t$  in equation 8, is a property of the turbulence and therefore varies with the development of the flow. Therefore it is necessary to determine a distribution for  $\nu_t$  in order to model the turbulent flow and equation 8 provides the base from which this model can be built. The k- $\epsilon$  model has been developed using the turbulent viscosity term defined by:

$$\nu_t = C_\mu \frac{k^2}{\epsilon} \quad (8)$$

Where  $\epsilon$  is the dissipation rate of the turbulent kinetic energy ( $k$ ), and  $k$  is defined by:

$$k = \frac{1}{2} \overline{u_i u_i} \quad (9)$$

The advection equation for turbulent kinetic energy is given as

$$U_j \left( \frac{\partial k}{\partial x_j} \right) = \frac{\partial}{\partial x_j} \left( \frac{\nu_t}{\sigma_k} \frac{\partial k}{\partial x_j} \right) + P_k - \epsilon \quad (10)$$

where  $P_k$ , the term describing the production of  $k$  is given by:

$$P_k = \nu_t \frac{\partial U_i}{\partial x_j} \left( \frac{\partial U_j}{\partial x_i} + \frac{\partial U_i}{\partial x_j} \right) \quad (11)$$

The differential equation governing turbulent dissipation takes a similar form.

$$U_j \frac{\partial \epsilon}{\partial x_j} = \frac{\partial}{\partial x_j} \left( \frac{\nu_t}{\sigma_\epsilon} \frac{\partial \epsilon}{\partial x_j} \right) + C_{1\epsilon} \frac{\epsilon}{k} P_k - C_{2\epsilon} \frac{\epsilon^2}{k} \quad (12)$$

The constants in the above equations were determined by Rodi by matching the mathematical model predictions with experimental measurements. The values for these constants are:

$$C_\mu = 0.09, \quad \sigma_k = 1, \quad \sigma_\epsilon = 1.3, \quad C_{1\epsilon} = 1.44, \quad C_{2\epsilon} = 1.92 \quad (13)$$

These values have been applied to a much wider range of flows than those from which they were derived. They are used in the SSIM and they cannot be changed by the user.





## **Appendix 2**

**Guidelines for using SSIM to model river groynes**





---

## Appendix 2 Guidelines for using SSIIM to model river groynes

---

### A2.1 SSIIM package

SSIIM executable may be downloaded from the Internet ( the address is <http://www.sintef.no>). It comes with a manual in which the theory and the options are described and with a library of test cases which are helpful in learning how to use the software. These test cases include an example of a river bend where the expected secondary flow is produced, an X-shaped channel crossing, a Y-shaped channel, a curved channel, a fish farm tank, a reservoir trap, a flood wave hitting a building, a turbidity current, a spillway and an erosion case. The source code of SSIIM is not supplied, so it is not possible to make changes to the model to include special effects.

SSIIM software runs on a PC under OS/2. The use of OS/2 operating system could be a limiting factor, but it is understood that support for other systems is planned. As with other 3D packages, SSIIM has a large memory requirement. As a guide, about 0.62 megabytes (Mb) of random access memory (RAM) are required for each 1000 cells plus 1.5 Mb for static data. An extra 4 Mb must be added for the program itself and the operating system. A further allowance is desirable to allow other systems such as the online graphics system to run concurrently. If the memory required is greater than the available RAM, then the hard disk is used as backing store. However this is usually unacceptably slow and may cause a program crash in some circumstances.

Although the software will run on a 486, a Pentium processor is strongly recommended to speed up the calculation. A 24 Mb, 60MHz Pentium was used for this study.

### A2.2 Description of files

#### A2.2.1 Storage of files and directories

A directory should be created to store the SSIIM executable and working data files. Since SSIIM uses specific filenames, it was found that the best way to run different simulations and models, is to create a sub-directory for each test. Prior to each run, the input files should be copied from the subdirectory to the SSIIM directory and, at the end of each run, results files should be copied to the subdirectory. This last action should be done before restarting SSIIM window because the first action performed by SSIIM is to write the Boogie file. This method will prevent SSIIM from overwriting valuable files.

#### A2.2.2 SSIIM input files

Two files are necessary to run SSIIM. The first is the **control** file which contains the size of the grid, the vertical distribution of the cells, the flow conditions, the boundary conditions and the specification of the parameters. Each option is defined by a letter and a number.

The second file required is the **koordina** file. This file contains the coordinates of the points at the bed. The format of the data is:

i j x y z

where **i** and **j** are the grid lines in the streamwise and cross-section direction and **x**, **y**, **z** are the coordinates of each point. In plan, four points define a cell. The vertical position of the cells are defined by the specified position of the bed, the calculated position of the free surface and the distribution of cells specified by options G3 or G16 in the Control file. SSIIM uses a cell-centred representation. Thus, the variables are calculated at the centre of each cell not at the co-ordinates defined in the koordina file. The first internal cells are numbered 2, and are delimited by lines 1 and 2. This is described fully in the SSIIM manual.



Other subsidiary files can be created to define the geometry and the boundary conditions more precisely.

- The **geodata** file contains the survey data that has been obtained from the field, a digitised map or a GIS system. This file can be used for three purposes. First, it can help to generate the grid using the grid editor. Second, it can be used for generating the z values for the bed using a linear interpolation. Finally, it can be used to create the Porosity file from the parameters in the Control file.
- The **bedrough** file may be used to specify a roughness height to individual bed cells.
- The **porosity** file defines the porosity at various z values in each cell. This file has been used to simulate a river bed covered with boulders. It may also be possible to use this file to specify the porosity of groynes. The porosity file is only used if the option G7 P is specified in the control file.
- The **inflow** file contains the upstream boundary conditions. The three components of the velocity are specified for each cell at the inlet section.
- The **interpol** file is used to define points where the user wants a vertical velocity profile (the option F48 is required in the Control file).
- The **verify** file is used as an input file for the “VerifyProfile” graphics option. The file contains the plan coordinates of the points, the vertical co-ordinate, and the velocity. Thus, experimental and computational results can be superimposed on a graph.

### A2.2.3 SSIM output files

The first file to be created is the **boogie** file which contains the following.

- 1 The memory requirement for the data arrays. To estimate the total memory requirement, at least 1Mb must be added to account for the memory required by SSIM and OS/2.
- 2 Geometric parameters: the wetted perimeter, hydraulic radius, water level and mean velocity for each section.
- 3 The residuals for each of the six variables. The residuals are output every iteration at the beginning and then every 100 iterations. This file enables the user to plot the residuals against the number of iterations to show the convergence rate. To create such a graph, the Boogie file must be read by Excel, converted using “delimited” “space” options for the format conversion. The beginning of the file must be deleted and the option “Use Relative References” in the pull-down menu “Tools” “Use Macro” must be selected. The macro shown below must then be run to remove alternate lines describing the residual in the continuity equation :

```
Sub Macro1()  
    For l=1 to ....  
        ActiveCell.Offset(1, 0).Rows("1:1").EntireRow.Select  
        Selection.Delete Shift:=xlUp  
        ActiveCell.Select  
    Next l  
End Sub
```



The comma must be replaced by a space and the columns "Iter:" and "Resid:" have to be removed before creating the graph.

The main output file of SSIIM is the **result** file. This file contains the results from the water flow calculation. This file is written every 100 iterations and when the solution is converged. For each cell, the following values are output: the three components of the velocity, the turbulent kinetic energy, the dissipation rate, the fluid fluxes on all the walls of the cells, and the pressure.

The **xcyc.las** file is created using the "Files" pull-down menu of SSIIM window. It contains the x, y, z coordinates for all the nodes and may be used for processing the data. This file is divided in five parts:

- Twelve lines of parameters
- Input velocities (u and v), k and e (four values on each line)
- x values for all grid lines
- y values for all grid lines
- z values for all grid lines

The FORTRAN code to read this file is:

```

DO 99 I=1,12
99  READ (9,'(1x)')

DO 100 J=2,JMAX
DO 100 K=2,KMAX
100  READ(9,*)U(1,J,K),V(1,J,K),KK(1,J,K),EPS(1,J,K)

READ(9,*) ((X(I,J,K), K=1,KMAX), J=1,JMAX), I=1,IMAX)
READ(9,*) ((Y(I,J,K), K=1,KMAX), J=1,JMAX), I=1,IMAX)
READ(9,*) ((Z(I,J,K), K=1,KMAX), J=1,JMAX), I=1,IMAX)

```

where IMAX, JMAX, KMAX correspond to xnumber, ynumber, znumber in the G1 data set in the control file

If the water surface update option is specified, then the Z values are corrected to the true water surface. Otherwise, the Z values are calculated from the backwater method. The corrected water surface may be obtained by subtracting (pressure/9810).

A file called **interres** is created to store vertical interpolated velocity profiles at the points specified in the Interpol file. This file contains the velocities, k and e for each point.

### A2.3 SSIIM control file options

The SSIIM manual provides information about the control file options listed by letter and number. This section summarises the options of the control file listed by topic.

#### Run Control

- |     |   |
|-----|---|
| F1  | Debugging                                       |
| F2  | Automatic execution                             |
| F7  | General run options described under each topic. |
| F20 | Repeated calculations                           |
| F38 | Maximum Residual                                |
| F43 | Underflow check                                 |



F53 Print frequencies

#### Grid Editor

F47 Interpolation parameter  
W6 NoMovePoint (Fixed points)  
W7 Attraction points

#### Geometry

G1 Grid lines  
F7\_D,J Double resolution (in x, y direction)  
G3 Vertical distribution (global)  
G16 Vertical distribution (local)  
G6 Water surface adjustment  
K1 Frequency of water surface adjustment  
F7\_G Blocks don't move with water surface (or bed)  
G13 Specify outblocks (inactive blocks)  
W3 Multiple blocks  
W4 Block walls

#### Boundary Conditions and Initial conditions

F9 Turbulent boundary conditions  
G7 Flow boundary conditions (see also F7\_I, F7\_C, inflow file)  
F15 Friction law where wall meets bed  
F16 Roughness height (see also bedrough file and Strickler numbers)  
K2 Friction laws at vertical walls and free surface  
W1 Overall Strickler number  
W5 Local Strickler Number  
W2 Initialisation sections  
G8 Initial velocities  
G11 Source velocities

#### Numerical Scheme

F21 Relaxation coefficient for the Rhie and Chow Interpolation  
F24 Turbulence model (k-e)  
F44 2D calculations  
F59 Gauss-Seidel iterations (10)  
K1 Maximum number of iterations  
K1 Surface update frequency  
K3 Relaxation factors  
K4 Number of sweeps for each equation  
K5 Block correction (POW only)  
K6 Numerical scheme (SOU/POW)  
K9 Pressure scheme (SIMPLE/SIMPLEC)  
K10 Matrix solver



### Sediment

F7 A,B,Z  
F4,6,8,10,11,12,18,23,26,28,30,37,40,41,54,56  
G5,12  
S,N,B

### Transients

F17 Timestep (define transient calculations)  
F33 Timestep and iterations per timestep  
F36 Transient free surface (TFS)  
F45 TFS  
F54 Residual limit  
F58 TFS parameters  
F37 transient sediment calculations

### Porosity

F22 Minimum porosity, relaxation coefficient  
F25 F22 + Porosity parameters  
F31 Porosity coefficients used in making a porosity file.  
F7\_P Perform porosity calculations  
see also porosity file and roughness height

### Graphics options

G15 Mouse scaling for animation  
G19 OpenGL\_3D surface parameters  
H Colour contouring options  
L Isoline values  
P Initial scaling for graphics display  
F7\_V Rotate by 90 degrees  
F7\_X Read grid from xcyc.las file  
T Graphics title

## **A2.4 Grid generation**

### *A2.4.1 Grid Editor*

The overall resolution of the grid is specified in the control file. This can be modified using "GridEditor" which is selected from "InputEdit" pull-down menu. This grid editor can be used for straightforward cases such as a rectangular or curved channel with a regular grid. The grid may be adjusted by specifying attraction points (PointAttraction) and fixed points (NoMovePoints). The overall distribution of the internal mesh may be also be altered. For example, the grid editor can interpolate a smooth elliptic grid using "Elliptic" option.

However, for more complex channels, like a sinuous channel or to create a fine grid around a groyne, it is probably better to use a spreadsheet. Using such a spreadsheet, a formula can be inserted in a table to generate the grid. This process was used to create most of the grids in this study.



#### A2.4.2 Simulation of groynes.

In this section, some methods which were used in this study to create groynes are described in detail with their advantages and their drawbacks.

##### Blocked-out cells

The easiest way of creating an obstruction in the flow is to use the G13 option in the Control file. This option allows a group of adjoining cells to be blocked out. Up to 11 G13 data sets can be used. This option is very convenient to create a rectangular groyne in any kind of channel. However, it has some limitations when creating a tapered groyne because the sloping tip cannot be properly modelled. In this case, other solutions should be used.

##### Raised bed

A raised bed may be used to create groynes with a more complex geometry. The grid must be fine close to the groyne and the bed be raised to the height of the submerged groyne. However, this method may create instability when it is used to create an unsubmerged structure because the water tends to flow over the groyne and that can lead to divergence. To overcome this problem, a combination of blocked-out cells and raised bed should be used. The bed is raised to create about 90% of the groyne height and the remaining 10% of the height is achieved by blocking out cells using the G13 options. This solution enables a partly submerged tapered groyne to be modelled.

##### Porous groyne

A porous groyne can be modelled by a structure with several holes but this solution is not satisfactory because of the large jet of water that flows from each hole. However, a porosity model has been implemented in SSIM to simulate a river bed with large stones. This model can be extended to create porous structure. The option F7 P must be added to the Control file and the relaxation coefficient of the Rhie and Chow interpolation must be set to 0.0 (option F21 in the Control file) and a minimum porosity of 0.5 must be specified and used in the porosity file. However, at this stage, further investigations need to be made to make sure that the results are physically realistic.

#### **A2.5 Choice of Parameters**

The correct choice of resolution, numerical scheme and other parameters is important in achieving an accurate solution in an acceptable run time. These matters are described in full in Section 10 but the following notes indicate the main points.

- The POW scheme is about 30% faster than SOU and is usually more stable but is less accurate where the grid is coarse and the flow is not aligned to the grid.
- Block correction accelerates convergence of the POW scheme but this may not work satisfactorily where blocked out cells are used.
- 
- The SOU scheme can create undershoots which may be the cause of instability in the k and epsilon equations.
- A very coarse grid may generate an oscillating solution, delaying or preventing convergence.



## A2.6 Choice of relaxation coefficients.

Relaxation factors are defined in the control file by data set K3. The default values are 0.8 for the velocities, 0.2 for pressure and 0.5 for k and epsilon. If the solution diverges then reduced relaxation factors are indicated, for example 0.3 for velocity and 0.2 for turbulence. Much lower values have been found necessary in some circumstances. If the solution oscillates after many iterations lower relaxation factors may be required. If the model is converging steadily but very slowly then the relaxation coefficients may be increased with caution. Convergence is monitored using a display of the residuals. The residuals are also written to the BOOGIE file which may be later processed and graphed as described in Section A2.2.3. Relaxation factors and other parameters may be altered while the program is running and this is described in the next section.

## A2.7 Modification of parameters during the run

Before making any changes to the parameters it is advisable to save the current state of the program using "Write Result". So, if the changes in parameters cause divergence, the control file can be edited and the program restarted from the saved state using "Read Result".

SSIIM provides a monitor window in which the residuals may be seen. The graphics display may also be run simultaneously with the simulation so that the flow patterns may be viewed. If problems are noticed, the user can modify several numerical parameters while a simulation is running. This is done by choosing "Waterflow parameters" in the pull-down menu "Input Edit" of SSIIM window. A dialogue box is displayed on the screen and the user can change the scheme for each variable, the relaxation factors, the algorithm for the pressure calculation and the condition of calculation for the updated water surface. These new numerical parameters can then be stored in a new Control file, choosing the option "Write Control.new" in the pull-down menu "Files" of SSIIM.

The user must be very careful when modifying the numerical parameters because such changes usually cause a large increase in the residuals and may lead to divergence. If alterations are made to the relaxation factors while the program is running then it is preferable to make small changes to the relaxation factors (e.g. a reduction of 0.1 or 0.05). Any change to the run parameters will cause a rise in the residuals but the solution usually settles down after 20 to 50 iterations. Note that a reduction in relaxation coefficient is not always the most appropriate course of action, since the failure to converge may result from an unsuitable choice of parameters or resolution as described above.

## A2.7 Graphics package provided with SSIIM

A graphics package is provided with SSIIM. Seven graphics modules can be invoked at any time during the calculation or afterwards. Here is a brief description of the capabilities of these modules:

- **Map :** plan view of the grid, velocity vectors, bar plots of all the variables.
- **Contour Map :** coloured contour lines of all the variables in a plan view.
- **Colour Map :** variables in colour and density patterns.
- **Longitudinal Profile :** grid, velocity vectors, vertical profile of all the variables.
- **Cross-Section :** grid, velocity vectors.
- **Verify Profile :** superimposition of numerical and experimental results at locations.
- **Animation :** particle movement in a plan view.

Note that an improved graphic package - Open GL was not available at HR at the time of these tests.

The available capabilities of the SSIIM graphics were too limited for our needs and thus another system - Rubens - was used to produce the majority of graphs for this report.



## A2.8 Rubens visualisation software

### A2.8.1 Summary

Rubens is a data visualisation package for displaying one or two dimensional data. This software was developed by E.D.F. (Electricite de France) for use with their finite element model Telemac. It runs under Unix and at HR it was used on a Sun Sparcstation. Rubens can read several formats of meshed data (such as finite difference and finite elements with triangular and quadrilateral elements). In addition, Rubens is able to visualise 1D or 2D experimental data in SCOP\_S or SCOP\_2D format. A useful capability of Rubens is that new variables can be derived from data at the same point. For instance, it is possible to visualise vectors [velocity = vecteur(Vx,Vy)] and vorticity [vorticity = rot(velocity)]. However Rubens is not able to calculate variables from data at several points. Thus depth averaged values were determined in the conversion software (ssiim\_conv) which is described below.

### A2.8.2 SSIIM to Rubens conversion

The transfer of data from SSIIM to Rubens comprises two parts: data transformation and formatting. The data transformation is performed by a C program (**ssiim\_conv**). This reads the result file (RESULT) and the output co-ordinates file (XCYC.LAS) from SSIIM and writes a temporary text file called **ssiim.dat**. The formatting is performed by a FORTRAN program (**ssiim\_leo**) which uses subroutines provided by E.D.F.. This writes a binary file in Leonard format suitable for input to Rubens. This file is called **leo.out**. The two programs are packaged in the script **sim2rub**. The process is shown in outline in Figure A-33.

Data transformation of both dimensionality and gridding is required because of the different design of SSIIM and Rubens. Rubens was designed to visualise 2-D unsteady flow, whereas the SSIIM results are 3-D steady flows. Thus, the time dimension in Rubens is used to describe one of the space dimensions in SSIIM. For example, when the results are to be displayed in cross-section, the time step in Rubens corresponds to the longitudinal direction in SSIIM. Note that this method assumes similarity in the direction being mapped to the time direction. Linear variations can be accommodated using scaling factors in Rubens. For this reason it was found most convenient to use a rectangular grid. Where this was not possible, the grid was aligned with the channel.

Grid transformation is required because the SSIIM values are cell-centred but Rubens is designed for a grid with values at the corner of the cells. To perform the transformation, the SSIIM co-ordinates defining the corners of each cell are averaged to determine the co-ordinates of the cell centres and additional nodes and values are created at the boundary of the flow domain so that the flow region displayed by Rubens is the same as that modelled in SSIIM. This averaging process causes some distortion of the grid where the grid spacing or the bed level is uneven.

It is often the case in open channel flow that the size of the flow domain is very different in each direction. This may be inconvenient for presentational purposes and thus an option is included in the transformation to stretch the vertical axis of the display.

### A2.8.3 Output from sim2rub.

The user can choose one of three views: plan view, cross-section view, longitudinal view

The variables that are created for each view are listed below:

- longitudinal velocity (Vx).
- transverse velocity (Vy).
- vertical velocity (Vz).



- pressure (P).
- turbulent kinetic energy (k).
- dissipation (epsilon).

In addition, the following variables are generated in plan view :

- bed level.
- surface level.
- depth-averaged longitudinal velocity ( $V_{x\_ave}$ ).
- depth-averaged transverse velocity ( $V_{y\_ave}$ ).

#### A2.8.4 How to use sim2rub and Rubens

- 1 - Copy the XCYC.LAS file and the RESULT file into a Unix directory created for a single test. It is not necessary to convert these files into a Unix format.
- 2 - Type sim2rub in the test directory where the XCYC.LAS file and the RESULT file are stored.
- 3 - Type the name of the files.
- 4 - Choose a view.
- 5 - Choose an exaggeration coefficient.

At the end of the conversion (which can last 5 minutes or more if the files are large), two output files are created: ssiim.dat and leo.out. The intermediate file ssiim.dat can be deleted but the leo.out file is now the input file for Rubens. For each view, a different leo.out file is created and from each file Rubens creates a separate project which is stored in a separate subdirectory. Experimental data from SCOP\_S or SCOP\_2D files are also held in separate project subdirectories. Results from different projects may be combined on the same graph; thus experimental results may be overlaid on numerical graphs. Also different views may be combined to create for example a cross-sectional view showing contours of streamwise velocity with secondary current vectors.





## **Appendix 3**

**Numerical experiments to optimise the use of SSIM**





---

## **Appendix 3      Numerical experiments to optimise the use of SSIIM**

---

In determining the optimum values for the parameters, a number of tests were conducted based on the results from the Hanover flume (see Table A3.1) and in the trapezoidal channel in the GP flume at HR (see Table A3.2). The numerical grids used in the tests on the Hanover flume (Test RAa) are shown in Figures A-4 and A-5. The numerical grid used in the trapezoidal channel is shown in Figure 9.1. This appendix describes the results from these tests which were used to determine capabilities of SSIIM outlined in Section 4.

The tests described were made throughout the project, but are presented here in the following order. The first issues considered relate only to the modelling method - for example the numerical scheme. The second set of issues relate to the numerical grid. Finally physical parameters are considered such as discharge and roughness.

### **A3.1 Numerical Scheme**

There are two numerical schemes available in SSIIM : POW - the first order power law scheme and SOU - the second order upwinding scheme. The technical description of these schemes is to be found in Section 4.5.

#### POW Scheme

The first test presented using the POW scheme is Test RAa-9. The results are shown in Figures A-10 and A-11. The length of the recirculation zone is indicated by the limit of the reverse flow region in Figure A-10. This shows a length of about 1.7m which does not compare well with the measured value of 2.88m. This discrepancy is also apparent in the lateral velocity profile at Section E. In addition, the strength of the recirculation zone at Section D is overpredicted. The relatively strong reverse flows in the numerical model are not seen in the experimental results.

The inaccuracy of this prediction is supported by the fact that significantly different results are obtained when the grid is refined in Test RAa-10 (Figures A-12 and A-13). Here the recirculation length is increased to 2.33m. However this is still not a good estimate of the recirculation length.

#### SOU Scheme

The results from using the SOU scheme (Test RAa-6) are shown in Figures A-6 and A-7. Here the recirculation length is increased to 2.78m. The predicted values fit the experimental data quite well in the recirculation zone. The shape of the velocity profile in the main flow at Section D is not as good. The overall improvement in the predictions indicate that this method would be acceptable as a predictive tool. However, later tests showed that this scheme may become unstable.

#### MIXED Scheme

After some experimentation, it was determined that the use of the SOU scheme for  $u$ ,  $v$  and  $w$  and the POW scheme for  $k$  and  $\epsilon$  improved stability while retaining the accuracy of the SOU scheme. This arrangement was termed the MIXED scheme. The results from the test (RAa-12) are shown in Figures A-17 and A-18. These can be seen to be very similar to the results from the SOU scheme shown in Figures A-6 and A-7. The improvement in the accuracy of the predictions is confirmed for the trapezoidal case, by comparing Test TA-1 Figure A-26 with Test TA-3 Figure A-27. The recirculation length is increased from 4.6m to 5.1m.

### **A3.2 Influence of block correction**

Block correction is a method for accelerating the convergence of the numerical scheme. Block correction can only be applied reliably to a variable which is calculated using the POW scheme. To see the influence of this option, five numerical tests were performed using the geometry and the flow conditions of the Hanover flume:



- RAa-8 : POW scheme with block correction on all the variables (Figures A-8 and A-9)
- RAa-9 : POW scheme and no block correction (Figures A-10 and A-11)
- RAa-12 : MIXED scheme and no block correction (Figures A-17 to A-19)
- RAa-13 : MIXED scheme and block correction on k and epsilon (Figure A-20)
- RAa-14 : MIXED scheme and block correction on p, k and epsilon (Figure A-21)

Comparison of the results from Tests RAa-8 and -6 show that the block correction option does not alter the accuracy of the results, but does reduce the overall computational time typically by 15%. The time required to perform one iteration is higher using block correction because of the additional calculations which are involved to average the correction. However, the number of iterations to reach the convergence is lower and the computational time is reduced. In later tests, the saved time was much greater. For example, in a unobstructed sinuous channel the time reduction was over 80%.

The comparison between the Tests RA-12 , -13 and -14 shows that when block correction is applied to the pressure equation the computational time is increased. The results for these tests shown in plan in Figures A-17, A-20 and A-21 show no noticeable difference. Consequently, it is advisable to select the block correction option only for k and epsilon. In some later tests, where there were several groynes, it was found that block correction could impair the stability of the scheme. Thus block correction was only used where the convergence of the scheme could be monitored.

### **A3.3 Influence of the number of sweeps**

In an attempt to reduce the computational time, we increased the number of sweeps of the turbulent kinetic energy and the dissipation rate (epsilon) because the decrease of their residuals was very slow. The number of sweeps is specified by option K4 in the Control file. The number of sweeps for k and e were increased from 1 in Test TA-4 to 4 in Test TA-5. As it can be observed in Figures A-28 and A-29, there is no difference between the solutions and the number of iterations was exactly the same. The option K4 is probably not yet implemented in the software. This option was not investigated further.

### **A3.4 Influence of the modification in the Control file on the residuals**

The residuals of a numerical scheme are a measure of how close the model is to convergence. At each node, the difference of the old and the new values is calculated, summed and normalised with reference to a characteristic flux at the inlet. The convergence criterion in SSIIM is that all the normalised residuals are less than  $10^{-3}$ . For steady convergence, a plot of the log of the residuals against number of iterations should be approximately linearly decreasing, see Figure A-1. However in some circumstances the solution oscillates and does not converge. Since the residuals are only recorded every 100 iterations, the oscillations may not be noticeable in the graph but the lack of convergence is readily seen in Figure A-2 between iterations 500 and 3500.

There are two ways of modifying the parameters in SSIIM:

- either save the results, stop SSIIM, edit the Control file and restart SSIIM reading the Result file.
- or open the window "Grid Editor" "waterflow Parameters" and change the parameters during the run.

Both of these options were tested in the run TA-2 and the log of the residuals was then plotted against a number of iterations. The model responded with a temporary increase in the residuals. (cf. Figure A-3 for the first option).

Obviously, low relaxation coefficients reduce the speed of convergence (see Appendix 2.6). However, sometimes it is necessary to use reduced relaxation co-efficients at the start of a run to prevent rapid



divergence. If low values are used at the beginning of a run, they can be increased during the run. In the same way, it is possible to change the scheme or the block correction option. But, as it can be seen on the Figure A-2, any change causes an abrupt jump in the residuals and this can lead to divergence. Therefore, the user must be very careful when modifying the parameters in the Control file because this sharp increase can immediately lead to a divergence of the computation. To avoid this problem, it is advisable to change the relation coefficients in steps of 0.05 or 0.1 and to wait about 100 iterations between changes so that the velocity field has time to stabilise.

### **A3.5 Influence of horizontal grid resolution**

While maintaining block correction from Test RAa-13 the grid resolution was doubled in the x and y directions, for Test RAa-16. The refined grid shown in Figure A-5 and the results are shown in Figures A-23 and A-24. Comparison with Test RAa-13 shows the influence of increasing the resolution in the MIXED scheme. It can be seen that there is a slight improvement in the predicted values in the recirculation zone at sections D and E. The width of the recirculation zone shown in Section D is over predicted. The vertical velocity profiles at points B3 and C3 are slightly improved and the flow direction at point C3 near the end of the recirculation zone is correct (see Figure A-24). However profile at point A3, near the groyne tip is not well predicted.

The slight improvement in accuracy obtained by using the refined grid resulted in a greatly increased run time. The run time was increased from 2 hours to 17½ hours.

Thus to obtain satisfactory results in an acceptable time the MIXED scheme was used with the relatively coarse grid used in Test RAa-13.

### **A3.6 Influence of the vertical grid resolution (number of layers)**

A good way of reducing the computational time would be to reduce the number of layers. Two tests, TA-3 and TA-4, were performed with respectively 12 and 3 layers. The results are shown in Figures A-27 and A-28. An additional test (TA-8) was added to determine the performance of a 2-D computation (see Figure A-32). The results are obviously different in the length of the recirculation zone but the velocities are roughly similar.

The recirculation lengths are estimated from the contour of zero mid-depth velocity in Figure A-27, A-28 and A-32. The recirculations lengths are estimated as 5.15m, 5.13m and 4.44m for the cases of 12 layer, 3 layer and 2D simulation.

It can be seen that the 2D simulation is inaccurate but in new situations it may be used to quickly determine the general pattern of flow and hence indicate where grid refinement is required. The run time for this simulation was 15 minutes. This compares favourably with 1.5 hours and approximately 8 hours for the case of 3 and 12 layers.

The results from the 3 layer and 12 layer models gave very similar results, but refinement near the bed is useful for determining potential scour. Also, vertical refinement is necessary for resolving the flow in the case of submerged groynes as can be seen in Figure 9.14.

Thus for consistency, the majority of the validation tests were conducted with 9 or 10 layers. However later examination of the vertical velocity distributions indicated that fewer layers would have been adequate in the majority of tests.



### A3.7 Influence of Water Surface Update

In common with many steady state 3D models, SSIIM uses a rigid lid approximation. Thus, energy losses or changes in velocity potential, result in changes in pressure rather than changes in water surface level. In some circumstances, this approximation leads to a significant error in water surface level and this may lead to errors in the velocity field, since the change in water level changes the flow area. The error is <sup>greater</sup> here at higher Froude numbers than those that apply in this test ( $Fr < 0.3$ ).

To overcome this problem, the numerical model can update the water surface to the level where the pressure is zero. This option was tested in Test RAa-11 which may be compared to RAa-9 in which the water surface is not updated. The results from Test RAa-11 are shown in Figures A-14 and A-15. There is no noticeable difference between these results and those obtained without water surface update (Figures A-11 and A-12). Since water surface update necessitates a change in the computational grid, this option significantly increases the time to convergence. The modified water surface may be obtained after convergence, using the expression

$$h_{\text{modified}} = h_{\text{backwater}} - \frac{P}{\rho g}$$

Later experimental measurements in a rectangular channel show that the predicted roller vortex upstream of the groyne is not observed. It had been thought that the water surface update might eliminate the roller vortex. However, as can be seen from Figure A-16, this is not the case.

### A3.8 Influence of the Reynolds number and of the Froude number

To see the influence of these two dimensionless numbers, the discharge of the Hanover flume was doubled in the Test RAa-15 to compare with the results of the Test RAa-13. To compare results, the figures representing the normalised X-velocity at 37½% from the bed are used. The results of the tests shown in Figures A-18 and A-22 are highly similar and the slight difference is due to the water slope which is different. The discharge is used to calculate the water slope using the Manning's equations and this affects the velocity field. Neither the Reynolds number nor the Froude number seem to alter the solution probably because the flow turbulence is not affected. This is consistent with the findings of Mayerle et al who state that contrary to expectations, the Froude number had little influence on the wave length.

		Test RAa-13	Test RAa-15
Discharge (m <sup>3</sup> /s)	Q	0.20	0.40
Area (m <sup>2</sup> )	A	0.575	0.575
Water depth (m)	h	0.23	0.23
Mean velocity (m/s)	$V_{\text{mean}} = Q/A$	0.348	0.696
Reynolds number	$Re = \frac{V_{\text{mean}} h}{\nu}$	61380	122760
Froude number	$Fr = \frac{V_{\text{mean}}}{\sqrt{gh}}$	0.232	0.464



Note  $v_{\text{water}} = 1.304 \cdot 10^{-6} \text{ m}^2 / \text{s}$

### A3.9 Influence of the Manning's n

The user can define a value of the Strickler coefficient  $M (= 1/n)$  for the whole channel (option W1 in the Control file) or specify the value of this coefficient in each section (option W5 in the Control file). To see the influence of the Manning's n on the computational solution, Tests TA-4 and TA-7 were conducted with a Manning's n of respectively  $1/50 = 0.02$  and  $1/60 = 0.001667$ . The configuration of the tests was the same as the experiment in the GP flume, a trapezoidal channel with one rectangular groyne. Results from these tests are shown in Figures A-28 and A-31. The difference is not really visible on this graph but, looking through both of the result files, the velocity is slightly less in Test TA-7 than in Test TA-4. For example, at test point 2, the X-velocity is  $-1.2\text{cm/s}$  for TA-4 and  $-1.17\text{cm/s}$  for the Test TA-7. The difference is only about 4%. This indicates that changes in bed roughness have little effect on the flow pattern.

### A3.10 Conclusions

The following conclusions are drawn from tests in prismatic channels with one or two groynes which create a recirculation zone.

1. The SOU scheme is recommended for the momentum equations since it improves accuracy and may reduce run times.
2. The POW scheme is recommended for the turbulence equations for greater stability.
3. The block correction scheme speeds the convergence of the k and epsilon equations particularly where there are long unobstructed regions of flow.
4. The horizontal grid should be refined in regions of highly varying flow, particularly at the groyne tip. This improves the accuracy of the solution both locally and downstream of the groyne..
5. The general level of refinement may need to be coarser than ideal in order to obtain acceptable run times.
6. A two dimensional model may be used for determining the general flow pattern but does not give accurate results.
7. The number of layers required in the 3D model depends on the particular circumstances. More layers are required where the geometry of the groyne causes three dimensional flow.
8. The water surface update has an insignificant effect on the results (although larger effects may be expected at high Froude numbers).
9. The normalised flow pattern was not altered by doubling the flow velocity. Further tests would be required to determine any significant influence of Reynolds number or Froude number.
10. Small changes in roughness have little effect on the normalised flow patterns.

**Table A3.1 Tests in rectangular channel to find the best tuning parameters**

run code	scheme	block correction	X	Y	Z	total	comp. time (minutes)	number of iterations	seconds/iteration	separation length $S_1$ (m)	recirculation length ratio $S_1/L$	comments
RAa-1	POW	no	41	20	10	8200	-	-	-			model length = 32.4 m
RAa-3	POW	no	41	20	10	8200	-	-	-			model length = 6 m
RAa-4	POW	no	49	39	10	19100	-	500	-			increased resolution
RAa-6	SOU	no	35	19	10	6650	172	517	19.96	2.84	11.36	Standard grid, SOU
RAa-8	POW	all	35	19	10	6650	123	338	21.83	1.79	7.16	POW and Block correction
RAa-9	POW	no	35	19	10	6650	133	390	20.46	1.79	7.16	POW
RAa-10	POW	no	70	38	10	26600	421	547	46.18	2.42	9.68	Finer grid
RAa-11	POW	no	35	19	10	6650	-	600	-	1.83	7.32	Surface update
RAa-12	MIXED	no	35	19	10	6650	137	349	23.55	2.84	11.36	Mixed scheme
RAa-13	MIXED	k, e	35	19	10	6650	120	349	20.63	2.84	11.36	Block correction K, e
RAa-14	MIXED	p, k, e	35	19	10	6650	123	338	21.83	2.84	11.36	Block correction P, k, e
RAa-15	MIXED	k, e	35	19	10	6650	120	352	20.45	2.75	11	double discharge
RAa-16	MIXED	k, e	70	38	10	26000	1050	713	88.36	3.16	12.64	Finer grid
										2.88	11.5	Experiment



**Table A3.2 Tests in trapezoidal channel to find best tuning parameters**

run code	scheme	block correction	X	Y	Z	total	comp. time (minutes)	number of iterations	seconds / iteration	separation length $S_L$ (m)	recirculation length ratio $S_L/L_c$	comments
TA-1	POW	no	54	29	12	18792	-	918	-	4.63	7.98	POW
TA-2	MIXED	no	54	29	12	18792	-	-	-	-	-	effects on residuals
TA-3	MIXED	no	54	29	12	18792	-	1200	-	5.21	9	SOU
TA-4	MIXED	no	54	29	3	4698	~ 90	306	17.65	5.14	8.6	3 layers
TA-5	MIXED	no	54	29	3	4698	~ 90	306	17.65	5.14	8.6	4 sweeps on k
TA-6	MIXED	no	54	29	3	4698	~ 90	306	17.65	5.14	8.6	4 sweeps on k, e
TA-7	MIXED	no	54	29	3	4698	~ 120	350	30.86	5.21	9.	N = 1/60
TA-8	MIXED	no	54	29	3	4698	-	-	-	4.5	7.76	2-D computation



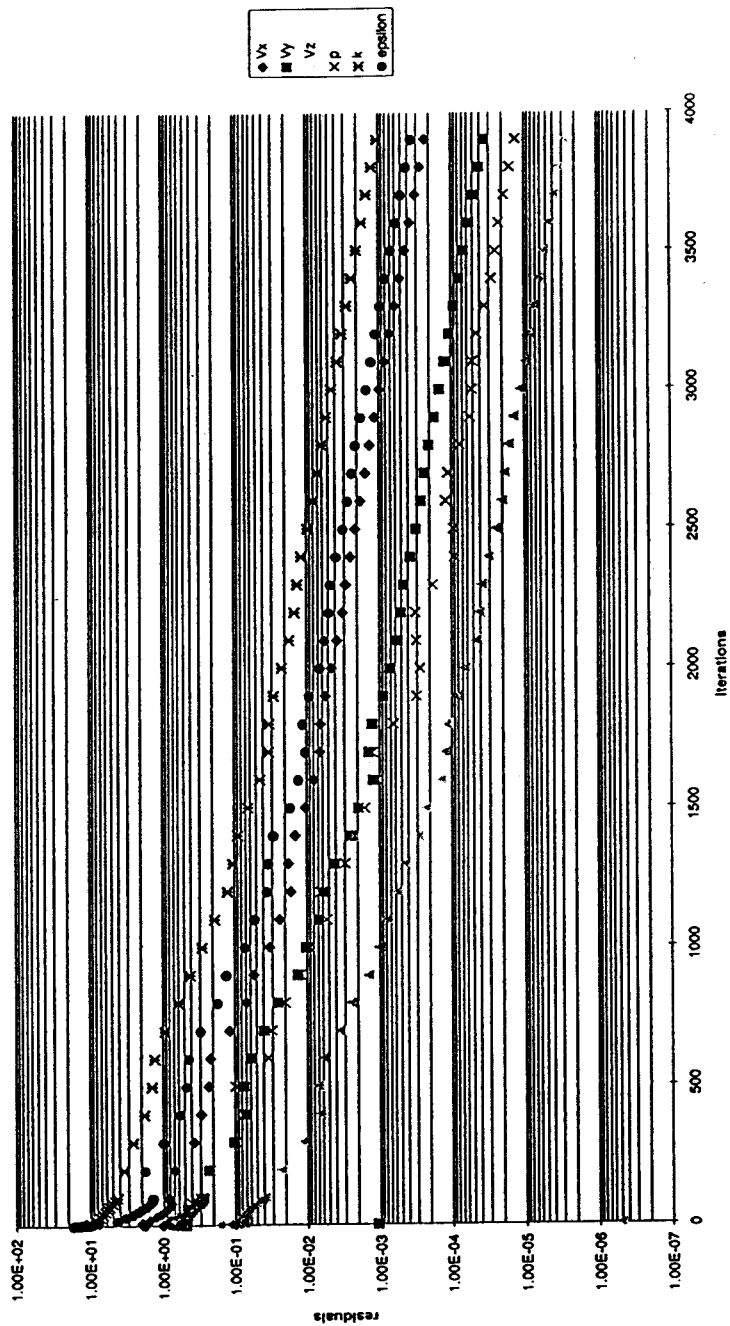


Figure A-1

Residuals plot: typical convergence slope

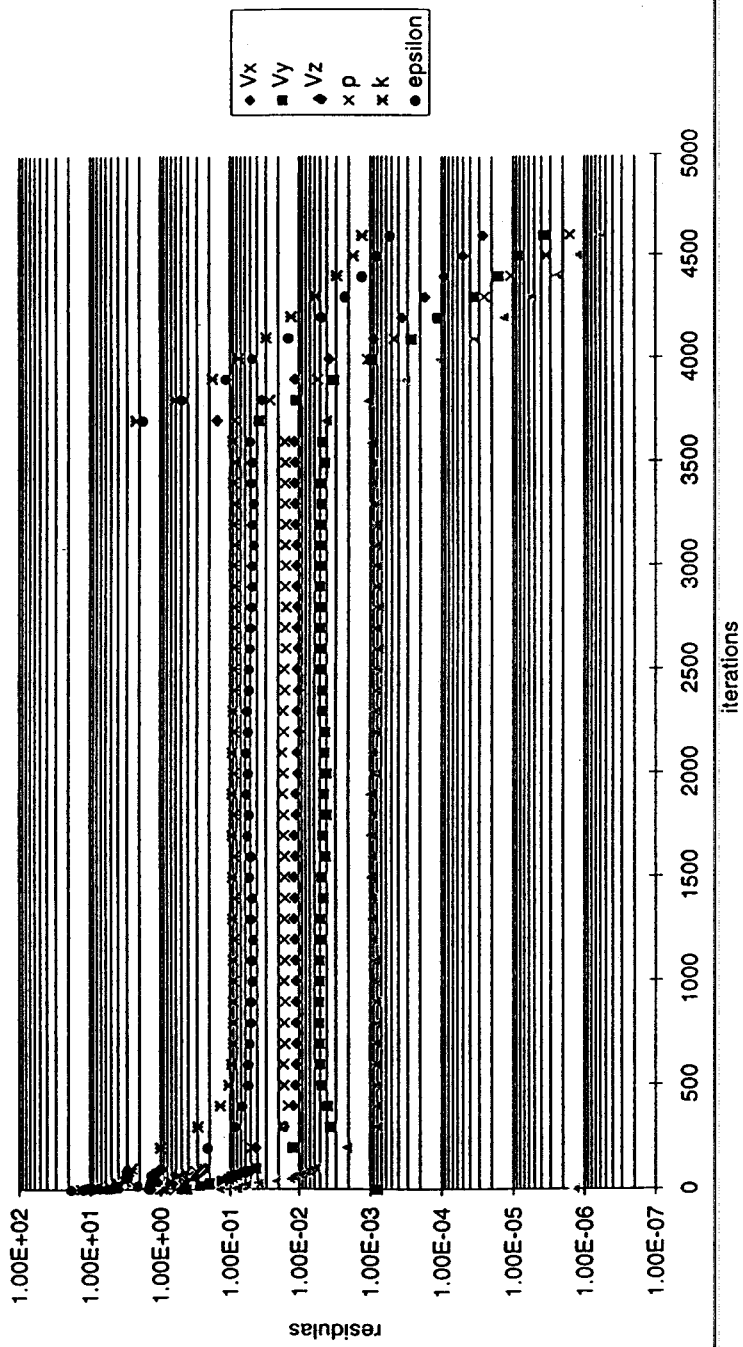


Figure A-2 Residuals plot: modification of parameters during the run



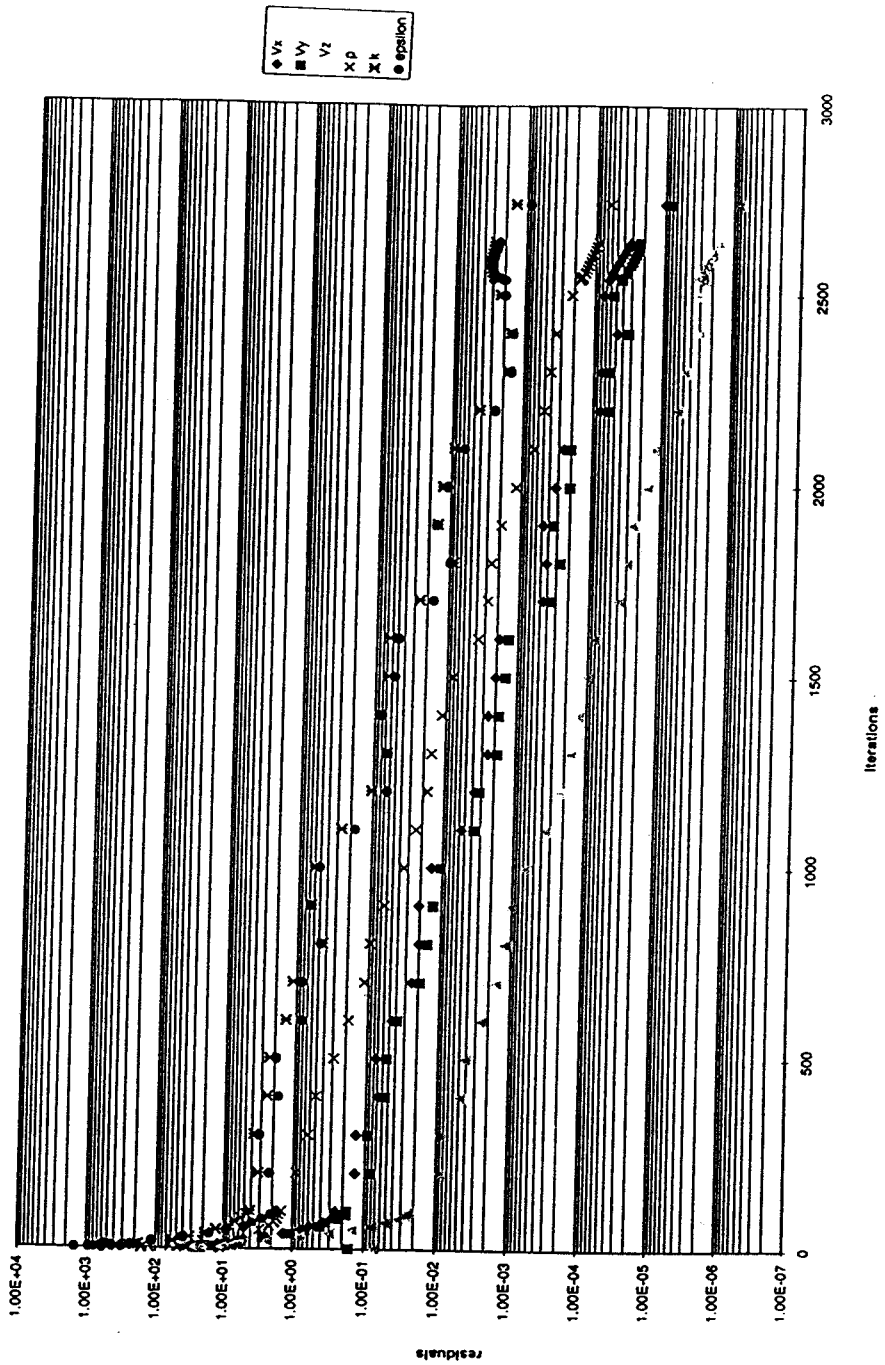
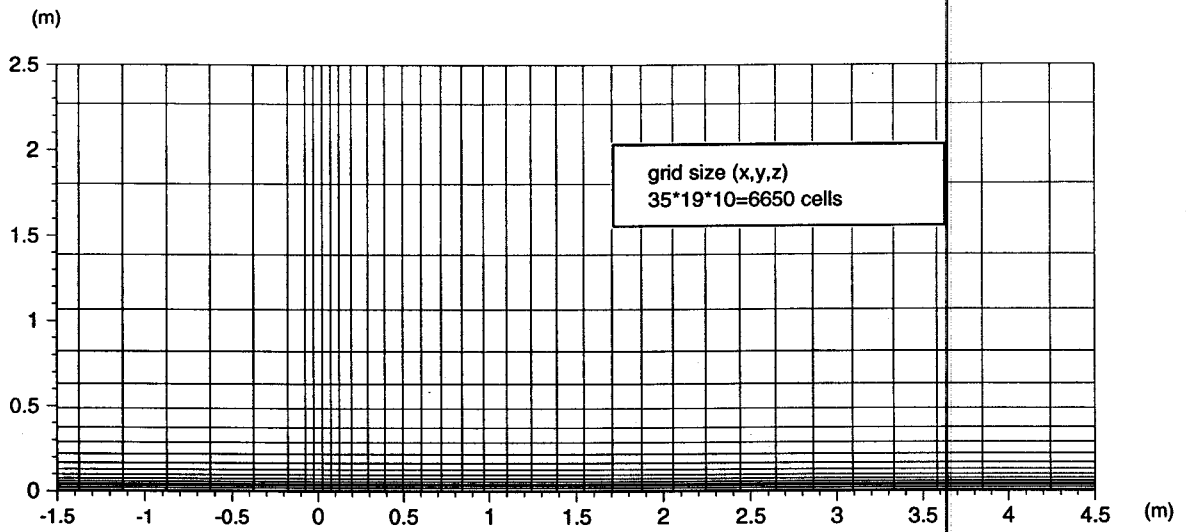
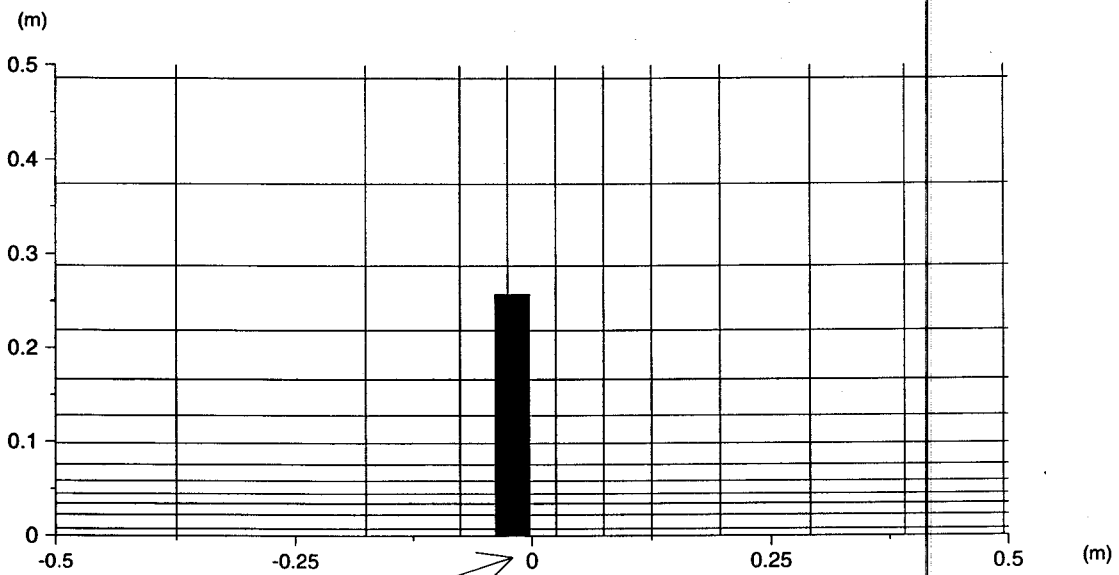


Figure A-3 Residuals plot: oscillations



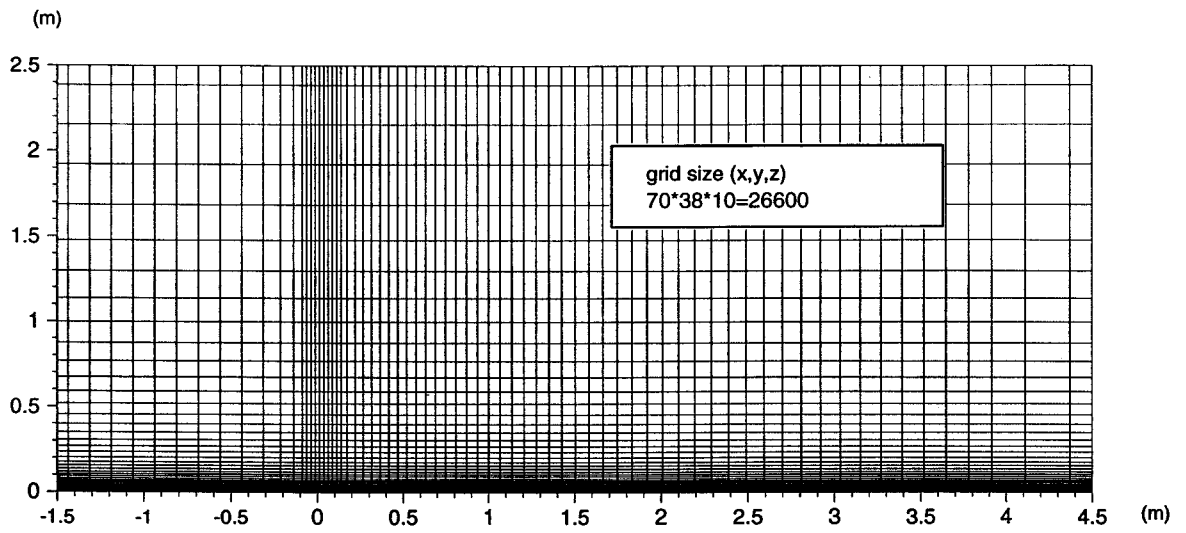
**Overall view**



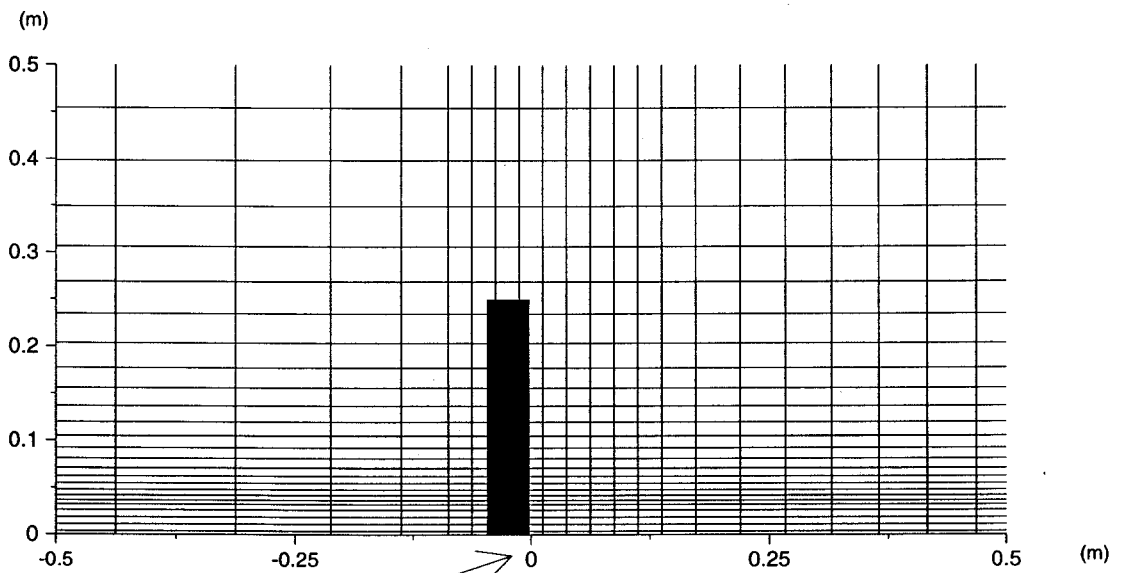
groyne  
yzx=250\*230\*5

**Zoom view**

**Figure A-4 Hanover flume - plan view of grid for tests RAa-6, -8, -9, -11, -12, -13, -14 and -15**



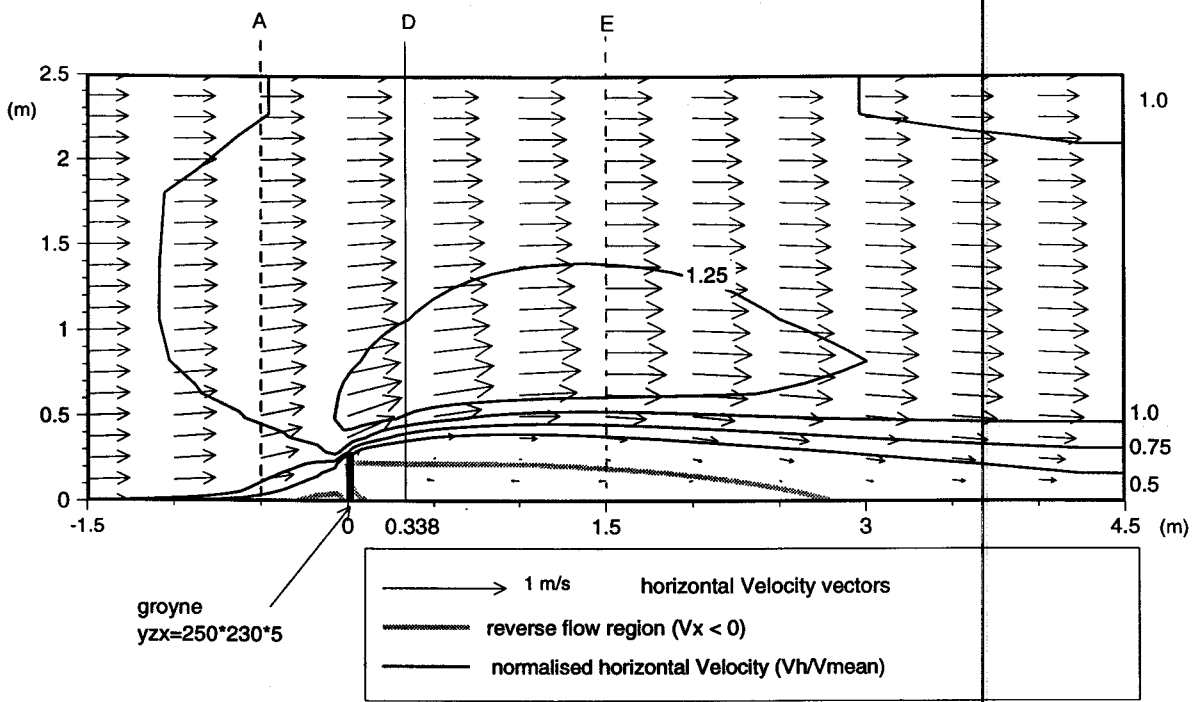
**Overall view**



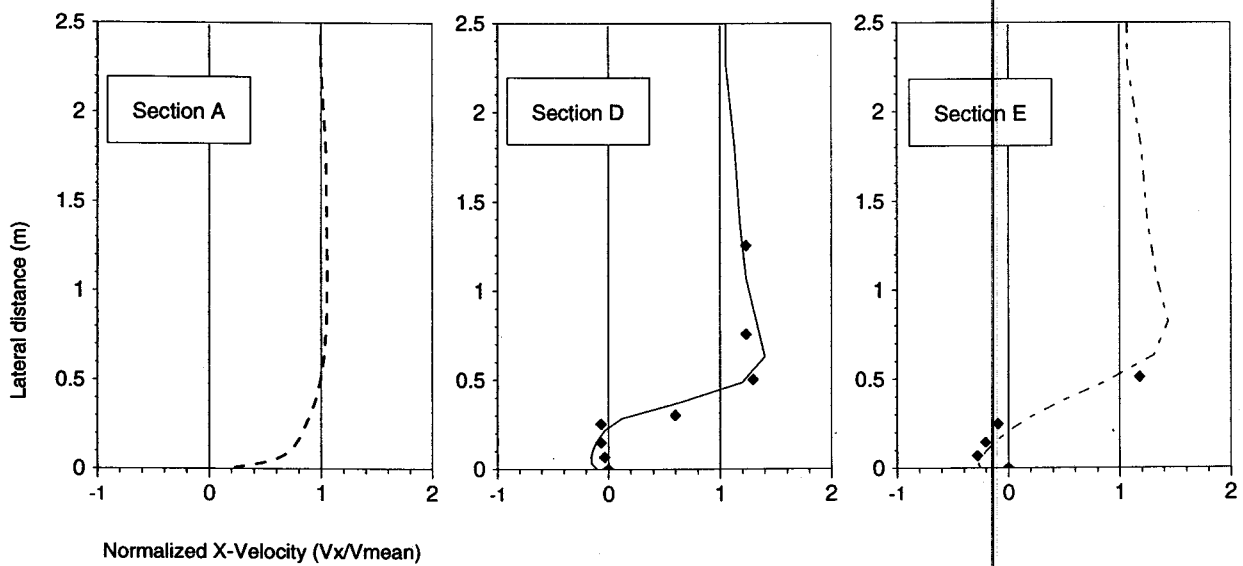
groyne  
yzx=250\*230\*5

**Zoom view**

**Figure A-5 Hanover flume - plan view of grid for tests RAa-10 and -16**



Velocity vectors and contours at 37.5% from the bed



Normalized X-Velocity profiles at 37.5% from the bed

Figure A-6 Test RAa-6 Hanover flume - one groyne - SOU scheme  
10 layers - No block correction

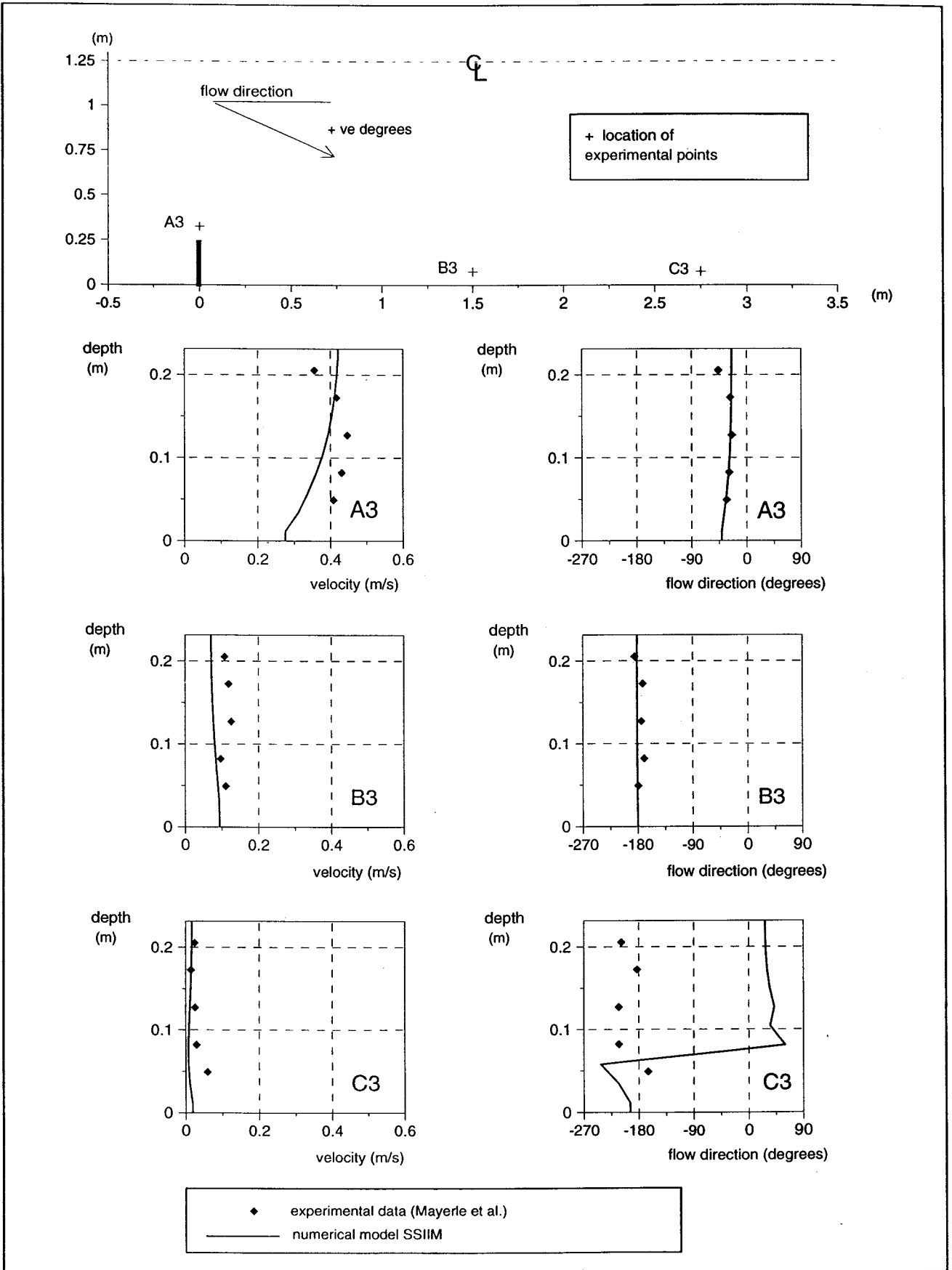
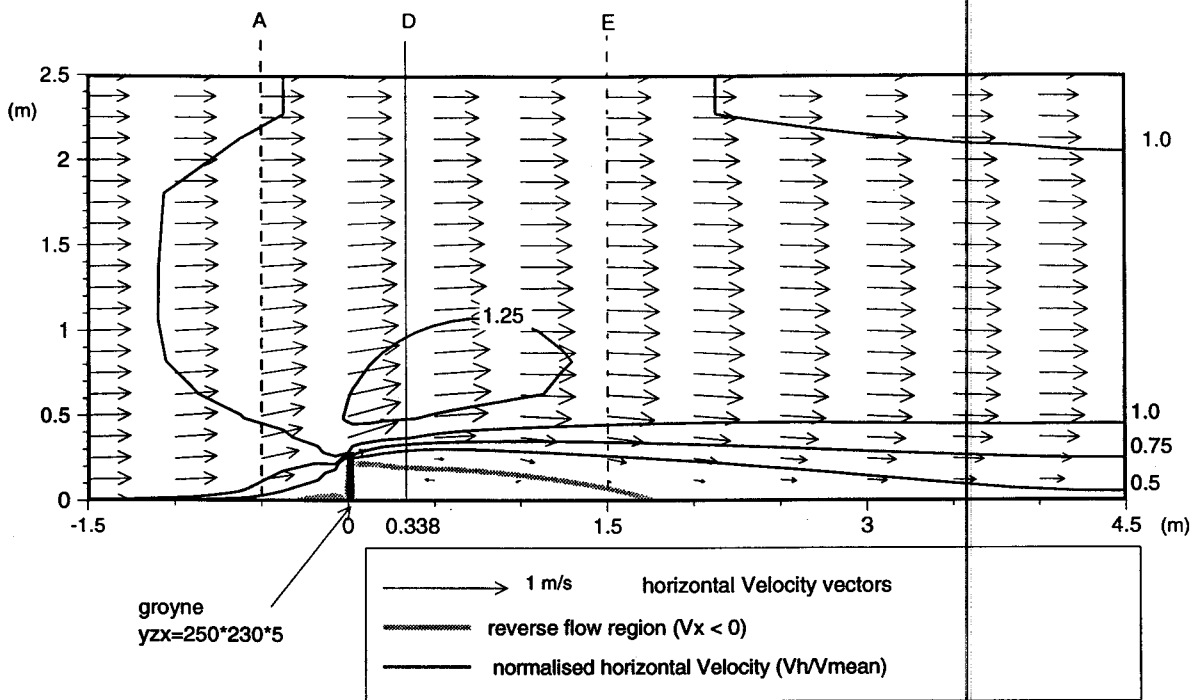
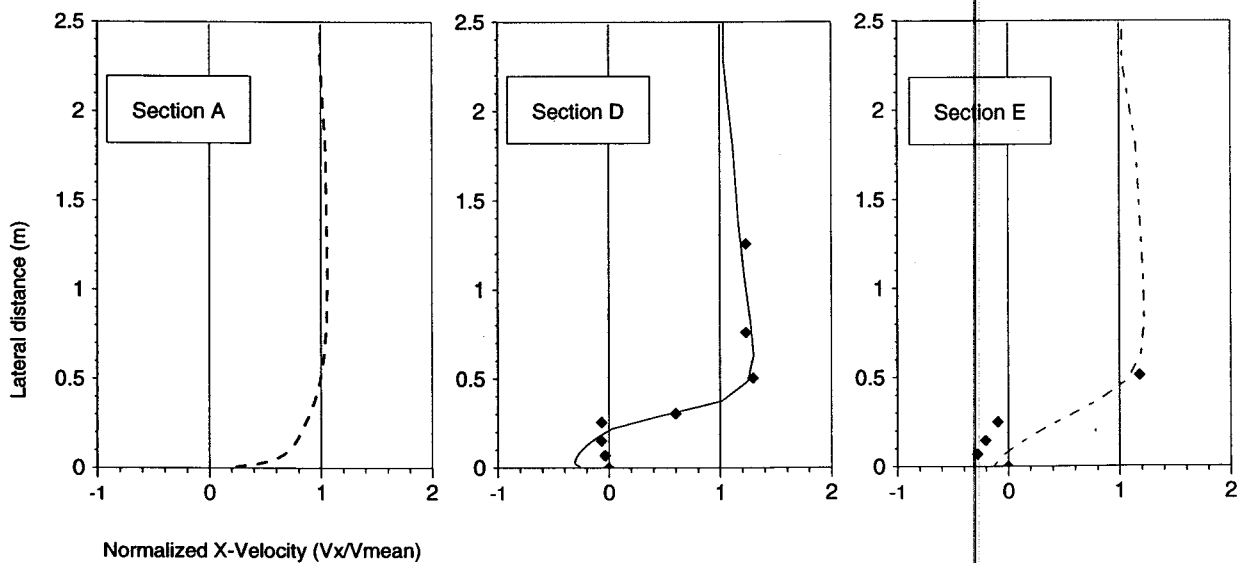


**Figure A-7 Test RAa-6 Hanover flume - one groyne - SOU scheme 10 layers - No block correction**



Velocity vectors and contours at 37.5% from the bed



Normalized X-Velocity profiles at 37.5% from the bed

Figure A-8 Test RAa-8 Hanover flume - one groyne - POW scheme  
10 layers - Block correction on u, v, w, p, k and epsilon

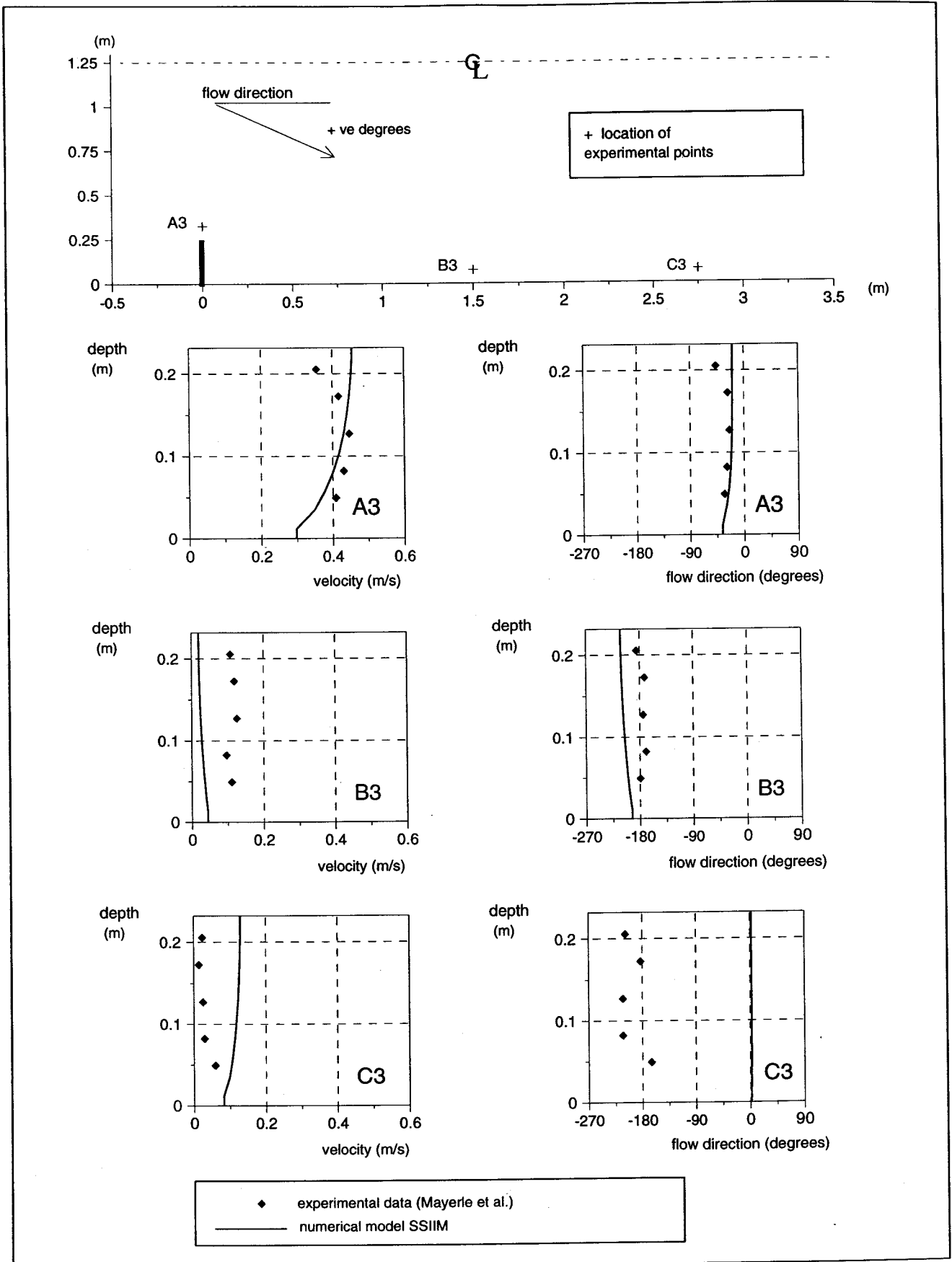
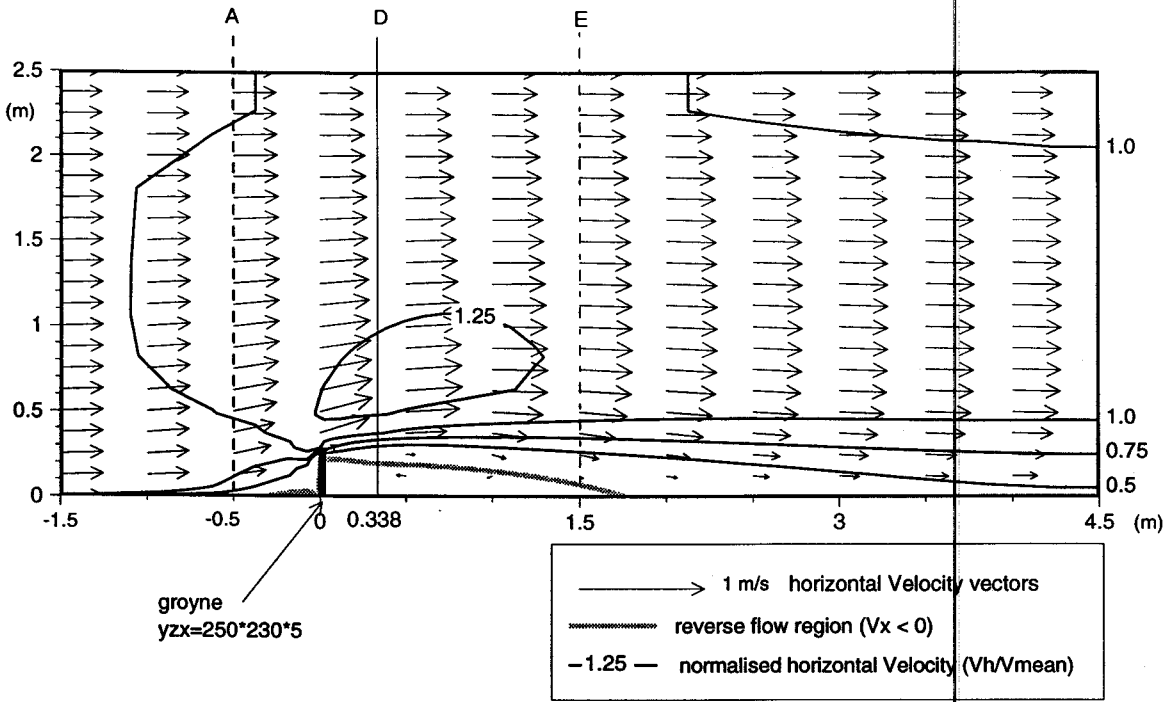
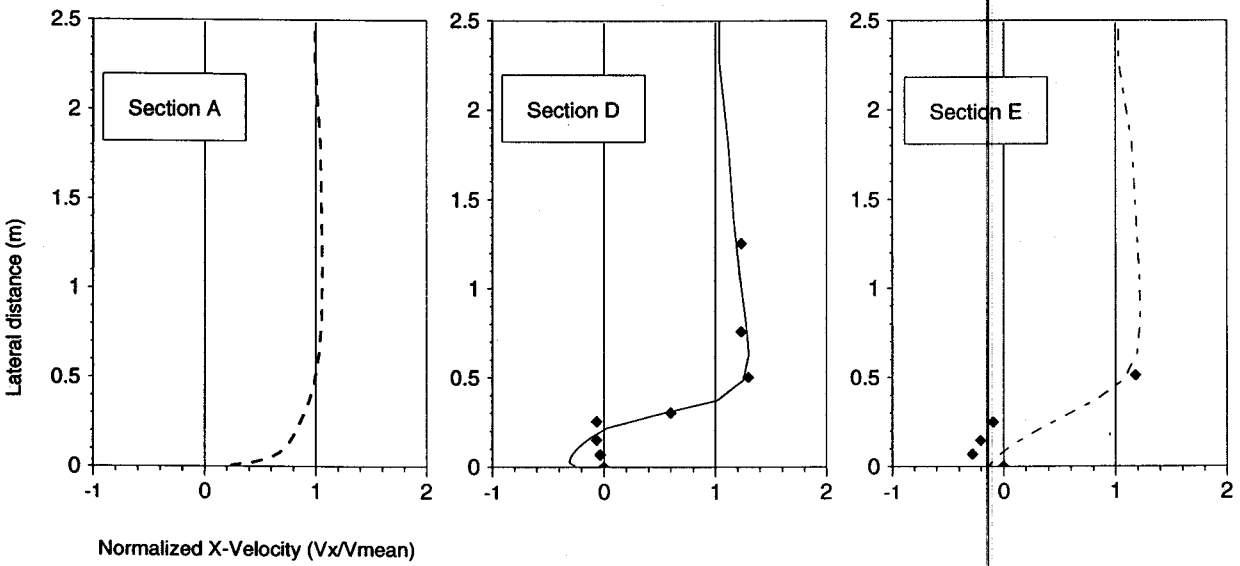


**Figure A-9 Test RAa-8 Hanover flume - one groyne - POW scheme 9 layers - Block correction on u, v, w, p, k and epsilon**



Velocity vectors and contours at 37.5% from the bed



Normalized X-Velocity profiles at 37.5% from the bed

Figure A-10 Test RAa-9 Hanover flume - one groyne - POW scheme  
10 layers - No block correction

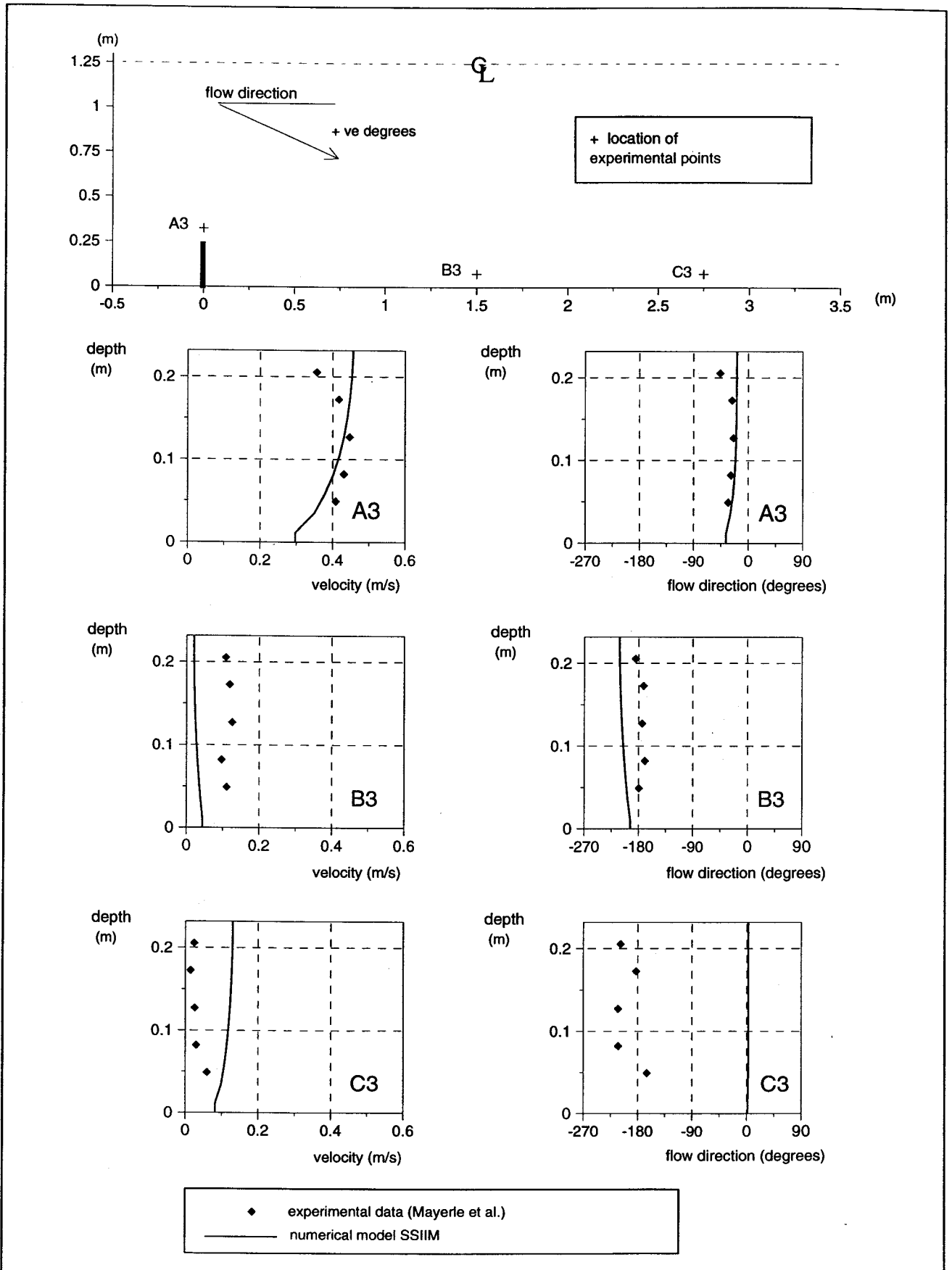


**Figure A-11 Test RAA-9 Hanover flume - one groyne - POW scheme 10 layers - No block correction**

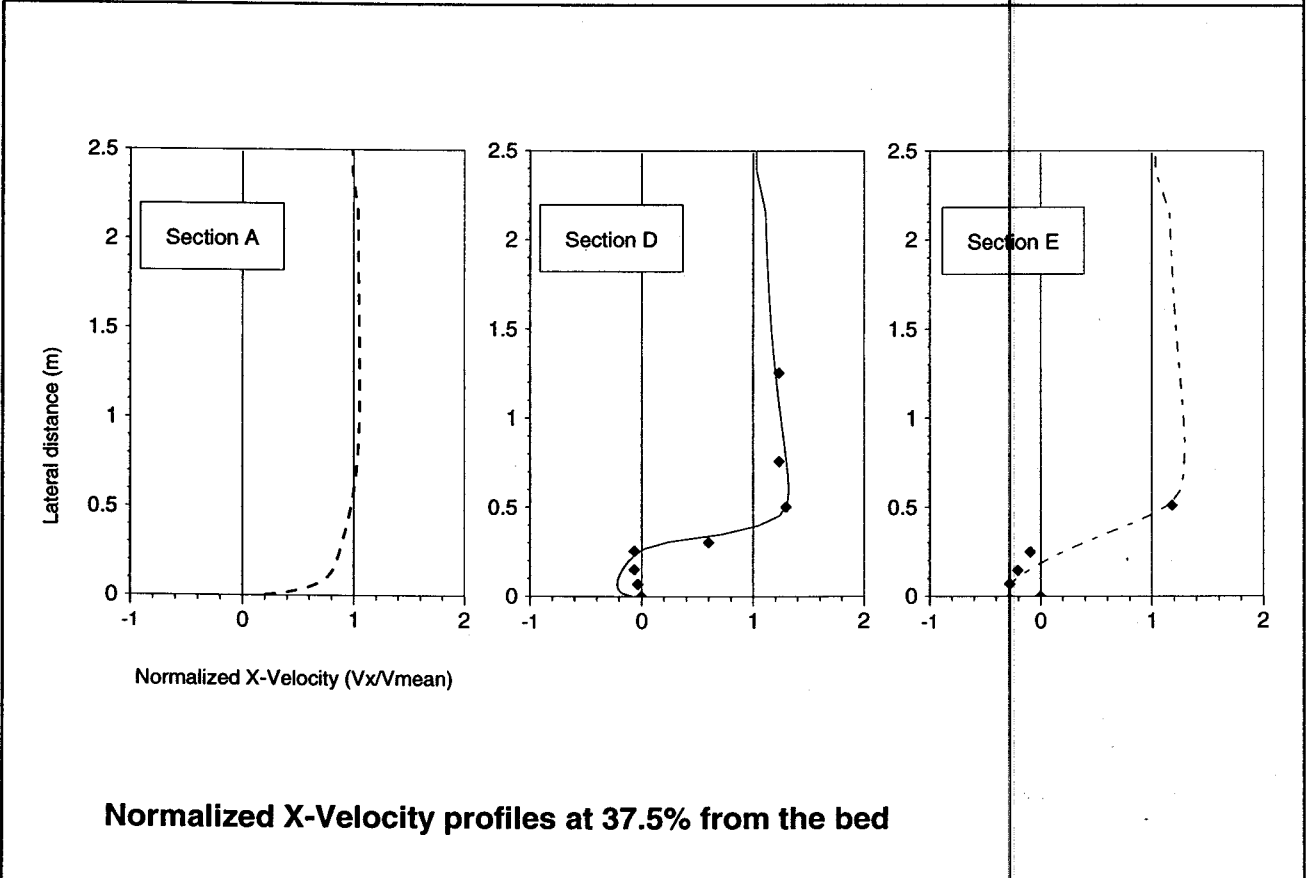
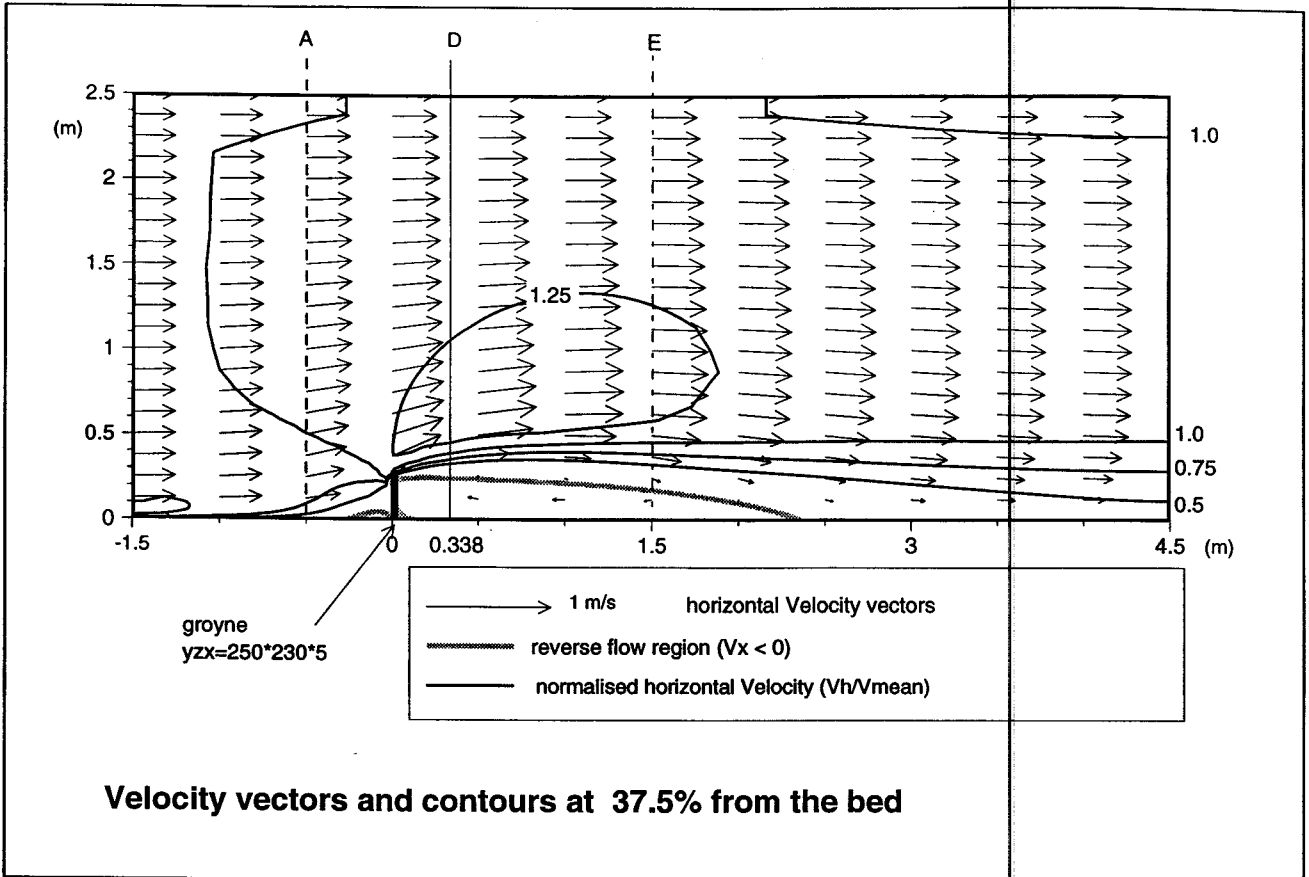
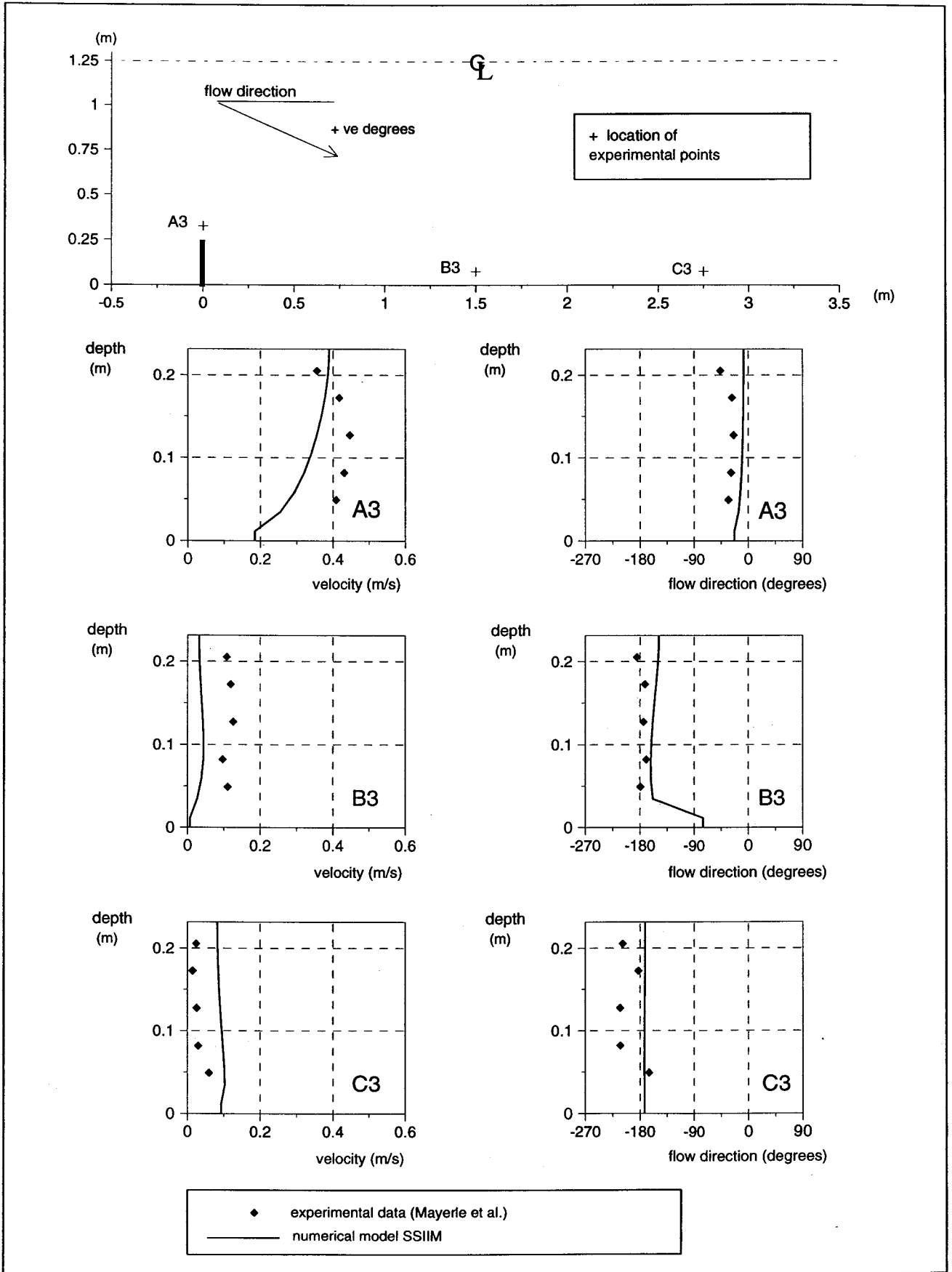
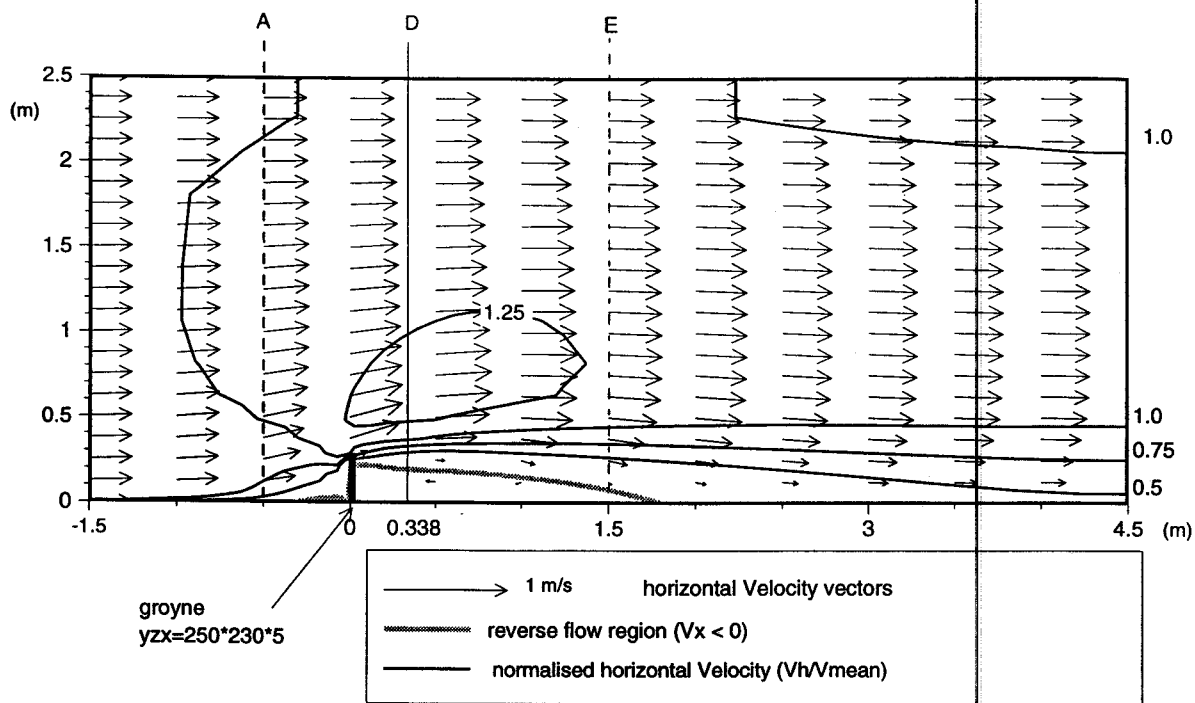


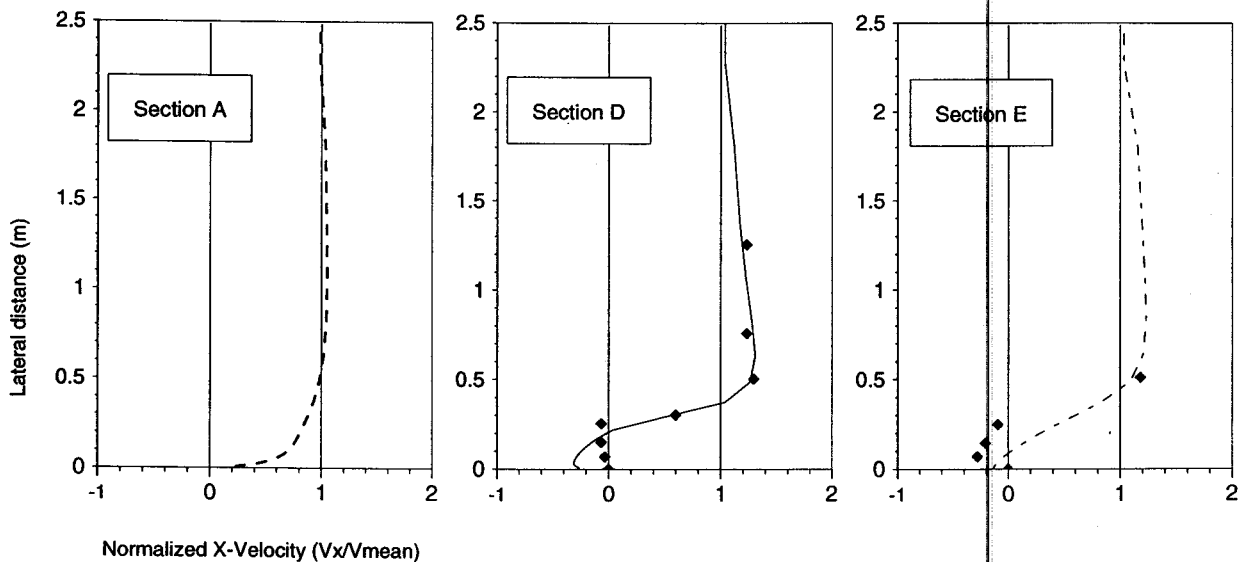
Figure A-12 Test RAa-10 Hanover flume - one groyne - POW scheme  
10 layers - No block correction - finer grid



**Figure A-13 Test RAA-10 Hanover flume - one groyne - POW scheme 10 layers - No block correction - finer grid**



Velocity vectors and contours at 37.5% from the bed



Normalized X-Velocity profiles at 37.5% from the bed

Figure A-14 Test RAa-11 Hanover flume - one groyne - POW scheme  
10 layers - No block correction - surface updated

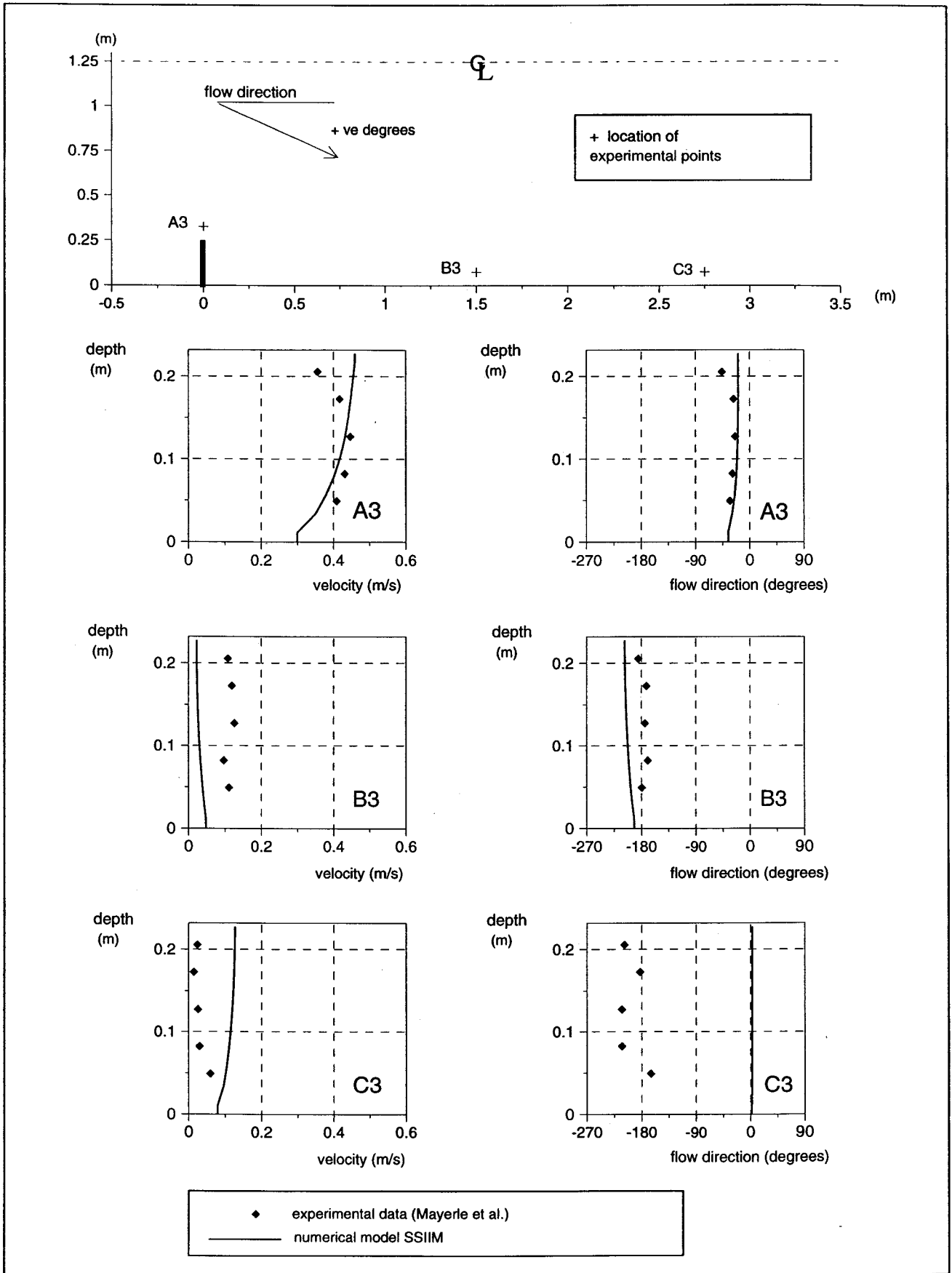


**Figure A-15 Test RAA-11 Hanover flume - one groyne - POW scheme  
10 layers - No block correction - surface updated**

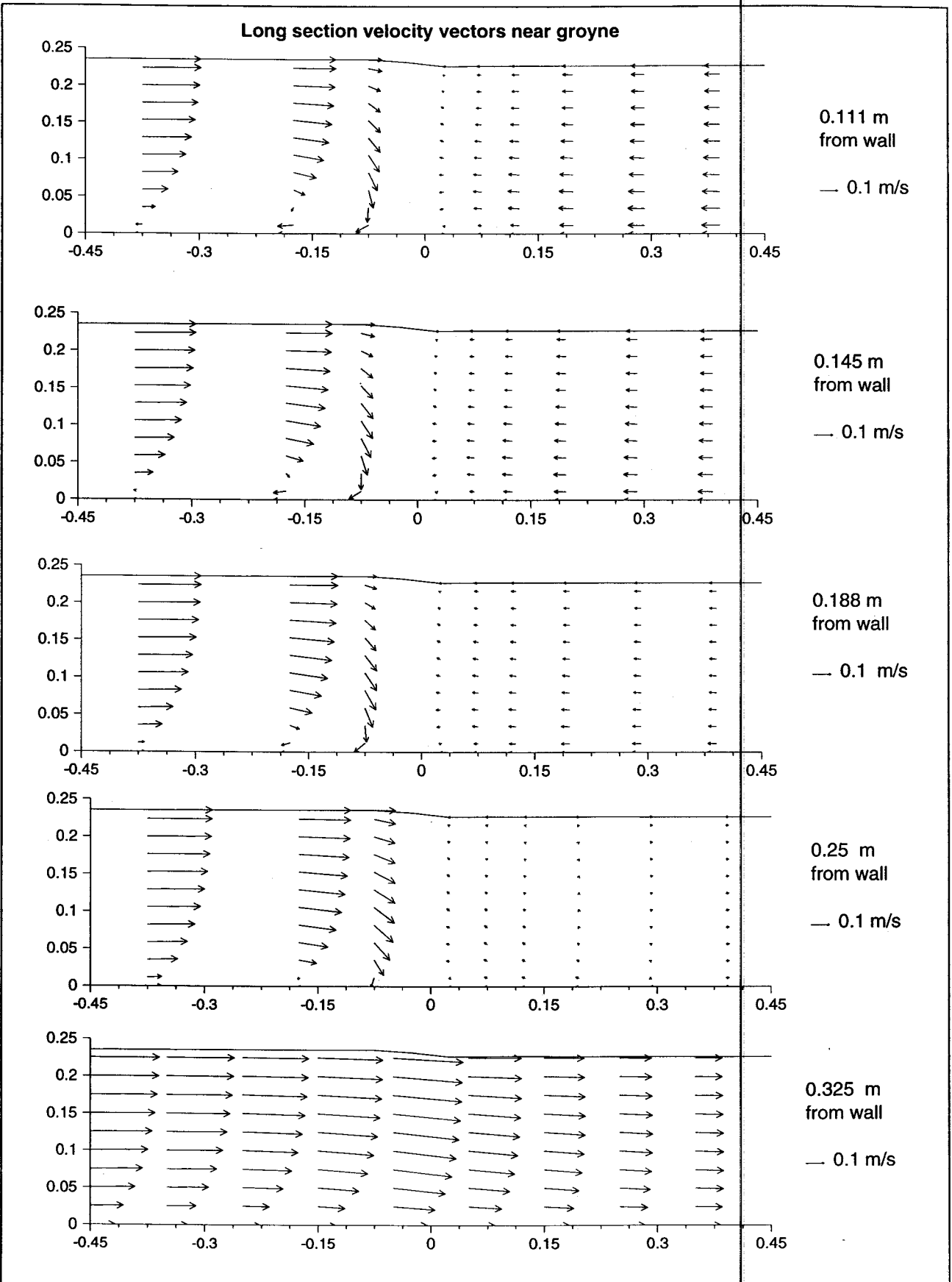


**Figure A-16 Test RAa-11 - Rectangular groyne in rectangular flume  
Hanover flume - water surface upated**

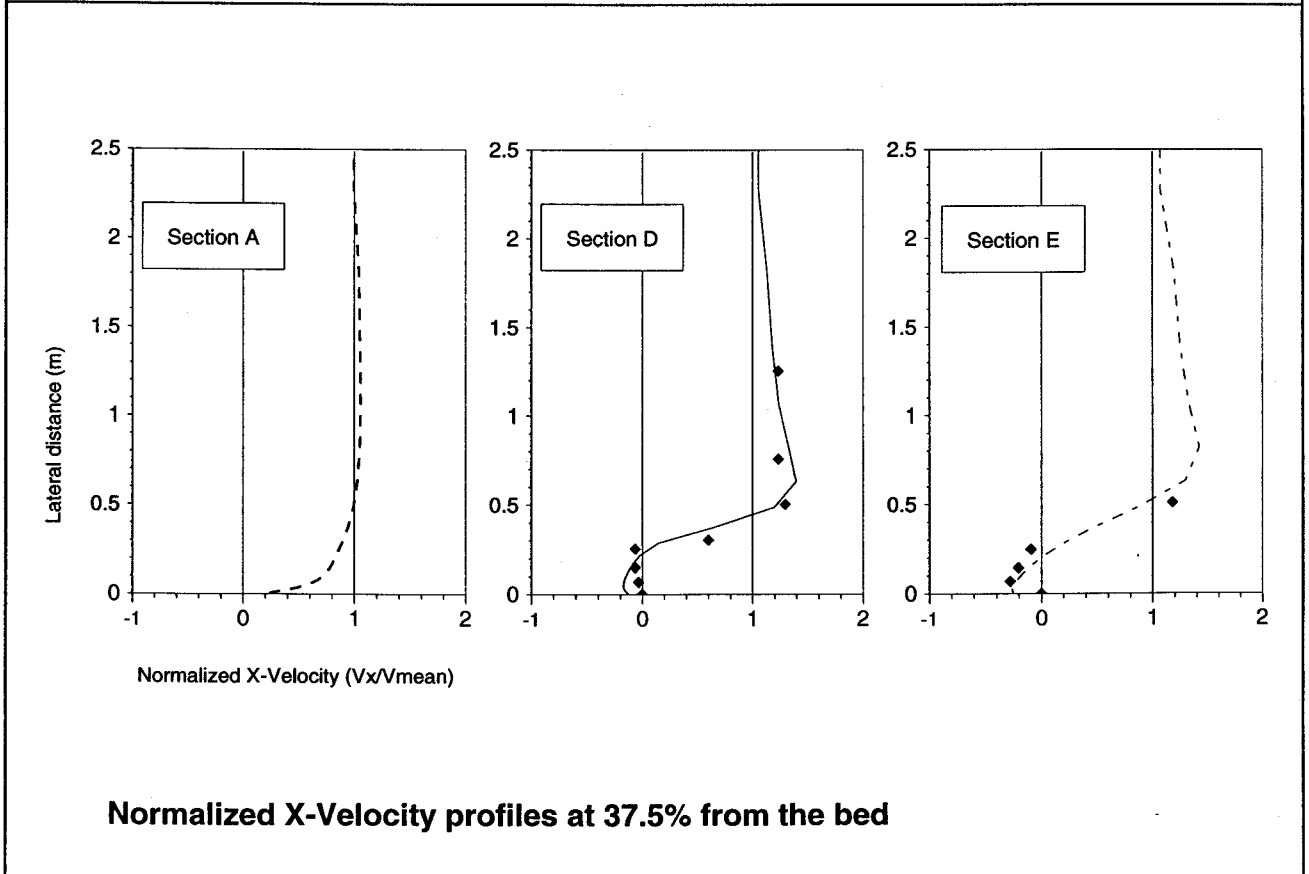
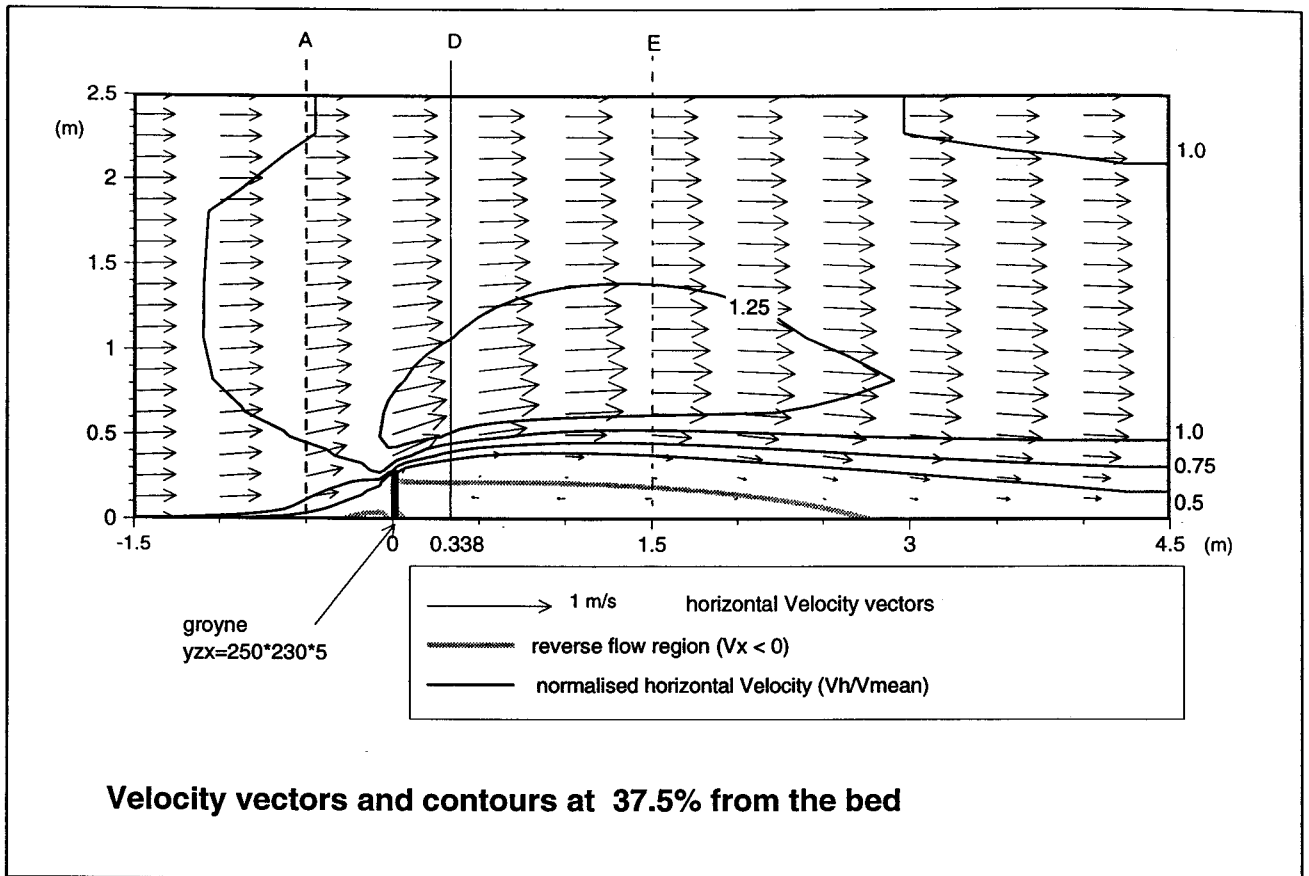


**Figure A-17 Test RAa-12 Hanover flume - one groyne - MIXED scheme  
10 layers - No block correction**

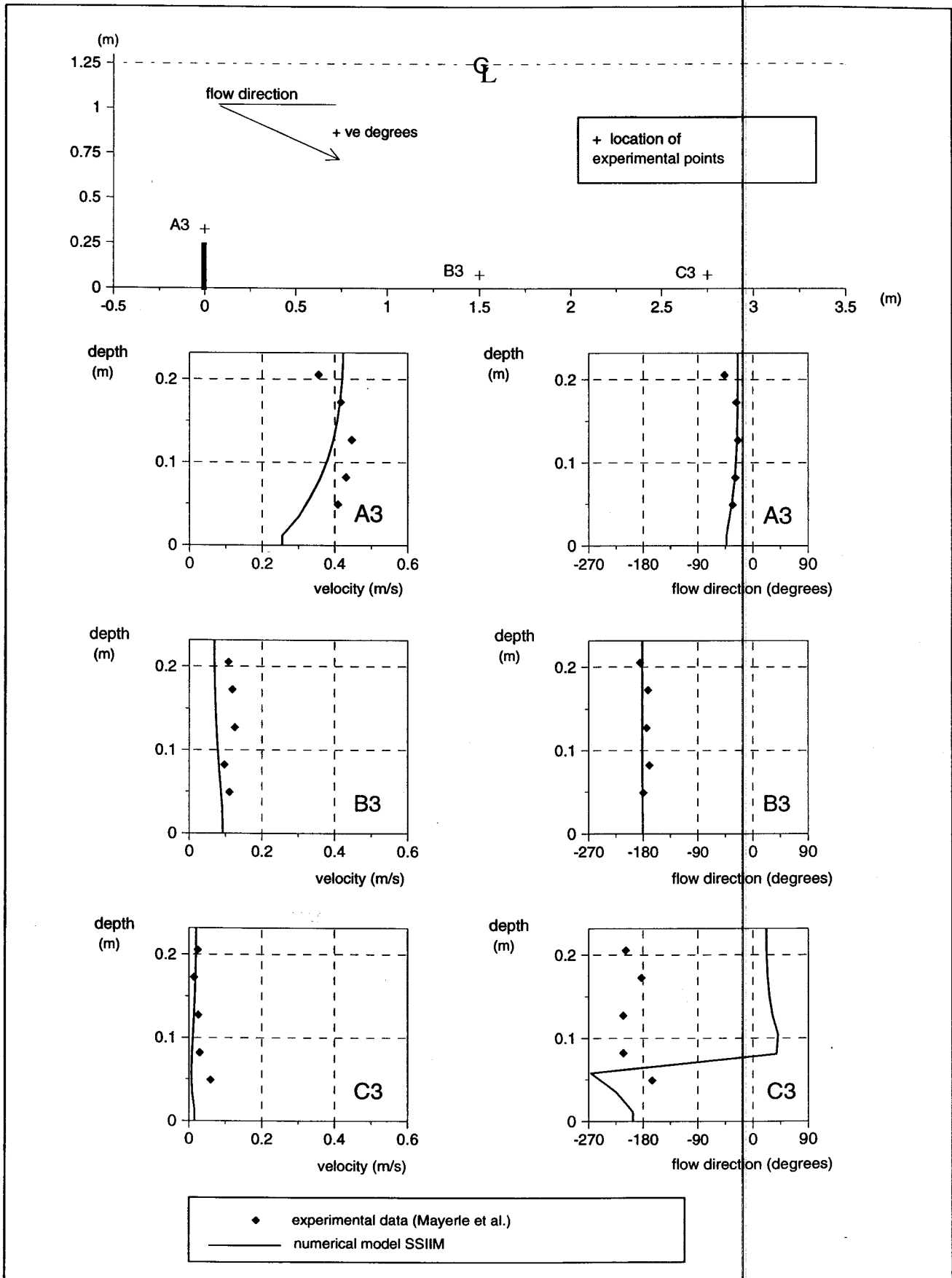


**Figure A-18 Test RAa-12 Hanover flume - one groyne - MIXED scheme  
10 layers - No block correction**

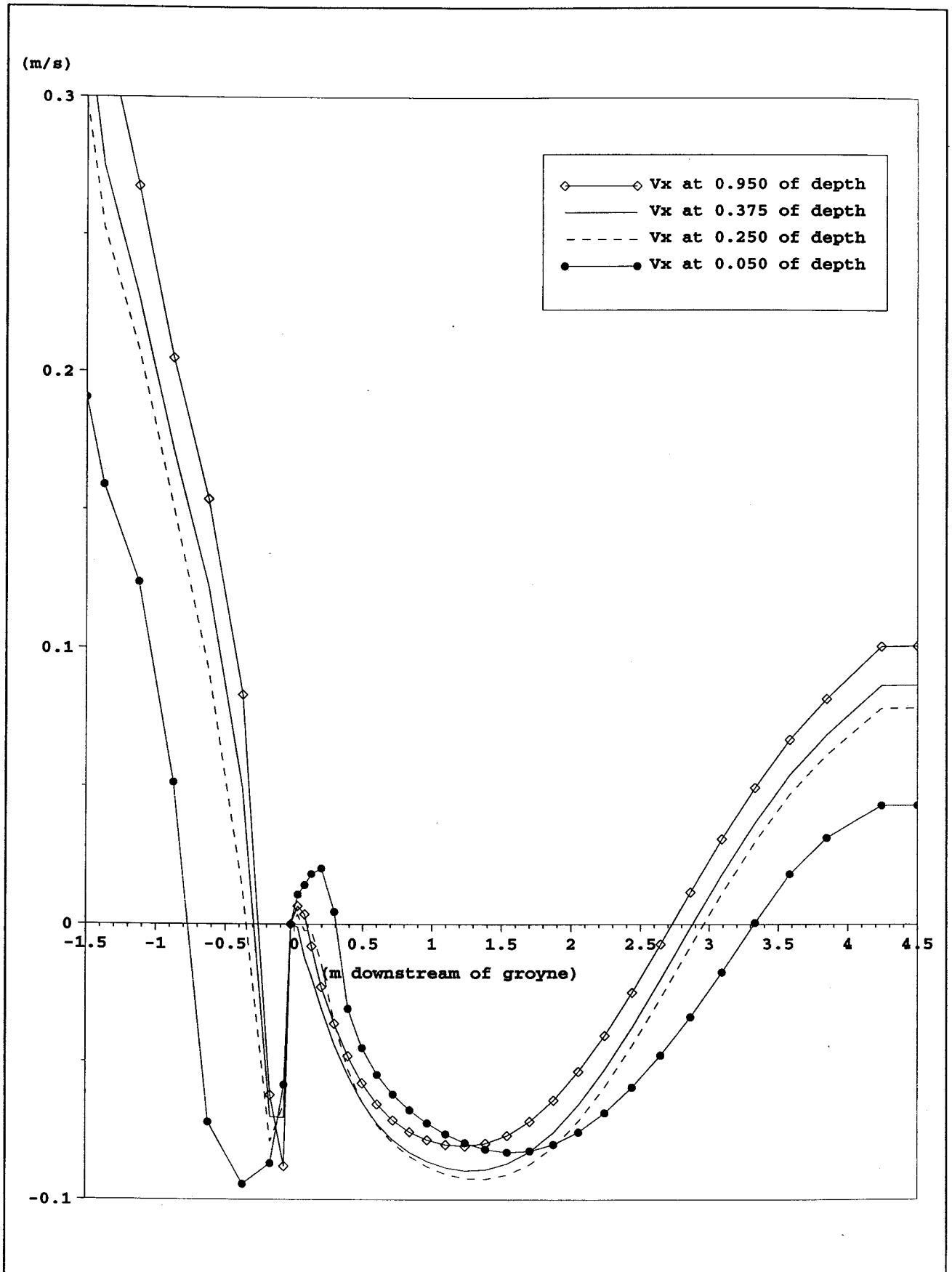
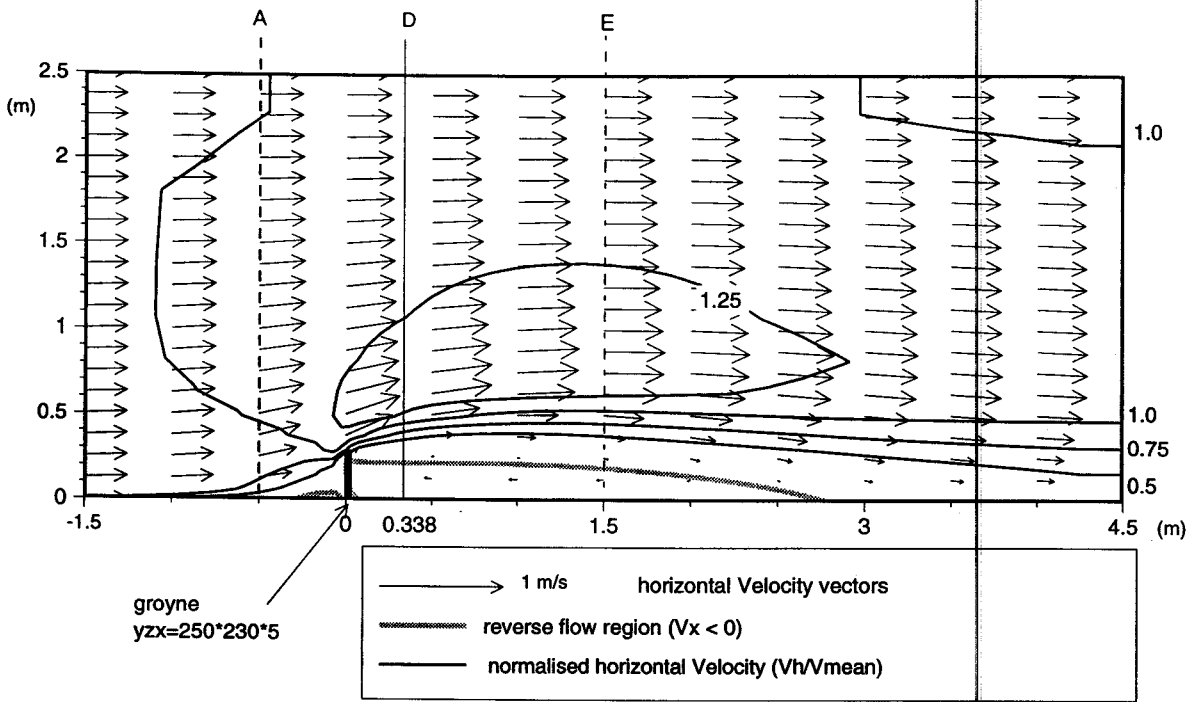
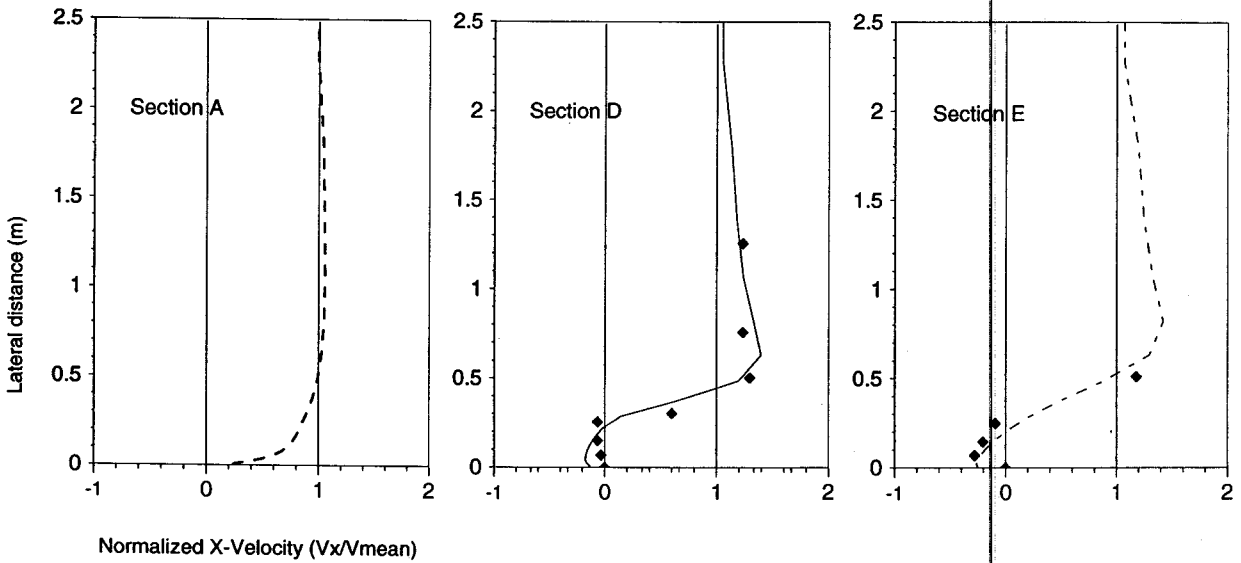


**Figure A-19 Test RAa-12 Hanover flume - one groyne - MIXED scheme  
Long section of longitudinal velocity close to wall**



Velocity vectors and contours at 37.5% from the bed



Normalized X-Velocity profiles at 37.5% from the bed

Figure A-20 Test RAa-13 Hanover flume - one groyne - MIXED scheme  
10 layers - Block correction on k and epsilon

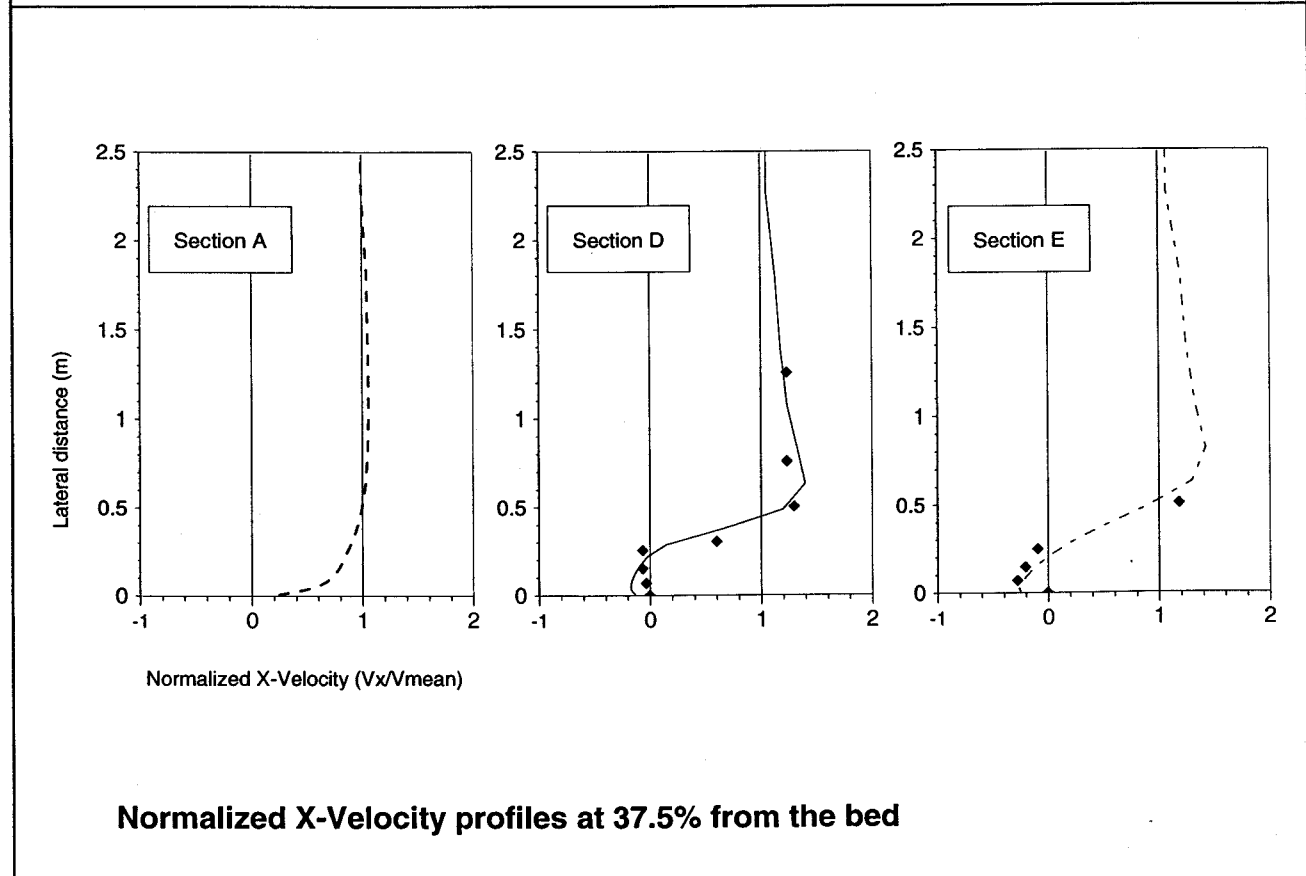
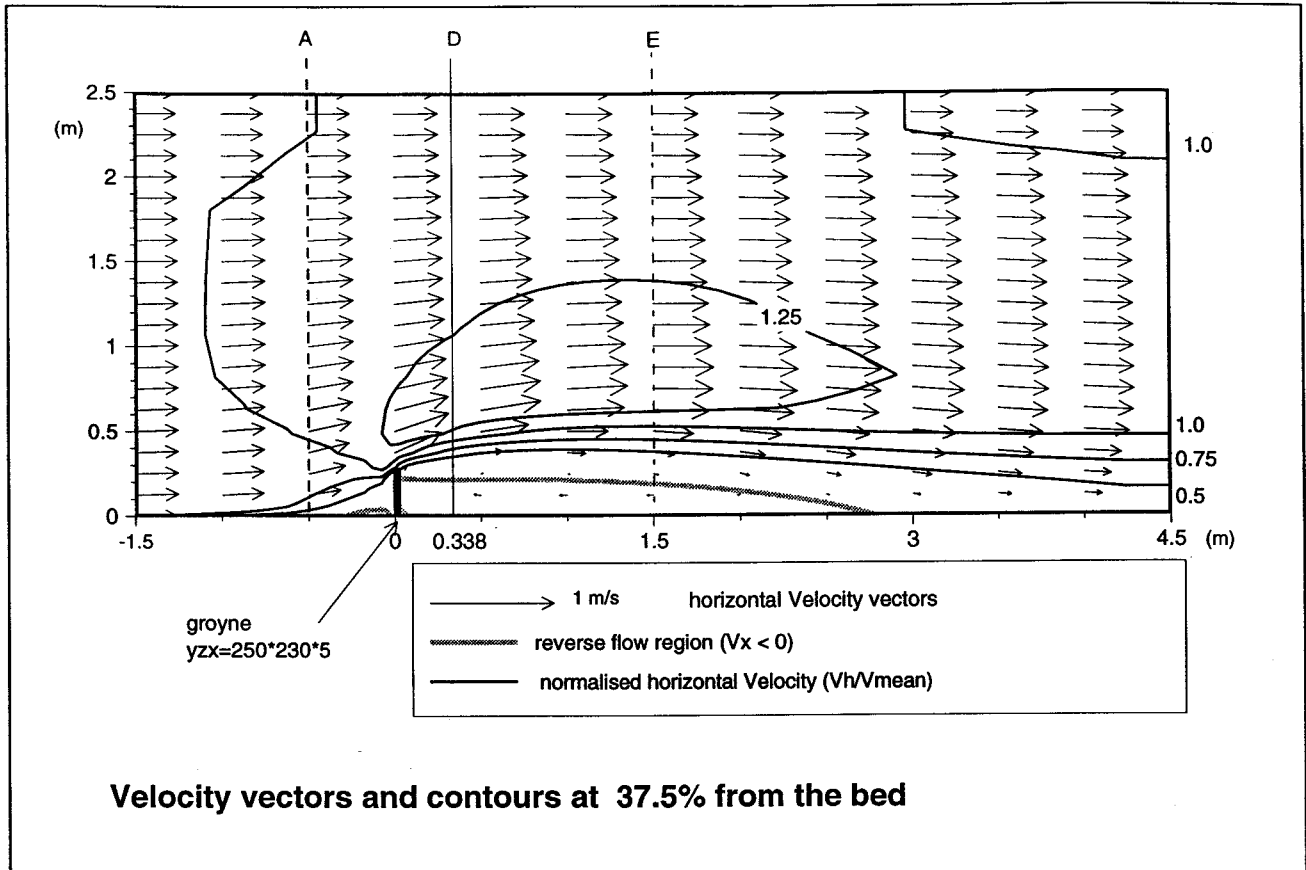
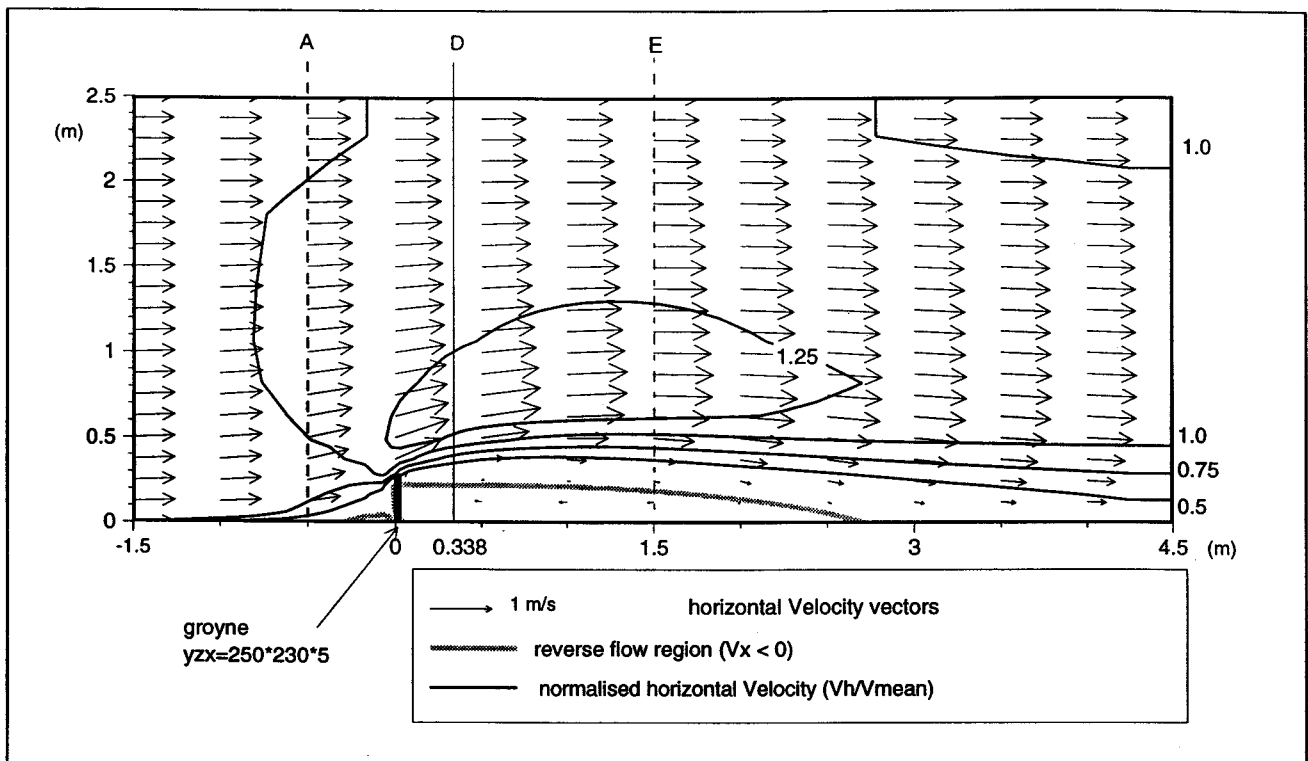
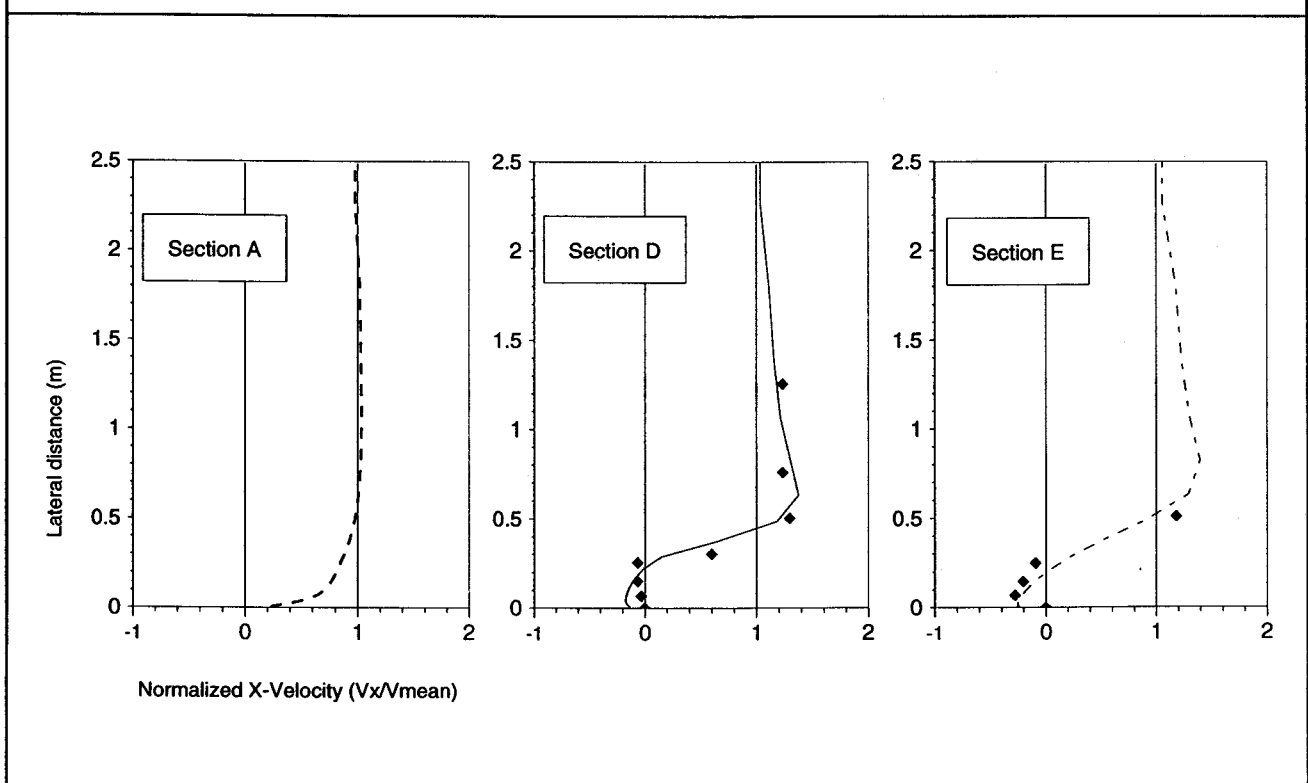


Figure A-21 Test RAa-14 Hanover flume - one groyne - MIXED scheme  
10 layers - Block correction on p, k and epsilon



Velocity vectors and contours at 37.5% from the bed



Normalized X-Velocity profiles at 37.5% from the bed

Figure A-22 Test RAa-15 Hanover flume - one groyne - MIXED scheme  
10 layers - Block correction on k and epsilon - double discharge

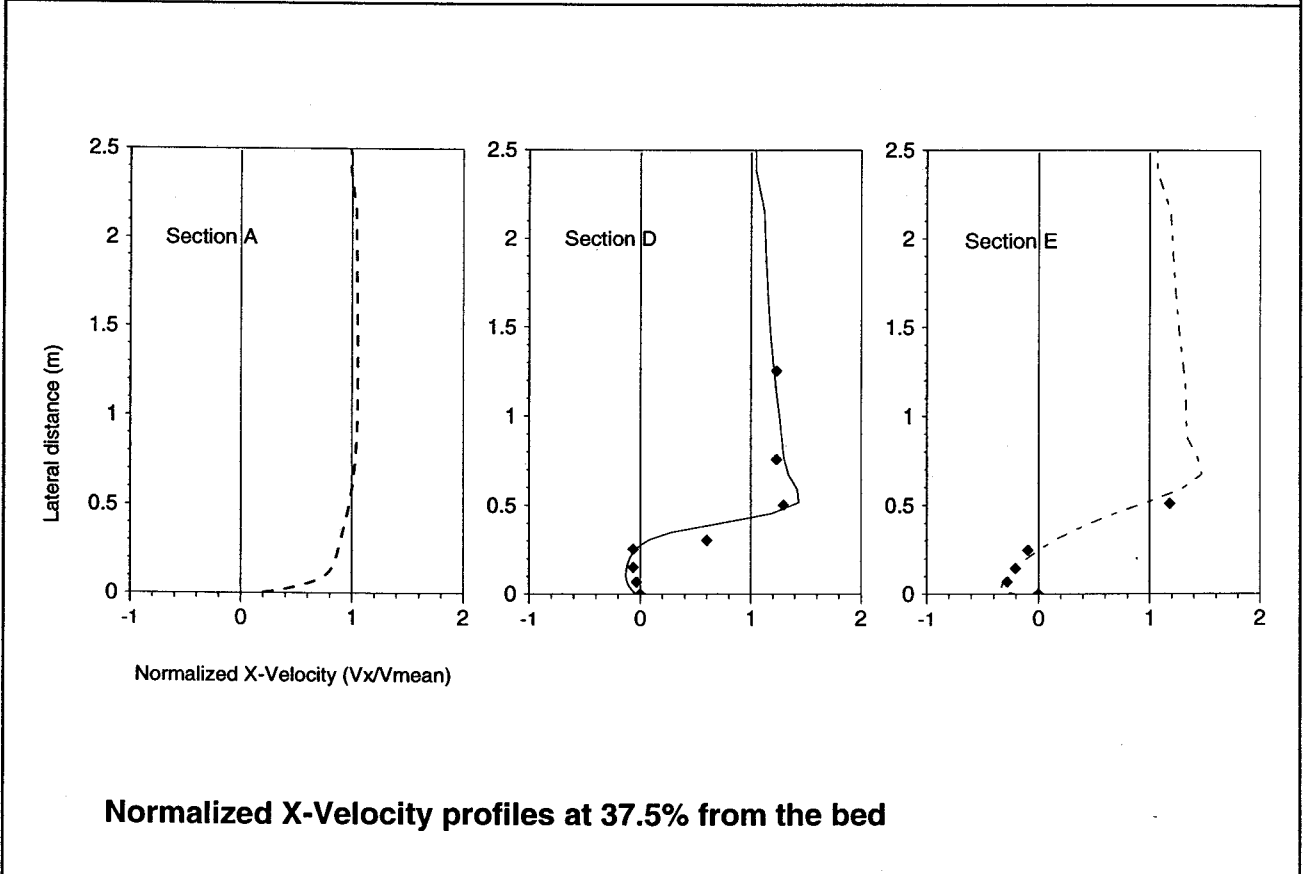
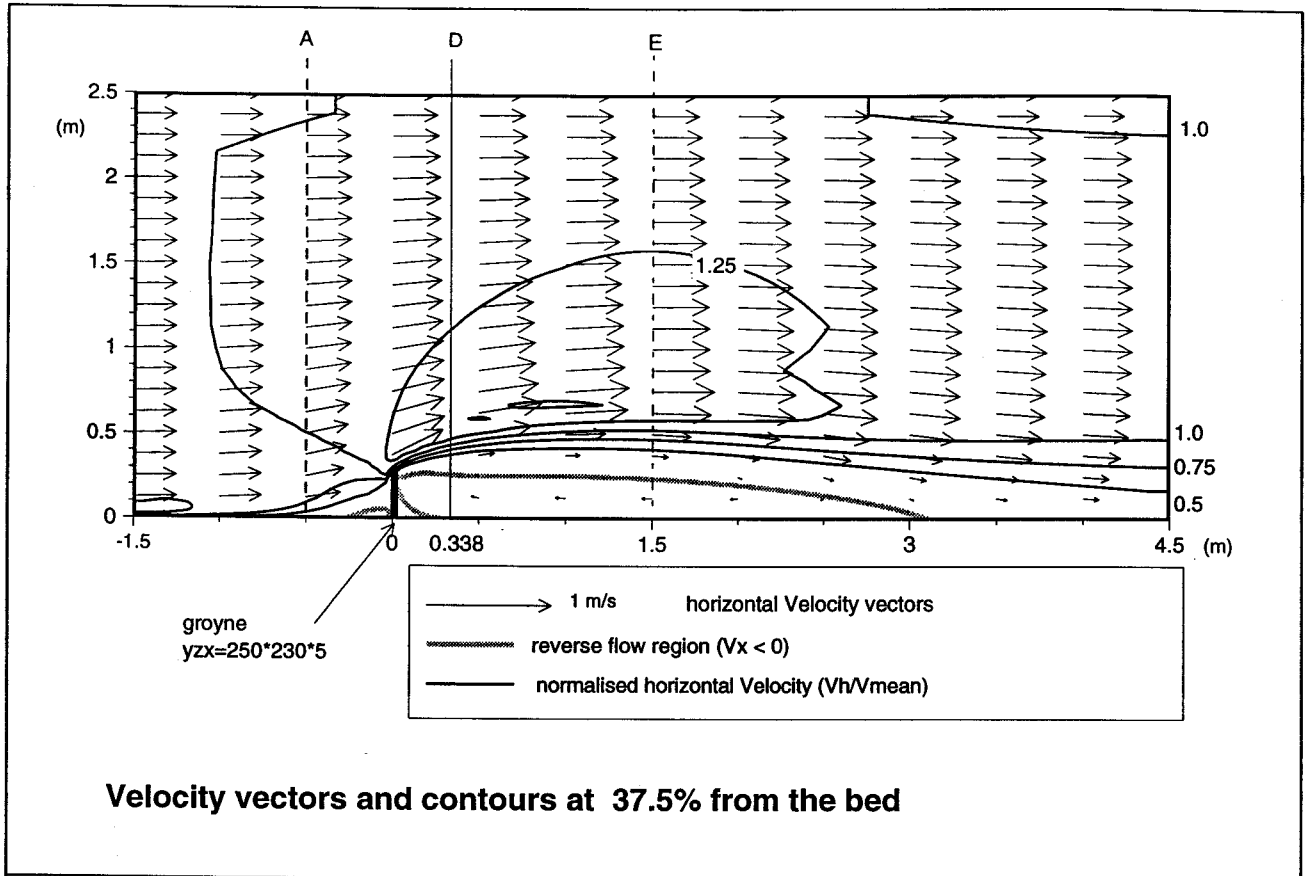


**Figure A-23 Test RAa-16 Hanover flume - one groyne - MIXED scheme  
10 layers - Block correction on k and epsilon - finer grid**

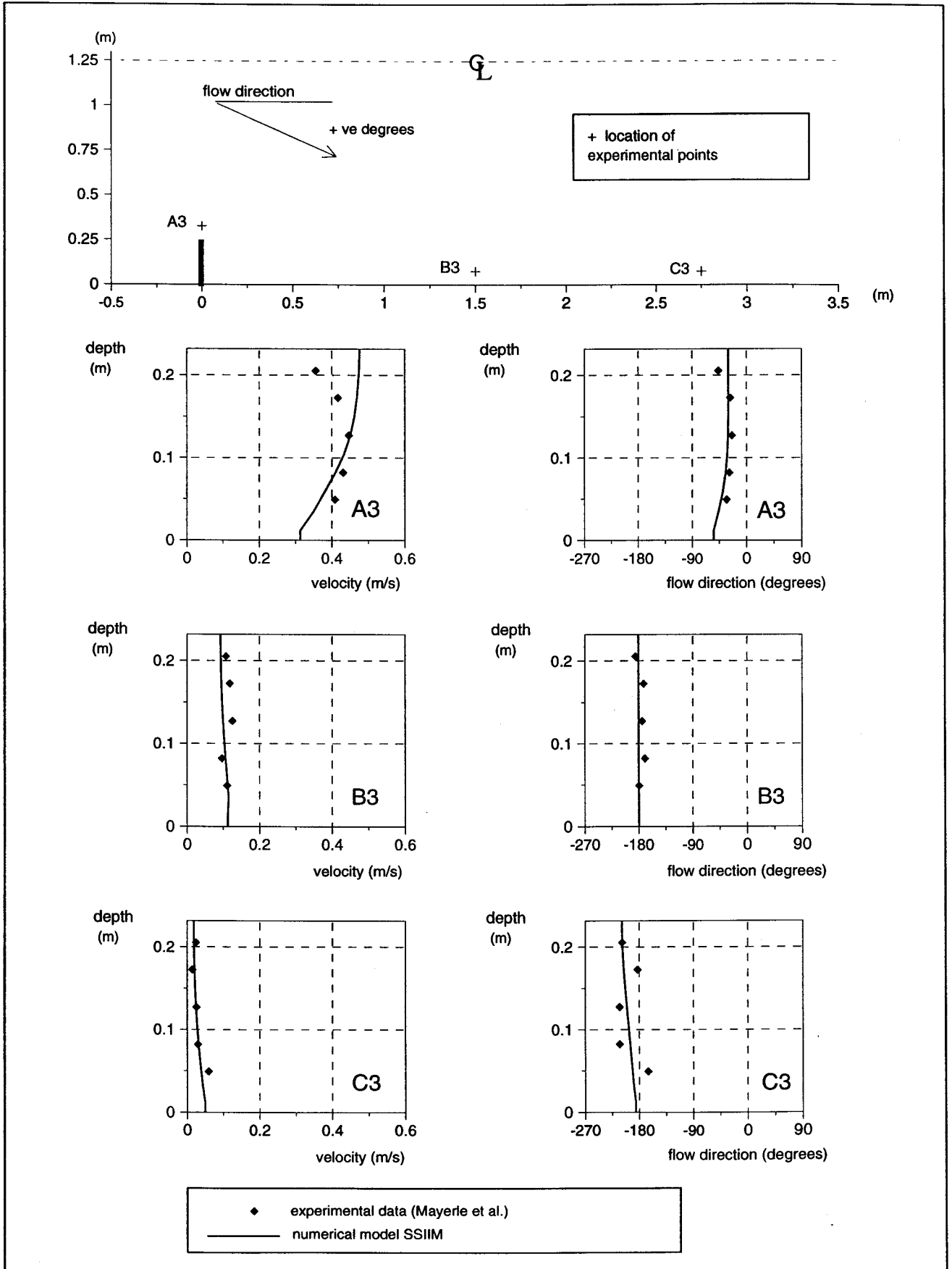


**Figure A-24 Test RAa-16 Hanover flume - one groyne - MIXED scheme  
10 layers - Block correction on k and epsilon- finer grid**

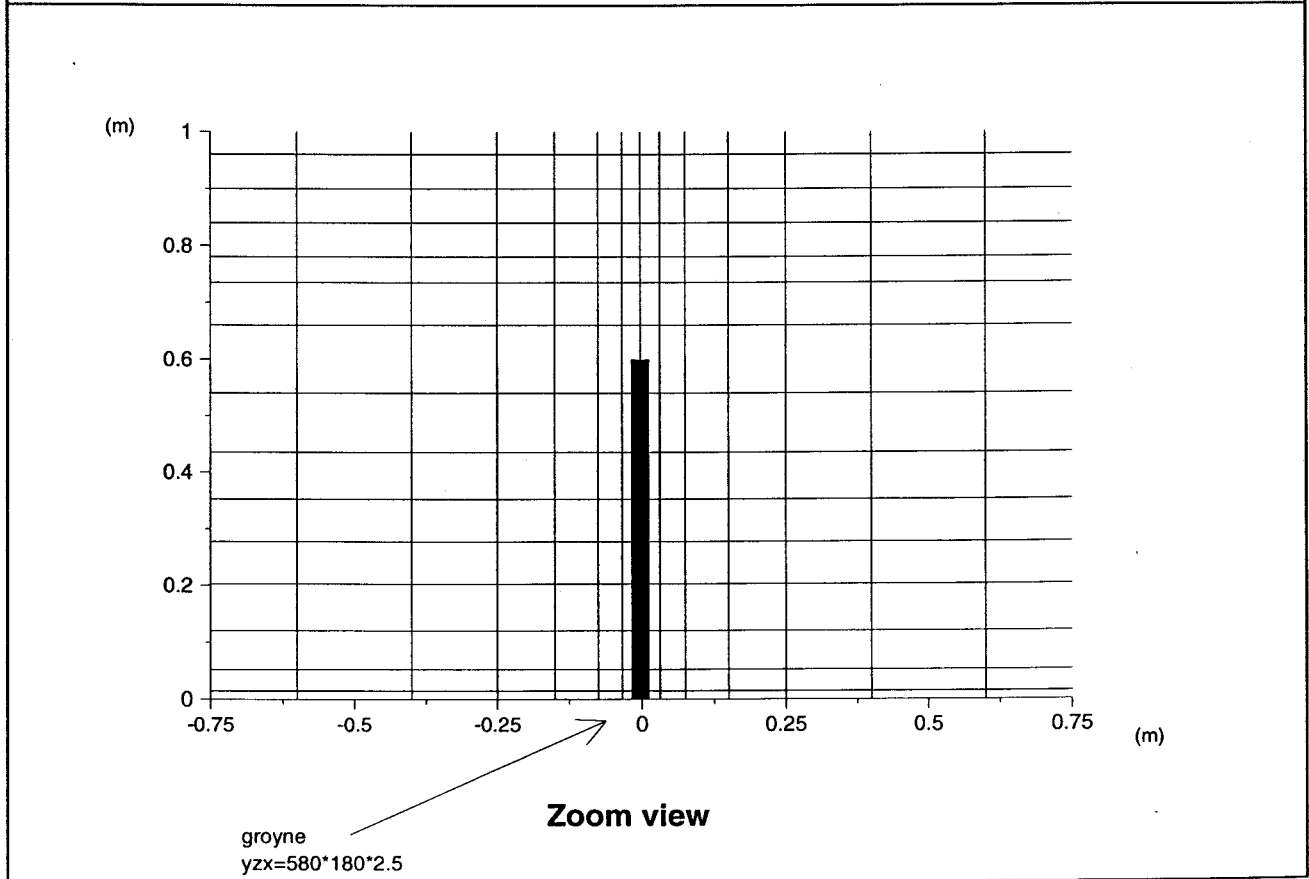
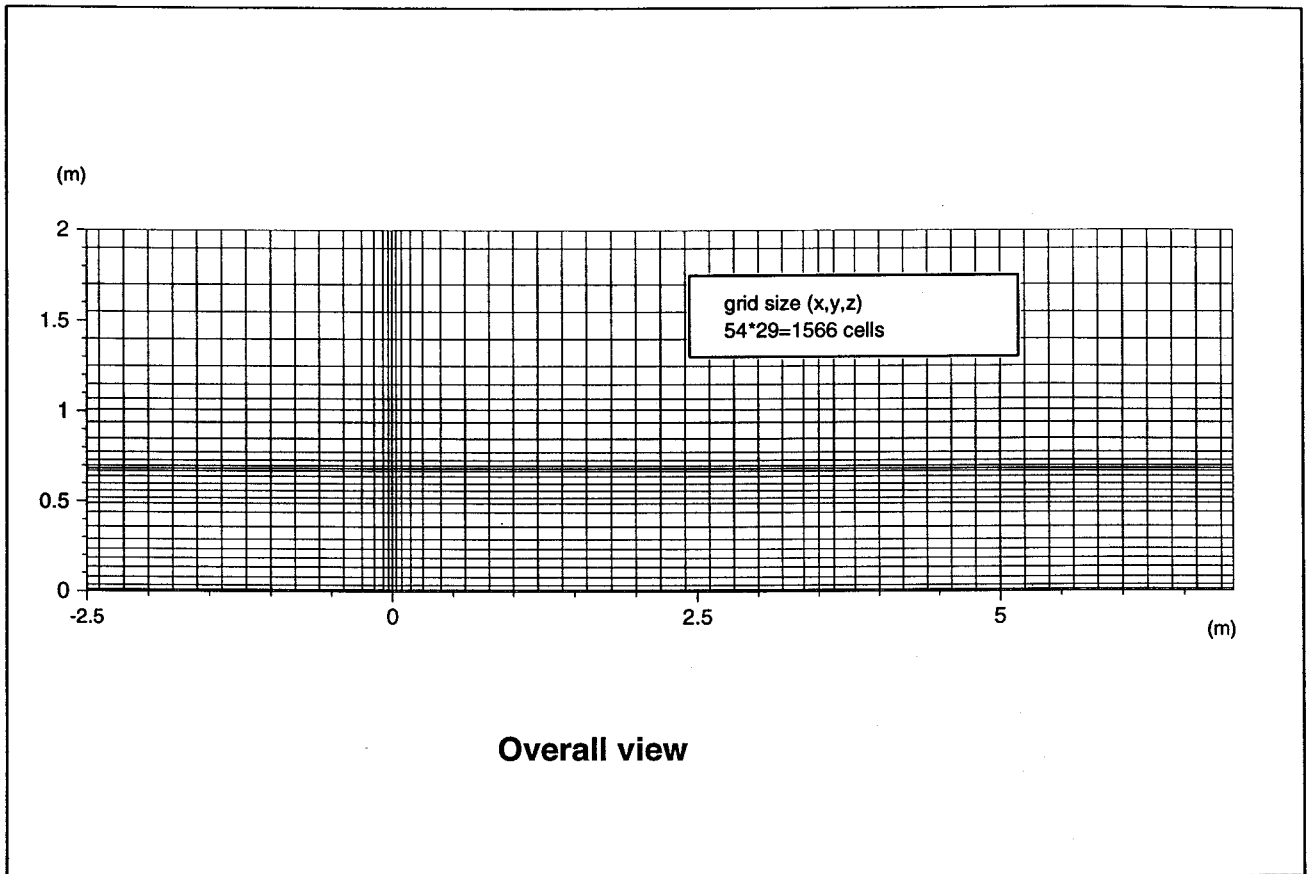
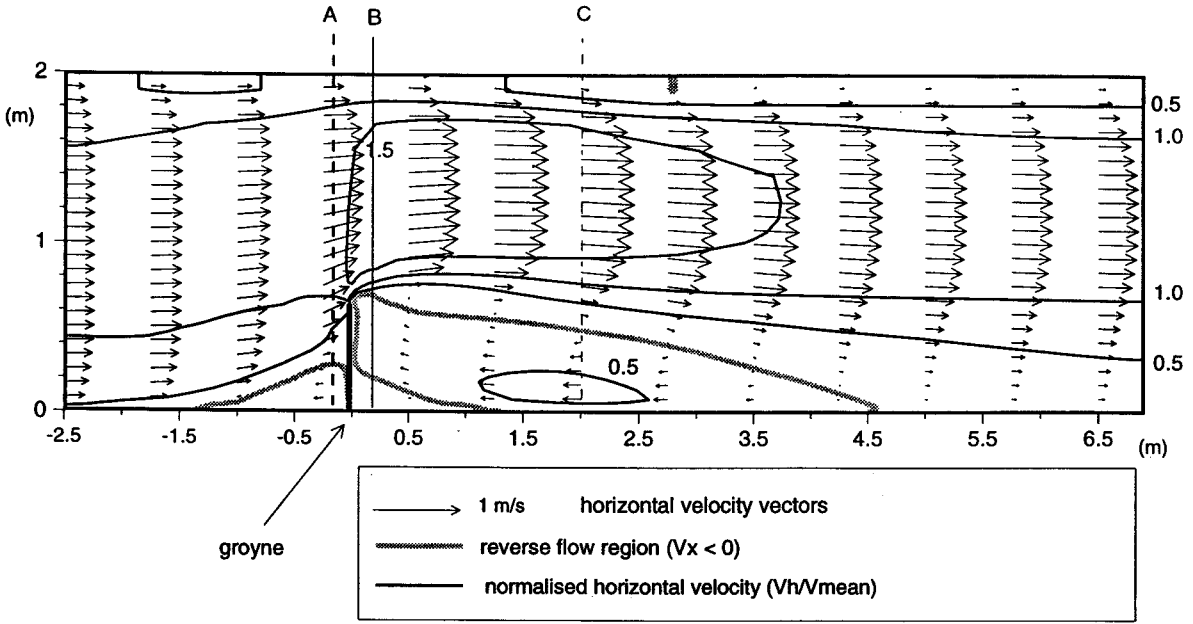
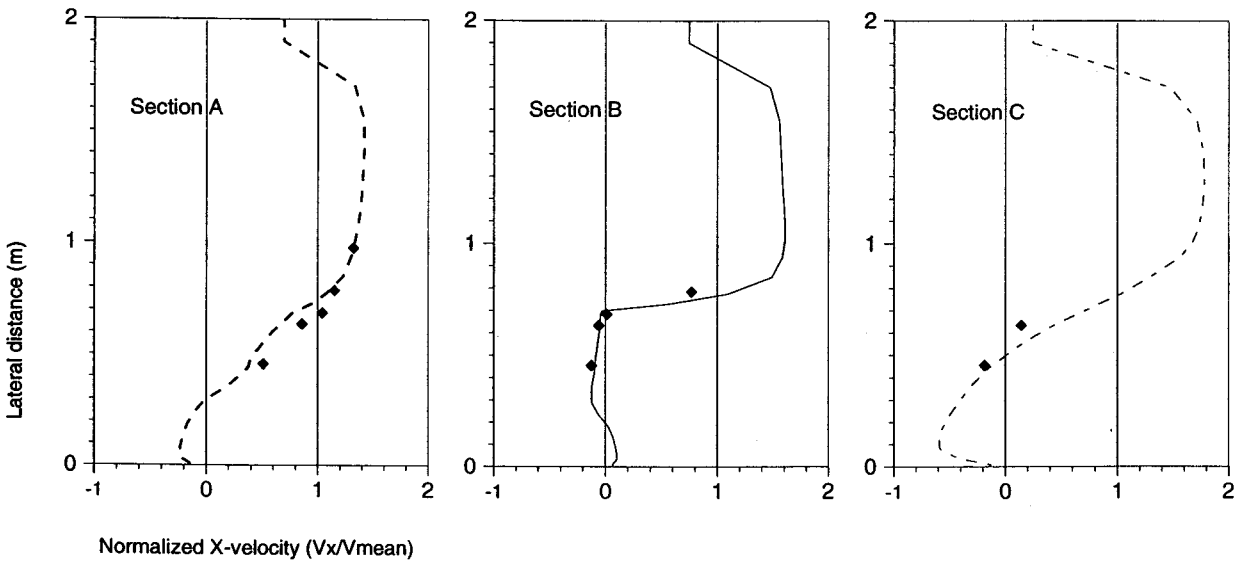


**Figure A-25 Plan view of grid for tests TA**

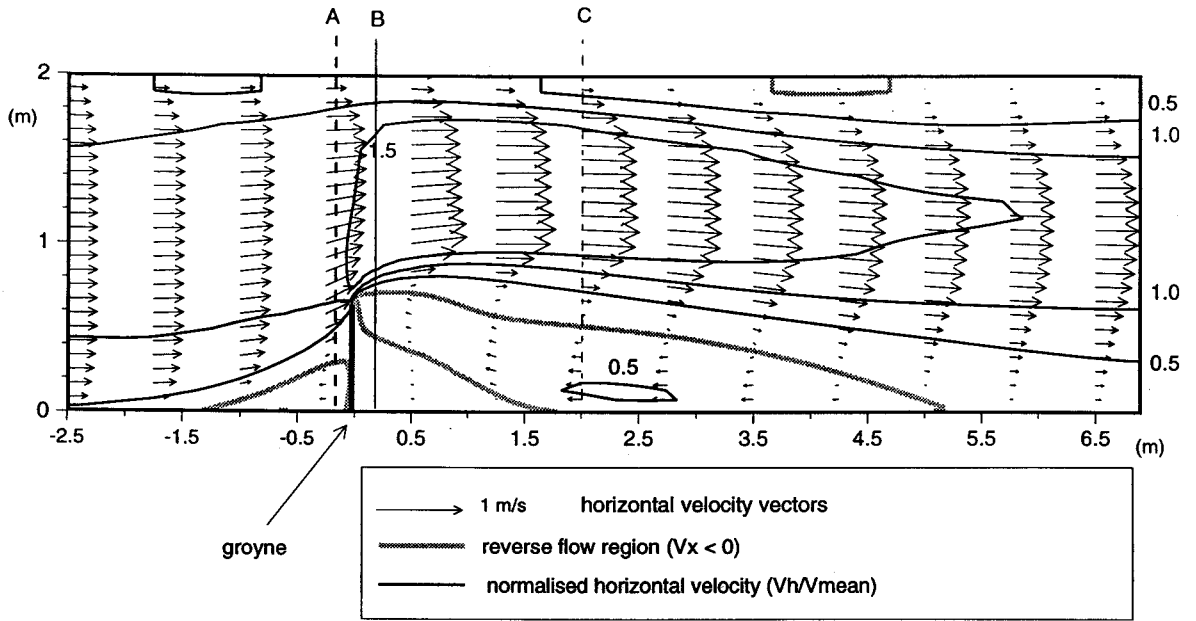


Plan view at mid-depth - velocity vectors and contours

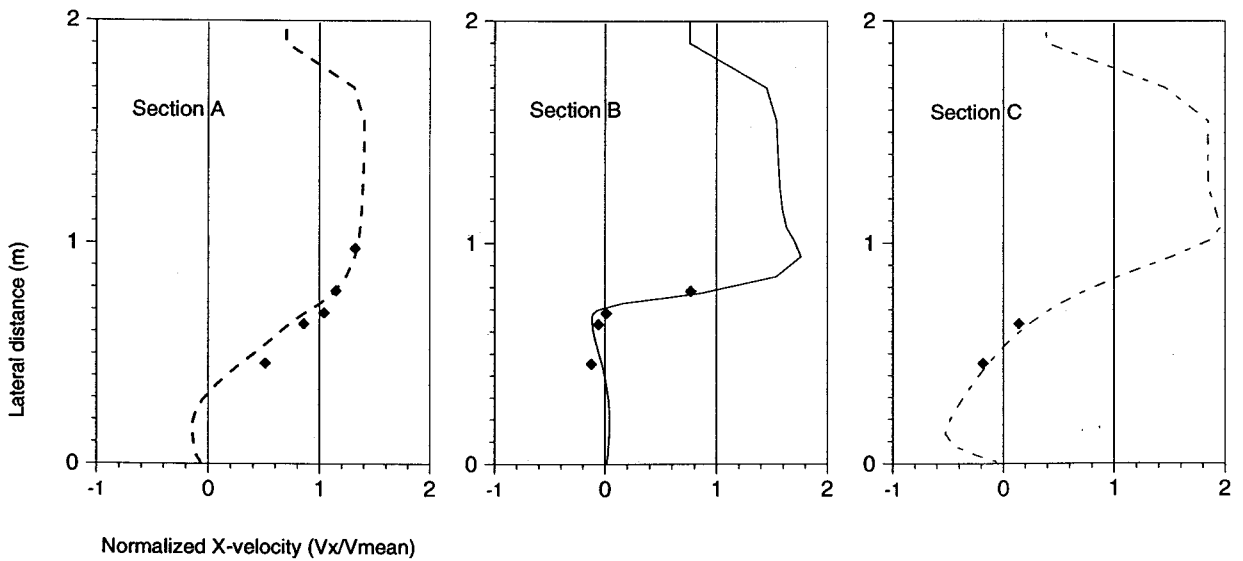


Normalized X-velocity profiles at mid-depth

Figure A-26 Test TA-1 - Trapezoidal channel - one groyne - POW scheme  
12 layers - No block correction

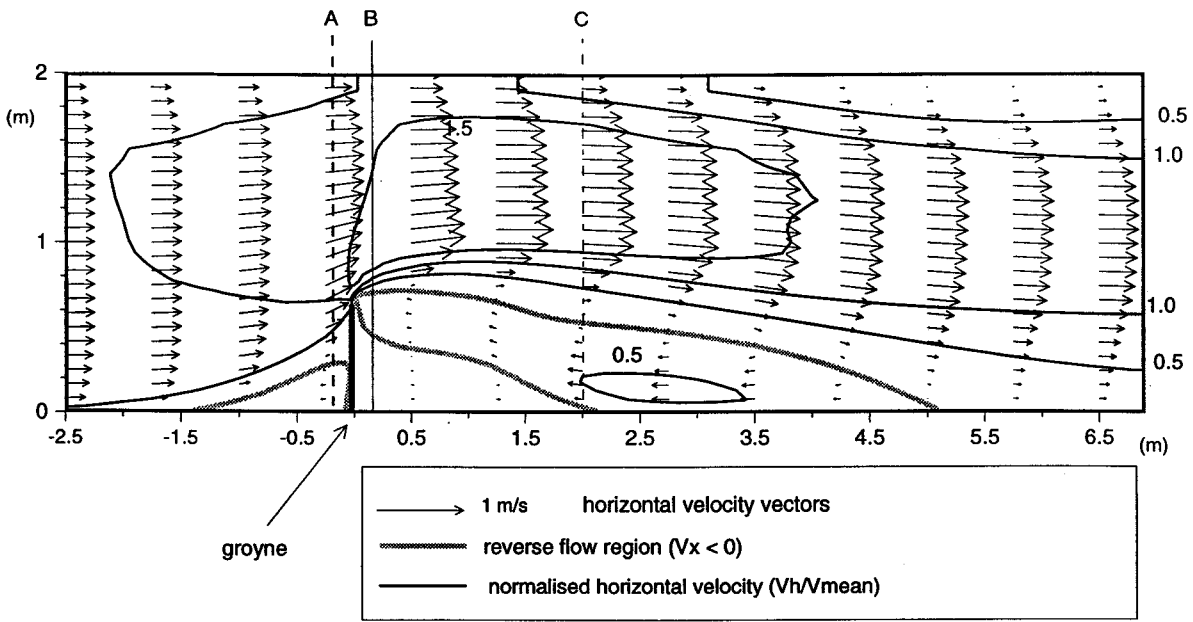


Plan view at mid-depth - velocity vectors and contours

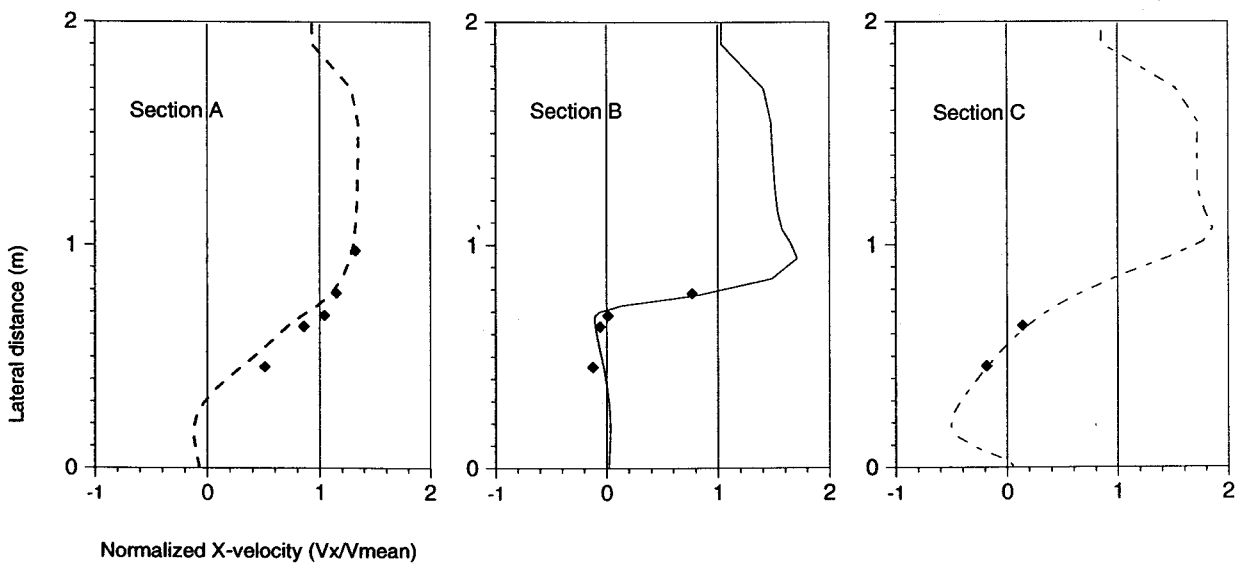


Normalized X-velocity profiles at mid-depth

Figure A-27 Test TA-3 - Trapezoidal channel - one groyne  
MIXED scheme - 12 layers - No block correction

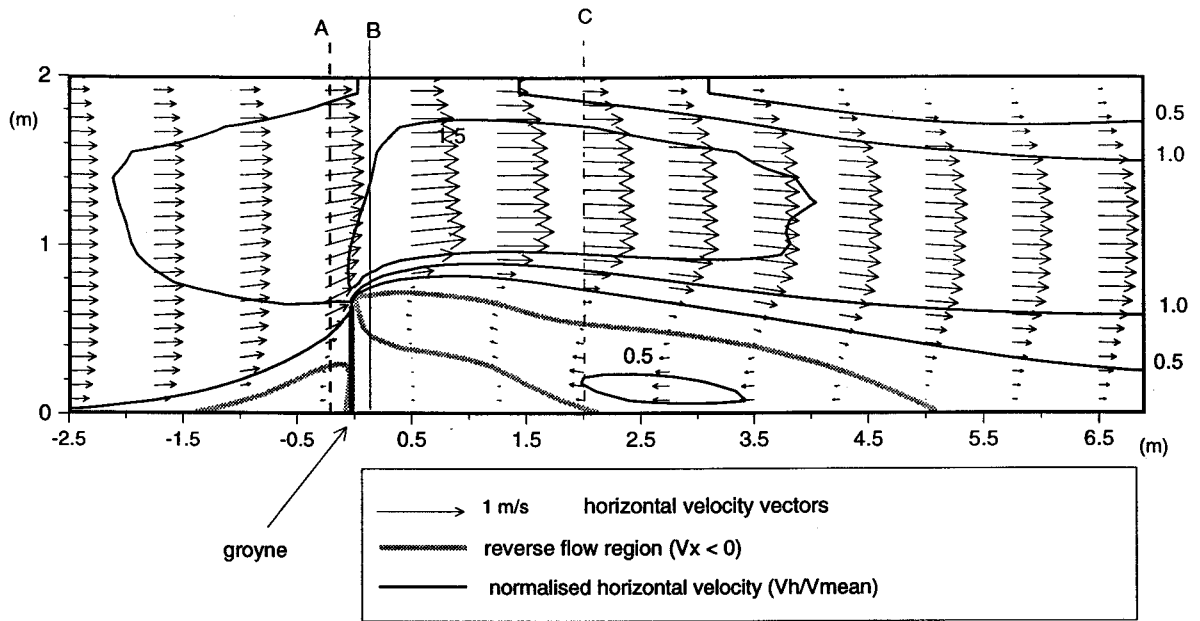


Plan view at mid-depth - velocity vectors and contours

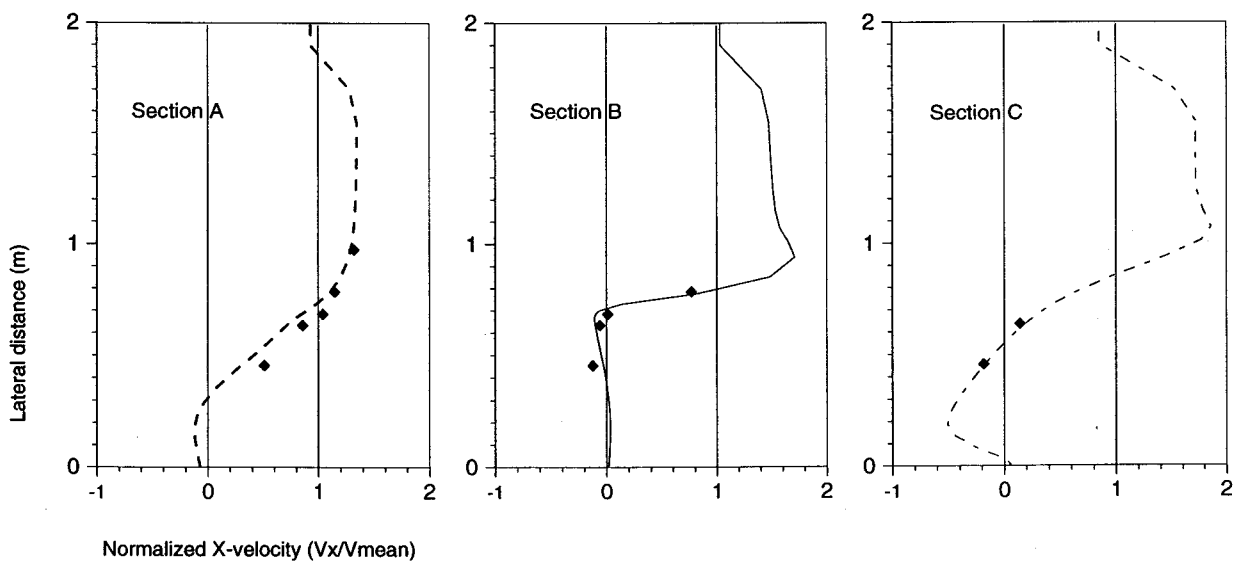


Normalized X-velocity profiles at mid-depth

Figure A-28 Test TA-4 - Trapezoidal channel - one groyne - MIXED scheme - 3 layers - No block correction

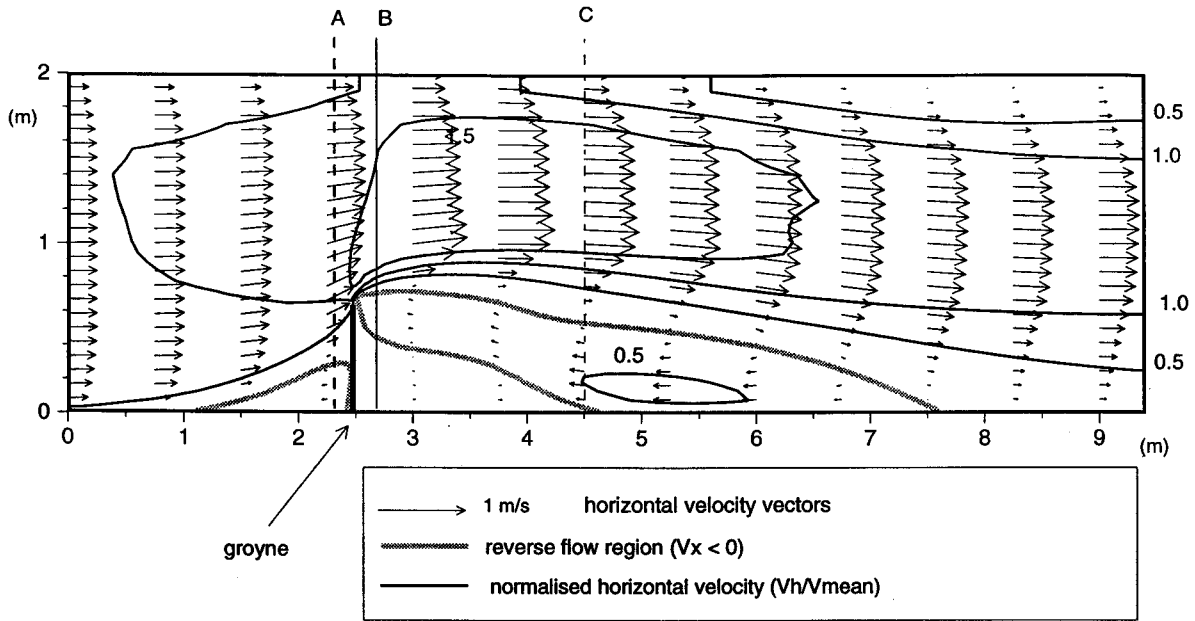


Plan view at mid-depth - velocity vectors and contours

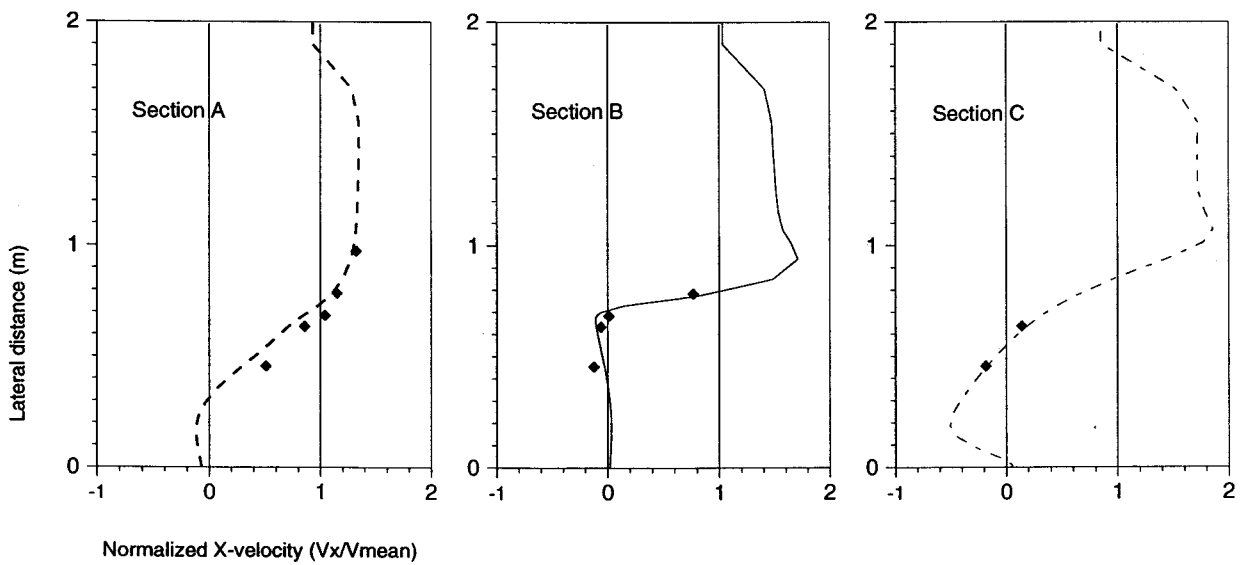


Normalized X-velocity profiles at mid-depth

Figure A-29 Test TA-5 - Trapezoidal channel - one groyne - MIXED scheme - 3 layers - No block correction - 4 sweeps on k



**Plan view at mid-depth - velocity vectors and contours**



**Normalized X-velocity profiles at mid-depth**

**Figure A-30 Test TA-6 - Trapezoidal channel - one groyne - MIXED scheme  
3 layers - No block correction - 4 sweeps on k and epsilon**

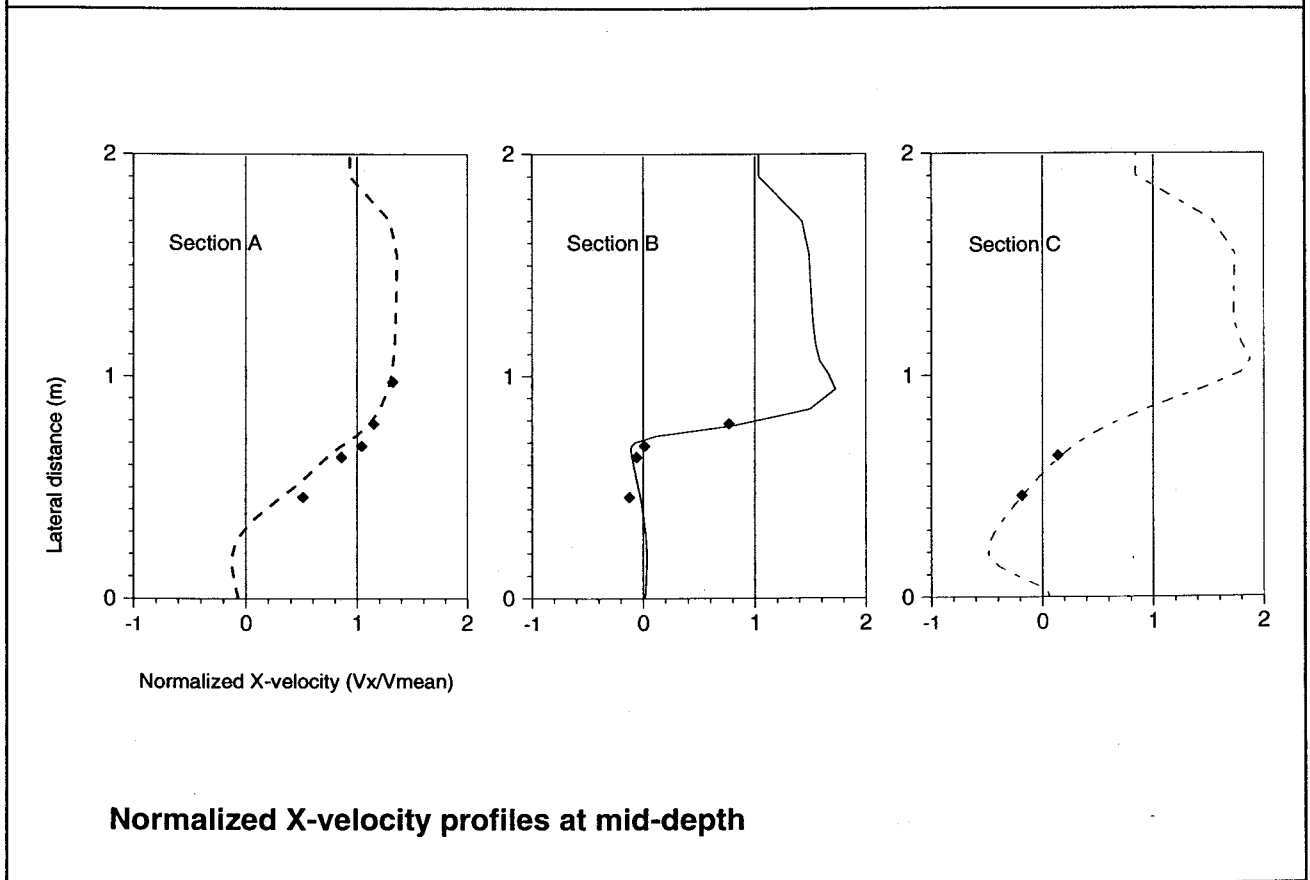
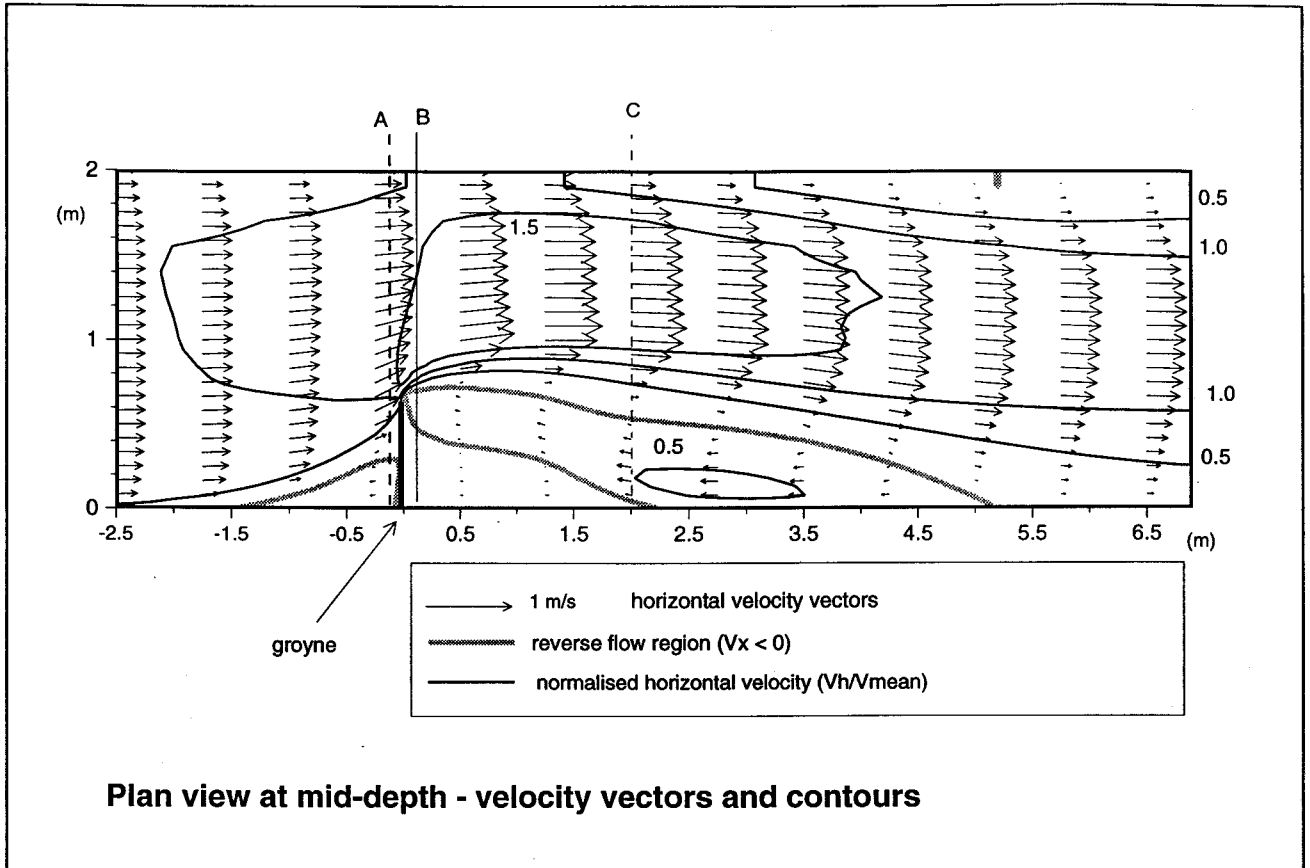


Figure A-31 Test TA-7 - Trapezoidal channel - one groyne - MIXED scheme 3 layers - No block correction increased roughness

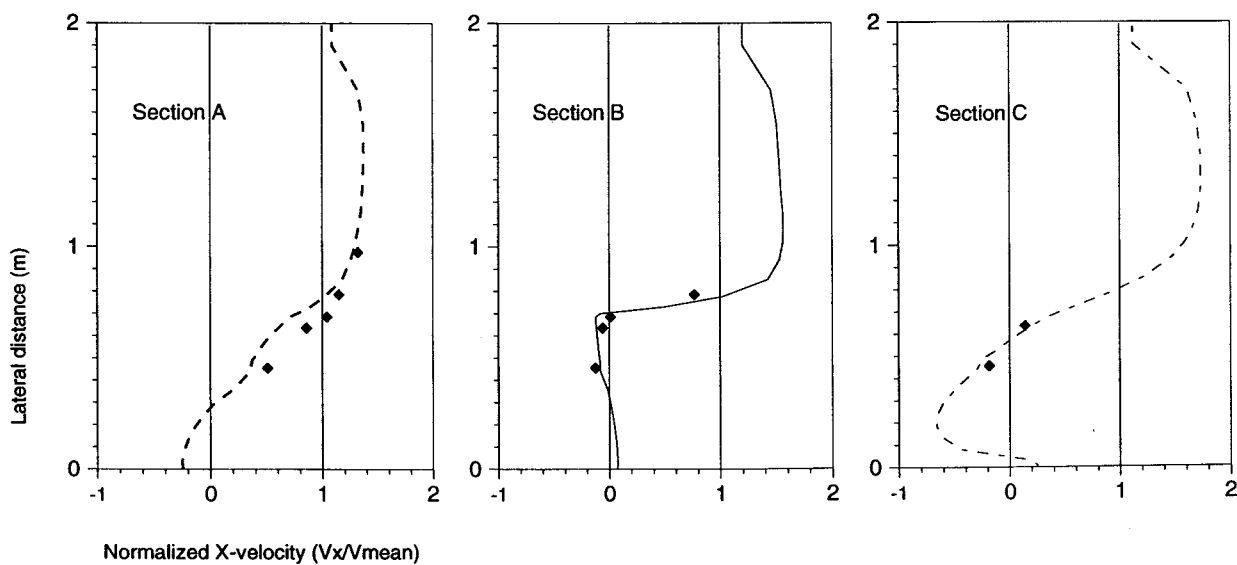
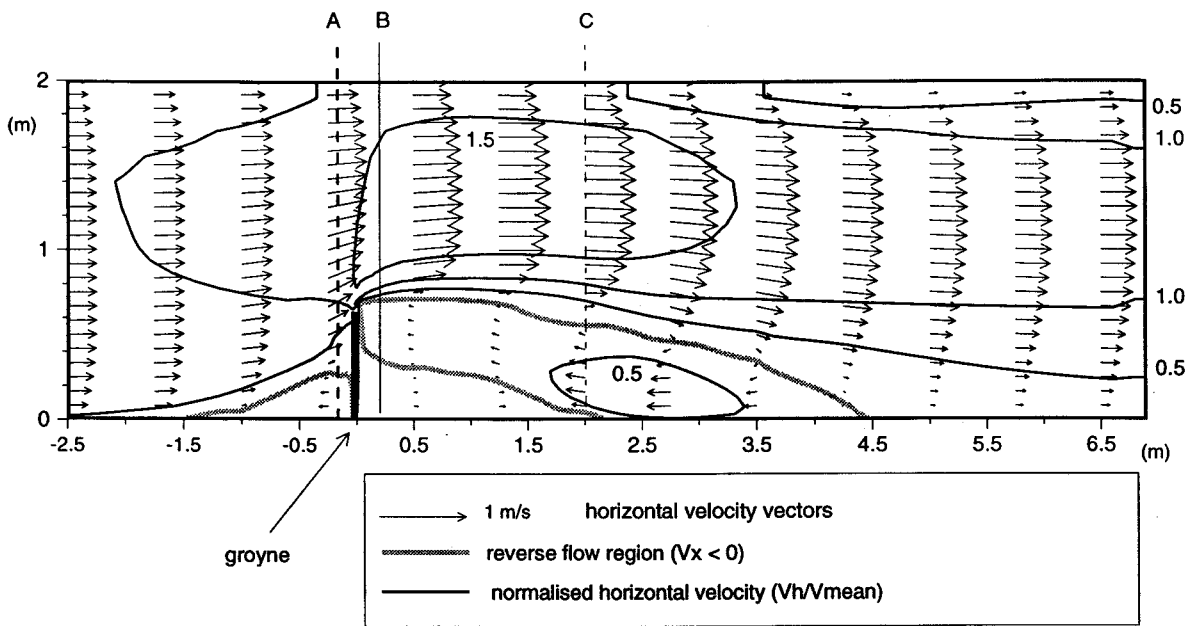


Figure A-32 Test TA-8 - Trapezoidal channel - one groyne - MIXED scheme - 3 layers - No block correction - 2-D computation

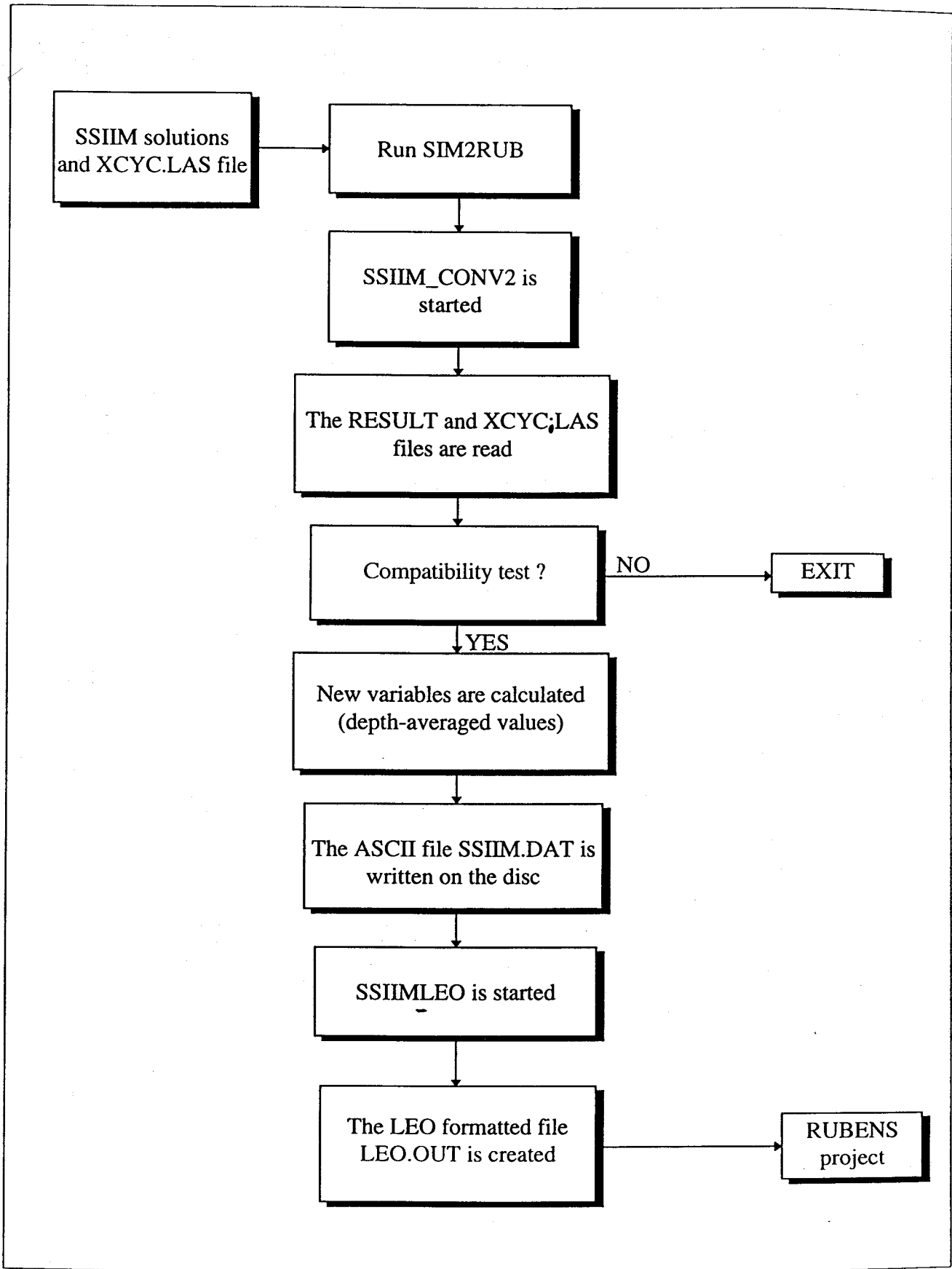


Figure A-33

Organizing chart of SIM2RUB